# Modelling visual-olfactory integration in free-flying *Drosophila*

Finlay John Stewart

Doctor of Philosophy

University of Edinburgh

2009

# Abstract

Flying fruit flies (*Drosophila melanogaster*) locate a concealed appetitive odour source most accurately in environments containing vertical visual contrasts (Frye et al, 2003). To investigate how visuomotor and olfactory responses interact to cause this phenomenon, I implement a tracking system capable of recording flies' flight trajectories in three dimensions. I examine free-flight behaviour in three different visual environments, with and without food odour present. While odour localisation is facilitated by a random chequerboard pattern compared to a horizontally striped one, a single vertical landmark also facilitates odour localisation, but only if the odour source is situated close to the landmark.

I implement a closed-loop systems-level model of visuomotor control consisting of three parallel subsystems which use wide-field optic flow cues to control flight behaviour. These are: an optomotor response to stabilise the model fly's yaw orientation; a collision avoidance system to initiate rapid turns (saccades) away from looming obstacles; and a speed regulation system. This model reproduces in simulation many of the behaviours I observe in flies, including distinctive visually mediated 'rebound' turns following saccades.

Using recordings of real odour plumes, I simulate the presence of an odorant in the arena, and investigate ways in which the olfactory input could modulate visuomotor control. In accordance with the principle of Occam's razor, I identify the simplest mechanism of crossmodal integration that reproduces the observed pattern of visual effects on the odour localisation behaviour of flies. The resulting model uses the change in odour intensity to regulate the sensitivity of collision avoidance, resulting in visually mediated chemokinesis. Additionally, it is necessary to amplify the optomotor response whenever odour is present, increasing the model fly's tendency to steer towards features of the visual environment. This could be viewed as a change in behavioural context brought about by the possibility of feeding.

A novel heterogeneous visual environment is used to validate the model. While its predictions are largely borne out by experimental data, it fails to account for a pronounced odour-dependent attraction to regions of exclusively vertical contrast. I conclude that visual and olfactory responses of *Drosophila* are not independent, but that relatively simple interaction between these modalities can account for the observed visual dependence of odour source localisation.

# Acknowledgements

It is with a certain sense of euphoria that I write this, because there have been times over the last four years when I seriously doubted that I ever would. There are many people I must thank for helping me to get this far.

First and foremost, thanks to my supervisors, Barbara Webb and Dean Baker. I have the utmost respect for Barbara's supervision style. She gave me a great deal of freedom to manage my own research, even though at times - particularly in the early stages - I wanted nothing more than to be told what to do. I pursued my share of month-long dead ends, but Barbara always made sure I didn't have quite enough rope to hang myself with. We only learn by making mistakes, and I feel that I'm a more capable researcher as a result. Dean played an invaluable role during both my Masters and my PhD coaching me, as someone who didn't even take biology at high school, to be able to hold my own in a *Drosophila* lab. While he was at Edinburgh he treated me with real warmth and friendship (not least during our Friday afternoon supervision meetings at the pub), and also helped to make me a little more streetwise about science operates.

I'd like to say a big thank you to Lincoln Smith at Sussex for allowing me to use his gantry and devoting a week of his time to helping me with my PhD. Thanks also to Andy Philippides for going out of his way to make me feel welcome during my time at Sussex. I'd like to extend my gratitude towards everyone at the Dickinson, Frye and Fry labs at Caltech, UCLA and Zurich respectively, for allowing me to visit and taking the time to discuss their ideas with me. I'd like to single out a couple of people for particular thanks: Andrew Straw for taking me under his wing at Caltech, and Mark Frye for being the most infectiously enthusiastic scientist I've ever had the pleasure to meet. I must also thank Mark for supplying me with Super Flies. On the subject of flies, I am grateful to the Finnegan and Armstrong labs here at Edinburgh for allowing me to use their facilities.

I'd like to thank everyone at IPAB (and IPUB) for making it such a pleasant place to work. Thanks especially to my colleagues from the old robot lab in JCMB – being there really didn't feel like work (possibly because it often wasn't). I must also say thanks to the DTC admin Pat Ferguson for going over and above the call of duty to look after me and my fellow students.

I would like to thank my 'urban family' (which is to say my friends) without whom my time in Edinburgh would have been much less enjoyable, and whom I very much hope will continue to be my friends once I leave. Let me mention a few people individually. Graham: you understand me and my

sense of humour better than anyone; you're (sadly) the closest thing I have to a soulmate. Jude: you've offered me so much support, from letting me vent my day-to-day PhD stresses to getting me through full-fledged personal crises. I don't know what I'll do without our coffee breaks. Danny: the man behind a million anecdotes, you're a bona fide eccentric genius and I've had countless hours of entertainment laughing both with and at you. Anisha: you're the most genuinely optimistic person I know. I don't know how you've put up with me over the years, but I'm immensely glad you have. Adam: talking to you is kind of like taking drugs (I imagine), but mostly in a good way. Thanks also to the many other people in Edinburgh that I haven't mentioned here but who have truly enriched my life.

This work was carried out as part of the Neuroinformatics Doctoral Training Centre programme, funded primarily by the EPSRC. I'd like to offer my sincere thanks / humble apologies (delete according to political conviction) to every UK taxpayer for paying for it.

Finally, thanks to my parents, for all your material and emotional support over the years. Thank you for always encouraging me to do what I wanted to do, not what others expected. Most of all, thank you for teaching me to think for myself, which I consider to be the most important thing a parent can do for a child. This thesis is dedicated to you, with love.

# Declaration

This thesis was composed by me, and describes my own work. The work has not been submitted for any other degree or professional qualification.

Finlay Stewart 25th June 2009

# Table of Contents

# 1. Introduction and motivation

Animals interact with their environment using a number of sensory modalities. Consider, for example, an airborne fruit fly searching for food. It could be alerted to the possibility of feeding by the odour of a fermenting banana, but in order to reach the fruit it may have to visually steer toward the yellow patch of its visual surround whilst avoiding obstacles such as branches.

One might suppose that a fly's behaviour is largely reactive, i.e. based on responses to sensory input rather than being the result of any coordinated planning. If this were the case, its banana-seeking behaviour would represent the result of various sensorimotor reflexes being executed in parallel. However, a fly has only one pair of wings with which to propel itself, and it cannot move in two directions at once. Thus there is a question of how input from multiple modalities should be combined to produce coherent behaviour; by naively attempting to pursue an odour plume and visually avoid collisions simultaneously the fly may succeed in neither objective. The issue is further complicated by the fact that different modalities can give conflicting information. For example, a strong headwind may suggest to the fly, via its mechanosensory and proprioceptive systems, that it is moving forward, while its vision would indicate that it is in fact moving backwards.

A clear example of the non-trivial nature of crossmodal integration is provided by Frye et al (2003). *Drosophila* are tracked flying in an arena which has a small vial of vinegar (an appetitive olfactory stimulus) concealed in its floor. The flies are only able to locate the food source when the walls of the arena are patterned, and furthermore the pattern must contain vertical contrasts. Thus, what one might at first assume to be a purely olfactory task relies upon features of the visual environment. The reasons for this phenomenon are poorly understood; why is a fly able to locate an odour source when surrounded by vertical stripes, but not when the same pattern is rotated by 90°?

This thesis presents my efforts to answer this conundrum by performing behavioural experiments in order to derive a detailed account – i.e., a model – of the interplay between vision and olfaction in *Drosophila* that can reproduce and thus explain the curious effect described above. The next chapter describes in detail what is known about the fly's senses of vision and smell, and how they shape its behaviour. For the remainder of this chapter, I provide motivation for this choice of problem and the approach taken.

## 1.1: Why study crossmodal integration?

The question of how we are able to combine all the sensations we experience into a single coherent perception of reality has troubled thinkers for thousands of years. Aristotle posited the notion that our five senses converge in our heart to produce a unified "common sense" (Modrak, 1987). While we have revised the hypothesised locus of this operation to the brain, one might be tempted to conclude that we are little closer to understanding the process than the ancient Greeks were. What a *Drosophila*'s perception of reality is like, and indeed whether it even possesses one, are questions that I shall leave to philosophers. However, by carefully characterising how just two senses interact in an insect, perhaps one can uncover some basic principles of multimodal information processing that apply to more sophisticated creatures.

The issue of combining information from many different kinds of sensors is of more immediate and practical importance to the designers of robotic systems, who refer to it as the *sensor fusion* problem. It is highly desirable that an agent can use multiple redundant senses to perceive its environment, as any given modality will typically suffer from ambiguities in certain situations (see Murphy (1996) for a review). Amalgamating these inputs is a difficult problem; if two senses give conflicting information, which should be believed? In a task requiring vision and proprioception, humans unconsciously but very accurately gauge the reliability of each of these senses and weight them in an optimal probabilistic fashion (Körding & Wolpert, 2004). Whether such mechanisms exist in insects, or whether their limited information processing capacity constrains them to simpler algorithms, remains an open question.

## 1.2: Why study odour localisation?

All animals need to eat, and most rely on their sense of smell rather more than humans do when locating food. Additionally, some animals (e.g. moths and butterflies) use olfaction to find mates, via the use of sex pheromones. As I shall discuss in detail in section 2.5.1, it is not generally straightforward to follow an odour plume back to its source because, over any distance greater than a few centimetres, the diffusion of chemicals in a fluid (be it water or air) becomes chaotic and unpredictable. Furthermore, wind or currents will distort the plume structure, and perturb the movement of flying or swimming animals. The latter observation may provide a clue as to why *Drosophila* use their eyes even when localising an invisible odour source: the visual environment provides a stable external reference with which a flying insect can estimate its own movement (section 2.2.1).

Since the difficulties outlined in the preceding paragraph are faced by many animals, it may be the case that similar mechanisms for dealing with them will have been preserved across many species. Parallel or convergent evolution may also have independently 'discovered' such solutions several times. For these reasons, a model of visual-olfactory integration in *Drosophila* may aid our understanding of creatures as diverse as seabirds (Nevitt, 1999) and sharks (Hodgson & Mathewson, 1971; see Vickers (2000) for a review).

As with crossmodal integration, there are also reasons why odour localisation is interesting from an engineering perspective. Humans currently exploit the superior olfactory abilities of well-trained animals such as sniffer dogs to locate various hard-to-find objects, including earthquake and avalanche survivors, explosives, truffles, and concealed drugs. Clearly, it would be desirable to use robotic as opposed to canine (or porcine) agents for these tasks (review in Russel, 2001).

## 1.3: Why study insects?

Insects are in general good candidates for neuroethological studies. (Neuroethology is the study of the natural behaviour of animals and its mechanistic control by the nervous system (Hoyle, 1984).) They are sufficiently complex to exhibit interesting behaviours (reviews: Giurfa & Menzel, 1997; Greenspan & van Swinderen, 2004), which are often more sophisticated, robust and adaptable than those of the most advanced robots built to date. Some illustrative examples include path integration for navigation in ants (Wehner, 2003), co-operative communication in honeybees (von Frisch, 1967), and aerial pursuit in blowflies (Boeddeker et al, 2003).

On the other hand, insects are simple enough that we can have some hope of understanding complete neural circuits from sensor to muscle. The fruit fly brain contains approximately $10^5$ neurons – roughly one millionth of the figure for humans. Furthermore, while insects are capable of learning (see Siwicki & Ladewski (2003) for a review of *Drosophila* learning) and 'spontaneous' behaviour (Maye et al, 2007), their behaviour is more rigidly stereotyped, and thus repeatable, than that of mammals.

Insects can thus be seen as halfway house between tractable but behaviourally limited organisms like the nematode worm *C. elegans*, and behaviourally fascinating but dizzyingly complicated animals like primates. Finally, from a practical standpoint, insects are small and cheap (see section 1.4), and one can perform experiments on them that would be unethical on vertebrates.

## 1.4: Why study *Drosophila*?

The fruit fly *Drosophila melanogaster* (fig 1.1) is an immensely popular model organism for all kinds of biological research, as evidenced by its distinction of being the first known animal sent to space, in 1947. There are a number of reasons why it is so beloved by scientists. It is small (~3mm in length) and very easy to maintain. A breeding population can be kept in a bottle containing a plentiful supply of food, which need only be refreshed around once a month due to the accumulation of corpses, empty pupal exoskeletons, and excrement. It has a short life cycle (~10 days) and high fecundity, making breeding very simple.

Figure 1.1: The fruit fly *Drosophila melanogaster*. This is a wild-type male, ~3mm in length with a wingspan of ~4mm. Picture credit: André Karwath.

*Drosophila* is primarily a model organism for genetics research. The discovery that genes are arranged linearly in fixed positions on chromosomes came from work on *Drosophila* (Sturtevant, 1913) and more recently it was among the first multicellular organisms to have its genome fully sequenced (Adams et al, 2000). An impressive array of genetic techniques exists for flies, allowing specific subsets of cells to be targeted for various manipulations, such as disabling a particular protein (or restoring it in a mutant animal lacking it), or suppressing neuronal activity by hyperpolarization (see Greenspan (2004), also Borst (2009) for a brief but recent overview). These spatially selective manipulations can even be triggered in a temporally selective manner by exposure to light or heat, allowing a fly to develop normally before subjecting it to an acute lesion, which can subsequently be reversed.

I do not take advantage of these genetic tools; no mutant flies are used in this study. Nevertheless, it is worthwhile to perform experiments on wild-type flies because of all that is known about them thanks to the powerful techniques available. Similarly, gathering detailed behavioural data about wild-type

flies can generate hypotheses that can subsequently be investigated using mutants.

Having said this, the decision to use *Drosophila* is a compromise, in that they are not ideally suited to neuroethological experiments of the type I am concerned with. Due to their small size even by insect standards, it is very difficult to take electrophysiological recordings of their cells. For this reason, rather more is known about the functional properties of neurons in larger insects such as blowflies (genus *Calliphora*) and house flies (*Musca domestica*). These larger flies are also easier to track in flight, so a more substantial body of free-flight behavioural data exists for them. Together with *Drosophila*, these animals are members of the order *Diptera*, the 'true' (i.e. two-winged) flies. While it is reasonable to assume that substantial similarities exist in their physiology and behaviour, one must always exercise caution when comparing data from different species.

## 1.5: Why use this experimental paradigm?

There are two broad schools of thought regarding the design of behavioural experiments. The traditional approach, exemplified by the classical studies of visual motion processing in flies (Hassenstein & Reichardt, 1956; Götz, 1968; see section 2.2.2) was to put animals in situations where their behavioural responses were highly constrained (e.g. by tethering) and present them with very simple stimuli (e.g. moving sinusoidal gratings). Thus as many variables as possible were eliminated by virtue of the experimental design.

In later decades there was a philosophical shift towards studying behaviour in more realistic settings, facilitated in part by technological advances in both experimental hardware and computational analysis. The importance of ecological validity was stressed (Gibson, 1979; Hoyle, 1984). For instance, insects did not evolve in a world composed of fixed-wavelength, fixed-contrast sinusoidal gratings, and they are found to estimate the velocity of more naturalistic visual stimuli considerably more reliably (Straw et al, 2008; see section 2.3.3.2).

However, simplifications must always be made in order that studies do not become mired in the countless sources of noise and variability that exist in naturalistic settings. Like all experiments, the free-flight paradigm pioneered by Tammero & Dickinson (2002a) and adopted for the purposes of this study represents a compromise. Flies are able to move freely, and thus receive realistic mechanosensory and proprioceptive input, as well as experiencing visual motion with realistic translational and rotational components. The use of a real odour plume ensures an appropriately complex olfactory environment exists. However, the visual environment is rather simplified, in that it

is static, flat (i.e. it gives no parallax cues), and only contains regular shapes in one of two tones (black and white). Unlike a natural setting, there is no wind.

There is a long tradition of studying illusions in cognitive psychology. An illusion is some contrived stimulus that tricks our perceptual systems precisely because it is unrealistic. For instance, humans normally have no difficulty in ascertaining which side of a cube is nearest to them, as they can utilise cues from binocular disparity, occlusion, perspective, texture, illumination, and so on. The famous Necker Cube illusion (Necker, 1832) removes all of these sources of information, and as a result the viewer experiences a curious visual ambiguity. This result tells us a great deal about how our visual perception systems work. The *Drosophila* free-flight paradigm can also be viewed in this way. An environment lacking vertical contrast is highly unrealistic, but the fact that it causes a breakdown in the odour localisation competence of flies provides a valuable insight into the algorithm that underlies this behaviour.

## 1.6: Why build models?

While I perform behavioural experiments (chapters 4 and 6), this study is, at its heart, an exercise in modelling. The rationale for writing computer programs in order to understand flies may not be readily apparent to all readers, so in this section I argue why this study should nevertheless be considered an example of science rather than engineering.

Having said this, the science/engineering distinction is perhaps, like so many dichotomies, somewhat artificial. To my mind, science is essentially a process of reverse engineering. This is especially clear in biology, where evolution has 'designed' ingenious devices over millions of years, and like industrial spies, we would very much like to understand that technology behind them. Given a mysterious artefact, be it man-made or biological, we can collect data on it in various ways: opening it up and looking inside, taking parts out and testing whether it still works, carefully studying its behaviour in different conditions, etc. However, data from all these different approaches may be difficult to unify into a coherent framework. I would argue that we can only be said to truly understand how the artefact works when we are able to build one ourselves.

This final step in the scientific process is the role of the modeller. Clearly, when discussing insects, building full working replicas from scratch is out of the question for the foreseeable future. However, as argued by Webb (2009), models can still be informative despite being abstracted, inaccurate and incomplete. In building even these pale imitations of biology, a modeller will often encounter many

issues that had not even occurred to experimentalists. This is because modelling forces one to be explicit in their hypotheses; quantitative details must be filled in. A flying insect is a closed-loop system, meaning that its behaviour at one instant will shape its sensory experience of the next, in turn affecting its subsequent behaviour. In these circumstances, it becomes very difficult to analytically predict the behaviour of even a well-understood system, since it is the product of a complex interaction between agent and environment (Simon, 1982). Modelling is thus especially useful in this case.

However, there are a number of ways in which modelling can fail to be useful if not performed properly. Firstly, while negative experimental results are usually still informative, a model that does not work is likely to be of little interest. It is difficult to go from a negative modelling outcome to a proof that a model of that kind cannot in principle solve the problem at hand. This is because any given model represents just one instance of a potentially infinite configuration space of the algorithm that it represents.

If a model works, in the sense that it reproduces all relevant experimental data, it may still be useless. A large database of the aforementioned data would succeed in this respect, but would contribute nothing to our understanding. To be considered valid, a model (like any scientific theory) must be able to make verifiable predictions. Finally, even a model which passes both of the above tests would be of limited value if it were too complicated to be understood. Rosenblueth & Wiener (1945) pithily remarked that "the best material model for a cat is another, or preferably the same cat". The point they are making is that the purpose of a model is not to merely duplicate the target system, but to explain it, which of course the cat 'model' is unable to do.

Webb (2001) identifies a number of dimensions on which a model can be assessed, several of which conflict to some extent. For instance, *generality* (i.e. being applicable to a wide range of biological systems) is often considered a desirable quality, but a highly general model risks lacking *accuracy*, i.e. faithfully representing the features of any particular target system. A modeller must always make compromises, while keeping the pitfalls discussed in the preceding paragraphs firmly in mind. These issues are discussed further, with particular reference to this study, in section 5.3.1.

## 1.7: Why combine modelling and experimentation?

I must stress that I do not see modelling as an alternative to empirical science, but rather as an

occasionally overlooked complement to it. Without a well-characterised target system to compare it to, it is difficult to validate one's model, or indeed to justify its existence (Webb, 2009). Furthermore, experimental results inform the modelling process. Biological data can provide values for model parameters, constraining the space of possible implementations and thus helping to avoid overfitting (see section 5.3.1). Conversely, the high level of algorithmic detail required to implement models highlights gaps in our understanding which can inspire new experiments. New experiments can also be conceived to attempt to confirm or falsify the hypotheses embodied by a model.

Webb (2006) makes the point that it is essential for a modeller to be very familiar with the data she is attempting to reproduce. In particular, she should go beyond the textbook accounts and concern herself as far as possible with the actual data, looking for phenomena that may have been missed (or deliberately downplayed). When faced with a mismatch between model and animal data, she should always consider the possibility that the experimental results are invalid for some reason.

The best way to have intimate knowledge of experimental data is to perform the experiments oneself. This is the approach I take in this study, alternating between the roles of behavioural experimenter and modeller. For the sake of clarity, I separate my presentation of experimental and modelling work as far as possible in this thesis, as outlined in the following section. However, these two lines of enquiry were followed in a more overlapping and iterative manner than this structure might suggest.

## 1.8: Thesis outline

The objective of this study is to derive a model of the interaction between vision and olfaction in flying *Drosophila* that explains why their ability to locate a hidden food odour source depends on the presence of vertical visual contrasts. Chapter 2 reviews in detail the literature relevant to this question. My experimental methodology is described in chapter 3, the majority of which is concerned with how I implemented a system to track flying *Drosophila* in three dimensions. I then begin my investigation by considering the behaviour of flies in the absence of food odour. Chapter 4 describes the results of my free-flight experiments in various visual environments, and chapter 5 presents my model of the observed behaviour. Having characterised unimodal behaviours in this way, I consider the issue of olfaction, first investigating odour localisation in the free-flight arena in chapter 6. Chapter 7 is a brief methodological digression, describing my approach to characterising odour plumes using a robot-mounted chemical sensor. Armed with this data, I investigate models of crossmodal integration in chapter 8. Having demonstrated the minimal model capable of reproducing the observed odour

localisation behaviour of flies, I assess its validity by introducing a novel experimental environment in chapter 9. Finally, chapter 10 offers my conclusions and suggestions of directions for future research.

# 2. Background

Having introduced this study's research question in the previous chapter, I shall now review the relevant literature. I begin with the studies most directly related to this one, i.e. those pertaining to the interaction of vision and olfaction in *Drosophila* (section 2.1). I then focus on the visual modality, considering evidence gleaned from behavioural (section 2.2), physiological (section 2.3) and modelling studies (section 2.4). Sections 2.5 to 2.7 then cover the olfactory modality in a similar manner.

## 2.1: Visual-olfactory integration

As discussed in chapter 1, my project is based around Frye et al's (2003) observation that *Drosophila* require certain types of visually structured environments to localise odours. I shall begin by describing the findings of this study in more detail.

A fly was placed in a cylindrical arena 1m in diameter and 60cm tall, with a black floor and black curtain canopy over the top. Ambient lighting was provided through the wall, which featured one of several black and white patterns, and a pair of cameras tracked the fly's position in 3D. Initial experiments were conducted in the absence of odour. Flies generally fly in relatively straight lines interspersed with rapid (~70ms duration) yaw turns of ~90°, termed *saccades*. When the walls were uniformly white, vertically striped or had a random chequerboard pattern, the fly would initiate saccades as it neared the wall, which would steer it in the appropriate direction to avoid a collision with greater-than-chance frequency. Horizontally striped walls reduced the frequency of saccades, with flies instead following smoothly curved trajectories close to the wall.

A small vial of apple cider vinegar – an attractive substance for flies – was concealed in the arena floor in order to investigate olfactory behaviour. In the chequerboard or vertically striped arenas, the fly would spend considerably more time in the region above the vial (though this is not quantified). This did not occur in the uniform white arena. In the horizontally striped arena, the addition of odour elicited saccadic flight, but as in the uniform condition, the fly did not localise the odour. It appears that proximity to the vial (and thus presumably high odour intensity) increases saccade frequency in all visual conditions, which leads to a slight bias towards the odour location due to non-directional kinesis (see section 2.5.3). However, only in the chequerboard and vertical stripe conditions did the

fly saccade closer to the wall when flying towards the odour source and further from it when flying away. The fly does not require visual 'landmarks' to associate with the odour, as localisation is successful in a homogeneous vertically striped arena. Rather, the authors suggest that it requires vertical contrasts to provide cues about its own motion in the horizontal plane.

'Tethered-flight' experiments offer a complementary approach to studying the interplay of vision and olfaction in *Drosophila*. In this paradigm, a fly is held by means of a rod glued to its dorsal thorax and put in a drum lined with LEDs that can be configured to show arbitrary moving patterns. Flies held in such a way will spontaneously beat their wings for prolonged periods despite receiving neither the visual nor mechanosensory cues associated with flight. Their behaviour can be measured either by analysing wingbeat statistics or directly measuring the torque it produces. This behaviour can optionally be used to control the presentation of the visual stimulus in a closed-loop manner, e.g. if the fly attempts to turn right the visual scene rotates to the left, simulating the visual feedback that would result if the animal was unrestrained.

Frye & Dickinson (2004) tether flies in this way and blow air over them from the front, periodically mixing food odour into the airstream. These bursts of odour were found to elicit increases in wingbeat amplitude and frequency, which would presumably correspond to an increase in forward thrust in an untethered animal. The flies were also challenged with lateral expanding visual patterns. These cause the wings to differ in beat amplitudes, corresponding to an evasive turning reflex (see section 2.2.3; Tammero & Dickinson, 2002b). Concurrent presentation of both stimuli results in a response very similar to the summation of responses to each one presented individually. The authors therefore argue that in this situation the two modalities not do substantially interact but rather are processed in parallel, even down to the level of the flight motor where they suggest that they modulate the activity of different muscle groups.

More recent tethered-flight studies have however identified interactions between the two modalities. Chow & Frye (2008) employ a closed-loop paradigm, with the fly's turning responses (estimated by means of wingbeat analysis) being used to control the yaw orientation of visual stimuli. The presentation of food odour increased the amplitude of responses to wide-field rotating stimuli (i.e. the optomotor response, see section 2.2.2), while weakening evasive turns evoked by wide-field expanding patterns (see section 2.2.3). No odour-dependent effects were observed when a small-field stimulus (i.e. a single vertical bar) was used (see section 2.2.5). For both rotating and expanding stimuli, a tighter correlation between visual input and behaviour was observed in the presence of odour, which the authors interpret as an increase in the saliency of visual motion.

Duistermars & Frye (2008) adopt a variant of the tethered-flight paradigm where the fly is attached to a pin held in a magnetic field, allowing it to rotate freely about its yaw axis. A precise odour delivery system ensures that the fly's head is only inside an artificial 'plume' of food scent for a narrow range of body orientations. They find that wide-field visual contrast enhances the fly's ability to stay inside the plume, but that a small field stimulus (a single vertical stripe) offset 90° from the plume does not. They conclude that small-field patterns are insufficient for odour tracking, but an alternative interpretation would be that attraction to the stripe (section 2.2.5) overrides plume-following behaviour.

Other groups have used tethered-flight experiments to investigate the issue of crossmodal learning. Guo & Guo (2005) train *Drosophila* to associate an aversive heat-shock stimulus with both a particular visual pattern and an odour. This bimodal training reduces the discrimination threshold for later unimodal memory retrieval. They also demonstrate 'memory transfer': if certain patterns and odours are repeatedly presented together (without punishment), then heat is associated with one, the fly will avoid the other.

Van Swinderen & Greenspan (2003) record local field potentials from the medial protocerebrum of tethered *Drosophila*. They discover an increase in power in the 20-30Hz band when a visual stimulus passes in front of the fly. When a puff of fruit odour is presented at the same time as the visual cue, this 20-30Hz response is selectively boosted in a non-linear fashion (i.e. compared to the response to each stimulus alone). A similar response is seen for aversive or novel stimuli, and coincides with the initiation of visual tracking, leading the authors to suggest that it represents a neural correlate of salience.

## 2.2: Visual behaviour

In this and the following two sections I shall discuss the visual system on its own, first drawing on evidence obtained from behavioural, then physiological (section 2.3) and modelling (section 2.4) studies. Though I shall focus as much as possible on *Drosophila*, I also consider data from larger flies (see section 1.4). Honeybees have also received much attention because of the impressive feats of vision-based navigation involved in their foraging behaviour. Though bees are somewhat distant relatives of fruit flies, and are generally considered to possess more advanced cognitive capabilities (Greenspan & van Swinderen, 2004), it is still helpful to draw comparisons between the species.

I shall focus almost exclusively on motion vision, because it is of particular relevance to the free-flight behaviour I intend to investigate. Furthermore, one might argue that the fly's visual system is heavily specialised for detecting motion. Each compound eye consists of only ~700 facets or *ommatidia* (fig 2.1) with which the whole visual hemisphere must be sampled, and each photoreceptor has a bell-shaped angular sensitivity function with a half-width of ~3.5° (Stavenga, 2003). Thus, the fly's ability to detect static patterns is limited. However, its eye has far superior temporal resolution than our own; the flicker fusion rate in the blowfly is >250Hz (Autrum, 1958).

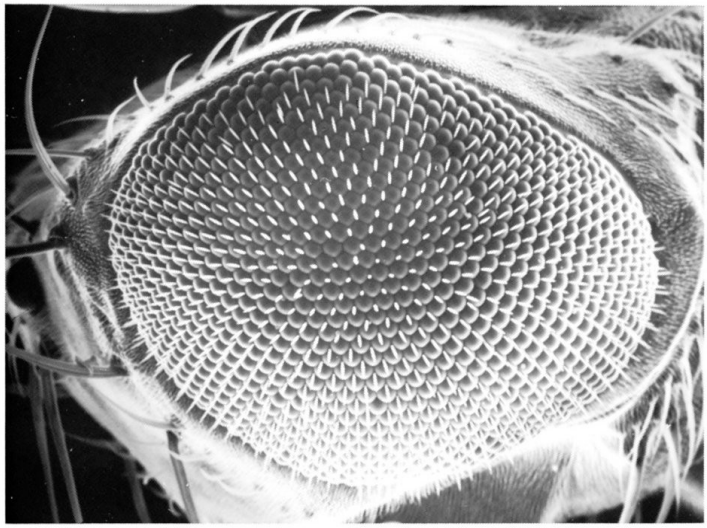

Figure 2.1: Scanning electron micrograph of a *Drosophila* compound eye. Each facet is a single ommatidium. Picture credit: T. Venkatesh.

### 2.2.1: Optic flow

Before discussing any experiments in detail, I shall briefly explain the concept of *optic flow*, which is central to understanding visuomotor behaviour. This refers to the characteristic patterns of image motion experienced by a moving agent, from which information about their movement can potentially be extracted (Gibson, 1950). Translation and rotation produce qualitatively different patterns, as illustrated in fig 2.2.

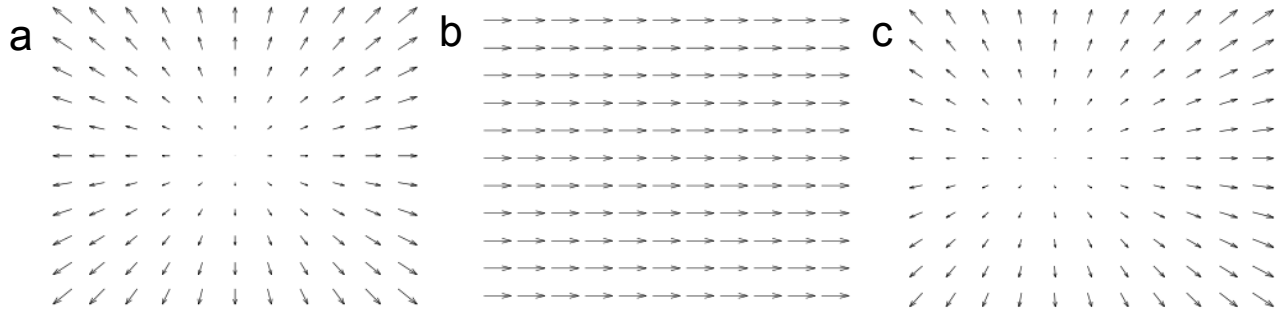


Figure 2.2: Example of optic flow fields. Arrow size denotes velocity of retinal motion. **a** A frontal expansion pattern corresponding to pure forward translation. **b** A pattern corresponding to pure leftward yaw rotation. **c** A field resulting from a combination of forward translation and a small amount of leftward rotation. The focus of expansion shifts to the left. Adapted from Higgins & Pant (2004), p422.

Rotational and translation flow differ in another important respect. The velocity of rotational flow is independent of the distance between viewer and object. In the case of translational flow, however, the velocity is inversely proportional to this distance. This phenomenon is well known to anyone who has looked out the window of a moving car and observed streetlights speeding past while distant mountains move imperceptibly slowly. Thus, translational flow encodes information about both one's own motion and the layout of the environment. While this could been seen as a confounding influence, many authors have argued that a proximity-weighted estimate of velocity is in fact ecologically useful (Gibson, 1950; Lee, 1976). For instance, the faster one is moving, the more clearance one wishes to give objects in order to avoid collisions (Kennedy, 1940; Franceschini et al, 2007).

### 2.2.2: The optomotor response

Seminal studies of the optomotor response (Hassenstein & Reichardt, 1956; Götz, 1964; Götz, 1968) represent the first attempts to rigorously characterise the relationship between visual stimulation and movement in insects. A tethered *Drosophila* was placed at the centre of a vertically-striped drum that was rotated about its vertical axis. The fly was found to produce a turning response in the same direction as the rotation, which is interpreted as a course stabilisation mechanism: the rotation of the entire visual surround suggests that some external force has perturbed the fly's yaw orientation, so it attempts to correct for this disturbance.

The magnitude of this turning response depends on the velocity of the drum rotation in a non-linear fashion: it increases up to a certain optimum velocity then deceases again, resulting in a bell-shaped profile. Interestingly, the optimal velocity changes as a function of the spatial frequency of the pattern, such that shorter wavelengths have a lower optimal velocity and longer ones higher.

However, if these curves are plotted as a function of temporal frequency (i.e. velocity x spatial frequency), then they are virtually identical for the different pattern wavelengths. It therefore appears that the system underlying the optomotor response is selective for the direction (left/right) of image motion, but does not accurately gauge its velocity.

It has been suggested that the direction of the 'retinal slip' caused by an external perturbation is all that is required for a feedback controller to successfully compensate, and that the attenuation of the response at high velocities may actually promote stability in such a controller (Warzecha & Egelhaaf, 1996). Evidence for a controller of this kind operating in free-flight is provided by experiments performed inside a rotating drum, as *Drosophila* fly in circles holding a constant position relative to patterns moving at up to $500°s^{-1}$ (Mronz & Lehmann, 2008).

The finding that the optomotor response depends on temporal frequency as opposed to velocity is the basis for the highly influential 'delay and correlate' elementary motion detector (EMD) model (Hassenstein & Reichardt, 1956; Reichardt, 1969), outlined in fig 2.3. It works by comparing the light intensity signal from one photoreceptor (B) with the delayed signal from an adjacent one (A). The signals will be more correlated when the image moves from A to B than when it is stationary or moving in the opposite direction. However, a single detector of this type will not be directionally selective, as it will respond to motion perpendicular to the line AB, and even to global changes in lighting. To resolve this issue, a second mirror-symmetrical detector is added taking input form the same pair of photoreceptors, and its output is subtracted from that of the first. Thus any directionally non-specific components of the response will be cancelled out.

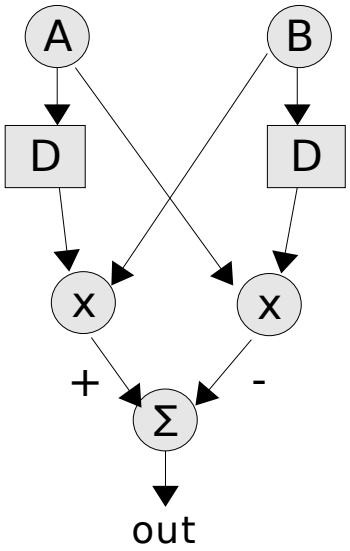


Figure 2.3: A 'delay and correlate' elementary motion detector (EMD). A and B are two adjacent photoreceptors. D denotes a delay operation. A first-order low pass filter (which introduces a phase lag) is most commonly used as this is more biologically plausible than either a pure delay or a higher-order filter. x is a multiplication operator, and Σ a summation. If the image is static or changes uniformly, both halves will cancel perfectly and the output will be zero. Movement to the right (A to B) will result in a positive response, and movement to the left a negative one. Adapted from Zanker et al (1999) p110.

The EMD model responds maximally to a certain temporal frequency rather than velocity, providing a good qualitative match to the data from the optomotor response experiments. However, one cannot conclude from these behavioural findings that a circuit like the EMD actually exists in the fly visual system, as there are so many stages of processing (optical, neural and mechanical) between the eye and the flight motor, any combination of which could give rise to the observed behaviour. In section 2.3.2 I review evidence for the EMD model from electrophysiological recordings of insect neurons.

### 2.2.3: Collision avoidance

There is strong evidence that the optomotor response as described above is not the only mechanism involved in *Drosophila* visual flight control. Tammero et al (2004) present moving stimuli confined to specific regions of a tethered fly's visual field. They find that in certain conditions, for instance when a rotating pattern is only shown in the rear hemisphere, the fly turns *against* the direction of image movement, the opposite of what the optomotor response model would predict. They introduce patterns where sections are moving in opposite directions, resulting in expansion and contraction poles in the image. From these experiments, they conclude that the fly's behaviour is best understood as an attempt to steer away from visual expansion, rather than to minimise retinal slip; response magnitudes are greater for expanding than rotating patterns, and flies are better able to stabilise their orientation relative to expansion than rotation patterns in closed-loop conditions. Since rapidly

expanding shapes are likely to represent objects moving towards the fly (or vice versa, see section 2.2.1), this behaviour would result in collision avoidance in an untethered animal.

The magnetic tether paradigm (section 2.1) allows flies to produce rapid yaw turns similar to the saccades observed in free flight. Bender & Dickinson (2006) challenge flies tethered in this way with various expanding patterns to determine what features trigger saccades. They find that these manoeuvres tend to be initiated when shapes reach a critical retinal size, regardless of the time course of expansion. This mirrors findings on the escape response of standing houseflies (Holmquist & Srinivasan, 1991). However, Bender & Dickinson (2006) point out that their results are consistent with expansion detection being based on the pooled responses of local motion detectors (i.e. EMDs), since highly textured shapes elicit saccades slightly sooner, while saccades away from shapes that only expand in one dimension are delayed.

The saccades themselves are found to be rather stereotyped manoeuvres, although their amplitude depends on the position of the looming shape relative to the fly, such that the fastest and largest turns occur in response to frontal expansion. However, the probability of initiating a saccade is lower for frontal than for lateral expansion. A previous study shows that *Drosophila* extend their legs in a stereotyped landing manoeuvre in response to frontal expansion (Tammero & Dickinson, 2002b), so it may be that flies frequently attempt to land on the visual object rather than avoid it in this situation. Similarly, houseflies exhibit landing reflexes when discs are moved frontally towards them. The timing of this response fits well with what one would predict if expansion were measured by spatial and temporal integration of the outputs of an ensemble of suitably arranged EMDs (Borst & Bahde, 1988).

Both the optomotor response and expansion-based collision avoidance are visual reflexes based on the detection of wide-field motion. It is therefore natural to ask to what extent they share common processing mechanisms. Duistermars et al (2007) compare the behavioural responses of tethered *Drosophila* to various rotating (i.e. optomotor) and expanding (collision avoidance) stimuli. They find that the temporal frequency tuning of the two systems is strikingly similar, suggesting that the same EMDs provide input to both. However, the spatial integration (see section 2.3.3.1), temporal dynamics and contrast sensitivity of the two responses differ, consistent with the existence of separate pathways beyond the stage of local motion detection.

It is difficult to relate expansion detection to free-flight studies, because it is unclear which features of the fly's visual input serve to trigger saccades or other evasive manoeuvres. Tammero & Dickinson

(2002a) attempt to address this issue by reconstructing the fly's visual experience, and using arrays of EMDs to calculate the magnitude of image expansion immediately preceding each saccade. The level was found to be similar across environments differing in textural properties, suggesting a simple threshold mechanism for triggering saccades.

However, I have some doubts about this analysis. Being unable to directly measure the fly's orientation, they assumed its head was aligned with its direction of movement at all times. This is in itself a reasonable approximation (and one that I make in this study), since side slip manoeuvres are rare in *Drosophila* (Mronz & Lehman, 2008; but see Fry et al (2003) and Ristroph et al (2009) for counterexamples). However, it means that the reconstructed optic flow patterns will always feature expansion poles in roughly frontal positions, since little rotation occurs during intersaccadic segments. In light of this, their decision to measure horizontal expansion using a filter centred at an azimuth of 45° (Tammero & Dickinson, 2002a; Fig. 11, p337) seems questionable.

### 2.2.4: Velocity sensitivity

Another way vision influences flight behaviour is by providing a means to regulate speed. Some clues about the properties of this mechanism come from experiments on honeybees. Bees were tracked flying along a corridor with vertical grating patterns on the walls. They maintain a straight path along the central axis of the tunnel even when the patterns on either side differ in spatial frequency or contrast. However, their lateral position is the corridor is perturbed if one or both of the patterns is moving. If the pattern moves in the direction of flight, thus reducing its apparent velocity, the bee will fly closer to that wall. Conversely, they will avoid a wall moving counter to their flight direction. In fact, the bee's lateral displacement is found to closely match the point at which both walls appear to be moving at the same velocity (Srinivasan et al, 1991).

The finding that bees fly centrally despite differences in pattern wavelength on either wall is interesting, as it indicates that they are extracting image velocity rather than temporal frequency. The EMD model discussed above cannot therefore account for this behaviour. This observation is further supported by experiments on honeybee foraging. A bee is trained to fly to a food source somewhere in a long, narrow tunnel. The food is then removed and the bee's searching behaviour is recorded; it tends to concentrate its search around where the food was positioned. If the wavelength of the grating patterns is altered between training and test sessions the bee still searches in the correct place, demonstrating that its 'odometer' is insensitive to the structure of the visual environment. However, horizontal grating patterns, which offer no horizontal movement cues, result in the bee searching uniformly over almost the whole extent of the tunnel (Srinivasan et al, 1997; Si et al, 2003).

*Drosophila* are not central-place foragers like honeybees, and thus have little need for an odometer. However, one may still ask whether they are capable of perceiving image velocity independently of spatial structure. Other than one experiment offering suggestive evidence that they could (David, 1982), little was known about this question until very recently. Fry et al (2009) subject flies to an innovative 'free-flight open loop' paradigm by tracking their flight in a wind tunnel in real-time and displaying patterns on the walls based on their movements, thereby achieving a level of control over the visual stimulation normally only possible in tethered experiments (Fry et al, 2008). They find that *Drosophila* can indeed estimate velocity independent of spatial frequency, and that their speed regulation system can be well approximated as a simple proportional controller subject to saturation for speeds above around $0.6ms^{-1}$.

It would be hasty to conclude that the EMD model is incorrect because it is unable to account for this observation. Rather, the question is what must be added to the basic EMD model to achieve this behaviour. Modelling studies have yielded some insights in this area (section 2.4.1). Another point to note is that a fixed wavelength pattern on a planar wall will generate a range of angular wavelengths from the fly's perspective, unlike the same pattern on a cylinder with the fly at its centre. Thus the properties of the stimulus itself could assist the fly in obtaining an unbiased estimate of its velocity. This could resolve the apparent paradox that the tethered flies of Duistermars et al's (2007) study exhibit temporal frequency tuning, while the free-flying animals in Fry et al's (2009) experiment exhibit velocity tuning.

### 2.2.5: Object fixation

Another visuomotor behaviour exhibited by the fly is object fixation. Walking (Horn & Wehner, 1975), tethered flying (Poggio & Reichardt, 1973; Duistermars & Frye, 2008) and free-flying (Frye et al, 2003; Maimon et al, 2008) flies will attempt to move towards a conspicuous feature of their visual environment. This feature may be (amongst other things) a dark stripe on a light background, a light stripe on a dark background, a dark target on a textured background, or a chance white patch in a random chequerboard pattern. Notably, this response appears to depend on motion detection; presenting a static bar to a tethered fly does not produce a turning response, but a bar with a fluctuating position does (Poggio & Reichardt, 1973).

*Drosophila*'s tendency for target tracking is sufficiently robust that a moving vertical stripe can be used to 'drag' magnetically tethered flies into a desired orientation (Duistermars & Frye, 2008). This response appears to depend on the shape of the target, as free-flying flies are attracted to a long

vertical pole but repelled by a much shorter object of the same thickness (Maimon et al, 2008). Both blowflies (Egelhaaf, 1987) and *Drosophila* (Duistermars et al, 2007) exhibit different frequency tuning for large- and small-field visual stimuli (i.e. grating patterns *versus* single vertical stripes), such that small-field responses peak at higher frequencies than large-field ones. This suggests that separate mechanisms are responsible for the two behaviours.

Some interesting effects are observed when the environment contains more than one feature. If two vertical stripes are <60° apart, *Drosophila* will fixate the midpoint between them, apparently treating them as a single feature. At higher separations, the fly's heading distribution becomes bimodal as it fixates one bar and then the other (Horn & Wehner, 1975). Schuster et al (2002) track the movements of walking *Drosophila* and use this to display 'virtual objects' on a bank of LEDs around the arena. They find that flies selectively fixate the object that appears to be closest, based on motion parallax cues, i.e. the speed at which the object traverses their retina during ego-motion.

## 2.3: Visual physiology

### 2.3.1: The fly visual system

I now turn my attention to attempts to peer inside the black box of the nervous system and uncover the mechanisms underlying the fly's visuomotor behaviours, so far as these are known. I shall begin by giving a brief overview of the anatomy of the *Drosophila* visual system, which is illustrated in fig 2.4. For reviews see Borst & Haag, (2002); Borst, (2009).

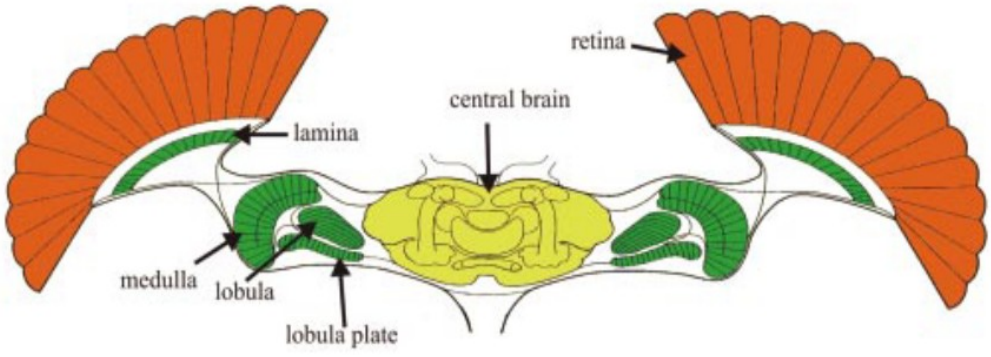


Figure 2.4: Schematic diagram of the Drosophila visual system. Taken from Borst & Haag (2002), p420.

Each eye consists of ~700 ommatidia, each containing a lens and eight photoreceptors. Together the eyes sample ~85% of the visual surround, with a small frontal band (~30° azimuth) that is seen by

both eyes (Heisenberg & Wolf, 1984; Krapp & Hengstenberg, 1996). *Drosophila* have a further three primitive single-lens eyes called *ocelli* on the top of their head (Hu et al, 1978). Photoreceptor axons project to part of the brain known as the visual ganglion, which is comprised of three neuropil layers: the lamina, medulla and lobula complex. These all exhibit a retinotopic arrangement of 'columns', each column being a stereotyped ensemble of neurons.

The lobula complex is divided into two parts: the lobula and lobula plate, which receive input from the medulla in parallel. The lobula plate contains several distinctive neurons with very large dendritic arbours, collectively known as lobula plate tangential cells (LPTCs). These have received considerable attention due to their size making them relatively easy to individually identify and record from, at least in larger flies. Some of the LPTCs make contact with descending neurons connecting the central brain to the thoracic ganglion, which is home to motoneurons innervating the muscles of the wings and halteres (Chan et al, 1998). (The halteres are tiny vestigial wings which provide no propulsion but beat in antiphase to the main wings and act as gyroscopes, measuring rotational velocity by sensing the Coriolis forces acting on them (Nalbach, 1994)).

### 2.3.2: Motion detection mechanisms

Little is known about the response characteristics of lamina and medulla neurons to visual stimuli, as their size makes them very difficult to record from, even in larger fly species. However, this procedure has been performed for a small subset of these cells, allowing parameters such as each one's degree of direction selectivity to be investigated (Douglass & Strausfeld, 1995; Douglass & Strausfeld, 1996). Based on these observations, a biologically feasible (though somewhat speculative) neural model of how a Reichardt EMD (section 2.2.2) could be implemented has been proposed (Higgins et al, 2004).

The LPTCs, with their wide receptive fields, integrate the responses of many local motion sensitive units. This makes it difficult to infer much about the properties of individual detectors from recordings of LPTC activity. Riehle & Franceschini (1984) overcome this problem by using sophisticated optical apparatus to present flashes of light to individual photoreceptors in a single ommatidium of the housefly eye while recording from the LPTC H1. Temporally offsetting flashes to adjacent photoreceptors in a manner mimicking preferred-direction motion of a visual object elicits excitatory responses in H1 corresponding to both the on- and offset of the motion stimulus. The reverse sequence has an inhibitory effect, which is found to be smaller in magnitude than the excitatory one, indicating an asymmetry in directional sensitivity.

By presenting a sinusoidal grating pattern though a narrow slit aligned perpendicular to the pattern gradient, Egelhaaf et al (1989) measured the integrated response of an ensemble of motion detectors receiving virtually identical stimuli, and thus inferred the behaviour of a single one. Using this technique, they found that the properties of the blowfly's motion detection mechanism closely match those of a Reichardt correlator. In particular, they conclude that the non-linear interaction between the input channels is very well approximated as a mathematical multiplication, as in the EMD model. However, the responses to forward and backward motion are not mirror-symmetrical, having different amplitudes and time courses. In addition, there was a positive response to 'flicker' stimuli that varied in intensity but did not move. These observations provide further evidence that the EMD is not perfectly balanced, i.e. one half-detector has a larger weighting than the other. As discussed in section 2.4.1, this may enhance the EMD's velocity sensitivity.

A conceptually similar but more technically sophisticated approach was taken by Single & Borst (1998), who used calcium imaging to measure the local membrane potential throughout the dendritic arbour of a blowfly LPTC, while presenting a moving sinusoidal grating stimulus. As predicted by the EMD model, they found a global de- or hyperpolarization (depending on the direction of the stimulus), overlaid with fluctuations matching the temporal frequency of the stimulus. The phase of these fluctuations varied with position in the lobula plate, and thus the position in visual space. They also found a small second harmonic in the response, which again suggests that the motion detectors are asymmetric. Haag et al (2004) also used calcium imaging to look for the hallmarks of Reichardt-type detectors in LPTCs, namely a pattern-dependent AC component superimposed on a DC signal that depends on temporal frequency rather than velocity. They conclude that the EMD model accurately predicts responses across a variety of different stimulus conditions.

### 2.3.3: The lobula plate tangential cells (LPTCs)

I shall now turn my attention to the LPTCs themselves. In the blowfly, these are a group of ~60 individually identifiable cells in each brain hemisphere. As we have seen, they respond to motion in a direction sensitive manner. The cells differ from each other in a number of ways (Borst & Haag, 2002):

- whether they respond primarily to horizontal or vertical motion
- their mode of signalling; these include non-spiking cells that encode information with graded membrane potential changes, fully spiking cells, and those that exhibit smooth membrane potential modulation with some superimposed spike-like depolarizations
- whether they project axons ipsi- or contralaterally
- whether they respond more to wide-field or small motion patterns; some cells' response increases

(though often saturates) as the retinal extent of the pattern increases, others have a diminishing response for patterns over a certain size.

In the following sections, I discuss some particular features of the information processing carried out by the LPTCs which are relevant to my investigations.

### 2.3.3.1 Dendritic integration

I mentioned above that some cells respond to patterns of increasing size with a monotonically increasing response, while others have peak sensitivity for small patterns. This raises the question of how the input from many local motion detectors is combined by LPTCs. I shall consider the wide-field class first, of which VS cells are examples. Fig 2.5 shows these cells' responses to patterns of increasing size. A saturation is evident, but note that the level at which the membrane potential plateaus varies with the velocity of the stimulus. This phenomenon has been termed *gain control*, and clearly cannot be due to a simple output saturation of the VS cell.

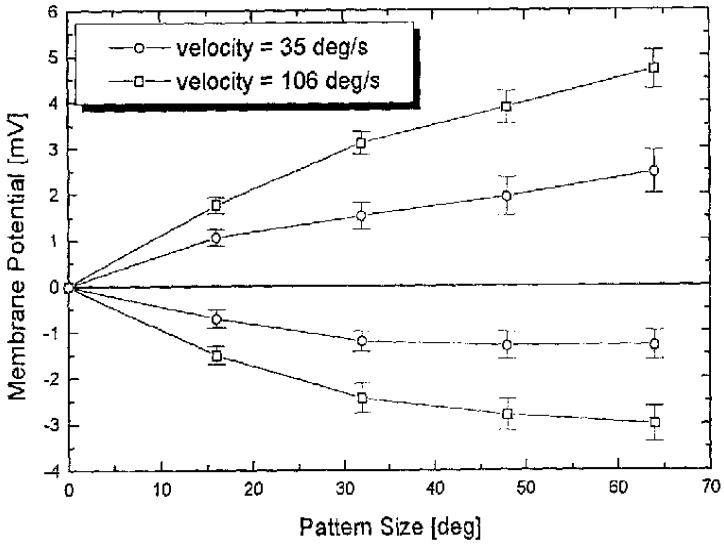


Figure 2.5: Responses of *Calliphora* VS cells to gratings of various sizes moving at differing velocities, both in the preferred and null directions. Taken from Borst et al (1995), p7.

An elegant explanation for this effect is provided by Borst et al (1995), who propose that each half of an EMD synapses directly onto an LPTC, with excitatory synapses in the case of preferred direction (PD) sensitive half and inhibitory for the anti-preferred direction. Recall that half-detectors are not fully direction selective; the anti-PD detector will still respond, albeit to a lesser extent, during PD motion. The dendrite potential will therefore be some intermediate value between the reversal potentials of the excitatory and inhibitory ions, weighted according to the relative activity of each polarity of detector. A constant-magnitude leak conductance also exists, with a reversal potential

equal to the resting potential. Thus, when small numbers of synapses are active the leak will have an appreciable effect, pulling the membrane potential towards resting. When many are active, corresponding to a large-field visual stimulus, the potential will be dominated by the excitatory/inhibitory ratio, creating the saturation effect described above.

This account is well supported by empirical evidence. Single et al (1997) block inhibitory input to the LPTCs using a GABA antagonist. Their observations are consistent with the model outlined above; most notably, they find that after blockade the responses to different stimulus velocities in the preferred direction are very similar.

Clearly, this mechanism cannot account for the properties of neurons such as the CI cells, which respond maximally to small patterns (fig 2.6). In this case it seems that a secondary 'pool cell' integrates inputs and inhibits the neuron in question (Reichardt et al, 1983). For instance, the small-field sensitive cell FD1 is inhibited by vCH, which displays wide-field sensitivity. Removing input from vCH, either by applying a GABA antagonist or photo-ablating the cell, abolishes FD1's small-field preference (Warzecha et al, 1993).

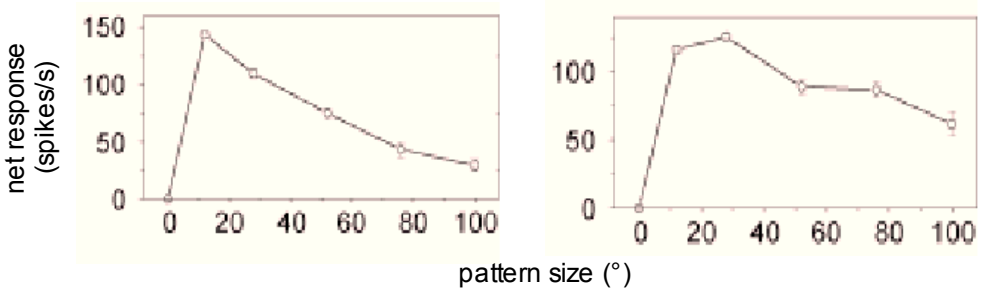


Figure 2.6: Responses of two different blowfly CI cells to moving stripe patterns. From Gauck & Borst (1999), p54.

### 2.3.3.2 What information do the LPTCs encode?

Though I have described LPTCs as being sensitive to either horizontal or vertical motion, many are in fact sensitive to different orientations of motion at different locations within their receptive field. By presenting a moving dot stimulus in a small (~10°) patch of visual space whilst recording from an LPTC, Krapp & Henstenberg (1996) ascertain its directional preference as well as its scalar sensitivity for motion in that region. Plotting this local motion sensitivity (LMS) data reveals some remarkably well-organised patterns (fig 2.7), which bear striking similarities to optic flow fields (section 2.2.1). The Hx cell shown in fig 2.7 appears to be tuned to translation in a nearly backwards direction, as it responds to image expansion in the caudal visual field and contraction in the frontal. Other LPTCs'

LMS fields lack this expansion/contraction pattern and thus seem tuned to detect self rotation; the VS cells for instance appear to detect rotations about various horizontal axes (Krapp et al, 1998).

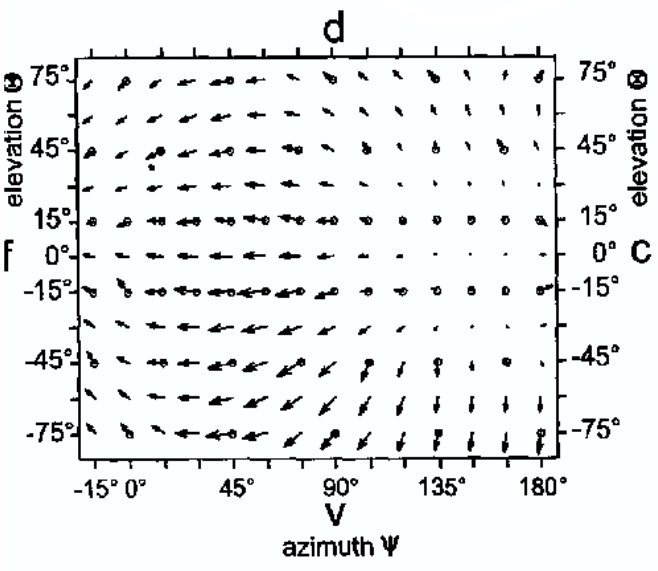


Figure 2.7: Local direction sensitivity of the Hx cell of the blowfly. Note the prominent singularity around (165°, 0°) from which all vectors radiate. Letters stand for dorsal, ventral, frontal and caudal. From Krapp & Hengstenberg (1996) p465.

Translation-sensitive cells tend to respond more to movement in the ventral part of the visual field, while rotation-sensitive ones are more sensitive dorsally (Krapp et al, 1998). Franz & Krapp (2000) show that this may in fact be optimal for a world where the ground tends to be closer than the sky. Recall that translational optic flow is proportional to proximity (section 2.2.1). The sky, being at a virtually infinite distance, provides rotation cues uncorrupted by translation, while the much closer ground offers the largest translation cues. It has also been argued that the arrangement of the ommatidial rows in the eye of the blowfly (which is not perfectly regular) may in fact be optimised to detect rotational flow patterns (Petrowitz et al, 2000). Taken together, these observations suggest that the fly visual system is highly specialised for extracting optic flow parameters.

Kern et al (2005; see also Boeddeker et al, 2005) record from the HSE cell while presenting visual patterns reconstructed from recorded outdoor flight paths. They find that it responds strongly to yaw rotation during saccades, but also to translation between saccades despite the image velocities involved being much smaller. They argue that this is possible because the two stimuli have different profiles in the frequency domain. The same procedure suggests a similar dual role for H1 during saccades and intersaccadic segments (van Hateren et al, 2005). It is suggested that the reason for flies' distinctive saccadic flight is to temporally separate translation and rotation cues, making each one

computationally more simple to decode.

Karmeier et al (2005) have looked in detail the information encoded by the VS cells. These 10 neurons are sensitive to rotation, with their axes ranging from azimuth ~80° (i.e. roughly equivalent to pitch), through 180° (roll) to ~240° (elevations are all ~0°). Performing a Bayesian analysis taking into account the noise present in the system, they show that these cells can accurately estimate the axis of rotation using a population coding scheme. Although it would be possible to do this using just two cells, having 10 allows integration times as short as 5ms to be used, which is clearly advantageous for flight control. Karmeier et al (2003) show that when VS1 is considered on its own, its tuning for rotation is actually coarser than one would expect based on local receptive field measurements. Additionally, it responds surprisingly strongly to vertical translation. They suggest that both of these effects are due to non-linear dendritic integration (see section 2.3.3.1).

The blowfly LPTC V1 also receives input from the ocelli, responding to patterns of illumination over these simple eyes that are consistent with the cell's directional sensitivity in the compound eye, i.e. rotation about an axis midway between pitch and roll (Parsons et al, 2006). This is thought to enhance the dynamic range of angular velocities to which it responds, as ocellar responses to visual motion exhibit a considerably higher velocity tuning than those from the compound eye (Hengstenberg, 1993).

Straw et al (2008) investigate the issue of contrast sensitivity in the HS cells of hoverflies. When presented with rotating sinusoidal gratings the responses depend strongly on the level of contrast, as the EMD model predicts. However, responses to natural scenes containing varying amounts of contrast are remarkably constant. It is unclear how this feat is achieved, but the observation once again demonstrates that the fly visual system is optimised to exploit properties of the natural world.

This section has drawn almost exclusively from data obtained from blowflies and other large dipterans. Because *Drosophila*'s small LPTCs traditionally evaded electrophysiological recording, one simply had to assume that their visual system functioned in a similar manner to those of their larger relatives. However, Joesch et al (2008) recently succeeded in recording from *Drosophila* VS cells. Happily, this assumption was vindicated, as the cells were found to have similar direction selectivity, spatial sensitivity, and velocity and contrast tuning properties to those of *Calliphora*.

#### 2.3.3.3 Connectivity in the LPTCs

I have given the impression that each LPTC's output is a non-linear summation of a population of

suitably positioned and oriented EMDs. Unfortunately, this picture is rather oversimplified. We have already seen that FD1 is inhibited by vCH. It turns out that vCH in turn (along with its sister dCH) does not receive direct input from EMDs, but rather 'piggybacks' the HS cells via dendro-dendritic electrical synapses. This has the effect of blurring the movement pattern, which may actually be desirable for enhancing motion contrast in order to perform figure-ground discrimination (Haag & Borst, 2002; Farrow et al, 2003).

In fact, connections between the LPTCs are too numerous to detail them all here. Adjacent VS cells have axo-axonal gap junctions which serve to spatially interpolate motion signals (Cuntz et al, 2007). Many LPTCs receive contralateral input, resulting in receptive fields spanning both eyes (Krapp et al, 2001). It even appears that recurrent loops exist, which may result in a winner-takes-all effect between the two hemispheres (Borst & Haag, 2002). These observations underline the difficulty of predicting the behaviour of any cell in isolation, and thus emphasise the importance of performing physiological experiments on intact animals, and using naturalistic stimuli wherever possible.

## 2.4: Visual modelling

### 2.4.1: Motion detection models

I have already discussed one model – the Reichardt EMD – in detail, as it is integral to our understanding of visual motion processing. However, I have detailed how it fails to account for invariances to pattern structure and contrast that insects exhibit in certain circumstances. This section describes some more sophisticated motion detection models that attempt to reproduce these abilities (see Srinivasan et al (1999b) for review).

Firstly, EMDs need not be fully symmetric; indeed, in section 2.3.2 I described evidence of directional asymmetry. The two halves of the circuit feeding into the summation step can be given different weights; in the most extreme case one could have a weighting of zero, giving a 'half-detector'. Although such a detector sacrifices directional selectivity (since signals unrelated to movement are no longer cancelled out), its optimum response velocity is found to be almost invariant with respect to pattern structure (Zanker et al, 1999).

Alternatively, an ensemble of symmetric EMDs tuned to different spatio-temporal frequencies could be used to produce a kind of population code for image velocity. This can be achieved by altering the angular separation of the input channels and/or the time constants of the low pass filters. A closely

related idea is that of using EMDs with more than two input channels, as these effectively have multiple spatial sampling intervals (Snippe & Koenderink, 1993). Experimentally, interactions between ommatidia separated by up to eight times the interommatidial angle have been found to contribute to LPTC responses in blowflies (Schuling et al, 1989).

Various adaptive processes have been identified in the fly visual system (e.g. contrast adaptation, motion adaptation) which are thought to maximise information transfer (Harris et al, 2000; Reisenman et al, 2003; Safran et al, 2007). Shoemaker et al (2005) add these features, along with various non-linearities including the gain control mechanism described in section 2.3.3.1, to a motion detection model with which they estimate the velocity of rotating natural scenes. The elaborations substantially reduce the model's sensitivity to textural properties of the stimuli, although these improvements are still unable to match the performance of a hoverfly HS cell.

A similar approach is taken by Lindemann et al (2005), who model the responses of a blowfly HSE cell to the reconstructed visual experience of an animal flying in a textured environment. While various elaborations to the peripheral processing stages yield slight increases in accuracy, the introduction of non-linear spatial pooling of motion signals on the LPTC (i.e. gain control) is found to offer the most significant improvement in performance. Hennig et al (2008) use a similar methodology to investigate the separate question of how selectivity for small-field motion is achieved in the FD cells (see section 2.3.3.1). They implement detailed models of various circuits by which suppression of large-field responses could occur, and find that presynaptic inhibition of the inputs to the FD cell is best able to account for the physiological data.

Rind & Bramwell (1996) describe a neural network model of collision detection closely based on the locust lobula giant motion detector (LGMD) cell. While this is less relevant to my investigation, it is noteworthy because it does not use any mechanism resembling an EMD. Instead, its response depends on a 'race' between feedforward excitatory connections and lateral inhibitory ones. This results in it responding specifically to accelerating and/or growing visual edges (corresponding to looming objects), as the real LGMD does.

### 2.4.2: Visuomotor models

The previous section described models of visual processing up to the level of the LPTCs. I shall now discuss models that allow visual stimuli to alter the behaviour of the agent, thus closing the loop between sensing and action. The difficulty of such an enterprise is illustrated by Lindemann et al's (2008) study which uses the blowfly HSE model described above to drive saccadic flight in a

simulated environment. While the model can be tuned to produce realistic behaviour in a particular visual setting, it is found to lack robustness with respect to variations in the textural properties of the environment. Reiser & Dickinson (2003) implement a robotic model closely based on *Drosophila* behaviour in the free-flight arena (Tammero & Dickinson, 2002a; Frye et al, 2003). This system achieves robust wall avoidance by detecting expansion, but lacks other visuomotor reflexes (e.g. the optomotor response) and is only investigated in a single visual environment. Similarly, while the LGMD model described in the previous section has been used to drive collision avoidance behaviour in mobile robots, this has not been related to locust behaviour in any detail (Blanchard et al, 2000; Yue & Rind, 2005).

Because of the difficulty of implementing a biologically realistic closed-loop visual controller, a more high-level approach to the problem has typically been adopted, taking cues from biology but not attempting to accurately reproduce the behaviour of any particular animal.

An early example of bio-inspired motion detection came in the form of Franceschini et al's (1986) electro-optic angular velocity sensor. This was based on single-ommatidium experiments on houseflies (Riehle & Franceschini, 1984; see section 2.3.2), but differs somewhat from the classical EMD specification, as it features a thresholding step which generates pulsed motion signals. Sensors of this type have been used to control a number of robotic systems, including a wheeled obstacle-avoiding vehicle (Franceschini et al, 1992), a hovercraft that negotiates a textured corridor environment (Serres et al, 2006), and a tethered miniature helicopter that modulates its thrust to control its altitude (Franceschini et al, 2007). The last study emphasises that the motion sensor's property of conflating velocity and proximity is computationally desirable, and could explain features of insect flight such as decreasing altitude in a headwind, or landing with a constant slope.

How exactly local motion signals should be spatially integrated to control behaviour is a question that has been addressed by modelling studies. Franz et al (1999) equip a wheeled robot with a camera and an array of EMDs. They use the statistical properties of its indoor environment to derive optimal matched filters for estimating forward translation and yaw rotation, and demonstrate that this results in a reliable odometer. In a similar vein, Neumann & Bülthoff (2002) describe experiments on a flying agent in a simulated outdoor environment. They break the problem of flight control into a number of parallel reactive processes:

- course stabilisation: compensating for yaw perturbations, i.e. the optomotor response
- obstacle avoidance by detecting differences in frontolateral image velocity, c.f. Srinivasan et al's (1991) centring response or Tammero & Dickinson's (2002a) collision avoidance

- altitude control by regulating ventral image velocity
- attitude control: adjusting pitch/roll to keep the sky in the dorsal visual field.

They learn optimal filters for these behaviours based on stimulus variance, using no prior knowledge about the environment. In both of the above studies, the learnt filters share features of the fly LPTCs such as greater sensitivity in the ventral field for translation, due to the proximity of the ground relative to the sky/ceiling.

Target fixation behaviour has also received considerable modelling interest. A high-level model of blowfly pursuit behaviour is described by Boeddeker & Egelhaaf (2003). Higgins & Pant (2004) demonstrate in simulation that a model based on the FD cells is able to detect and approach an object in a textured environment, though they suggest some elaborations to improve performance. Experiments on a wheeled robot suggest that target fixation and the optomotor response may be mediated (at least in part) by the same neural circuit (Huber et al, 1999). This model relies upon the assumption that front-to-back image motion generates a greater turning response than back-to-front motion of equal velocity, which is supported by the evidence for asymmetric EMDs.

A somewhat different approach to visuomotor modelling is to base one's model closely on a particular insect behaviour, but to implement a system with little regard for biological plausibility. For example, robotic models of both honeybee centring (Coombs & Roberts, 1992; see section 2.2.4), and landing behaviours (Chahl et al, 2004) have been implemented based on Srinivasan's (1994) image interpolation algorithm, which estimates velocity by analytically computing the deformation between successive image frames. Such an approach allows one to focus on the computational properties of a particular visuomotor system without being concerned with its algorithmic details, as insufficient data might exist to make modelling at this level of description feasible (Srinivasan et al, 1999a).

Other biorobotic modellers have focussed on the question of how fly-like visual computation can be performed using specialised analogue electronics. Systems of this type typically consume much less power than traditional serial architectures, and because local motion detection can be carried out in a parallel manner, can be much faster. Harrison & Koch (1999) implement Reichardt EMDs in analogue hardware and demonstrate that their system's responses to grating patterns exhibit many similarities to fly LPTCs. They go on to use the optical chip for optomotor control in a wheeled vehicle, showing that it is able to stabilise its course despite having an imposed steering bias. Similar work is presented by Liu & Usseglio-Viretta (2001) who achieve both optomotor stabilisation and fixation-like behaviour in a wheeled robot using an analogue hardware EMD implementation.

Finally, some researchers take inspiration from insect visuomotor control but are primarily interested in the challenge of engineering robust autonomous air vehicles, rather than investigating insect behaviour. An impressive example of work of this kind comes from Zufferey et al (2007), who describe a free-flying robot which weighs only 10g and avoids obstacles by comparing bilateral translational optic flow (Zufferey & Floreano, 2006).

## 2.5: Olfactory behaviour

I now turn my attention to the fly's sense of smell. This modality has been less thoroughly investigated than vision, and as a result I shall draw on findings from other species more heavily in this and the following sections. In addition, I shall focus more on experiments concerned with odour intensity than identity, as the latter is less relevant to the paradigm employed in the current study, where the composition of the attractant does not vary. Before describing any behavioural experiments, I shall briefly discuss some properties of odour diffusion in air that constrain the kinds of algorithms that animals can use to locate odour sources.

### 2.5.1: Odour plumes

Generally speaking, odours do not diffuse from a source to produce a smooth spherical gradient. This is because there are two main processes by which chemicals travel in air: molecular and turbulent diffusion. The former refers to the random movement of molecules, and results in smooth gradients. It is a small-scale and slow process. The latter is due to currents in the air deforming this gradient, resulting in highly heterogeneous distributions of odour. Although turbulence depends considerably on environmental conditions (e.g. the presence and strength of wind), it is typically the dominating factor in determining the structure of the odour plume outside the immediate vicinity (i.e. on the order of centimetres) of the source. Because turbulent diffusion is driven by movements of air, the diffusion pattern of a chemical does not depend on its molecular weight. This is useful, as it allows one to use tracer chemicals to visualise the diffusion of otherwise undetectable compounds.

The odour concentration at any point in a plume fluctuates considerably over time, with 'bursts' of odour being interspersed with periods of clear air. These bursts are on average weaker, longer in duration and have longer gaps between them further from the odour source. As one nears the source, this intermittency (quantified as the peak/mean ratio) decreases. Thus there are subtle spatiotemporal cues that an organism could use to locate the source of a plume. For a comprehensive review of plume

dynamics, see Murlis et al (1992).

### 2.5.2: Upwind odour localisation

The insect whose olfactory behaviour has received most attention is the moth. Male moths locate mates by means of a pheromone secreted by the female. The flight paths they follow have a characteristic structure of upwind forward 'surges' alternated with lateral crosswind 'casts', resulting in a zigzag trajectory. Interestingly, qualitatively similar paths are seen in the odour following behaviour of diverse species such as birds and lobsters (review in Vickers, 2000).

Vickers & Baker (1994) presented free-flying moths in a wind tunnel with pulses of sex pheromone. They find that each pulse would elicit a surge, so that by increasing the pulse frequency increasingly direct upwind flightpaths would be produced. If no odour was encountered for >0.3s, the moth would cast sideways. The intermittency of the odour stimulus is essential for plume following; moths do not maintain upwind flight in constant intensity, unbroken pheromone plumes (Willis & Baker, 1984).

Mosquitoes use olfaction to locate human hosts. They can use at least two different cues to do this: exhaled carbon dioxide and human skin odour. Geier et al (1999) find that intermittent $CO_2$ presentation elicits sustained upwind flight, as with moth pheromone following, whereas mosquitoes respond better to homogeneous clouds of skin odour. This finding demonstrates that different odour following algorithms can exist even within one species. Similar wind tunnel experiments were recently performed on *Drosophila* by Budick & Dickinson (2006). Flies surge upwind upon encountering food odour and initiate lateral casting manoeuvres when they lose contact with the plume, in a manner very similar to moths. However, unlike moths, flies are able to follow a homogeneous (i.e. non-turbulent) plume directly to its source.

Of particular relevance to the current study is Goyret et al's (2007) investigation of the visual and olfactory components of feeding behaviour of moths in a wind tunnel paradigm. Moths are more strongly attracted to an object that both looks and smells like a flower than to objects possessing just one of these attributes. Presenting an odourless flower and an odour source just 10cm apart significantly decreases attraction. However, temporal separation (e.g. brief exposure to odour prior to reaching the flower) has a less detrimental effect.

These studies prompt the question of how flying insects detect and follow the wind direction (*anemotaxis*). While mechanosensory information from the antennae play a role in this behaviour in *Drosophila* (Budick et al, 2007), purely mechanosensory cues cannot be used, as it is impossible to

distinguish between air movement due to wind and that due to egomotion. It appears that visual information is used as an external reference. Moving floor patterns disrupt the ability of moths (Kuenen & Baker, 1982) and flying beetles (Fadamiro et al, 1998) to locate an upwind odour source. It is hypothesised that the optomotor response is the mechanism underlying this ability, detecting drift due to wind and causing the fly to steer into it (Willis & Cardé, 1990).

### 2.5.3: Non-anemotactic odour localisation

The vast majority of work on odour localisation has adopted wind tunnel based paradigms. This is understandable, as in the natural environment wind is an important determinant of plume structure. The presence of wind can be seen to simplify the problem of plume following by providing a directional cue; the fly can simply fly upwind upon encountering odour and it will tend to move towards the source. However, the study that forms the basis for this one (Frye et al, 2003) took place in still air. It should be noted that small air currents (e.g. due to convection) are still likely to exist and thus the plume would have been to some extent filamentous, although unfortunately its structure was not characterised in the study.

Moths, like *Drosophila*, are able to locate odours in still air. When doing so, they still exhibit a temporally regular zigzag flight pattern, which is taken as evidence that turns are driven by some internal oscillator (Willis & Cardé, 1990). However, this finding is rather difficult to interpret as the plume structure is unknown.

Although a variety of well-established olfactory behaviour assays exist for *Drosophila* (see Devaud (2003) for review), these tend to be rather simple and artificial tests, such as T-mazes where the fly displays a preference for one odour over another by the path it takes at a junction. One exception is an experiment where a fly is tethered in total darkness and its yaw torque is continually measured to trace out a trajectory in imaginary space (assuming constant speed). In this space are zones which, if the fly enters, it is given an appetitive odour stimulus. The concentration of this odour increases the closer the fly is to the centre of the zone. In such conditions, the fly steers to spend disproportionate time inside the zones (Wolf & Heisenberg, 1991). This would seem to suggest that *Drosophila* can locate odours without visual input, but it is important to bear in mind that this is a very artificial situation, as no attempt is made to simulate the structure of an odour plume or the dynamics of free flight.

Borst & Heisenberg (1982) present different concentrations of odour to each antenna of a tethered *Drosophila* walking on a trackball. Flies were able to produce strong turning responses towards the

side with the higher concentration, and unilaterally antennectomized flies would always turn towards the intact side. While this demonstrates that flies can detect odour gradients across their antennae, it seems very unlikely that this mechanism alone could guide free-flight odour localisation. As discussed in section 2.5.1, instantaneous local concentrations in a plume are highly variable, and even if they were not, the antennae are so close together that the differences in concentration would be very small at any substantial distance from the source. The competence revealed by this study is presumably more appropriate for guiding a standing fly's feeding behaviour over a very short range.

This issue is addressed in a recent and elegant study of odour localisation in *Drosophila* larvae (Louis et al, 2007). Maggots are tracked moving across a substrate with a known distribution of food odour, and are found to exhibit *chemotaxis*, i.e. they turn preferentially in the direction of the odour gradient. Mutant larvae with only one functional olfactory receptor neuron (ORN, see section 2.6.1) still display this competence, indicating that it does not depend on bilateral comparisons of odour intensity. Instead, the authors believe that gradient estimation is achieved by the animals sampling olfactory input while sweeping their heads from side to side. Larvae with two functional ORNs – one on each side – exhibit stronger chemotaxis, but the authors argue that this can be attributed to an increase in signal-to-noise ratio rather than an ability to perform bilateral comparisons.

An example of how odour localisation can be achieved without any directional information comes from the nematode worm, which uses chemical cues to locate food. It appears to calculate the first temporal derivative of concentration. If this is positive the worm moves forwards; if it is negative it makes a tight turning manoeuvre (Ferrée & Lockery, 1999). In this way the animal's movement is biased to spend more time in regions of high odour intensity. This non-directional process is referred to as *chemokinesis*. In fact, a similar mechanism is employed by the bacterium *E. coli* (Berg & Brown, 1972). It should however be noted that at the scale over which these organisms move molecular diffusion dominates, resulting in considerably more benign chemical gradients than flying insects would typically encounter.

## 2.6: Olfactory physiology

### 2.6.1: The fly olfactory system

Adult *Drosophila* have two olfactory organs: the third antennal segment and the maxillary palp, which is a mouthpart. These both contain sensory hairs called *sensilla*, with ~500 in the antennal segment and ~60 in the maxillary palp. Each sensillum contains up to four olfactory receptor neurons (ORNs) (Carlson, 1996). These cells express odorant receptor (Or) molecules, which are thought to be

G-protein coupled receptors activated by the binding of atmospheric chemicals. *Drosophila* have a total of 62 different types of Or, and in most ORNs only a single type is expressed (Couto et al, 2005).

The ORNs project to the antennal lobe (AL), which is comprised of ~50 distinctive globular structures called *glomeruli*. There is an almost perfect one-to-one mapping between Or types and glomeruli. The glomeruli appear to have a topographic arrangement, with similar odorants (in terms of carbon chain length and aliphatic *versus* aromatic character) exciting nearby glomeruli (Couto et al, 2005). From the glomeruli, cells known as *projection neurons* (PNs) send axons to the lateral horn (LH) of the protocerebrum and the mushroom bodies (MBs). The MBs are heavily implicated in learning and memory, while the LH is thought to mediate more immediate responses to odours. The LH projects to areas also receiving visual and mechanosensory input (Tanaka et al, 2004). The whole olfactory system is summarised in fig 2.8.

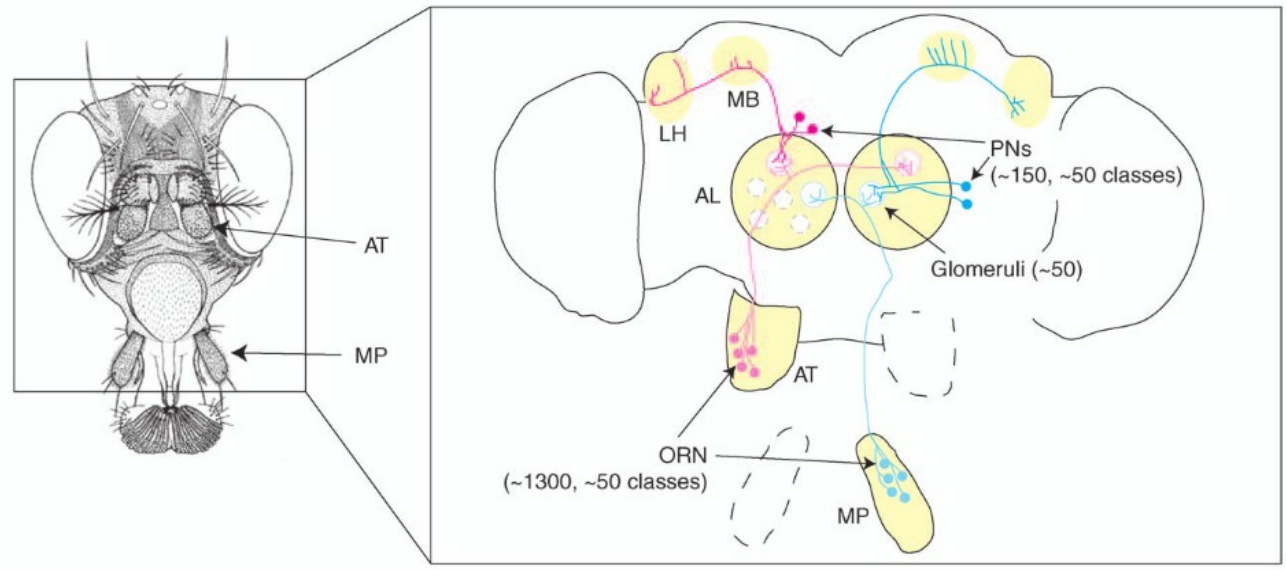


Figure 2.8: Schematic diagram of the *Drosophila* olfactory system. MP: maxillary palp, AT: third antennal segment, AL: antennal lobe, PNs: projection neurons, MB: mushroom bodies, LH: lateral horn. Taken from Komiyama & Luo (2006), p68.

## 2.6.2: Physiological studies

One can characterise the peripheral transduction of odour signals by means of an electroantennogram (EAG), which measures a field potential from a number of ORNs. The temporal dynamics of these cells are of particular relevance to odour localization as the odour signal experienced by the fly will fluctuate rapidly as it flies though the plume.

Once again, moths have traditionally been a popular organism in this area. Justus et al (2005)

compared moth EAG responses in turbulent pheromone plumes with measurements from a photoionization detector (PID), a device that gives high temporal resolution measurements of the concentration of organic compounds in the air. They calculated the coherence of the two signals in various frequency bands, and found that the antenna could be well modelled as a first order low-pass filter such that frequencies up to ~35Hz could be reliably resolved. (For comparison, the highest frequency humans can perceive is ~0.2Hz (Wang et al, 2002).) They also found that frequencies <1Hz were attenuated, which they suggest is due to adaptation in the ORNs. Similar findings were obtained by measuring EAG responses to artificially pulsed pheromone stimuli (Bau et al, 2002).

A recent study on *Drosophila* adopted a similar methodology and also concluded that antennal responses had a first order low-pass filtering characteristic, with time constants varying from 4.4 to 35.5ms (i.e. cut-off frequencies of 36 to 4.5Hz) depending on the odorant used (Schuckel et al, 2008). Single-ORN recordings also reveal marked differences in temporal resolution for different substances (Yao et al, 2005), presumably reflecting differing reaction dynamics between the various odorant molecules and receptors. This could of course serve a useful purpose in odour identity coding.

ORNs also display high-pass (i.e. adaptation) characteristics. Single unit recordings suggest some rather subtle adaptation takes place over a timescale of hundreds of milliseconds (Dobritsa et al, 2003; Yao et al, 2005). After one minute of exposure to a high concentration of a particular odorant, EAG responses to that chemical are virtually eliminated for at least 30s afterwards, and do not fully recover for more than six minutes (Störtkuhl et al, 1999). It thus seems likely that multiple homeostatic mechanisms exist, operating on timescales ranging from seconds to several minutes.

Vickers et al (2001) record simultaneously from the antenna and AL PNs of tethered moths in a turbulent pheromone plume. They found that the PN responses were tightly bound to the fine-scale structure of the plume, with both their instantaneous firing rates and number of spikes produced being strongly correlated with odour intensity as measured by the EAG. Experiments on *Drosophila* indicate that synapses in the AL between ORNs and PNs are very strong, but exhibit pronounced short-term depression (Kazama & Wilson, 2008). Lateral connections between glomeruli are primarily inhibitory, serving to sharpen the tuning curves of the PNs (Olsen & Wilson, 2008). Perhaps surprisingly, glomerular organisation of the PNs may not be a necessary precondition for odour localisation behaviour. Moths lacking proper glomeruli due to a lesion during development were able to fly upwind to a pheromone source with no obvious behavioural deficits compared to controls (Willis et al, 1995).

Stopfer et al (2003) address the question of how odour intensity is encoded in the AL of locusts. Unlike the ORNs, overall activity in the PNs does not change as a function of odour intensity. Different PNs respond to different concentrations of the same odorant, suggesting that identity and intensity could potentially be confounded. However, by analysing the activity of many PNs over time, they found that different odours were represented by distinct clusters in high-dimensional spatio-temporal activity space, within which intensity is represented in a relatively ordered fashion. Similarly, behavioural experiments on mutant *Drosophila* indicate that distinct ORNs respond to different concentrations of the same odorant (Kreher et al, 2008).

Moving further downstream in the olfactory system, a topographic representation of odour is maintained, with PNs from the same glomerulus projecting to the same localised regions of both the MBs and LH in *Drosophila* (Wong et al, 2002). Wang et al (2004) use calcium imaging to visualise the odour-evoked activity patterns across the MBs. They find evidence for a sparse coding scheme, with small numbers of neurons responding to any given odour. Some cells respond to a wide variety of concentrations of the same odorant, while others display a narrow tuning curve for intensity.

The functional roles of these higher brain centres are poorly understood. Curiously, blocking neurotransmission in the MBs (but leaving the LH unaffected) disrupts attraction to odours but does not affect olfactory repulsion behaviour in *Drosophila*, suggesting that different aspects of olfactory behaviour may be segregated (Wang et al, 2003). A presumed function of both regions is the integration of multimodal information. In the ventral nerve cord of the moth, axons projecting from the protocerebrum (which contains the LH) are found which respond in a directionally selective fashion to moving visual stimuli, but whose activity is modulated by the presence of pheromone (Olberg & Willis, 1990).

## 2.7: Olfactory modelling

A modelling approach was taken by Belanger & Arbas (1998) in an attempt to elucidate the algorithm underlying anemotactic odour localisation in moths. They simulated a wind tunnel containing a pheromone plume, and tested a number of systems-level models. In particular, they sought to differentiate between 'counterturning' behaviour, with regular zigzags whose angle was modulated by pheromone contact, and a surge-cast model as discussed in section 2.5.2. Their findings were inconclusive, with neither model achieving the success rate of real moths. The study did however provide some unexpected insights to the problem, such as the potential similarity in behaviour produced by different models, and the importance of odour detection latencies.

Similar experiments have been conducted in a wind tunnel using a gantry-mounted robot (named *Robo-Moth*) fitted with an ion detector (Rutkowski et al, 2004; Edwards et al, 2005). The robot is able to track the plume to its source in three dimensions. However, the robot has no visual or wind sensing capabilities. The problem is rather simplified as the robot knows the wind direction *a priori* and its movement is not affected the wind. Some of these issues are addressed by Pyk et al (2006), albeit in two dimensions. They combine a surge-cast olfactory algorithm with visual collision avoidance in a wheeled robot operating in a wind tunnel. Kuwana et al (1999) take a novel approach to modelling moth odour localisation by mounting freshly dissected antennae on a mobile robot and using EAGs as sensor inputs, though this work should perhaps be viewed more as a technical proof of concept rather than an attempt to faithfully reproduce insect behaviour.

*RoboLobster* is a wheeled robot that moves along the sea bed, mimicking the lobster's ability to track water-borne odour plumes (Grasso & Atema, 2002). In a manner reminiscent of the surge-cast model of moth chemotaxis, *RoboLobster* moves upstream on detecting odour and searches laterally on losing the odour signal. In both the animal and the robot, this behaviour can be carried out with a single antenna, but performance is improved by comparing concentration at the two antennae to guide casting behaviour.

Apart from the above examples, most odour sensing robot projects have tended to be motivated more by technological than biological goals. Hayes et al (2002) implement a wheeled wind-sensing robot that locates odours in a manner comparable to moths. However, anemotaxis is rather simper for a vehicle on a solid substrate than an airborne one. Odour localisation is, as I have discussed, more difficult in the absence of wind, as there are no directional cues and the effects of turbulence become more unpredictable. This latter problem is addressed in a robot presented by Lilienthal et al (2001), which moves at a fixed speed to introduce a constant airflow over its chemosensors and thereby locates odours in one dimension. A more impressive implementation comes from Lilienthal & Duckett (2003), who describe a robot which builds up a spatial map of odour intensity in a wind-free environment. By using repeated measurements to construct the map, the effects of temporal fluctuations due to turbulence are minimised.

## 2.8: Key points

The most popular paradigms for investigating insect sensorimotor behaviour are tethered-flight (both open- and closed-loop) and free-flight studies. Free-flight investigations of vision have typically taken

place in still air, while olfactory experiments have often used wind-tunnels. Because this study extends the work of Frye et al (2003) I shall adopt a still air, free-flight paradigm very similar to theirs. The merits of this approach are discussed in section 1.5.

It is essential that my modelling efforts are grounded as far as possible in reality. While this will partly be achieved by performing my own experiments to obtain detailed behavioural data (see section 1.7), many modelling decisions shall be based on the literature. Below is a list of experimental findings that I use to guide my model implementation. A discussion of details which are *not* included in the model, and the reasons why they are omitted, can be found in section 5.6.2.

**Vision**

- *Drosophila* eyes have low resolution, with an interommatidial angle of ~5° and a similarly wide acceptance angle for each ommatidium.
- Local motion detection is achieved using Reichardt elementary motion detectors (EMDs). While there is evidence that fly motion vision has some properties that this model cannot account for, the EMD is a well-studied model supported by considerable electrophysiological evidence, and as such represents a sound approximation for the computation performed in the fly optic lobe.
- Local EMD responses are pooled by cells with very large receptive fields (LPTCs), which respond to patterns of movement corresponding to translational or rotational optic flow.
- The optomotor response stabilises flight by producing smooth turns in the same direction as visual yaw rotation (i.e. presumed retinal slip).
- Saccades are initiated in response to visual expansion, though the details of this reflex remain unclear.
- Flight speed is regulated based on translational optic flow.

**Olfaction**

- Odour plumes have a complex, heterogeneous, dynamic structure.
- Peripheral olfactory processing has both low-pass and high-pass characteristics, corresponding to signalling dynamics and adaptive processes respectively.

# 3. Free flight experimental methodology

This chapter describes how I measure the behaviour of flies. First I discuss the configuration of the experimental arena (section 3.1), then the issues involved with rearing the experimental animals (section 3.2). I will then describe how I approached the problem of tracking a fly's movement (section 3.3). Once a fly's trajectory in three dimensions has been reconstructed (section 3.4) it must be analysed (e.g. to detect saccades), which is the subject of the final section (3.5).

## 3.1: Free-flight arena

As a main objective of this study was to extend the work of Frye et al (2003), I attempted to make my experimental arena as similar as possible to theirs. This dictated that it be a cylinder 1m in diameter and 60cm tall (fig 3.1). The walls were made from 2mm transparent acrylic. Due to the difficulty and expense associated with having a cylinder of this size manufactured, the arena walls consisted of two 180x60cm sheets bent into a circle and bolted together at the top and bottom. The arena walls were lined with one of a number of 'wallpapers', made from white paper with opaque black card shapes glued to it. Clearly, the bolts would provide a potentially undesired visual cue, so to conceal them a constraint was introduced that all wallpaper patterns (see below) must have black bands running along the top and bottom 3cm.

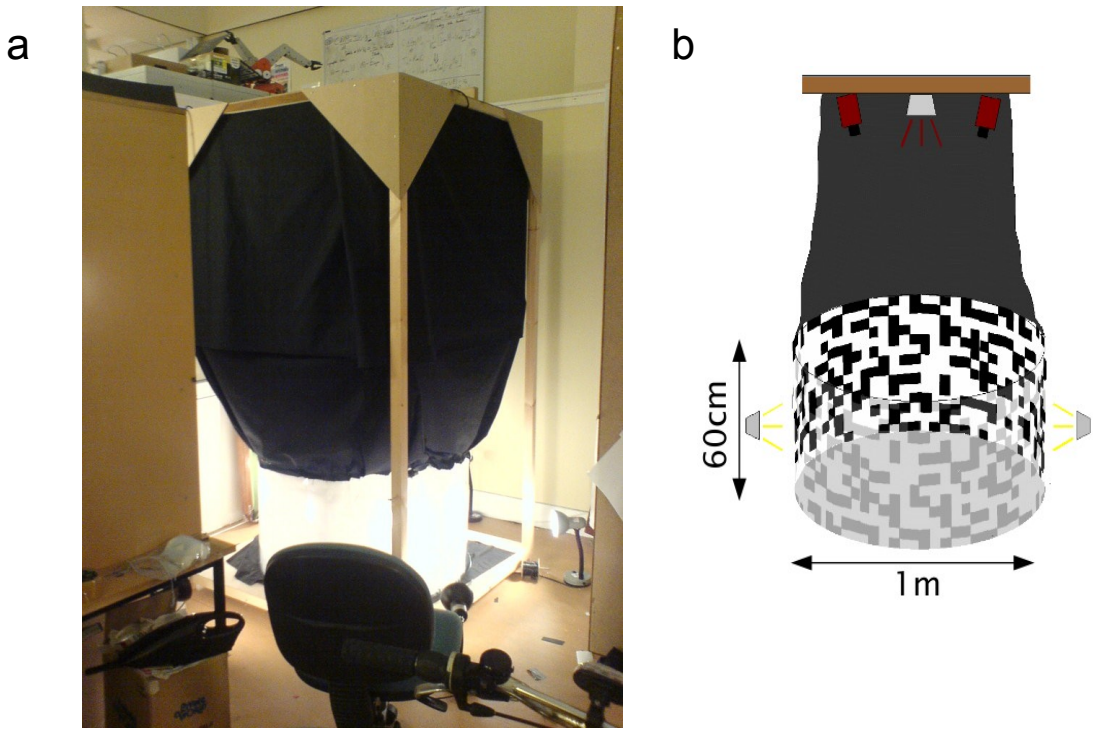


Figure 3.1: **a** Photograph of experimental arena. **b** Schematic representation.

In order to track the fly, two cameras were mounted on the ceiling of the experimental chamber, approximately 1.65m above the arena floor, diametrically opposed at a distance of about 35cm from the central position. Blackout curtains extended from the top edge of the arena wall (where their fixture was concealed by the black band) to the ceiling. This served to prevent flies from escaping whilst providing minimal visual stimuli. The ceiling itself was lined with the same black material, and the camera mounts were wrapped in the material to conceal them as far as possible.

The arena was illuminated from the outside by a ring of six evenly spaced 60W incandescent lamps. I found that the light provided by the lamps around the arena was insufficient for tracking (see section 3.3), so a 300W theatrical floodlight was suspended from the centre of the ceiling. A filter consisting of three layers of 'Congo Blue' filter and two 'Primary Red' was put over the lamp. This meant that virtually no visible light would escape, but infra-red light (detectable by the cameras, but not flies or - of course - humans) would be transmitted. The lamp itself was painted black.

The arena floor was also lined with black material. There were three holes in the floor, positioned 25cm from the centre of the arena, 120° apart (fig 3.2). These holes accommodated small (1ml capacity) vials that contained either water or vinegar depending on the experiment. The vials were painted black and positioned within the floor in order to minimise their visibility.

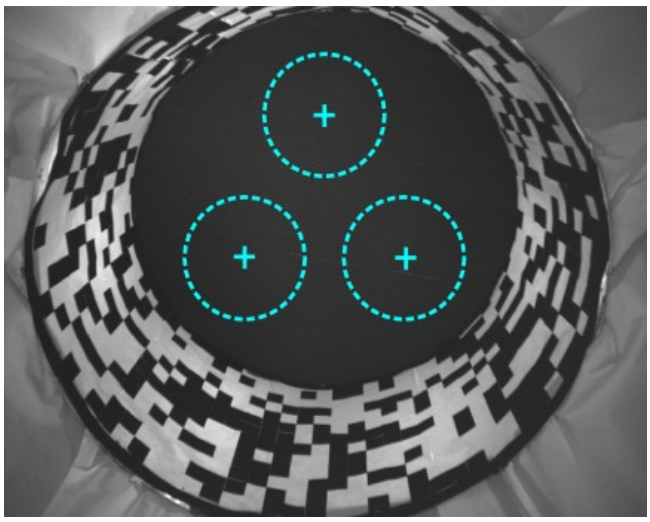

Figure 3.2: A image taken from one of the two tracking cameras. The positions of the vials and the extent of the zones used to quantify odour localisation behaviour are indicated. The curtain around the arena is black, but reflects near IR light to which the camera is sensitive. The floor absorbs both visible and IR light.

Flies are easier to detect against a white background than a black one (see section 3.3.3.1). As the arena floor makes up the lion's share of the image, a white floor was initially trialled. This approach was abandoned for the following reasons:

- The floodlight caused the fly to cast a fairly distinct shadow on the floor, which would often be tracked instead of the fly itself, resulting in erroneous traces.
- It was more difficult to conceal the vials in a white floor.
- Frye et al (2003) use a black floor, so changing this element of the experimental paradigm would make it more difficult to draw comparisons between their study and my own.
- Based on observations by eye, it seemed that the flies were less disposed to make long flights when the floor was white. Blowflies exhibit a reflex known as the *dorsal light response*, whereby they attempt to roll in order to keep the brightest region of their visual field at the top (Schuppe & Hengstenberg, 1993). Thus, the ground being brighter than the 'sky' may cause problems for flies' flight stabilisation mechanisms.

For the purposes of camera calibration (see section 3.4.1), eight LEDs were mounted on the wall: four evenly spaced around the top edge and four around the bottom edge. These LEDs were off during flight experiments.

My experimental arena closely matches that described by Frye et al (2003). The main differences are the presence of the IR floodlight (they provided additional illumination using a ring of IR LEDs

around the top edge of the arena), and the existence of three slots for odourant/water vials in the floor, as opposed to just one.

## 3.2: Animals

Behavioural experiments are notoriously difficult due to the variability of animals' actions. While variability can be overcome by large numbers of replicates, it is generally advisable to take whatever steps one can to control biological variables in order to obtain clean data.

I tried a number of different wildtype *Drosophila* strains. Oregon-R flies were abandoned early on, as they had a tendency to land quickly rather than fly for prolonged periods. Canton-S flies would fly adequately, but displayed very weak odour localisation performance. This strain had been laboratory-bred for many hundreds of generations, so it may be the case that the lack of selection pressure for foraging ability weakened their competence. Finally, so-called 'Super Flies', the same wildtype strain used by Frye et al (2003), were obtained. These animals exhibited better odour localisation performance, so were used for all experiments.

Although it is claimed that no behavioural sexual dimorphism exists in the free-flight odour localisation paradigm (Frye et al, 2003), I chose to use only one sex to eliminate this potential source of variability. I selected females because they are slightly larger and thus easier to track. When the flies eclose, females are collected and put in fresh vials, with no more than six flies to a vial. After two days, they are transferred to a vial containing only moistened cotton wool but no food, and some males are introduced. This is to ensure that all females are mated, as the sexual experience of a female fly can have a profound effect on its behaviour, at least in courtship situations (Xue & Noll, 2000).

Flies were fed with standard cornmeal food and reared at 20°C in an incubator with a 12/12hr light/dark cycle. To breed experiment-ready flies, I would put five females and three males in a vial for four days. The adults are then removed, leaving eggs and larvae. Once these reach adulthood they are collected. This procedure ensures that food competition is low (due to the small population), improving the likelihood of the flies being healthy.

Prior to experiments, flies are starved overnight (approximately 19hr). This is to ensure motivation for locating the food odour, but obviously must also be done before no-odour experiments for consistency. Experiments begin three hours after the flies' artificial dawn. As circadian rhythms have

pronounced effects on flies' activity (Sarov-Blat et al, 2000; see Chang (2006) for review), I confine experiments to a three-hour window each day. Even within this period, evidence of circadian effects is seen. For instance, intersaccadic velocity (section 3.5.3) is correlated with time of day ($\rho(42)=.354$, $p=.022$, see fig 3.3).

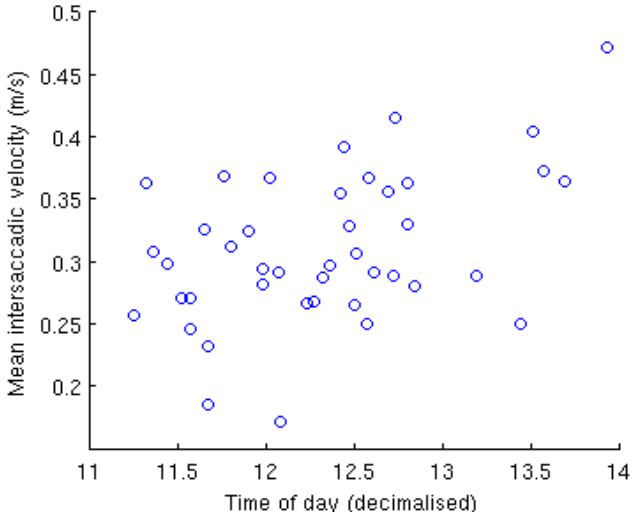


Figure 3.3.: Flightspeed *versus* time of day (24hr clock). Data is taken from the single landmark arena with no odour present, recorded over five days.

## 3.3: Video tracking

### 3.3.1: Hardware constraints

Automatically tracking flying *Drosophila* in a volume as large as my arena is a technically challenging problem. In a nutshell, the problem is that fruit flies are small and fast, and cameras with both high resolution *and* high framerates are very expensive. The cameras I chose (Marlin F131B, Allied Vision Technologies) represented what I considered to be the best compromise of resolution and framerate within the constraints of my budget. These are monochrome cameras that transmit data via a FireWire bus. They have a maximum resolution of 1280x1024 pixels, and can operate at arbitrarily high framerates, subject to limitations of bandwidth and shutter timing (see below). In the following paragraphs, I shall discuss in more detail the issues involved in obtaining suitable spatial and temporal resolution.

#### 3.3.1.1 Resolution

As the area to be imaged is circular, we are limited in resolution by the shorter dimension of the camera image, i.e. the height (1024 pixels). At the top edge of the arena, this means that each pixel represents just under 1mm. Due to perspective, at floor level each pixel corresponds to 1.53mm. A typical *Drosophila* female has a body length of around 3mm and a wingspan of ~4mm. A flying fly may therefore occupy as few as four pixels in the worst case. Given that images will be affected by phenomena such as sensor noise and motion blur (see below), the system needs to operate very close to the limits of tracking feasibility. Clearly, estimating the orientation of the fly's body is out of the question.

#### 3.3.1.2 Framerate

Naturally, high framerates are desirable because they provide richer behavioural data. There are a number of less obvious benefits that a high framerate also confers. Firstly, shorter exposure times mean less motion blur in each frame. This is a serious issue, since a typical flightspeed is $0.3ms^{-1}$, meaning that a fly takes only 10ms to move a whole body-length. Second, the shorter the interval between the capture of frames, the easier it is to track the fly, as it cannot move far between one frame and the next. Thus, although more frames per second must be processed, the processing may be simpler at a higher framerate. Third, high temporal resolution means that occasional skipped frames due to tracking errors are a less serious concern, as it will be more reasonable to interpolate data from the neighbouring frames.

As mentioned above, the two factors limiting framerate are exposure time and bandwidth. I shall discuss these issues in turn.

#### 3.3.1.3 Exposure time

The exposure time imposes an upper limit on the framerate: if we require the shutter to open for 25ms, clearly the maximum framerate is 40fps. Of course, the true framerate will be considerably lower as reading data from the CCD (charge-coupled device) takes some time. Short exposure times mean dim images, as fewer photons reach the sensor each frame. While it is straightforward to increase the cameras' gain to ensure that the full 8-bit intensity range is being properly utilised, this inevitably results in a poorer signal-to-noise ratio (SNR) as the effects of quantum noise are magnified.

The only way to circumvent this problem is to allow more light to reach the sensor. One way of doing

so is increasing the lens aperture, but this has the undesirable effect of decreasing the focal depth. As I need to image flies over a wide range of distances, focal depth must be maximised. Having said this, it is more important to have sharp focus at the floor level (where the targets are smallest) than high in the arena, so the focal length is adjusted accordingly.

Another solution to this problem is simply to use more illumination. My options in this respect were limited because: a) I wished to keep the level of ambient lighting similar to that in Frye et al's (2003) experiments (15 lux) and b) lights inside the arena would disrupt the experiment by adding unwanted visual features. I overcame these problems by using infrared illumination. In common with virtually all digital cameras, the CCD used in the Marlin F131B has some sensitivity in the IR range (half-maximal at 840nm; quarter-maximal at 920nm). Normally, a cut filter is used to prevent this light from reaching the sensor. I simply removed the filters to allow the cameras to 'see' both visible and near-IR light. As mentioned in section 3.1, a suitable IR source is obtained by fitting a wide-angle stage floodlight with a combination of filter gels that block out all visible light.

#### 3.3.1.4 Bandwidth

The Marlin has no internal memory on which to record footage, so all data must be streamed over a FireWire (IEEE 1394) connection to a computer for recording or processing. This imposes another serious limitation on the system's performance. The FireWire protocol has a maximum transfer speed of 400Mbit/s. If we specify a frame to be 1024x1024 pixels with 8 bits per pixel, this corresponds to 8.39Mbit. Since there are two cameras, this means the theoretical maximum framerate is 400/(8.39*2) = 23.8fps. Preliminary tests indicated that this was too slow, for the reasons discussed above.

Fortunately, the Marlin has the useful facility that one can specify an arbitrarily sized and positioned region of interest (ROI) within the frame and only read data from this area. Ignoring portions of the image allows one to achieve much higher framerates without any loss in resolution. The obvious drawback is that the fly must now be tracked in real-time, as it is no longer possible to record footage of the whole arena and analyse it offline. Clearly, this places some limitations on the computational complexity of the tracking algorithm (see section 3.3.2).

In testing prototype tracking systems, a further constraint on framerate became apparent. The overall brightness of the image was found to fluctuate considerably between frames, and I ascertained that this was due to flickering of the arena lights at 50Hz, the frequency of a.c. mains electricity in the UK. This flickering was problematic for the tracking algorithm. While it may have been possible to programatically compensate for this phenomenon, it could be eliminated by simply running the

cameras at exactly 50fps (or 25, 12.5, etc.). As this framerate was suitable for my purposes, I adopted it.

### 3.3.2: Tracking algorithm

My tracking system treats the two image streams coming from each camera independently. Therefore, in this section I shall discuss the problem of monocular tracking in a 2D image. Integrating data from two viewpoints to produce a 3D trace is the subject of section 3.4.

Background subtraction is a very popular approach to object tracking. In essence, an image of the empty arena ('background') is stored and each frame of footage is compared to this on a pixel-by-pixel basis. If a suitably large group of adjacent pixels differ from their counterparts in the background image, this is assumed to represent a target object. However, this approach can be rather brittle. If the image changes gradually, e.g. due to shifting levels of ambient lighting, false positive pixels will become increasingly common, degrading the tracker's performance. Furthermore, any noise in the background image could generate persistent spurious targets. These issues can be resolved by using adaptive background subtraction, where the background image is a continually updated average of a number of frames. Although the presence of the target will contaminate the background image, as long as it is moving it will have little effect on the stored scene as each frame only makes a small change to the average values (Balch et al, 2001). This approach has the benefit that the arena need not be empty at the start of recording.

My tracking algorithm initialises by taking twelve frames of the whole arena (1280x1024) to produce the background image. From then onwards, it can be in one of two states at any time: *acquiring* or *tracking* (fig. 3.4). Regardless of which state it is in, every 25th frame is used to update the portion of the background image corresponding to the current ROI. The update is weighted such that the time constant of this adaptation is 7.49 updates, or 3.74s assuming the tracker is running at full speed (section 3.3.1.2).

The algorithm begins in *acquire* mode, the details of which are sketched in box 3.1. The ROI (which is a square of size 624 pixels, see section 3.3.3.2) is positioned centrally, and incoming frames are subtracted from the appropriate portion of the background image. The resulting difference image is thresholded (see section 3.3.3.1) to produce a binary image of 'hits'. The program then finds connected regions of hits ('blobs'). If the largest blob is of roughly the right size to be a fly (i.e. big enough that we can be confident it does not merely represent noise, but small enough that it is not an obvious error), the program enters *track* mode.

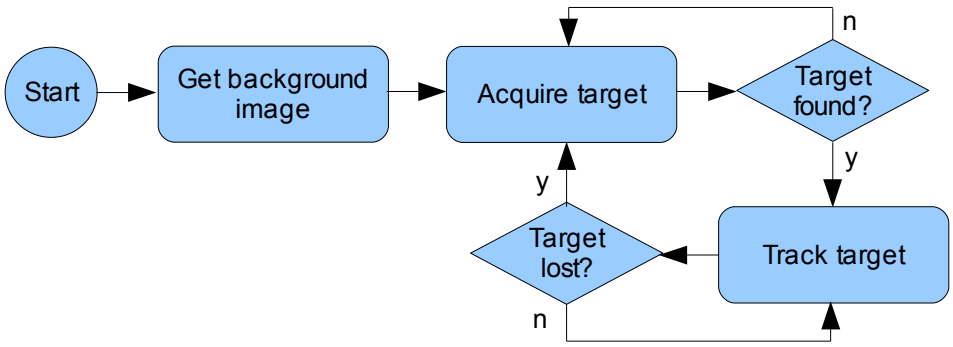


Figure 3.4: State transition diagram of the algorithm running for each camera.

```
Acquire():
    while not targetFound:
        currentImage = camera.getImage(ROI)
        differenceImage = background – currentImage
        hits = differenceImage.threshold()
        biggestBlob = hits.findLargestConnectedRegion()
        blobSize = biggestBlob.pixelCount()
        if minSize < blobSize < maxSize
            targetFound = true
    track(biggestBlob.getCentreOfMass())
```

Box 3.1: Pseudocode outline of the *acquire* algorithm.

When the program is in *track* mode, it has an estimate of the fly's recent position and can therefore perform a much more targeted search. The algorithm is outlined in box 3.2. The fly's future position is predicted by linearly extrapolating its recent movement, and only a small window around that location is searched. If the program fails to find the fly, the search window increases in size for the subsequent frame. If the search window reaches the edge of the camera ROI, this is repositioned such that the fly's predicted position is in the centre. If the tracker is unable to locate the fly for several consecutive frames, it is considered lost and the program reverts to *acquire* mode.

```
Track(flyPosition):
    camera.moveROI(flyPosition)
    searchWindowSize = large
    while lockedOn:
        currentImage = camera.getImage(ROI)
        currentImage.crop(flyPosition, searchWindowSize)
        differenceImage = background – currentImage
        hits = differenceImage.threshold()
        biggestBlob = hits.findLargestConnectedRegion()
        blobSize = biggestBlob.pixelCount()
        if minSize < blobSize < maxSize
            newFlyPosition = biggestBlob.getCentreOfMass()
            writeToFile(newFlyPosition, timestamp)
            flyVector = newFlyPosition – flyPosition
            searchWindowSize = small
            framesSinceLock = 0
            flyPosition = newFlyPosition
        else
            increase searchSize
            searchWindowSize = min(searchSize, ROI_Size)
            framesSinceLock++
            if framesSinceLock > timeOut
                lockedOn = false
        projectedFlyPosition = newFlyPosition + flyVector
        if not searchWindowFullyInsideROI
            camera.moveROI(projectedPosition)
            searchWindowSize = large
    acquire()
```

Box 3.2: Pseudocode outline of the *track* algorithm. Note that the search window size is always set *large* when after the ROI has been moved. This is because moving the ROI causes the camera to skip a few frames, so the fly's position becomes uncertain. A *small* search window is 25x25 pixels, a *large* one is 615x615 (i.e. almost the entire ROI), and the window grows by 12 pixels for each unsuccessful frame.

## 3.3.3: Optimisation

I have already discussed reasons why the experimental paradigm presents a particularly difficult tracking problem given the hardware available (section 3.3.1). It was therefore important to do all I could to optimise the tracker's performance. Unfortunately, it is difficult if not impossible to objectively compare different instances of the program, because there is no way of providing standardised test input. Instead, we must rely on the highly variable behaviour of flies for evaluation purposes. This section is therefore rather anecdotal in nature, and serves more to illustrate some of the issues involved in fine-tuning the system, rather than conclusively demonstrating the optimality of a particular implementation.

There are two key trade-offs involved in choosing an implementation. The first is accuracy *versus* efficiency. The complexity of the tracking algorithm is constrained by the fact that it must be able to reliably process 100 images per second (50fps from two cameras). Thus, while sophisticated probabilistic methods exist for target tracking, e.g. Kalman filtering (Walther et al, 2004), the computational requirements of such approaches make them unsuitable for my requirements. A closely related issue is that of robustness. If the camera sends a corrupted frame (a not infrequent occurrence), it is better that the system quickly detects this and discards the image, rather than attempting to analyse it.

The other type of trade-off that I must deal with is the likelihood of false positives *versus* false negatives. The system should be as sensitive as possible, but must be able to distinguish between a fly and noise. This issue is particularly important because the tracker uses the results of previous frames to direct its future search, so a single frame tracking error could have serious consequences. The thresholding procedure used to find hit pixels explicitly attempts to maintain this equilibrium, as I discuss in the following section.

### 3.3.3.1 Adaptive thresholding

Hit pixels are those that differ substantially between the current and background images, and thus could potentially represent the target. Of course, the threshold for considering differences 'substantial' will greatly influence performance. However, a single threshold value may not be suitable for all occasions. Consider, for instance, trying to track a fly high in the arena, where it will appear large, brightly lit (due to its proximity to the floodlight) and out of focus, *versus* a small, sharp, dimly illuminated fly near the floor. For this reason, I decided to allow the system to adjust its threshold at runtime. The mechanism by which it does this is shown in box 3.3. Notice that it is biased

towards raising the threshold in *acquire* mode and lowering it in *track* mode. This reflects the idea that we want to wait for a clear sighting of the target before entering *track* mode, but once we are tracking we require higher sensitivity because the search is already tightly localised.

```
hitProportion = hitCount / pixelsSearched
if mode == acquire:
        if hitProportion == 0:
                threshold--
        else if hitProportion > 0.07%:
                threshold++
if mode == track:
        if hitProportion < 0.5%:
                threshold--
        else:
                falseHitProportion = (hitCount – blobSize)/pixelsSearched
                if falseHitProportion > 1.7%:
                        threshold++
```

Box 3.3: Adaptive thresholding algorithm. *blobSize* is the size of the biggest blob, i.e. the target.

A simple way to reduce the frequency of false positive hits, thereby increasing accuracy, is to take into account the polarity of differences between the current and background images. The environment consists of very dark and very bright regions with few intermediate intensity values (fig 3.5). The fly typically appears dark against a white background and bright against a black one. It is thus possible to divide the image into ‘light’ and ‘dark’ pixels, and only accept as hits those pixels that differ in the appropriate direction for that region.

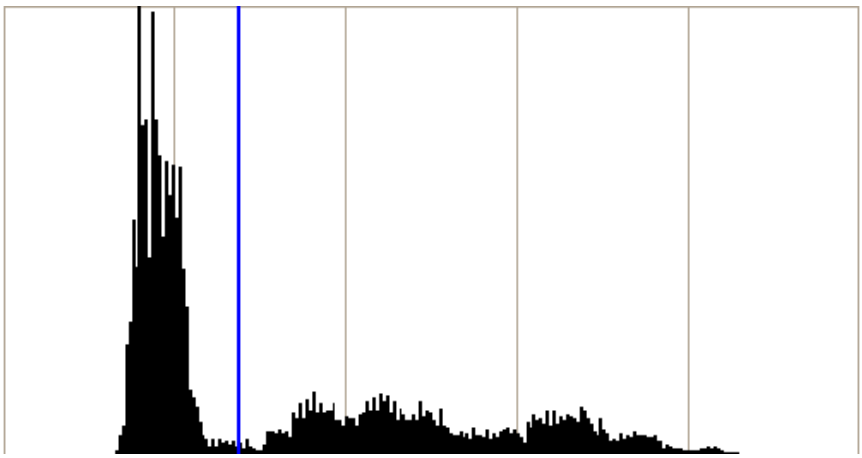

Figure 3.5.: Histogram of pixel intensity values, with the cut-off between 'light' and 'dark' marked.

A further refinement comes from the observation that the fly's average shade is closer to that of the dark regions than the light ones. It is desirable that the system has similar sensitivity to dark-on-light targets as light-on-dark, so that the adaptive thesholding mechanism does not need to compensate whenever the fly moves between backgrounds. This issue is addressed by making the threshold for light areas 33% greater than that for dark ones.

#### 3.3.3.2 Region of interest (ROI) size

A small ROI results in a shorter CCD readout time, offering the benefit that a longer exposure time can be used whilst keeping the framerate constant. However, a small ROI will need to be repositioned more frequently as the fly traverses the arena. To move the ROI, the camera's image capture must be briefly interrupted, resulting in the loss of typically three or four frames. Because the fly's movements during this period are unknown, a large area must be searched when the camera comes back online. Furthermore, the first frame following a ROI move appeared to have a heightened probability of being corrupted. Clearly, there are good reasons to strive to reduce the frequency of such events. A ROI size of 624x624 pixels was found to represent a suitable compromise between these issues, allowing an exposure time of 7.0ms.

#### 3.3.3.3 Minimum blob size

Another false positive *versus* false negative trade-off exists in deciding the minimum size at which a cluster of hit pixels ('blob') can be considered to represent the target. Generally, I found 3 pixels to be a suitable minimum, given that the adaptive thresholding mechanism (section 3.3.3.1) serves to keep the number of spurious hits at a constant low level. I added a couple of minor tweaks to this scheme to improve performance: in *acquire* mode, the biggest blob had to account for at least 3.3% of the hit

pixels in the frame, to prevent single noisy frames from producing erroneous target locks. Similarly, in *track* mode, if only one blob was found in the search window (meaning that the frame was particularly clean) a blob of only two pixels could be accepted as the target. This again reflects the intuition that false positives are more problematic when *acquiring*, while false negatives are of greater concern while *tracking*.

## 3.4: 3D reconstruction

The previous section described how each camera independently attempts to track the fly in the 2D image plane. In this section I discuss how these two asynchronous, incomplete trajectories from two perspectives are combined to produce a single 3D trace.

### 3.4.1: Geometry

A projection matrix *P* describes the transformation carried out by a camera's optics to convert a position *(x,y,z)* in space to a position *(u,v)* on the image plane (equation 3.1). Conversely, the projection matrix tells us, for any point on the image plane, the line in 3D space (which can be visualised as a ray coming out of the lens) to which it corresponds. Intersecting two such lines from different cameras allows one to pinpoint a unique 3D location.

$$\begin{bmatrix} u \\ v \\ 1 \end{bmatrix} = P \begin{bmatrix} x \\ y \\ z \\ 1 \end{bmatrix} \tag{3.1}$$

It is possible to define the projection matrix of a camera if its position, orientation, and various properties of its optics are known. However, a rather simpler and more robust method is to compute the matrix by identifying in the image a number of points whose 3D positions are known. For this purpose, eight LEDs are mounted on the arena walls, four at 0°, 90°, 180° and 270° positions at floor level, and four at 45°, 135°, 225° and 315° along the top edge of the wall (60cm above the floor).

The LEDs can easily be detected by switching them on while the arena lights and IR floodlight are off; simple thresholding then produces eight blobs. It is straightforward to automatically solve the correspondence problem (i.e. matching blobs to specific LEDs) since their approximate positions can be estimated *a priori*. This gives us matched pairs of points of the form $\{(u_i,v_i), (x_i,y_i,z_i)\}$, where i = 1...8. *P* is obtained by solving the set of simultaneous equations represented by the large matrix in

equation 3.2, and rearranging the coefficients as shown in equation 3.3.

$$\begin{bmatrix} x_1 & y_1 & z_1 & 1 & 0 & 0 & 0 & 0 & -u_1x_1 & -u_1y_1 & -u_1z_1 & -u_1 \\ 0 & 0 & 0 & 0 & x_1 & y_1 & z_1 & 1 & -v_1x_1 & -v_1y_1 & -v_1z_1 & -v_1 \\ & & & & & & & \vdots & & & & \\ x_8 & y_8 & z_8 & 1 & 0 & 0 & 0 & 0 & -u_8x_8 & -u_8y_8 & -u_8z_8 & -u_8 \\ 0 & 0 & 0 & 0 & x_8 & y_8 & z_8 & 1 & -v_8x_8 & -v_8y_8 & -v_8z_8 & -v_8 \end{bmatrix} \begin{bmatrix} m_{11} \\ m_{12} \\ \vdots \\ m_{34} \end{bmatrix} = 0 \tag{3.2}$$

$$P = \begin{bmatrix} m_{11} & m_{12} & m_{13} & m_{14} \\ m_{21} & m_{22} & m_{23} & m_{24} \\ m_{31} & m_{32} & m_{33} & m_{34} \end{bmatrix} \tag{3.3}$$

Notice that equation 3.2 is in fact overdetermined, and therefore may be impossible to solve exactly. This is because only six known points are required to uniquely specify a projection matrix. I chose to use more points to introduce redundancy and thereby reduce sensitivity to errors in the placement or detection of the markers. A least-squares method is used to find the optimal values for *P*.

The method outlined above assumes that projection is linear, which may not be the case. It is probable that the cameras' images are subject to some degree of radial distortion (fig 3.6), particularly as the lenses have fairly large angles of view. I quantified the magnitude of this effect by placing a straight edge on top of the arena wall (60cm from floor) forming a chord to the circle with its midpoint 10cm from the wall. Some concave distortion (fig 3.6b) is evident in the camera images; fitting a circle to the distorted line yields a radius of ~18,000 pixels. Assuming one pixel corresponds to one millimetre (section 3.3.1.1), a fly flying in a straight line at a typical speed of $0.3ms^{-1}$ would appear to have an angular velocity of approximately $1°s^{-1}$ due to radial distortion. This is more than an order of magnitude smaller than the typical intersaccadic angular velocities observed in flies (see section 4.3), so this effect can safely be ignored, especially since it will be be present across all experimental conditions.

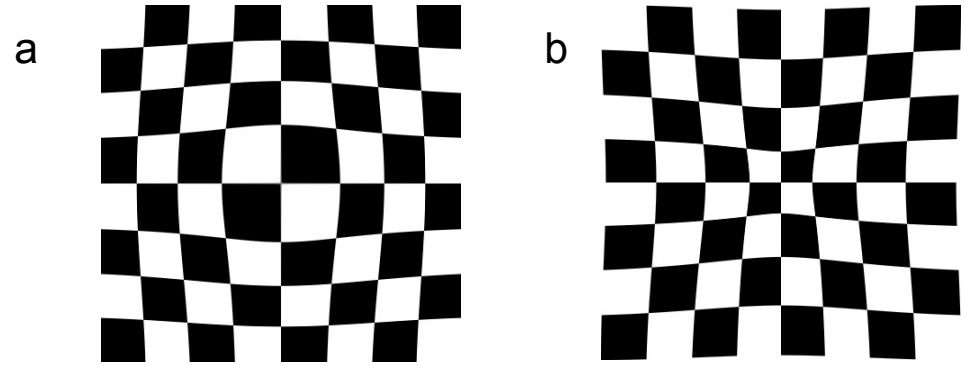


Figure 3.6.: Simulated radial distortion on a chequerboard pattern. Convex distortion is shown in **a**, concave in **b**.

Given a point in the 2D image, the pseudo-inverse of the projection matrix can be used to find some arbitrary point $g$ in 3D space that lies on the ray from the camera to the target object (equation 3.4). The focal point $f$ of the camera itself can also be obtained from $P$ (equation 3.5). These two points define a line in 3D along which the target must lie. Any position $q$ along this line can be specified by a scalar, $\mu$ (equation 3.6).

$$g = P^{-1}\begin{bmatrix} u \\ v \\ 1 \end{bmatrix} \tag{3.4}$$

$$f = -\begin{bmatrix} m_{11} & m_{12} & m_{13} \\ m_{21} & m_{22} & m_{23} \\ m_{31} & m_{32} & m_{33} \end{bmatrix}^{-1}\begin{bmatrix} m_{14} \\ m_{24} \\ m_{34} \end{bmatrix} \tag{3.5}$$

$$q = f + \mu(g - f) \tag{3.6}$$

In general, two lines in 3D cannot be assumed to intersect. However, one can find the point on each line that is closest to the other line, by minimising the function in equation 3.7 (the subscripts denote the different lines specified by the two cameras) and substituting the obtained values for $\mu_1$ and $\mu_2$ back into equation 3.6. The 'intersection' of the lines can then be taken as the midpoint of the line between these points (equation 3.8).

$$sqDist(\mu_1,\mu_2) = |f_1 + \mu_1(g_1 - f_1) - f_2 - \mu_2(g_2 - f_2)|^2 \tag{3.7}$$

$$r = \frac{q_1 + q_2}{2} \tag{3.8}$$

The length of the line joining the two rays (equation 3.7) is actually highly pertinent to my application. If it is large, the two rays are unlikely to be passing through the same object, so one or both cameras must have made a tracking error. This provides a very useful sanity check for the monocular traces, meaning that false positive target fixes are not a serious problem. The only way that two distinct objects could produce rays that 'intersected' (i.e. had a small inter-line distance) would be if they were coplanar with the cameras, which would produce a phantom object at an erroneous depth. This is exactly the principle by which 3D glasses and stereograms work.

### 3.4.2: Reconstruction algorithm

Each camera outputs a list of timestamped 2D positions, and in the previous section I explained the process by which these can be converted to 3D rays. These traces are asynchronous, intermittent (figs 3.7, 3.8) and potentially noisy. This section describes how these issues are dealt with to produce as accurate a 3D trajectory as possible.

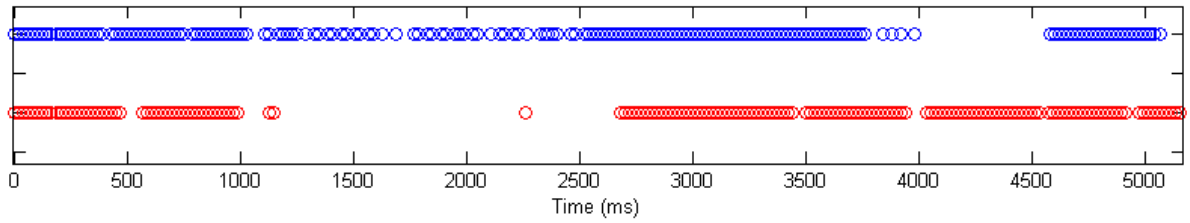


Figure 3.7: Intermittency of monocular traces: The two horizontal lines represent the two cameras, with each circle being an instant at which a target position was reported. The periodic small gaps (e.g. red trace, t=500, 4000) are the result of moving the ROI. The longer gaps (e.g. blue trace, 4000<t<4500) are times when that camera lost the fly and reverted to *acquire* mode. During *track* mode traces can become patchy, with many frames in which no target could be found (e.g. blue trace, 1100<t<2400). Note that this sample is not representative, but rather shows an occasion when the tracker was having difficulty following the fly.

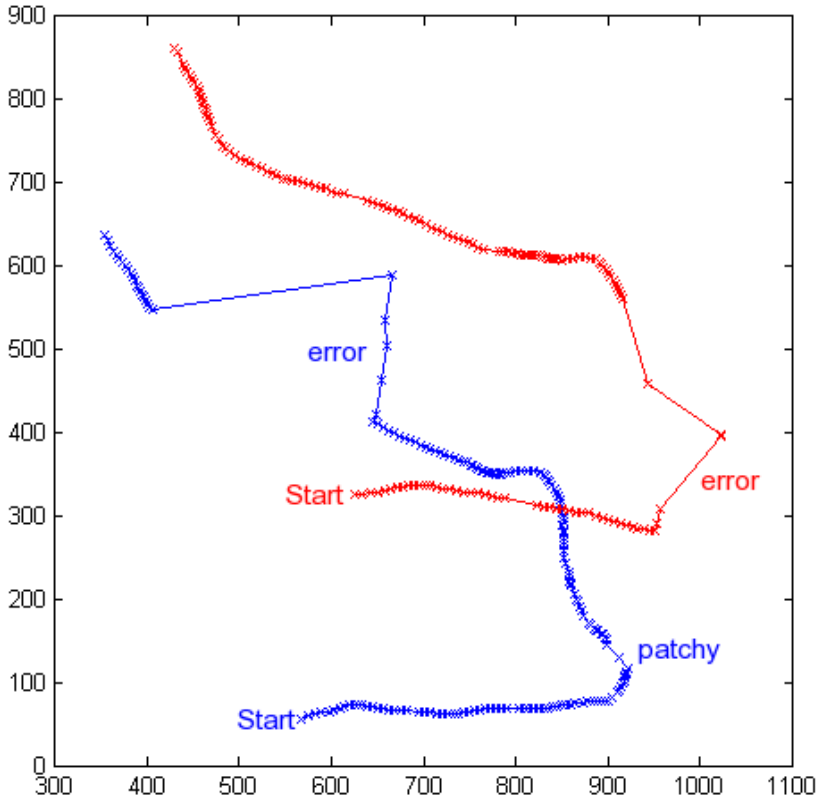


Figure 3.8: Sample traces. These are the 2D traces produced for the 5s depicted in fig 3.7, showing the fly's position as seen from both cameras. Each one loses the fly once and subsequently records a few erroneous positions. Scale is in pixels.

First of all, each 2D trace is subsampled at regular 15ms intervals by simply interpolating linearly between the timestamped sightings. Where long gaps exist, this will give the clearly incorrect impression that the fly moved slowly in a perfectly straight line between the positions bookending the gap. Nevertheless, the algorithm uses the procedure described in section 3.4.1 to attempt to obtain a 3D point for each 15ms timestep.

The next step is to detect the many invalid points that are likely to exist in this trajectory. The primary method by which this is done is by measuring the distance between the two rays (see equation 3.7). If this is greater than 8mm, this is judged not to be a true intersection, and thus the timestep is flagged as erroneous. A number of other sanity checks are used to detect bad 3D points:

- Is the fly's position substantially outside the arena walls, or beneath the floor?
- Is the fly moving at an unrealistically high speed (>1ms$^{-1}$)?
- Is the fly's absolute vertical velocity greater than 60cms$^{-1}$?

The result of these checks is a long binary string designating timesteps as good or bad. This is dilated six times and then eroded six times, which has the result of removing any short (<13 timesteps)

sequences of 'good' points. Unbroken strings of bad points are then identified. If these are longer than 3s, that portion of trajectory is abandoned. Otherwise, an attempt is made to 'patch' the problematic period.

Patching is done by identifying which camera has more target sightings during that interval; the one which does is assumed to be more reliable. The trajectory is then interpolated from the last good 3D point before the patch to the first one after it, using the monocular data and assuming that the fly's altitude changes linearly. The assumption reflects the observation that flies tend to hold a relatively stable position in the vertical dimension (Frye et al, 2003), but is clearly invalid over long periods of time, which is the reason for the 3s limit. If the patched trajectory segment breaks any of the above sanity checks it is abandoned, otherwise it is incorporated into the 3D trace (fig 3.9a). If, after patching, there are any trajectory segments less than 6s long, they are discarded.

Finally, the 3D trajectory segments are resampled at 20ms intervals. Rather than using a linear interpolation, points are sampled using a Gaussian weighted average (s.d. = 28ms). This serves to smooth the trajectory, removing jitter and helping to minimise the effects of any small jumps that may coincide with switching between patched and unpatched potions of the trace (fig 3.9b).

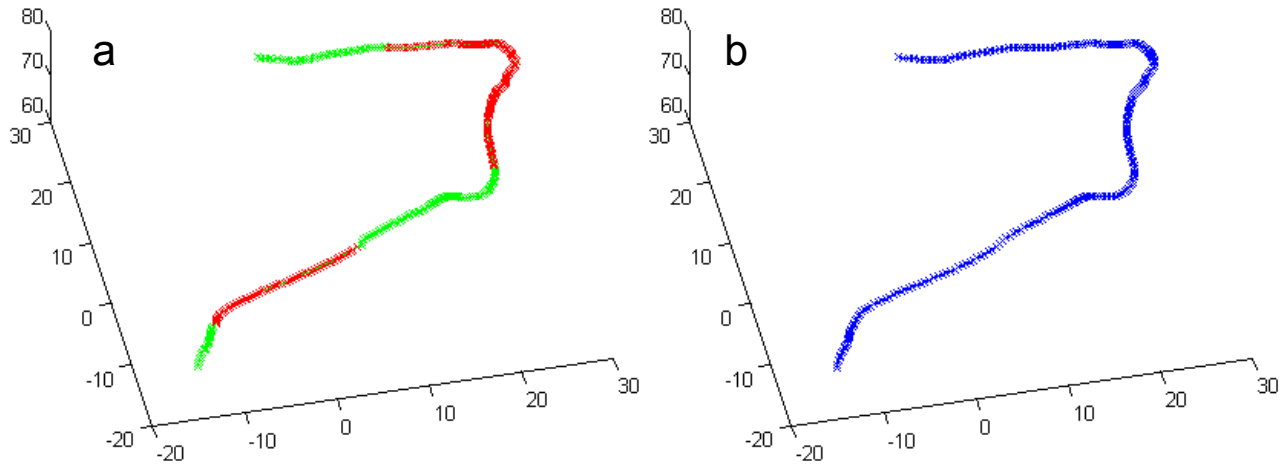


Figure 3.9.: The 3D reconstruction of the 5s segment shown in fig 3.8. **a** The patched trajectory, green sections are based on binocular data, red on monocular interpolations (patches). **b** The final trajectory, smoothed and resampled.

## 3.5: Trajectory analysis

The previous section described how I produce a 3D trace of the fly's flight, or more accurately, a

series of 3D trajectory segments. This is a rich dataset; for each fly I may have several minutes of flight recorded at 50Hz. This final part of the chapter is concerned with how this data can be processed to extract meaningful behavioural features.

### 3.5.1: Spatial distribution

One of the simplest ways to analyse the free flight data is to look at which regions of the arena the fly is most often found in. It is straightforward to split the arena into a grid and record the proportion of time the fly spends in each square. One might argue that this approach is biased, as it will over-represent regions in which the fly tends to move more slowly.

An alternative approach is to measure the frequency with which the fly passes though each grid square. I shall henceforth refer to this as *transit probability*. A fly is considered to have passed though a square if its entrance and exit points are more than half the width of the square apart. This measure is intended to prevent spurious transitions from being recorded due to the fly jittering between squares.

The above methods are useful for visualising the fly's behaviour. However, they are not well suited for making statistical comparisons between experimental conditions. Toward this end, I define cylindrical zones of radius 16cm around each of the odourant/water slots (section 3.1) extending from the floor to the top of the arena walls (60cm). An odour localisation index (OLI) can be computed based on the time spent by the fly in each zone, according to equation 3.9. An OLI of 1 corresponds to perfect localisation; zero means perfect avoidance, and the chance baseline level is 0.333. Using this statistic, I can compare the proportions of time the fly spends in each zone to detect a significant directional bias within an experimental condition, or compare the magnitude of these effects across conditions.

$$OLI = \frac{time_{odour}}{time_{odour} + time_{control1} + time_{control2}} \tag{3.9}$$

### 3.5.2: Saccade detection

The most conspicuous feature of *Drosophila* flight is the rapid yaw turns or *saccades* that they periodically make. Recall that the tracker is unable to detect the orientation of the fly's body; instead I must assume that it is always aligned with its direction of motion. This approach has been adopted by a number of studies (Tammero and Dickinson, 2002a; Frye et al, 2003; Maimon et al, 2008). One might argue that this assumption is realistic because there is evidence to suggest that for a small fly

like *Drosophila*, flight dynamics are dominated by frictional forces, meaning that side-slip is minimal (Hesselberg and Lehmann, 2007; Mronz and Lehmann, 2008). However, this conclusion is not universally accepted (Fry et al, 2003), and it has recently been demonstrated that *Drosophila* are capable of performing lateral flight manoeuvres (Ristroph et al, 2009; Sugiura & Dickinson, 2009). Thus, it should be recognised that this method's estimation of orientation is an approximation. The fly's instantaneous angular velocity is estimated by measuring the angle between consecutive 20ms segments of the trajectory. Because saccades are turns about the yaw axis, I project the trajectory to the horizontal plane to perform this analysis.

A simple threshold on angular velocity can be set to detect instances of saccades (fig 3.10). I chose a value of $450°s^{-1}$, which is rather more conservative than the cut-off of $300°s^{-1}$ used by previous studies (Tammero & Dickinson, 2002a; Frye et al, 2003). Of course, it is impossible to say with certainty whether a given manoeuvre represents a saccade or not, so setting this threshold is necessarily somewhat subjective. However, it was my feeling some of the events detected using a threshold of $300°s^{-1}$ were not true saccades, as the total angle of the turn was only a few tens of degrees. It should be pointed out that the aforementioned studies used a different smoothing procedure, so the values are not directly comparable.

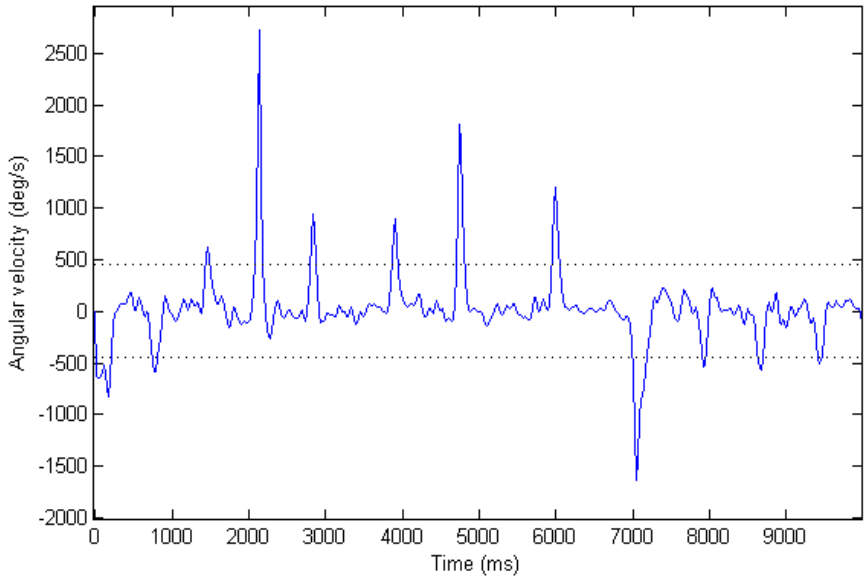


Figure 3.10.: A fly's angular velocity over 10s. Saccades are clearly evident as sharp peaks. The saccade detection threshold is marked.

If two instances of suprathreshold angular velocity occur within 100ms, these are treated as the same saccade. The motivation for this is to prevent spurious saccade events being generated due to

fluctuation around the threshold value. Any saccade whose total size is less than 17° is discarded.

Having identified a saccade, I can compute a number of statistics to quantify its features and context (fig 3.11). These are listed below. In many cases, some duration of unbroken intersaccadic flight is required prior to the saccade in order to perform the calculations. If this does not exist (either because the data is missing, or because another saccade occurred in that period) then the saccade is excluded from this analysis.

Some terms must first be defined. The *onset* of a saccade is the first timestep where the angular velocity exceeds the threshold value; the *offset* is the last one before it drops below it. The *midpoint* is the timestep midway between these events (equation 3.10).

$$t_{midpoint} = floor\left(\frac{t_{onset} + t_{offset}}{2}\right) \tag{3.10}$$

Saccade features include (refer to fig 3.11):

- *Distance from wall* (*d*). The radial distance from the edge of the arena, as measured at the saccade midpoint.
- *Distance to collision* (*c*). The distance from the saccade midpoint to the wall, in the direction the fly was moving between 220 and 160ms prior to the saccade midpoint.
- *Saccade size* ($\sigma$). The sum of the yaw angles between consecutive 20ms trajectory segments from 40ms before the saccade onset to 40ms after the offset.
- *Wall approach angle*. ($\omega$) A tangent of the fly's trajectory 160ms before the saccade midpoint is extrapolated until it meets the wall. The angle between this line and one perpendicular to the wall is calculated. This is defined such that in fig 3.11 both this and the saccade size would be positive, i.e. a saccade in the 'correct' direction to avoid the wall has the same polarity as the wall approach angle.
- *Pre-saccade velocity*. The fly's mean horizontal speed between 220 and 160ms before the saccade midpoint.
- *Time since last saccade*. Measured midpoint to midpoint.
- *Distance since last saccade*. The straight-line distance between the positions of the midpoints.

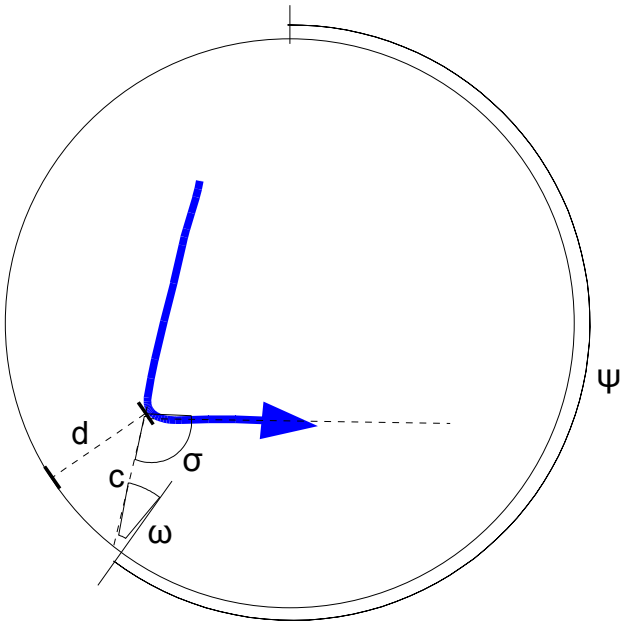


Figure 3.11: Saccade features, see sections 3.5.2 and 3.5.3. The blue line is a segment of the fly's trajectory.

## 3.5.3: Intersaccadic segments

It is also desirable to be able to analyse behaviour in the relatively straight bouts of flight between saccades. Of course, it is not clear at which point a fly 'decides' to saccade, and nor is it clear when a saccade is 'finished' and normal stable flight has resumed. In fact, I find that a counter turning reflex persists several hundred ms after the fly's angular velocity drops below threshold (section 4.4.3). For these reasons, I must be rather conservative in designating portions of flight to be intersaccadic if I am to avoid artefacts caused by the preceding or following saccade. For this reason, I ignore the first 500ms after the offset of the previous saccade and the last 220ms before the onset of the next. The remaining segment must be at least 120ms long to be included. Furthermore, a segment should be discarded if there is a possibility that it includes an undetected saccade. Thus if the angular velocity exceeds 80% of the saccade detection threshold (i.e. $360°s^{-1}$) the segment is excluded.

In a similar manner to saccades, I measure various features of intersaccadic segments:

- *Mean velocity*.
- *Wall approach angle*. This is based upon a tangent of the beginning of the intersaccadic trajectory.
- *Mean angular velocity*. This provides a measure of the straightness of the segment.
- *Angle to x*. Based on the start of the segment, the azimuthal position of some physical feature (e.g. the odour source or a visual landmark) with respect to the fly is calculated. Relating this

to the mean angular velocity gives an indication of whether the fly is steering towards that feature.

- *Arena heading* ($\psi$ in fig 3.11). The angular position on the arena wall towards which the fly is headed.

### 3.5.4: Statistical methodology

Data is rather cheap in this paradigm, since many flies can be recorded in a day, and each fly provides very rich behavioural information. This means that I can be relatively confident of avoiding type II errors, i.e. failure to detect a significant effect due to having insufficient statistical power. Of perhaps greater concern is the possibility of type I errors, i.e. finding a spurious result due to a flawed methodology.

Statistical tests assume that samples are independently drawn from a population. In the case of two saccades made one after the other by the same fly, this assumption may well be invalid; one could imagine that presaccadic velocity, for instance, would be correlated in this situation. Therefore, whenever I compare averages of these features, I first compute the average *for each fly* and use this as one observation. Thus, the *n* used for the statistical test is the number of flies, not saccades or intersaccadic segments. When computing a correlation between two variables (e.g. presaccadic velocity and saccade size, see section 4.4.2) it does not make sense to apply a similar procedure, so in this case I do treat events (i.e. saccades in this example) as independent. This caveat should be kept in mind when interpreting results of this kind.

Parametric tests (e.g. t-test, Pearson's r) assume that data is normally distributed. Non-parametric tests (e.g. Mann-Whitney U, Spearman's $\rho$) make no such assumptions, but due to this universality are weaker, in the sense that they have less sensitivity to small-magnitude effects. I use non-parametric tests throughout.

# 4. Visuomotor behaviour

This chapter is concerned with the free-flight behaviour of flies in various visual environments, without any food odour present. After explaining some details of how these experiments were conducted (section 4.1), I describe how differences in the visual environment affect the general shape of the flies' trajectories (section 4.2). I then look in detail at how intersaccadic flight (section 4.3) and saccadic turns (section 4.4) are affected, before finally discussing the implications of my results (section 4.5).

## 4.1: Methodology

My general methodology is discussed in detail in the previous chapter; this section briefly covers aspects specific to the experiments discussed in this chapter.

### 4.1.1: Visual stimuli

Three different 'wallpapers' are used to create distinct visual environments for the fly (see section 3.1 for details of the arena). The *random chequerboard* (CB) wallpaper is a grid of 43mm squares comprising either blank white paper or opaque black cardboard with equal probability (fig 4.1a). Each square subtends a visual angle of 5° from the centre of the arena. The *horizontal stripes* (HS) wallpaper consists of alternating bands of black and white (fig 4.1b), each 43mm wide (i.e. the same size as the squares in the CB arena). Finally, the *single landmark* (SL) wallpaper is similar to the horizontal stripes one, except for the presence of a vertical white band 244mm wide (or 18° when viewed from the centre of the arena) with a single black stripe of width 70mm (8°) running down its centre (fig 4.1c).


Figure 4.1: Arena wallpapers. **a** Chequerboard (CB). **b** Horizontal stripes (HS). **c** Single landmark (SL). Each measures 314x60cm.

Preliminary experiments were carried out with an entirely blank white wallpaper, but I was concerned that the flies were able to make use of residual texture created by imperfections in the arena and/or uneven lighting. This confounding phenomenon has been identified in another free-flight study (Frye and Dickinson, 2007). The patterns above all contain strong contrasts throughout their extent in order to ensure that the flies' contrast adaptation mechanisms are saturated, hopefully preventing them from detecting these subtle textures.

### 4.1.2: Experimental procedure

At the beginning of each replicate, a fly was introduced to the arena by means of an aspirator. It was allowed to fly for ~10s in order to remove any positional bias that might arise from the starting location. The tracking system was then started, running for four minutes. The resulting trajectory recording would typically be rather less than four minutes long, due to a) tracking failures, b) the fly landing, or c) the fly flying up into the region of the cameras. Only trajectories of total length >30s were included in my analysis. Once the tracking was finished, the fly was removed from the arena using a handheld vacuum cleaner.

## 4.2: Spatial distribution

Fig 4.2 shows samples of individual trajectories recorded in the three visual environments, and fig 4.3 gives transit probability plots (see section 3.5.1) averaged over many flies. It is immediately apparent that flies stay more centralised in the chequerboard (CB) arena than the horizontally striped one (HS), as Frye et al (2003) reported. This difference is significant: the flies' average distance from the wall in the CB arena is 31.6cm, *versus* 26.5cm in HS ($U(24,24)=73$, $p<.0001$).

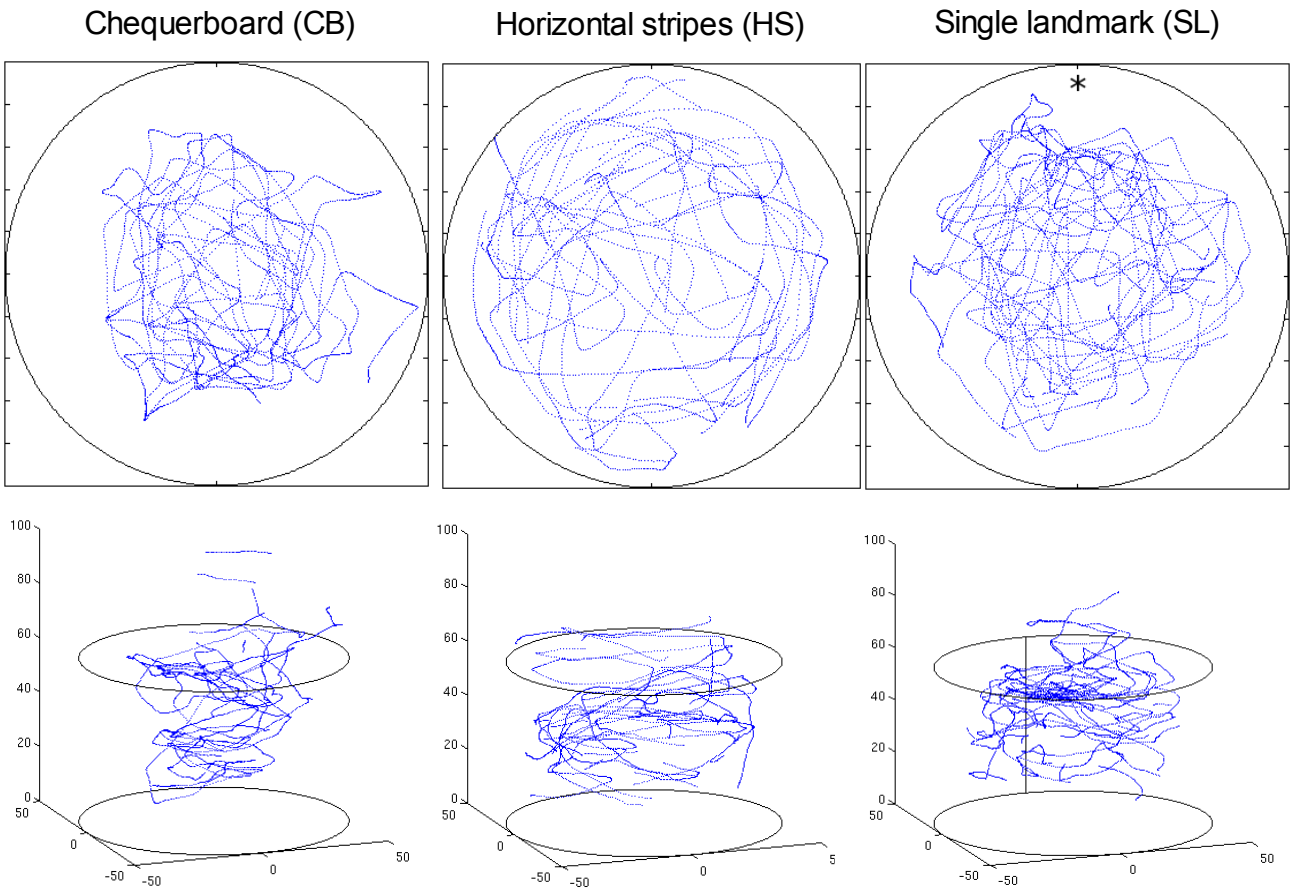


Figure 4.2: Sample trajectories from the three arenas. Dots represent the fly's position at 20ms intervals, giving an impression of speed. The overhead and 3D views show the same trajectories. In the SL arena, the stripe is located at the 12 o'clock position (marked by an asterisk) on the overhead plot, which is the far side of the 3D plot (marked by the vertical black line). Scale is in cm.

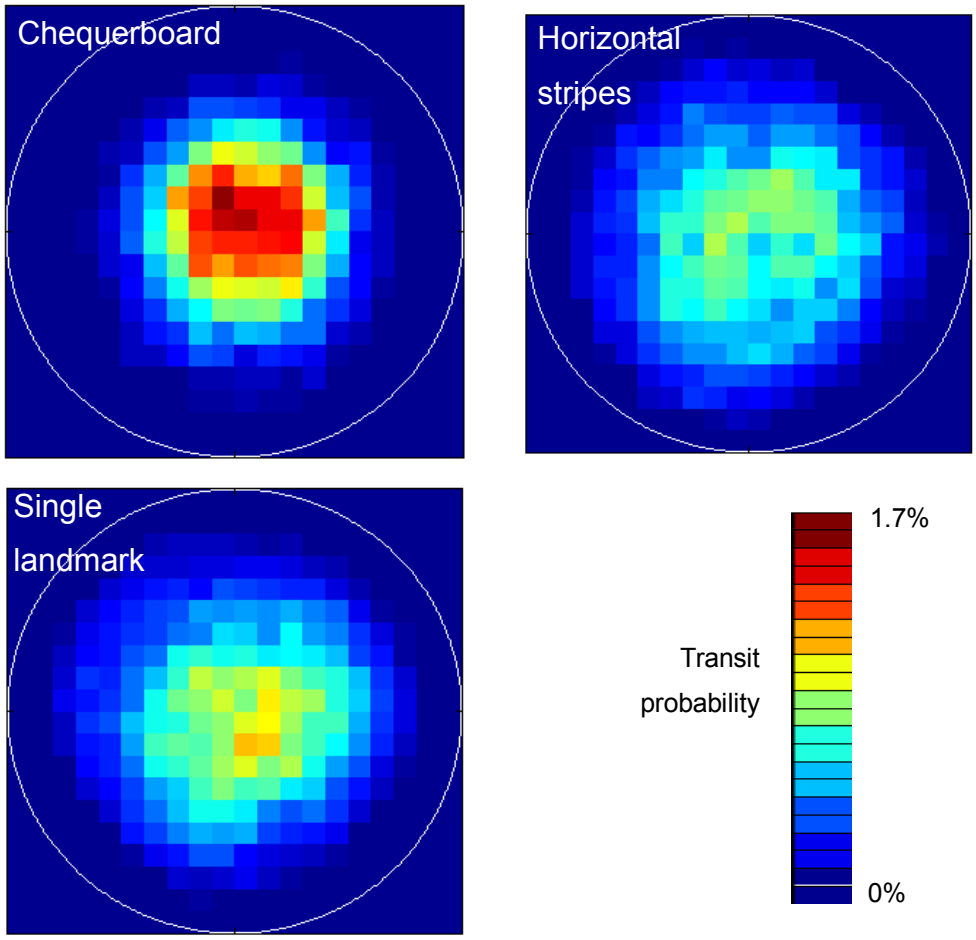


Figure 4.3: Transit probability plots. Each box is 5cm across, and its colouring represents the probability (i.e. proportional frequency) with which the fly passes through that box. Again, the stripe is at the 12 o'clock position in the SL arena. The data is averaged across replicates, meaning that each fly contributes equally regardless of the length of its trajectory. $n_{CB}$=24, $n_{HS}$=24, $n_{SL}$=42.

Interestingly, it appears that flies are neither strongly attracted to nor repelled by the vertical stripe in the SL arena. There is no significant difference between their average distance from the wall in the half of the arena containing the landmark and that in the half directly opposite it (27.8cm *versus* 28.3cm, T(42)=319, p=.098). Furthermore, they spend 48.7% of their time in the half of the arena closest to the landmark, which is not significantly different from chance (sign test, n=42, p=.64). Note that a larger number of flies (42) were used in this condition to search for such biases, but the results remained negative.

There is no difference in mean altitude across the three conditions (CB: 46.6cm, HS: 46.9cm, SL: 51.2cm; Kruskal-Wallis K=3.20, p=.20).

In the following sections I look in more detail at particular features of flight in different visual contexts. Often, I will compare behaviour in the CB and HS arenas, as these are both homogeneous

and represent two extremes in terms in the abundance of vertical contrast. The SL arena will be discussed less frequently, though I shall consider what it can tell us about target-oriented behaviour.

## 4.3: Intersaccadic flight

In this section I turn my attention to the behaviour of flies during the relatively straight bouts of flight that occur between saccades. Details of how these events are identified can be found in section 3.5.3.

### 4.3.1: Homogeneous environments

The most striking difference between intersaccadic flight in the CB and HS arenas is its speed: 26.7cms$^{-1}$ in CB *versus* 38.1cms$^{-1}$ in HS ($U(24,24)=48$, $p<.0001$). It seems plausible that this phenomenon is a direct effect of the relative paucity of visual contrast in the HS arena, as *Drosophila* are known to regulate their flightspeed with respect to their visual surroundings (David, 1982; Fry et al, 2009). In interpreting any subsequent differences found between behaviour in these two environments, one must carefully consider whether they are truly visual effects, or rather secondary consequences of this change in flight velocity.

The straightness of intersaccadic flight is similar between the two environments. In the CB arena, flies' mean absolute intersaccadic angular velocity is 34.0°s$^{-1}$, compared to 35.4°s$^{-1}$ in HS ($U(24,24)=306$, $p=.71$). However, a systematic bias appears to exist in the HS arena such that flies steer away from the nearest wall during intersaccadic segments. (I shall henceforth refer to this phenomenon as 'veering'.) Angular velocity is correlated with wall approach angle ($\rho(246)=.171$, $p=.007$) in the HS arena, but not in the CB one ($\rho(624)=-.012$, $p=.76$), as shown in fig 4.4. This effect can be seen in the sample trajectories of fig 4.2, where the flightpaths in the HS arena have a distinctive convex shape which the CB ones lack.

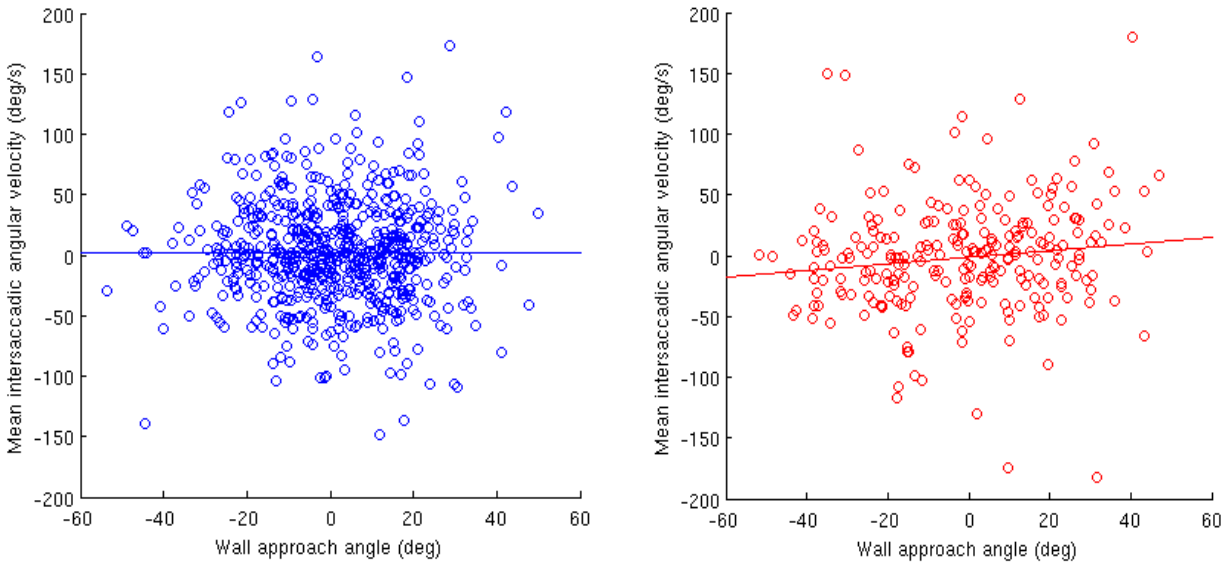


Figure 4.4: Intersaccadic turning and wall approach angle. CB arena is in blue, HS in red. Each datapoint is an intersaccadic segment, with the wall approach angle based on the starting position and orientation. If the angular velocity has the same polarity as the wall approach angle, the fly is turning away from the wall. Lines are linear regression fits to the data.

### 4.3.2: Landmark behaviour

Simply looking at how much time flies spend in each half of the arena failed to demonstrate any significant bias towards or away from the landmark (section 4.2). However, this is a rather crude measure. Investigating how intersaccadic flight is affected by the position, relative to the fly, of a vertical landmark could perhaps reveal some target-oriented behaviour.

One might suppose that flies would steer gradually towards the landmark. If one considers those intersaccadic segments which begin with the landmark in the fly's frontal visual hemisphere (i.e. at an azimuth between -90° and 90°), one would expect to find a correlation between the landmark angle and the fly's angular velocity if this were the case. No such correlation exists ($\rho(282)=.049$, $p=.41$).

Alternatively, the length of intersaccadic segments can be considered. There is a significant (though not particularly large) negative correlation between absolute angle to the landmark and segment duration ($\rho(585)=-.117$, $p=.005$). (This is significantly different ($p=.018$) to a Monte Carlo baseline, see section 6.3.1.) No such correlation exists for speed and landmark angle ($\rho(585)=.031$, $p=.45$), indicating that any tendency to approach the landmark is due more to suppressing saccades when it is frontally positioned, rather than modulating intersaccadic velocity.

## 4.4: Saccades

As my intention is ultimately to model saccadic flight, there are two main issues regarding saccades to consider when interpreting the free-flight data:

- What can be inferred about the visual conditions which trigger saccades?
- Do saccades represent an entirely stereotyped, fixed motor program, or do any of their features vary according to the visual environment?

I shall address these questions in turn in the following sections. See section 3.5.2 for details of how saccade parameters are calculated.

### 4.4.1: Saccade triggering

There is no significant difference between the frequency of saccades between arenas (mean intersaccadic interval: CB: 809ms, HS: 826ms, SL: 855ms; K=3.34, p=.19). However, the intersaccadic distance is greater in HS than CB due to the higher flightspeed (U(24,24)=40, p<.0001).

If flies generally venture closer to the walls in the HS arena than in CB, then one would expect that the distance from the wall at which they initiate a saccade is less. This is true, both in terms of their radial distance to the wall (CB: 29.6cm *versus* HS: 23.9cm; U(24,24)=80, p<.0001) and in terms of distance to collision (CB: 35.5cm *versus* HS: 30.1cm; U(24,24)=62, p<.0001). When one considers that flies generally move substantially faster in the HS arena, then clearly there is an even greater difference in *time* to collision (CB: 1425ms *versus* HS: 846ms, U(24,24)=56, p<.0001).

By finding occasions where the pre-saccade wall approach angle has an absolute value greater than 8°, I can identify instances where one would expect the fly to saccade in a particular direction in order to avoid a collision. Interestingly, flies frequently turn in the 'wrong' direction in this scenario (CB arena: 25.3% wrong, HS: 26.4%; U(24,24)=310.5, p=.64).

I find that in both visual conditions, these wrong-direction saccades are significantly larger than correct ones (CB: wrong: 118.0°, correct: 92.8°; T(24)=6, p<.0001; HS: wrong: 110.6°, correct: 86.6°; T(24)=16, p=.0001). As flies tend to veer away from the walls of the HS arena, one might be concerned that some of the small saccades in the correct direction might not be true saccades but merely instances of sharp intersaccadic turning. However, the fact that the pattern is just as evident in the CB arena, where flies do not veer away from the walls, suggests that this is a genuine effect. Some

possible explanations for this observation are offered in section 4.5.5.

## 4.4.2: Features of saccades

In this section I look closely at what occurs during a saccade, and how this may be affected by the fly's visual environment.

Saccade size is not significantly different across the two homogeneous arenas (CB: 101.3° *versus* HS: 96.1°; U(24,24)=208, p=.099). What difference there is may be best interpreted as a result of the difference in flightspeed (fig 4.5), as there is a negative correlation between pre-saccade speed and saccade amplitude in both arenas (CB: ρ(2539)=-.112, p<.0001; HS: ρ(852)=-.118, p=.0006). This is consistent with the suggestion that increasing flight force reduces manoeuvrability by constraining wing kinematics (Lehmann and Dickinson, 2001).

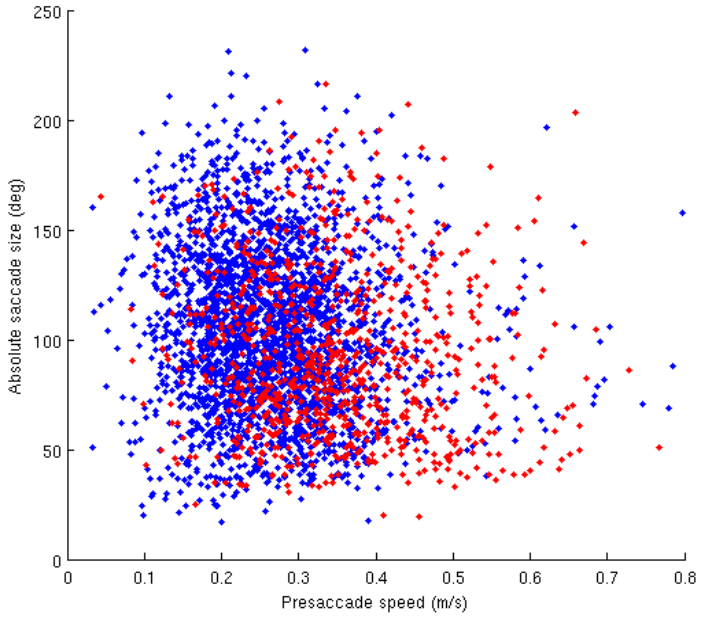


Figure 4.5: Flightspeed and saccade size. CB arena is blue, HS is red. Note that because of my operational definition, the minimum possible saccade amplitude is 17° (section 3.5.2).

Saccade amplitude is negatively correlated with distance to collision, i.e. larger saccades tend to occur when wall contact is imminent (CB: ρ(2539)=-.271, p<.0001; HS: ρ(852)=-.175, p<.0001). Of course, correlation does not imply causation. Presaccade velocity is also positively correlated with distance to collision (CB: ρ(2539)=.179, p<.0001; HS: ρ(852)=.101, p=.003), so it could be that this effect is a by-product of speed regulation rather than a specific mechanism to produce larger evasive manoeuvres for more imminent collisions.

Saccade amplitude is also negatively correlated with absolute wall approach angle, such that larger saccades are observed when the wall is being approached head-on (CB: $\rho(2539)=-.184$, $p<.0001$; HS: $\rho(852)=-.248$, $p<.0001$). This correlation is harder to dismiss as an indirect effect mediated by flight speed, as there is no significant correlation between absolute wall approach angle and presaccade velocity in the HS arena ($\rho(852)=-.026$, $p=.46$) and in CB a significant correlation exists in the wrong direction to account for this effect ($\rho(2539)=-.081$, $p<.0001$). This issue is discussed further in section 4.5.6.

Fig 4.6 shows the horizontal speed of flies before, during, and after a saccade. This data is computed by identifying saccades with at least 500ms of uninterrupted intersaccadic flight preceding and following them, computing the average velocity profile for each fly, and then taking the mean across animals. In both arenas, the fly slows down to approximately two-thirds of its intersaccadic velocity at the peak of the saccade. In both cases we see a distinctive asymmetric pattern, with the fly slowly decelerating into the saccade and then quickly accelerating out of it. From this observation, it is tempting to conclude the the fly is 'planning' a saccade several hundred milliseconds before peak angular velocity is reached. However, it must be borne in mind that typically, the fly will have a larger distance-to-collision after a saccade than before it. If this is the case, velocity regulation based on visual expansion could account for the pattern in fig 4.6.

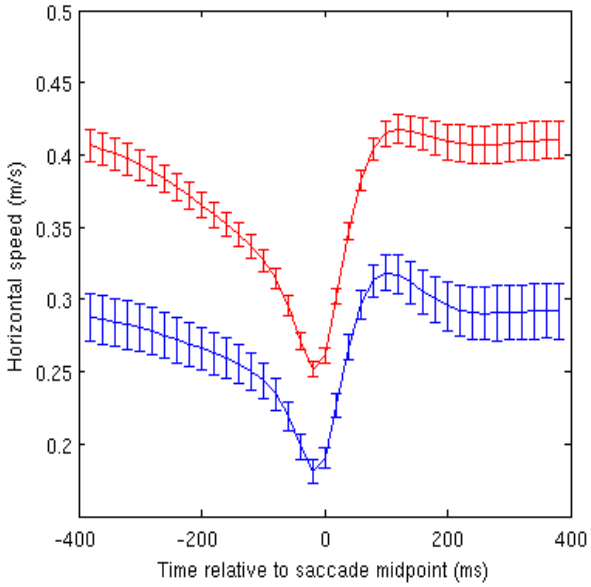


Figure 4.6: Event-triggered horizontal velocity profiles. CB arena in blue, HS in red. Bars are ±1 s.e.m.

Immediately after the saccade, there is a more pronounced velocity overshoot in the CB case (fig 4.6, t=100ms). A possible explanation for this phenomenon is that the flies may be moving at close to their maximum velocity in the HS arena, so the resulting ceiling effect could mask this post-saccade surge.

Fig 4.7 shows the average vertical *displacement* (not velocity) around the time of a saccade. Flies reach peak altitude at the same time they reach peak angular velocity, though it should be pointed out that the vertical speeds are not particularly high. Flies in the HS arena drop substantially more quickly immediately following a saccade. Once again, this may be linked to their increased speed; *Drosophila* can produce a maximum of around 150% of their weight in thrust, so as this is diverted to horizontal acceleration the fly may lose lift and hence drop in altitude (Lehmann & Dickinson, 2001; Sugiura & Dickinson, 2009).

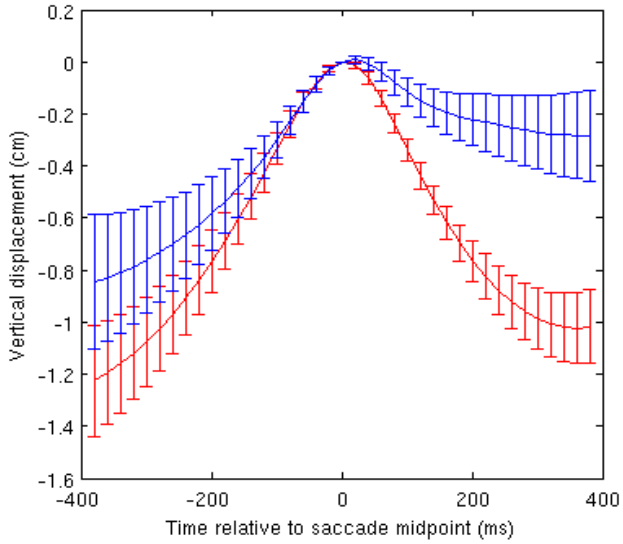


Figure 4.7: Event-triggered vertical displacement profiles. CB arena is in blue, HS in red. Bars are ±1 s.e.m.

Fig 4.8 shows the mean absolute angular velocity during a saccade. Saccade duration (defined as the length of time that the angular velocity is supra-threshold) is approximately 100ms. It should be borne in mind that trajectories are subject to Gaussian smoothing with s.d. = 28ms (section 3.4.2), which may slightly elongate this profile. During the saccade, the profiles for CB and HS are strikingly similar, supporting the view that saccades are produced by a stereotyped motor program that uses little or no visual input.

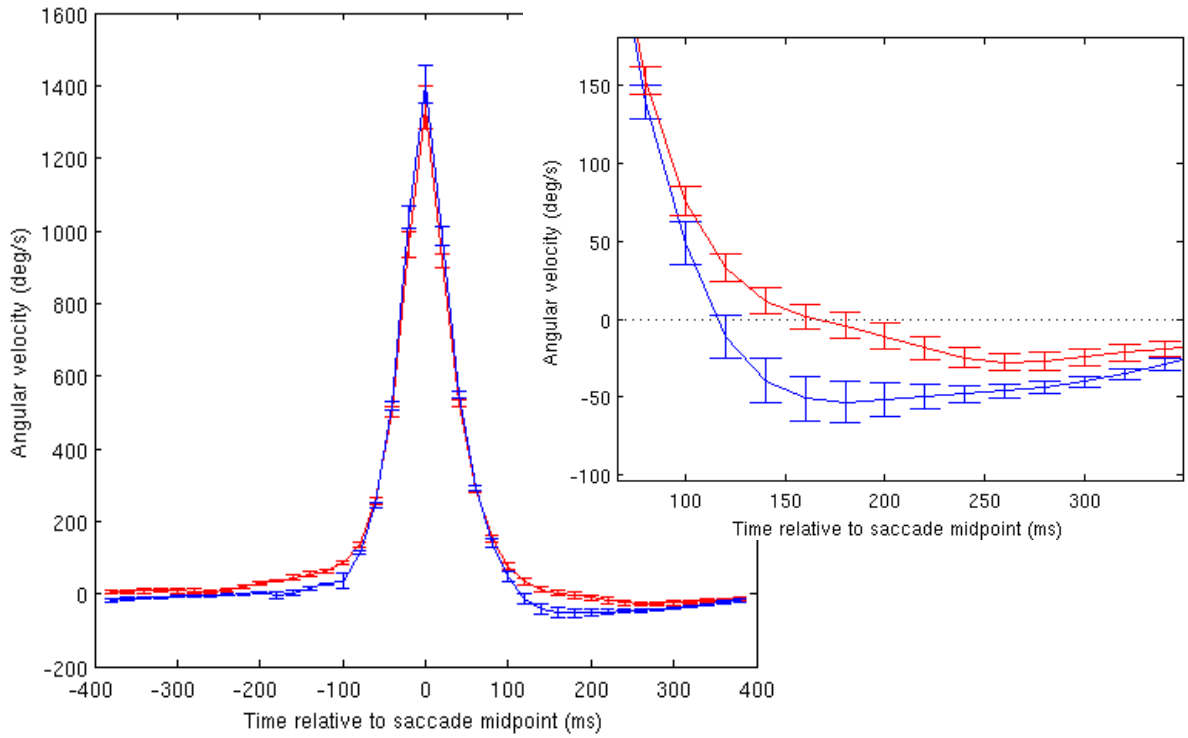


Figure 4.8: Event-triggered angular velocity profiles, normalised such the the saccade direction is positive. CB arena is blue, HS is red. Bars are ±1 s.e.m. Inset: Zoomed view of the plots, showing the 'rebound' phase following the saccade.

### 4.4.3: Optomotor rebound

While the angular velocity profiles of saccades in the two arenas are very similar, a curious phenomenon is seen immediately after the saccade. In the CB arena, the fly's angular velocity becomes substantially negative, i.e. it turns in the opposite direction to the saccade (fig 4.8 inset). This can even be seen in the fly's trajectory, which is noticeably concave (fig 4.2). While the same thing happens in the HS arena, the amplitude of this counter-turn is much smaller. The difference, as measured at t=160ms, is significant ($U(24,24)=132$, $p=.0013$). Furthermore, this 'rebound' appears to have a different timecourse in the two environments, as it reaches a peak 180ms post-saccade in CB, but not until 260ms in HS.

While it is possible that the counterturn is part of the saccade motor program (indeed, Fry et al (2003) argue that *Drosophila* have sufficient inertia to require them to generate a countertorque to terminate a saccade, though Hesselberg & Lehmann (2007) dispute this conclusion) this would not explain why its magnitude and timing differ based on the visual environment. It is also difficult to see how the difference in horizontal velocity could cause this effect, given that the angular velocity profiles are so

similar during the heart of the saccade.

Instead, I hypothesise that this rebound is due to the optomotor response causing the fly to compensate for the visual rotation it experienced while saccading. The CB arena is richly textured, giving strong rotational cues, so we see a pronounced rebound. Conversely, the fly receives very little yaw information from the HS arena, so the rebound is greatly reduced.

An alternative interpretation of this data is that the rebound is in fact part of the saccade motor program, and it is simply masked in the HS arena because the fly veers away from the wall, and usually this will mean turning in the same direction as the saccade. These two effects cancel each other out, resulting in an angular velocity close to zero. Indeed, this intersaccadic turning in the HS arena could account for the difference seen between CB and HS *before* the saccade (fig 4.8, t=-150ms).

To investigate this hypothesis, I identify the rather rare cases where the post-saccade wall approach angle is such that we would expect the fly to veer in the opposite direction to the saccade. If the above account is true, the post-saccade rebound should be even larger than it is in the CB arena, because the veering effect would now be added to the rebound portion of the saccade manoeuvre. However, fig 4.9 reveals that this is not the case – the rebound does not appear to depend on the post-saccade wall approach angle. I therefore reject this hypothesis and reiterate my view that the rebound is caused by compensation for the visual rotation experienced during a saccade. For this reason, I term the phenomenon *optomotor rebound*. It is discussed further in section 4.5.3.

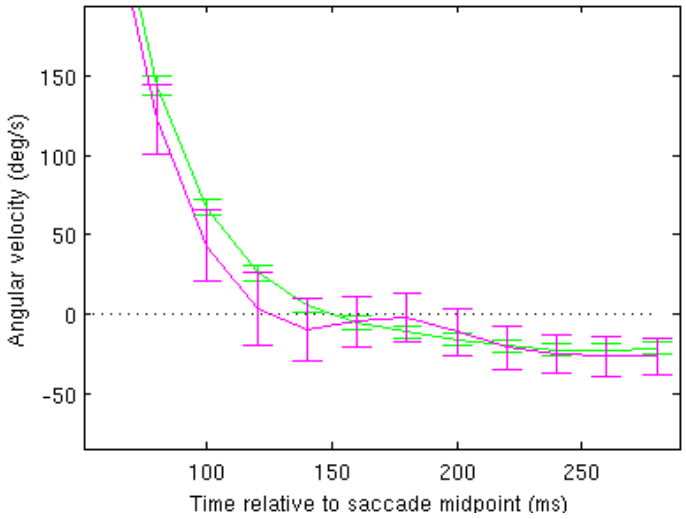


Figure 4.9: Event-triggered angular velocity profiles for saccades in the HS arena. The post-saccade wall approach angle is calculated based on flight 160-200ms after the saccade peak. Only cases where the absolute angle is greater than 8° are included, to ensure a clear directional bias. Green data represents cases where veering away from the wall would cause the fly to turn in the same direction as the previous saccade (i.e. positive angular velocity), magenta data the less common case where it would turn in the opposite direction (negative). Note that due to scarcity of data, this figure uses averages over saccades, not flies. $n_{green}$=587, $n_{magenta}$=68. Bars are ±1 s.e.m.

### 4.4.4: Landmark behaviour

Do flies saccade towards or away from the vertical stripe in the SL arena more frequently than chance would predict? To address this question I compute the angular position of the landmark relative to the fly, based on its pre-saccade orientation. I identify cases where it was on either the fly's left or right, discarding occasions where the absolute angle was <10° or >170°. It can then be determined whether the subsequent saccade was in the appropriate direction to orient towards the stripe. Averaging over flies, the mean probability of turning towards the stripe is 50.1%, which is not different from chance (sign test: n=42, p=1.0). This indicates that the landmark has no effect on saccade direction.

## 4.5: Discussion

### 4.5.1: Conclusions

The main findings of my free-flight experiments in the absence of food odour are as follows:

1. Flies more closely approach walls that are horizontally striped (HS) and thus lacking in vertical contrast than those which carry a richly textured random chequerboard (CB) pattern.

2. Flight is considerably faster in the absence of vertical contrasts.
3. While the straightness of intersaccadic flight is similar between CB and HS, flies veer away from the walls in the HS arena but not in CB.
4. The timecourse and amplitude of saccades is similar across the arenas, but flies in the CB arena make a significantly larger 'rebound' turn following a saccade than those in HS.
5. Flies appear to be neither attracted to nor repelled by a single vertical bar in an otherwise horizontally striped arena. The only landmark-oriented effect found was a slight suppression of saccades when the bar was frontally positioned on the fly's retina.

### 4.5.2: Comparison to previous studies

Tammero & Dickinson (2002a) was the first study to adopt the experimental paradigm of tracking free-flight in a circular arena. The two visual conditions they used were a random chequerboard pattern and blank white walls. While the untextured arena can be considered analogous to my HS condition inasmuch as they both lack vertical contrasts, they are not truly equivalent, since the fly is quite possibly making use of faint, uncontrolled textures on the ostensibly blank walls. This point is made explicitly by Frye & Dickinson (2007).

Tammero & Dickinson (2002a) report that intersaccadic segments in their chequerboard arena are significantly biased away from the nearest wall, in disagreement with my observations (point 3 above). The paper does not go into detail about how intersaccadic segments are processed, but it may be the case that differences in this aspect of methodology could account for the discrepancy. I have shown that saccades are followed by rebound turns lasting several hundred milliseconds (section 4.4.3), and for this reason I consider an intersaccadic segment to 'start' 500ms after the preceding saccade. It is also possible that differences in the smoothing or saccade detection algorithms could influence this computation.

The previous study expresses the viewpoint that "saccades might represent the feedforward output of a stereotyped motor program performed without any sensory feedback" (Tammero & Dickinson, 2002a, p339). My observations support this account, at least as regards the visual modality; the amplitude, duration and temporal structure of saccades do not appear to depend on the textural properties of the visual environment (but see section 4.5.6). However, I would argue the effects of visual feedback are seen in the counter-turn which immediately follows a saccade. I discuss this phenomenon in greater detail in the section 4.5.3.

Frye et al (2003) made use of both horizontally striped and blank walls, and found some clear differences in the behaviour elicited by them. Compared to a random chequerboard pattern, they reported that flies approach horizontally striped walls much more closely, a finding that I replicate (point 1). While it is not quantified statistically, it appears that flies veer away from horizontally striped walls in quite a pronounced fashion (Frye et al, 2003; Fig 13A, p851), also in agreement with the present study (point 3). Frye & Dickinson (2007) add a few more details to this picture, including the finding that exclusively horizontal contrasts elicit considerably faster flight than vertical ones, as I have also shown (point 2).

Perhaps the biggest surprise in my free-flight data is the flies' apparent indifference towards a conspicuous vertical bar in an otherwise horizontally striped environment (point 5). Both tethered flight (Poggio and Reichardt, 1973; Duistermars and Frye, 2008) and free-flight studies (Maimon et al, 2008) reveal that *Drosophila* are normally strongly attracted to long vertical objects. I consider the most reasonable explanation for this difference in behaviour to be the presence of horizontal stripes in the rest of the arena, as the aforementioned studies use backgrounds with minimal texture. As noted previously, horizontally striped surfaces elicit considerably closer approaches than walls with no ostensible texture whatsoever (Frye et al, 2003; Frye and Dickinson, 2007). It may therefore be the case that the flies' 'attraction' to the horizontal stripes counteracts their attraction to the vertical landmark.

### 4.5.3: Post-saccade optomotor rebound

In section 4.4.3 I argue that the counter-turn following a saccade cannot be explained as merely part of the saccade manoeuvre, but rather is a result of the optomotor response to the optic flow experienced during the fly's rapid rotation. To my knowledge, this phenomenon has not been previously reported in *Drosophila*. Of course, it is very difficult to definitively establish a causal relationship in an observational experimental paradigm like this one. Experiments using a magnetic tether (section 2.1) would be able to prove more conclusively that flies attempt to compensate for the visual rotation generated by their own saccades (section 10.2.2.1).

Assuming that this is the case, it is quite a surprising result. Generally, some form of efference copy is employed to suppress compensatory feedback when an animal makes a 'deliberate' movement (Webb, 2004). While it remains entirely possible that such a mechanism exists and attenuates the rebound turn, some residual feedback would still appear to occur. Alternatively, the diminishing response of the fly's motion detection system to very rapid movement may be sufficient to prevent large oscillations following a saccade (Warzecha & Egelhaaf, 1996).

In any case, the identification of this behaviour is serendipitous for the purposes of modelling (chapter 5), as it provides rich data on the magnitude and temporal properties of the optomotor response in different visual situations.

### 4.5.4: Intersaccadic veering

Why might flies steer away from horizontal contrasts, but not vertical ones? I hypothesise that this effect is also a result of the optomotor response. The absence of vertical contrasts and the circular geometry of the arena may create an illusion of rotation against which the fly attempts to compensate, resulting in a path that curves away from the wall.

To understand how this could occur, consider a fly attempting to traverse the arena in a straight, off-centre line as shown in fig 4.10. If the walls are horizontally striped, the only directional cue available to the fly is the distortion of the pattern due to perspective. At the beginning of the intersaccadic segment (point A), the wall behind and to the left of the fly will appear to bulge vertically. By the time it reaches point B, this bulge will have swept to a more frontal retinal position. Thus the world appears to have rotated to the right, causing the fly to steer right (i.e. away from the wall) to compensate.

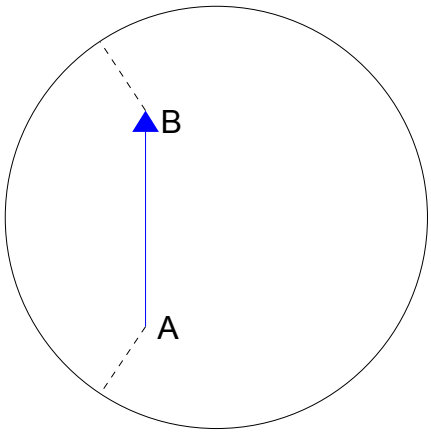


Figure 4.10: Hypothetical intersaccadic segment. The blue arrow is the fly's path. The dotted lines indicate the angle to the closest part of the arena wall.

This effect does not occur in the CB arena because the moving vertical contrasts sweeping towards the posterior visual field shatter the illusion of back-to-front motion. In fact, this front-to-back motion will be faster on the left hand side (in the situation shown in fig 4.10), because retinal velocity is inversely proportional to distance (section 2.2.1). It has been noted (Srinivasan et al, 1999b) that a simple optomotor response would cause a moving animal to steer *towards* obstacles because of this

effect. The fact that I do not observe this behaviour suggests that the optomotor response is overridden in situations where the optic flow pattern more closely resembles translation than yaw rotation. Again, this provides a useful constraint for modelling visuomotor behaviour.

### 4.5.5: Saccades in the 'wrong' direction

When a fly is approaching the arena wall at a shallow angle, there is clearly a preferable direction to turn in order to guide it away from the impending collision. However, in ~25% of cases, flies are observed turning *towards* the wall (section 4.4.1). Why might they do this?

Perhaps the simplest explanation is that the fly is simply 'mistaken'. Because of its limited visual acuity and/or neural signals being corrupted by noise between the eye and the flight motor, it might fail to make the appropriate evasive manoeuvre. However, this account does not explain the observation that 'wrong' saccades are significantly larger in amplitude than 'correct' ones. Rather, this phenomenon suggests that wrongly-directed saccades are in some way planned. To put it less anthropomorphically, it indicates that saccade direction may be influenced by factors other than the immediately preceding visual experience of the fly.

These large saccades might serve to enhance collision avoidance performance. If a fly is to turn in the wrong direction to avoid a collision, then it is desirable that it makes a large turn. For instance, if the wall approach angle is 30°, then a turn of >60° in the correct direction or >120° in the wrong direction will result in the fly moving away from the wall. Section 4.5.6 discusses whether flies are able to control the size of their saccadic turns. Why the fly would 'decide' to turn towards the wall in the first place remains unclear, although there is some suggestion that free-flying *Drosophila* persistently saccade in the same direction to improve foraging efficiency (Reynolds & Frye, 2007).

In the CB arena, there is a 71.0% chance that any given saccade will be in the same direction as the preceding one. (In HS: 69.4%, CB *versus* HS: $U(24,24)=317$, $p=.55$.) It would be fallacious to conclude from this that flies have an instinctive tendency to persistently saccade in the same direction, as one would expect the directions of subsequent saccades to be correlated if an animal is making roughly right-angle turns in a circular arena. The best way to determine whether this probability is higher or lower than we would expect based on purely environmental factors is to compare it to the behaviour of a model which has no directional bias. Such a model is described in the following chapter.

My discussion thus far has made the implicit assumption that saccades occur for the purpose of collision avoidance. Certainly, a tethered fly will generate saccades away from expanding visual patterns (Tammero & Dickinson, 2002b; Bender & Dickinson, 2006), consistent with this account. However, flies are also found to make spontaneous saccades in the absence of any sensory stimulation (Maye et al, 2007). It is reasonable to assume that an endogenously generated saccade of this kind would be in a random left/right direction, so this process could be the cause of the apparently misguided saccades. If this is the case, then one could hypothesise that endogenously generated saccades are larger than those triggered by exogenous visual stimuli, perhaps even being the result of a separate motor program. While this is only a tentative suggestion based on my data, it is a question that would be relatively straightforward to address in a tethered flight experiment (section 10.2.2.2).

### 4.5.6: Are saccades stereotyped?

The quote I gave from Tammero & Dickinson (2002a) in section 4.5.2 perhaps conflates two separate issues. The first is the question of whether saccades are performed in an open-loop manner without sensory feedback. The second is whether they always follow an identical open-loop program, or whether this can be modulated as a function of the visual input preceding the manoeuvre. Essentially, can a fly 'choose' how large a saccadic turn to make?

In section 4.4.2, I identified a clear association between presaccade velocity and saccade size, but I would suggest that this has more to do with aerodynamic and muscular constraints than visual processing. The observed relationship between collision distance and saccade amplitude can be viewed as a corollary of this effect. However, it appears that a genuine visually-mediated modulation of saccade size may occur on the basis of the angle at which the wall is approached, with shallow angles resulting in smaller saccades. It is noteworthy that this effect is clearer in the HS arena than in CB. A possible explanation for this is that the lack of vertical contrast could make the expansion pole appear to be laterally positioned; laterally presented expansion patterns elicit smaller turns than frontal ones (Bender & Dickinson, 2006).

I would hesitate to take this observation as definitive evidence for visual modulation of saccade amplitude. It is only possible for the fly to approach the wall at a shallow angle if it is close to it, which introduces a number of confounding factors, e.g. aerodynamic effects. Also, if spontaneous saccades are larger than visually evoked ones (as I hypothesise; see section 4.5.5), this could contribute to the correlation, since saccades close to the wall are more likely to be visually triggered.

### 4.5.7: Time-to-contact (*tau*)

It has been argued that time to contact (or *tau*), which is inversely proportional to rate of retinal expansion, is an invariant property used by a wide variety of animals to detect looming objects (Lee, 1976; Lee & Reddish, 1981). An example relevant to this study is Wagner's (1982) claim that the point at which houseflies approaching a target initiate deceleration corresponds to a critical ratio of image expansion velocity to image size, i.e. tau. More recently, the tau hypothesis has been criticised, as experiments have shown that time-to-contact judgements are situation-dependent, and reflect constraints of the nervous system (reviewed in Wann, 1996; Tresilian, 1999). Borst & Bahde (1988) show that landing responses in houseflies depend on a number of variables besides tau, including pattern position and pattern size. They argue that their findings point towards a system where expansion signals are temporally integrated until a threshold value is reached. More recently, tethered *Drosophila* have been found to saccade away from highly textured looming targets earlier than uniform ones (Bender & Dickinson, 2006), contradicting the tau account.

In section 4.4.1 I identified that because flies in the HS arena move faster and saccade closer to the walls, their projected time to collision when making saccades is markedly shorter than that of their CB counterparts. This parallels Bender & Dickinson's (2006) observation that flies are much slower to respond to shapes expanding in only one dimension, as this is essentially the case in the HS arena. My findings thus represent further evidence against the tau hypothesis, as they highlight the fact that the structure of visual objects can have a profound effect on the animal's ability to estimate their expansion. Attempting to ascertain the precise nature of the algorithm used by the fly to detect expansion is one of the key objectives of the modelling work described in the following chapter.

# 5. Modelling visuomotor behaviour

This chapter describes the implementation of a closed-loop model of visual flight control in simulation, based upon the *Drosophila* behaviour presented in the previous chapter. I begin describing how local motion detection is achieved (section 5.1). After briefly covering how the environment is simulated (section 5.2), I discuss in detail how wide-field motion signals can be used to control various behaviours (section 5.3), and how parameters of these visuomotor controllers can be tuned (section 5.4). Having built a model it is of course essential to characterise its behaviour and compare it to that of real *Drosophila* (section 5.5). I conclude the chapter with a discussion of the model's validity (section 5.6).

## 5.1: Peripheral visual processing

### 5.1.1: Optics

The two most important biological parameters for modelling the optical characteristics of *Drosophila's* compound eye are the interommatidial angle, i.e. the separation between adjacent facets, and the angular sensitivity of each ommatidium, which can be modelled as a 2D Gaussian distribution centred on its optical axis (Neumann, 2002). Together, these parameters define the spatial resolution of the fly's vision. According to Stavenga (2003), the average interommatidial angle is approximately 5°, and the s.d. of the sensitivity function is 1.5°.

To simulate the optical properties of the *Drosophila* eye I generate a visual scene at a resolution higher than that of the eye and then downsample it using Gaussian receptive fields with s.d. = 1.5°. Each Gaussian represents a single ommatidium. For efficiency, the Gaussian function is truncated, restricting the weighted sum to a 9x9° square around the central pixel (fig 5.1). The resolution of the initial image represents a trade-off between precision and performance; higher resolution means that the Gaussian functions are more closely approximated, but the number of computations per ommatidium increases quadratically. Because the model will need to be run many, many times to properly explore its parameter space (section 5.4, also see chapter 8), I have opted to use a relatively coarse inter-pixel angle of 1.8°.

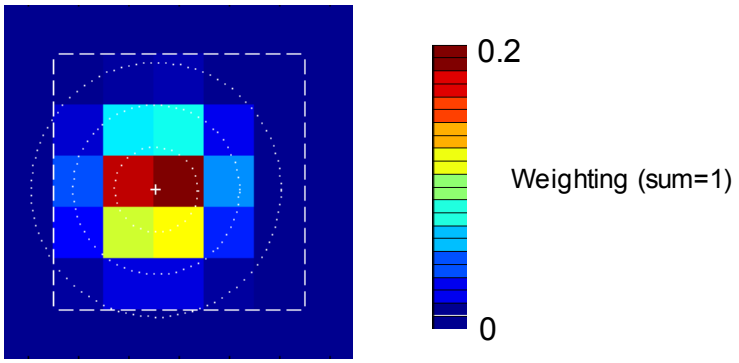


Figure 5.1: Heat-map showing weightings of pixels for an ommatidium centred on the position of the white '+'. Pixel size is 1.8°. Dotted circles show 1, 2 and 3 standard deviations (s.d. = 1.49) of the Gaussian sensitivity function. The dashed box shows the extent of the local neighbourhood that contributes to the Gaussian; all pixels outside of this region are given zero weighting.

For the sake of modelling simplicity and flexibility, I do not insist that ommatidia are arranged into a regular grid, like the hexagonal lattice of the *Drosophila* eye. Instead they can be placed arbitrarily on the retina (section 5.3) using the procedure illustrated in fig 5.1. However, the two input channels of any EMD (section 5.1.2.1) will always be separated by exactly 5°, i.e. the interommatidial angle of the fly.

## 5.1.2: Motion detection

### 5.1.2.1 Methodology

Motion detection is achieved by means of 'delay-and-correlate' elementary motion detectors (EMDs, see section 2.2.2). This mechanism represents a very well established theory of insect motion detection supported by electrophysiological recordings (Single & Borst, 1998; Haag et al, 1999; Haag et al, 2004), which has been used as the basis for many modelling studies (e.g. Reiser & Dickinson, 2003; Higgins et al, 2004; Borst et al, 2005; see chapter 2).

EMDs respond in a direction-selective manner to local movement, by comparing the current input from one ommatidium to a delayed signal from an adjacent one (Götz, 1968). In a canonical EMD, two mirror-symmetric half-detectors of this type are paired and the output of one is subtracted from that of the other, which serves to cancel out components of the signal not due to movement. A biologically reasonable way of introducing a delay to one of the two channels is by using a first-order lowpass filter (LPF). The time constant ($\tau$) of this LPF defines the optimal temporal frequency of a canonical EMD as described by equation 5.1 (Zanker et al, 1999). Duistermars et al (2007) showed that *Drosophila* respond optimally to temporal frequencies around 7Hz, corresponding to a $\tau$ of 23ms.

$$f_{optimal} = \frac{1}{2\pi\tau_{LPF}} \tag{5.1}$$

Clearly, the signals from many EMDs must be combined if wide-field motion is to be detected. To achieve this I follow the method proposed by Borst et al (1995), described in equation 5.2. This deviates slightly from the canonical EMD specification, representing a highly simplified model of the dendritic integration that takes place on the LPTC (see section 2.3.3.1).

$$output = \frac{\sum_{i=1}^{n} exc_i - \sum_{i=1}^{n} inh_i}{\sum_{i=1}^{n} exc_i + \sum_{i=1}^{n} inh_i + n \cdot leak} \tag{5.2}$$

$exc_i$ and $inh_i$ are the outputs of the two symmetrical halves of EMD *i*, and *leak* is a constant analogous to the LPTC leak current. The positions and orientations of the EMDs included in the set which is summed over determine the type of optic flow (section 2.2.1) to which this wide-field filter will be sensitive. The above mechanism can be used to achieve the phenomenon of *gain control* that is seen in some fly visual cells (2.3.3.1), whereby the response increases sub-linearly with increasing pattern size. The extent to which this occurs is determined by the *leak* parameter (section 5.1.2.1).

Compared to simply summing or averaging the outputs of EMDs, normalising the response in this way creates a problem: spurious signals (i.e. those not related to motion) are no longer cancelled out at the level of ommatidium pairs, and can therefore drown out genuine movement signals. For instance, imagine the situation where both ommatidial inputs to an EMD are seeing a constant white image. The two channels will be highly correlated, so both half detectors (i.e. $exc_i$ and $inh_i$) will output a large signal despite the fact that no visual movement is taking place. This will dilute the output of the ensemble towards zero (see equation 5.2).

This issue is addressed by adding first-order high-pass filters (HPFs) with $\tau$=10s to the input lines. This models photoreceptor adaptation, and means that parts of the visual scene which never vary will gradually be ignored. This elaboration has the side-effect of shifting the EMD tuning curve towards higher frequencies, so I empirically adjusted $\tau_{LPF}$ to 40ms to maintain the optimum response at 7Hz. The addition of HPFs also means that the motion detection system takes several tens of seconds to reach equilibrium, so it is important to allow it to adapt appropriately before beginning an experiment. The whole system is summarised in fig 5.2.

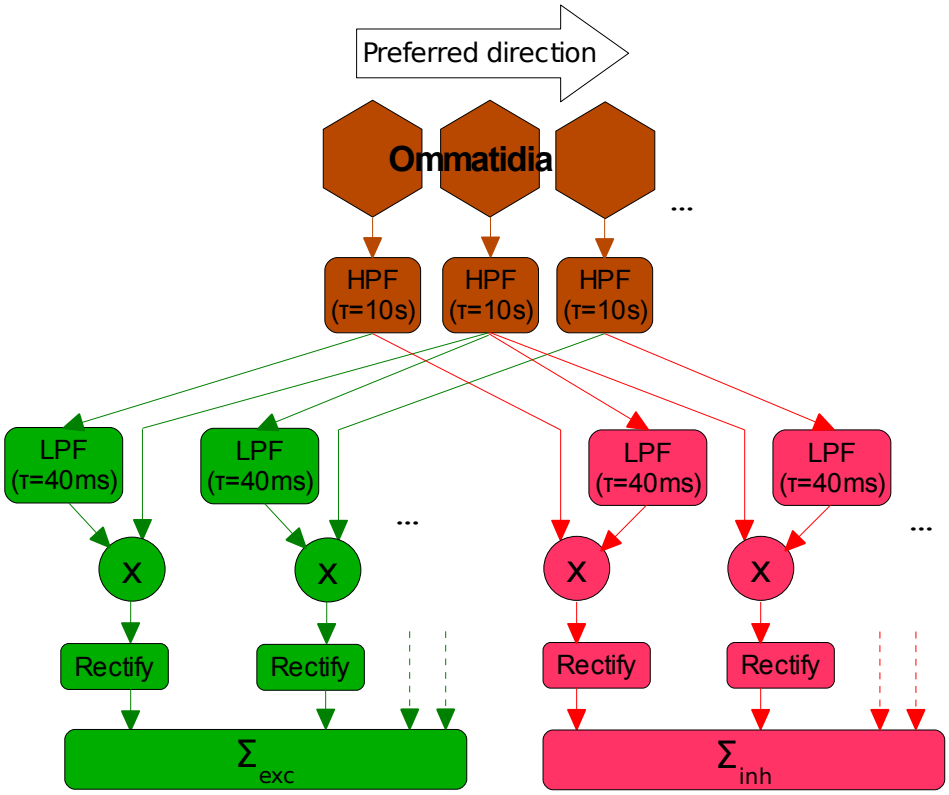


Figure 5.2: Schematic representation of the motion detection system. The brown portion represents the inputs from the compound eyes. Signals from adjacent ommatidia are fed to a half-detector which responds to movement in the preferred direction (green) and a mirror-image counterpart (red). Each half detector multiplies the delayed signal from one ommatidium with the undelayed one from another, and rectifies the result (i.e. sets negative values to 0). The outputs from many such units are summed, and the sums are combined as shown in equation 5.2 to produce a scalar output.

#### 5.1.2.2 Results

This section gives the results of some simple test runs to characterise the behaviour of an ensemble of EMDs. I use a 1D array of 35 EMDs evenly spaced around the full 360° of azimuth. The interommatidial angle for input pairs is 5°. The ensemble is exposed to a rotating square-wave pattern, using a simulation timestep of 1ms.

Fig 5.3 shows the raw output of the ensemble over a sample run. Note that a steady-state value is never reached, but rather the system oscillates continually about a fixed point. It reaches a relatively stable state within a few hundred ms. This would appear to be at odds with my earlier claim that the system would take tens of seconds to adapt. The reason for this is that all of the EMDs are receiving highly variable inputs, so little slow adaptation of photoreceptors is taking place.

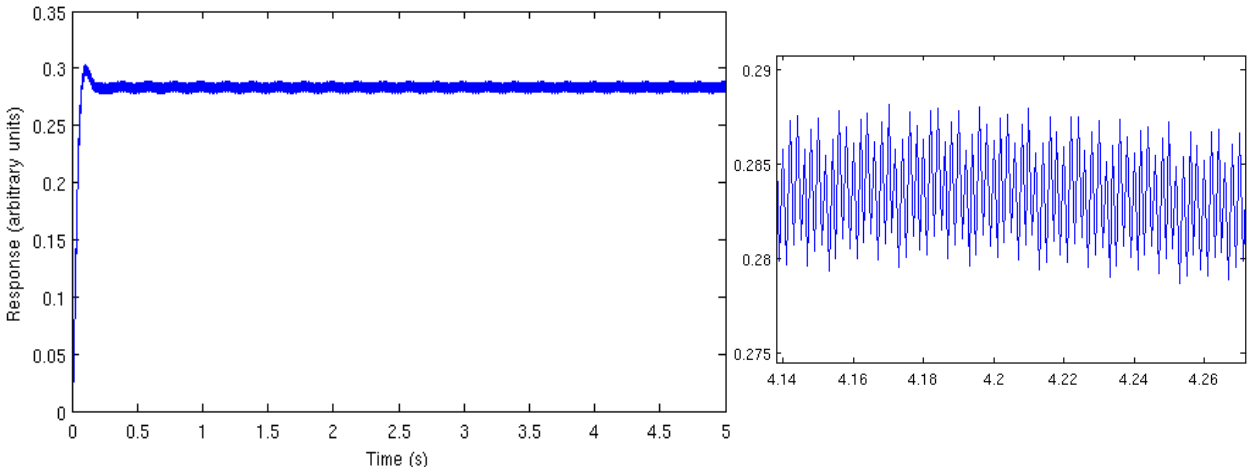


Figure 5.3: Output of the EMD array. Pattern wavelength (λ) = 20°, pattern velocity (v) = 100°s$^{-1}$. (Therefore, temporal frequency (f) = 5Hz.) On the right is a zoomed view showing fine temporal structure.

This situation can be changed by adding an additional 35 'distractor' EMDs, which receive high input (i.e. white) at all times. As fig 5.4 shows, it takes around 30s for the output to level off. This ensemble reaches a lower stable range, because of the increased 'leak' caused by the extra EMDs (equation 5.2). However, note that the response is slightly greater than half of that seen in fig 5.3, indicating that some degree of gain control is occurring.

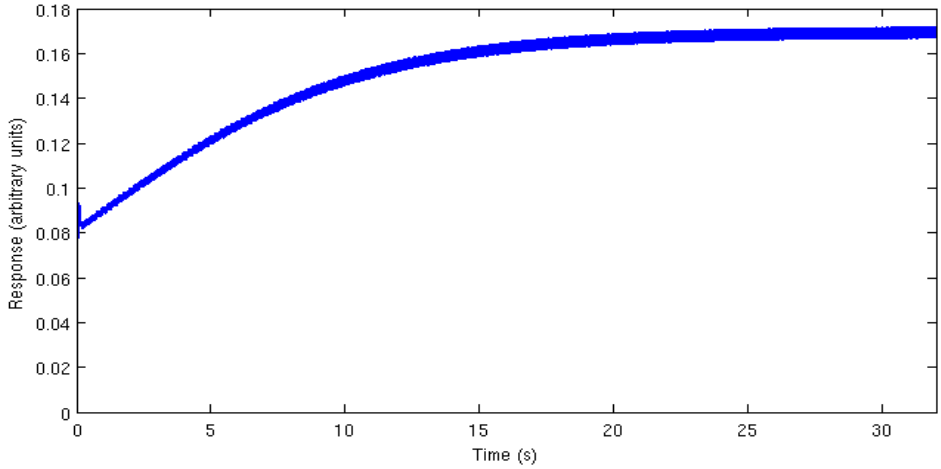


Figure 5.4: As fig 5.3, but with the addition of 35 'distractor' EMDs that receive constant high inputs.

It must be borne in mind that the constant-velocity rotating patterns I use in these tests are highly unnatural stimuli; typically a fly would not receive the 30-plus seconds of exposure to the same retinal motion pattern required to reach a stable state. These experiments are merely intended to demonstrate that the fly's stimulus history (or lack of it) extending back tens of seconds can influence its current response, which must be taken into account when performing further tests. Thus, although the distractor EMDs will not be included in the following experiments, each experiment shall be

preceded by 40s of adaptation time, using a large simulation timestep (125ms). The system is then run at full (1ms) temporal resolution for 5s, and the output value is calculated by taking the mean signal over the final second. The purpose of the following experiments is simply to characterise the behaviour of the motion detection system in tightly controlled conditions as a precursor to investigating the model in more realistic scenarios.

Fig 5.5 shows the results of varying both the speed and the wavelength of the square wave pattern. It is immediately obvious that the system's response depends upon temporal frequency (see section 2.2.2), since the optimal velocity increases as the wavelength does. At the smallest wavelength (11.25°), performance drops off catastrophically. This is because the spatial frequency of the pattern is approaching the Nyquist frequency, defined as half of the sampling frequency. Since the interommatidial angle is 5°, patterns of wavelength <10° will cause the system to give erroneous outputs due to aliasing. Of course, given the angular sensitivity of the ommatidia (section 5.1.1), it would not be able to properly resolve these patterns anyway. A more gradual decline in response amplitude is seen for large wavelengths, caused by the patterns becoming increasingly sparsely textured.

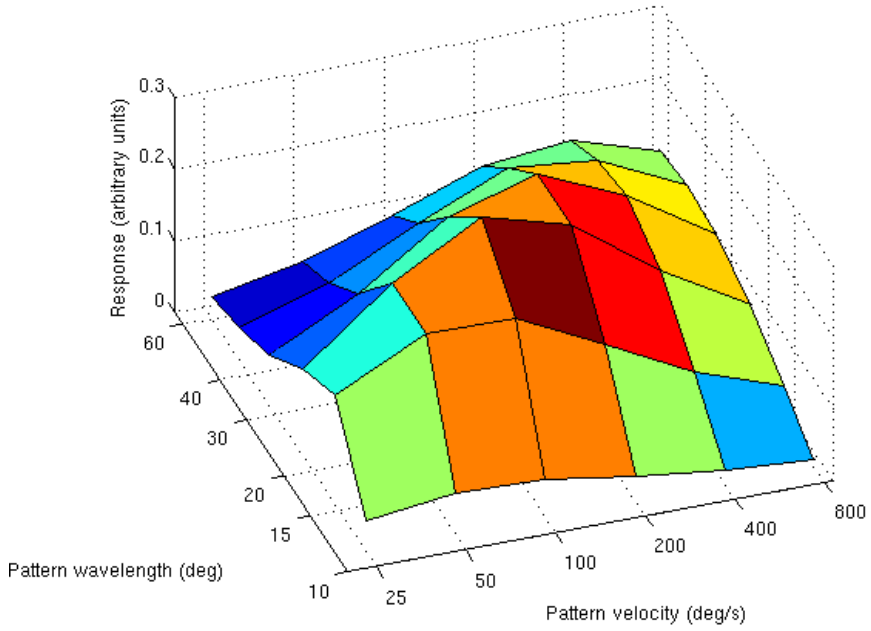


Figure 5.5: Mean stable response of the 35 EMD ensemble to square-wave patterns of varying velocity and wavelength.

The leak parameter determines the extent to which the EMD ensemble's response saturates with increasing pattern size. This point is illustrated in fig 5.6, which shows the response to a stimulus consisting of the square wave pattern covering 180° of azimuth and uniform grey covering the other

half. This is plotted as a proportion of the response to the full-size pattern. As *leak* gets smaller, the ensemble's response becomes increasingly invariant with respect to pattern size.

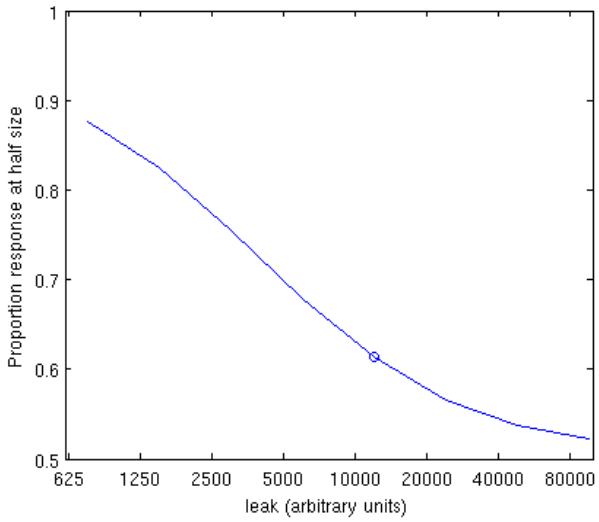


Figure 5.6: The leak parameter determines saturation. Graph shows the EMD ensemble's response to square wave patterns (λ=22.5°, v=100°s$^{-1}$) of size 180°, expressed as a proportion of the response to the full-size pattern. A small leak constant causes the proportional response to approach 1, corresponding to pattern size invariance. Large values for this parameter result in a value tending towards 0.5, i.e. output increasing linearly with pattern size. The circle marks the value used in the model.

It is not possible to use biological data to set a value for this parameter for a number of reasons:

- I do not intend to model specific LPTCs, so it is not clear which cell(s) would offer a suitable basis for the model. Furthermore, most experiments detailing the response properties of LPTCs are performed in larger flies.
- Even if LPTC electrophysiological data were available, it is very likely that this signal would be subject to many non-linear transformations and modulations before reaching the flight motor, making the task of accurately modelling any single LPTC's response somewhat futile.
- Conversely, while some detailed data exists regarding tethered *Drosophila*'s behaviour responses to various visual stimuli (Tammero et al, 2004; Bender & Dickinson, 2006) it is extremely difficult to relate these findings to individual LPTCs.

In all subsequent experiments the leak parameter is set to $1.2 \times 10^4$ (fig 5.6). This value is the result of manually tuning the closed-loop visuomotor model (section 5.3) to produce appropriate behaviours across the various visual conditions. Note that high values for this parameter tend to increase the model's sensitivity to the spatial density of moving visual contrasts, thus promoting larger perceptual differences between the richly textured CB and sparsely textured HS environments.

## 5.2: Environment simulation

In the previous section I described the implementation and performance of EMDs - the basic components of the model fly's visual motion detection system - and how these can be combined into wide-field motion filters. Before addressing the question of how these filters may be used for flight control, I first discuss the other half of the closed-loop system: the simulation of the environment which supplies the sensory inputs to the model fly based upon its actions. This section also includes those elements of the model fly's behaviour which are outside the control of the visuomotor system, as they can in some sense be considered part of the environment in which the controller operates.

### 5.2.1: Simulation of visual input

The fly's visual environment is simulated by means of a custom written Java program. The walls of the simulated arena are patterned identically to the wallpapers used in the free-flight experiments, and have 100% contrast. The floor and ceiling are uniformly black.

As described previously (section 5.1.1), the visual surround is mapped onto a 2D image at 1.8° resolution, and the ommatidal inputs to the visual system are obtained by subsampling this using the appropriate Gaussian sensitivity profile. While the 2D projection step is not strictly necessary, it greatly improves the program's efficiency (not to mention simplicity) compared to computing multiple ray-trace operations for every EMD input.

One cannot map the spherical visual surround onto a plane without introducing distortions. Perhaps the most intuitive mapping is a Mercator projection (fig 5.7), which is directly analogous to the system used to identify positions on the globe, with elevation and azimuth replacing latitude and longitude, respectively. Essentially, it approximates the eyes as a cylinder (with a vertical axis) onto which the visual surround is projected, since unwrapping a cylindrical surface to a plane is trivial. This scheme maintains a near-orthogonal representation of the area around the equator (i.e. elevation = 0°), but stretches the space near the poles (i.e. elevation = ±90°; the fly's dorsal-ventral axis) in the azimuthal dimension. Thus while the angle between any pair of ommatidia forming the inputs to an EMD is always 5° in Euclidean space, near the poles it may be considerably less in 3D space. While this caveat should be borne in mind, it is in fact of little consequence, as only one of the optic flow filters (see section 5.3.3) features EMDs at extreme elevations (i.e. < -60°) , and due to their orientations they have small azimuthal components. Furthermore, unless the fly is very close to the wall, there is no visual texture at extreme elevations, since the floor and ceiling are black (fig 5.7).

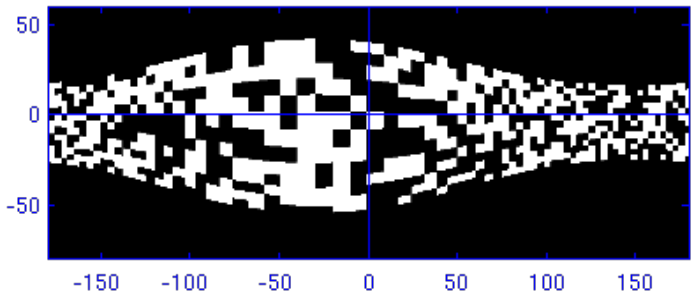


Figure 5.7: A sample of the model fly's retinal image in the chequerboard arena. Angles in degrees.

To simulate the fly's visual experience one needs to know not only its position, but also the yaw, pitch and roll orientation of its head. Due to the limited resolution of the free-flight tracking system, this data is unavailable. I have already argued that the fly's yaw orientation can be reasonably approximated by assuming it is aligned with its direction of flight (section 3.5.2). I make the further assumption that the fly maintains a perfectly constant pitch and roll orientation, as would be the case if it moved its neck to compensate for changes in body orientation associated with flight manoeuvres. Indeed, blowflies are known to at least partially cancel out body movements by such a mechanism (Gilbert et al, 1995; van Hateren and Schilstra, 1999; Huston & Krapp, 2008).

### 5.2.2: Non-visual flight control

For the sake of modelling parsimony, I hold the model's altitude constant. Although models of visual altitude regulation exist (Neumann & Bülthoff, 2002; Franceschini et al, 2007), it is difficult to envisage how these apply to this paradigm, where the floor of the arena is ostensibly untextured, but very probably has uncontrolled irregularities which flies can detect and utilise. Because flies' mean altitude does not differ across any of the visual environments tested (section 4.2), it seems reasonable to treat altitude regulation as being independent of vision in this experimental paradigm. The altitude is set at 36cm, which is lower than the mean altitudes reported in chapter 4, but is typical of free flight behaviour in the presence of food odour (chapter 6). I decided it was most appropriate to keep this parameter constant to facilitate more direct comparisons between odour and no-odour behaviour of the model.

If the model fly comes within 8cm of the arena wall, and is not already performing a saccade, it will initiate an 'emergency' saccade away from the wall. While this is included for primarily practical reasons to prevent wall collisions by the simulated fly, there are a number of possible mechanisms the fly could use for such emergency turns, e.g.:

- Backwash from the fly's wingbeats could be detected within a few cm of the wall (Robert &

Göpfert, 2002),

- A visual collision avoidance system could exist that initiates escape manoeuvres when expanding shapes reach a critical threshold size (Holmqvist & Srinivasan, 1991; Bender & Dickinson, 2006). This would be distinct from the wide field motion integration system of collision avoidance introduced in section 5.3.4.
- The fly's collision avoidance system could be stimulated by fine contrasts on the walls (e.g. the texture of the paper) that would only be resolved at very close range, and are not included in the simulated arena.

## 5.3: Visuomotor system implementation

This section is concerned with the issue of mapping visual motion signals to flight behaviour. My visuomotor model consists of three parallel subsystems: the optomotor response controlling gradual turning; a speed regulator based upon translational optic flow; and an expansion detector used to initiate saccades for collision avoidance. These are described in turn. First though, I feel a brief digression to remind ourselves of some of the issues involved in scientific modelling is warranted.

### 5.3.1: Modelling approach

In section 1.6 I discussed the general philosophy of how modelling can contribute to scientific understanding, and also how it can go wrong. In this section I consider how these issues relate to the particular problem at hand.

Developing a model that adequately reproduces the target system can be thought of as a search problem. Unfortunately, in this case the search space is essentially infinite, as there are limitless ways in which EMDs can be combined to produce wide-field filters, countless transfer functions to map the time-varying output of these filters to motor commands, and so on. One approach I take to address these problems is to, whenever possible, impose constraints based upon reasonable assumptions.

For example, I have already assumed that all EMDs have the same time constants. This constraint is based upon the the finding that optomotor and collision avoidance responses exhibit the same frequency dependence despite having (presumably) different sets of EMD inputs (Duistermars et al, 2007). This greatly reduces the space of possible filters. I further constrain the search by making the assumption that filters match the optic flow patterns corresponding to pure translational or rotational optic flow, since electrophysiological data from blowflies shows that the optimal stimuli for wide-

field motion sensitive neurons bear a close resemblance to such patterns (Krapp and Hengstenberg, 1996; Krapp et al, 1998; see section 2.3.3.2).

A more general constraint is that algorithms must be biologically plausible. This is a somewhat ill-defined concept, as it is currently not fully understood what types of computations can or cannot be performed by neural systems. I take the pragmatic approach that all computations must be essentially analogue (though of course they are performed on a digital computer), i.e. that the addition of Gaussian noise to signals would not result in catastrophic failure.

Another guiding principle is that of favouring parsimony, often referred to as Occam's razor. This is another slightly slippery concept, as it is in general difficult if not impossible to determine objectively that one model is simpler than another. I interpret this maxim to mean that every elaboration to the control loop must be justified, either by empirical data indicating that such a mechanism must exist, or by demonstrating that the target behaviour cannot be produced without it.

## 5.3.2: Optomotor response (OMR)

The optomotor response (OMR) is perhaps the most straightforward visual reflex to model, as it is reasonable to assume that the appropriate optic flow filter is one corresponding to pure yaw rotation. Fig 5.8 shows an example of such a filter. It is truncated at around ±60° elevation, since little retinal movement is seen near the axis of rotation, and as previously noted (section 5.2.1), the projection becomes highly distorted at extreme elevations.

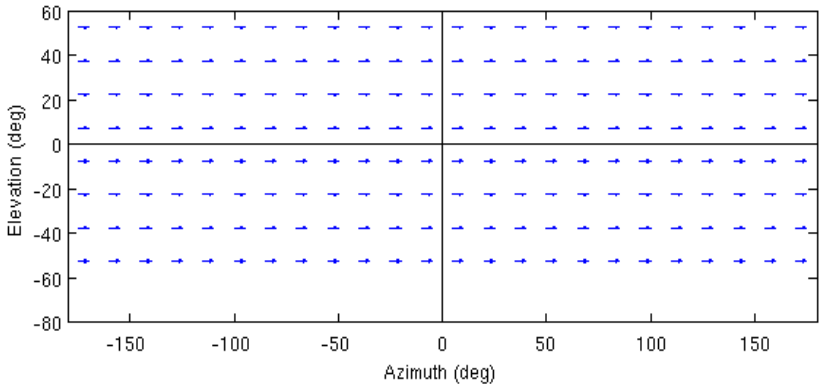


Figure 5.8: Candidate filter to drive the optomotor response. Each arrow represents a single EMD, with the endpoints denoting the positions of the two ommatidia giving input. The separation between the input channels is always 5°. The field corresponds to pure yaw rotation.

While the filter shown in fig 5.8 was used initially, after some investigation I settled upon the one presented in fig . Once again, the EMDs are all aligned with the the optic flow field corresponding to pure yaw rotation, but they are now distributed non-uniformly according to equation 5.3,

$$azimuth_i = i^2 + i + 1 \tag{5.3}$$

where $azimuth_i$ is the azimuth in degrees of the 'to' channel in the left hemisphere, or the 'from' channel in the right hemisphere (fig , blue and red respectively) of EMD column $i$, $i$=1...12. This increases their density in the frontal portion of the visual field, which serves to selectively enhance the OMR system's tendency to steer the model towards vertical contrasts, as is explained in section 5.4.4.

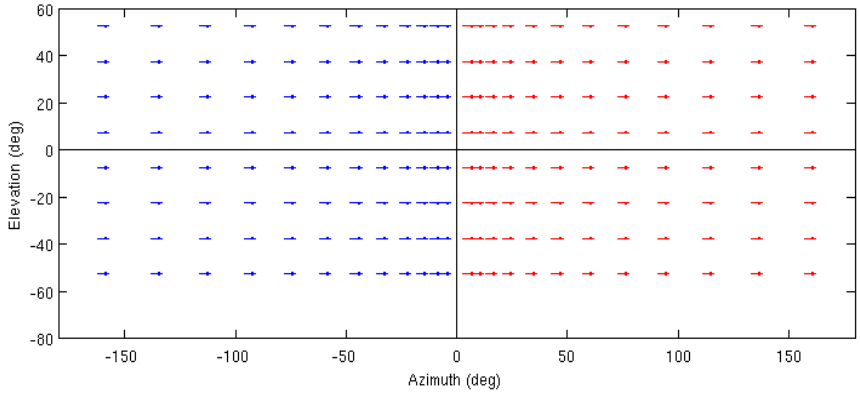


Figure 5.9: The actual OMR filters used in the model. There are two separate filters, one for each visual hemisphere. Comparing the signals from either side allows the model to distinguish translational optic flow from rotational (fig 5.10). EMD azimuths are determined using equation 5.3, elevations are at 15° intervals from -52.5° to +52.5°.

The response is passed through a first-order lowpass filter (τ=40ms) to model the dynamics of neural signal transduction. This is then passed to a leaky accumulator (τ=300ms) to remove noise by temporal averaging. The level of this accumulator is used directly to control angular velocity, via a gain parameter which must be manually tuned (section 5.4.4).

As I mentioned in section 4.5.4, a naive implementation of the OMR would cause a moving animal to steer *towards* obstacles, because the side on which objects are closer will experience more rapid front-to-back motion. However, I do not observe this behaviour in the chequerboard arena (section 4.3.1), suggesting that the OMR is overridden in situations where the optic flow pattern more closely resembles translation than yaw rotation. Hence, the OMR is driven using two large field cells, one for

each visual hemisphere (fig ). The outputs of these are multiplied, and if the product is below a negative threshold value (i.e. if the two signals are of different polarity and neither is close to zero), the optomotor response is suppressed entirely. The whole process is illustrated in fig 5.10.

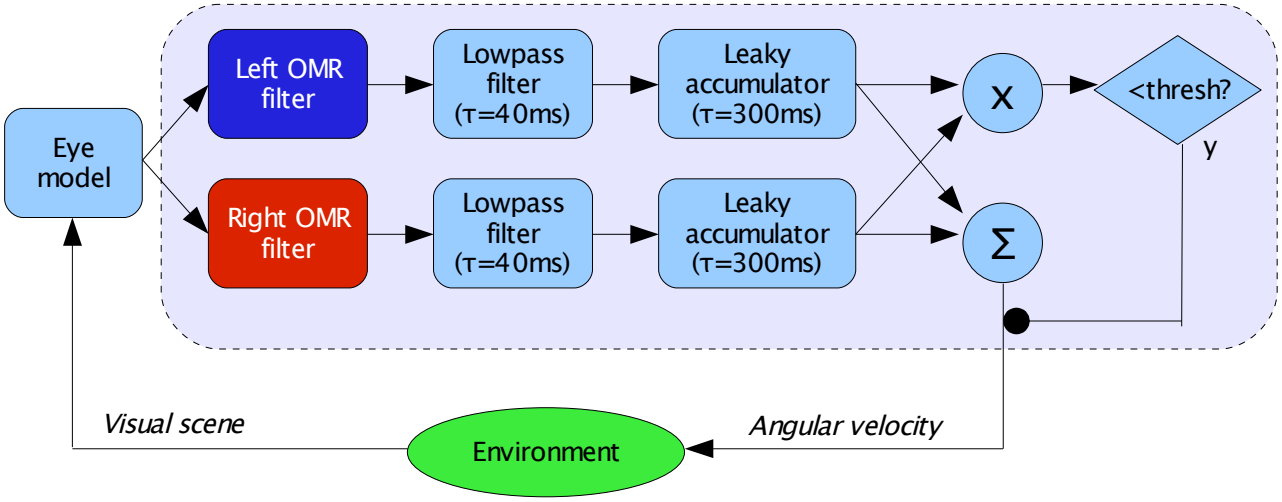


Figure 5.10: Control diagram of the OMR system. The dark blue and red boxes represent the filters shown in fig ), which detect optic flow patterns corresponding to yaw rotation in the two visual hemispheres. The round-headed arrow represents an inhibition that entirely suppresses the signal on the line on which it impinges, which occurs if the left and right cells have strong but opposite sign responses; *thresh* = -2.0. The gain with which this system modulates angular velocity (in $°s^{-1}$) is 10.0 per ms. The dotted box represents the boundary of the OMR system.

### 5.3.3: Speed regulation (SR)

*Drosophila* clearly use visual information to modulate their flightspeed, as their average speeds vary significantly in different visual surrounds (Tammero & Dickinson, 2002a; Frye & Dickinson, 2007), and they adjust their speed to compensate for motion of their visual environment (David, 1982; Mronz and Lehmann, 2008). A frontally-oriented expansion field is a suitable filter to use for regulating velocity. Additionally, the ventral portions of the visual surround most reliably indicate flight speed (Neumann & Bülthoff, 2002) because the ground will generally be closer than the sky (thus giving a larger signal) and at a more constant distance than objects to the sides. Thus, the filter used is as shown in fig 5.11.

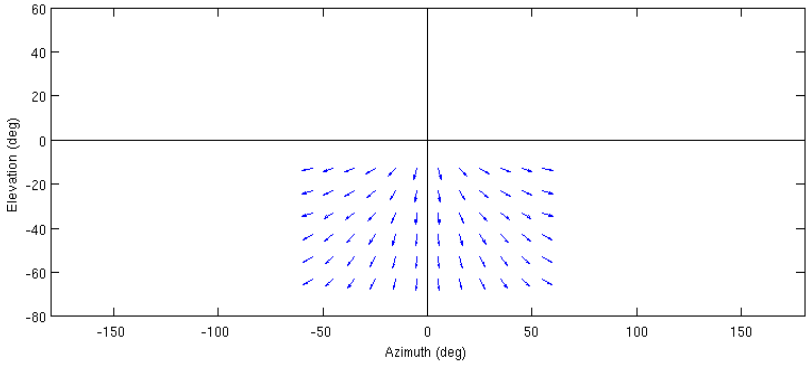


Figure 5.11: The filter driving speed regulation. Azimuths of the 'from' channels of the EMDs are at 10° intervals from -55° to 55°; elevations are at 10° intervals from -13° to -63°. EMD orientations are aligned with translational optic flow originating from (0,0).

A simple proportional controller is used to attempt to keep the visual velocity at a set point, as shown in fig 5.12. Recent work indicates that this is an appropriate model for speed regulation in *Drosophila* (Fry et al, 2009). Although I do not model altitude regulation, a control system of this type has the property that flightspeed increases proportionally with altitude (Franceschini et al, 2007). Note that there is no accumulator in this control loop, as I found that the lag introduced by such a mechanism caused pronounced oscillations in flightspeed.

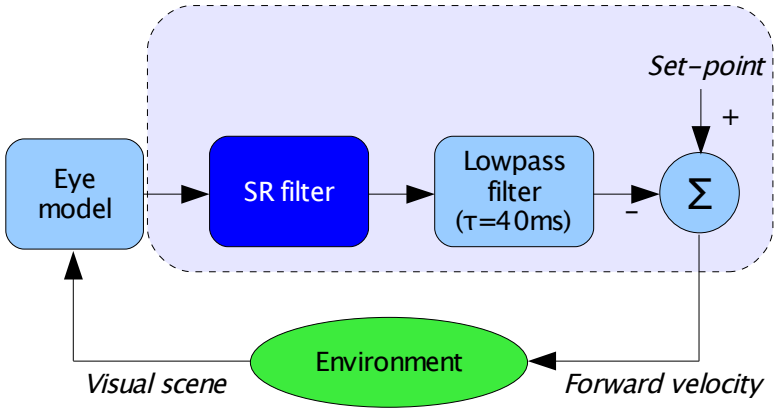


Figure 5.12: Control diagram for the SR system, which uses translational optic flow cues to control the model fly's forward velocity. Set-point is 0.021; the gain with which forward velocity (in $cms^{-1}$) is modulated is 0.18 per ms. The dark blue box represents the filter shown in fig 5.11.

## 5.3.4: Collision avoidance (CA)

In *Drosophila*, expanding patterns trigger collision avoidance saccades directed away from the focus of expansion (Tammero & Dickinson, 2002b; Bender and Dickinson, 2006). One might therefore

suppose that two expansion detectors centred at reasonably large azimuths to either side (as illustrated in fig 5.13) would be an appropriate design for the visual collision avoidance system. Indeed, this is essentially the approach taken by Reiser & Dickinson (2003).

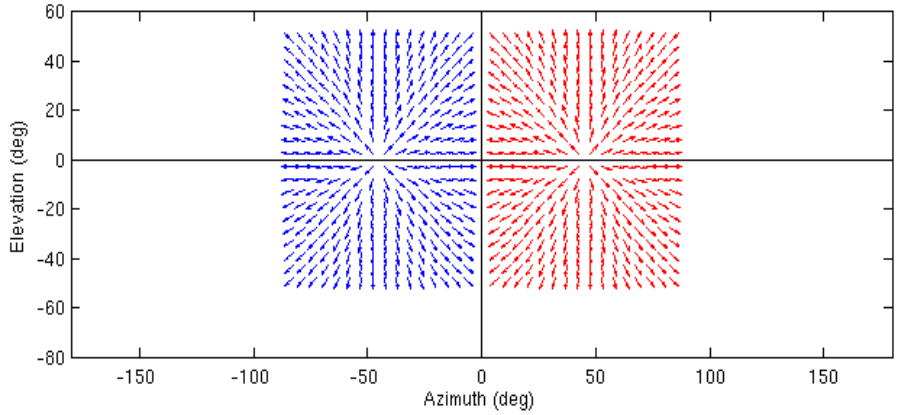


Figure 5.13: A potential configuration of collision avoidance filters, with expansion poles at ±45° azimuth. The blue cell would drive saccades to the right, the red left.

There are however some problems with this scheme (see section 2.2.3). We have assumed that flying *Drosophila* do not side-slip substantially (see section 3.5.2). If this is the case, and the fly is moving in a roughly straight line, then the focus of expansion will always be frontally positioned. These 'matched filters' therefore represent highly unnatural stimuli. Consequently, they will frequently cause the fly to saccade in the wrong direction in situations where horizontal motion cues must be relied upon, as illustrated in fig 5.14.

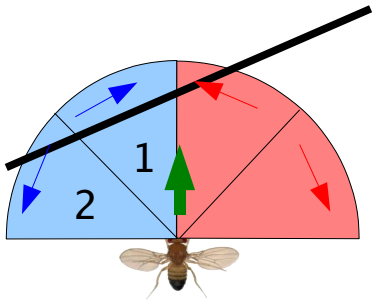


Figure 5.14: The thick black line is a textured wall, the green arrow the fly's vector of motion. The segments represent the receptive fields of the expansion detectors, see fig 5.13, split according to which direction of horizontal motion they are responsive to (red and blue arrows). The more distant an object, the smaller a motion signal it will give, because its retinal velocity will be lower and the fly's eye will be unable to resolve its fine contrasts. Thus, segment 1 will generate a large negative signal, while the positive signal from segment 2 will be attenuated. This will have the result of inhibiting a saccade to the right, i.e. the appropriate direction to avoid a collision. Note that this problem only applies to horizontal motion, which comes from vertical contrasts. A vertically striped arena would therefore represent the worst case for this control scheme, but flies are observed to behave normally in such arenas (Frye et al, 2003).

A frontally-centred expansion pattern split into two halves (as shown in fig 5.15) would resolve the

issue described above, but suffers the problem that a rightward rotation would cause the whole image to move left, promoting a rightward saccade (the blue filter) and inhibiting a leftward one (red), and vice versa.

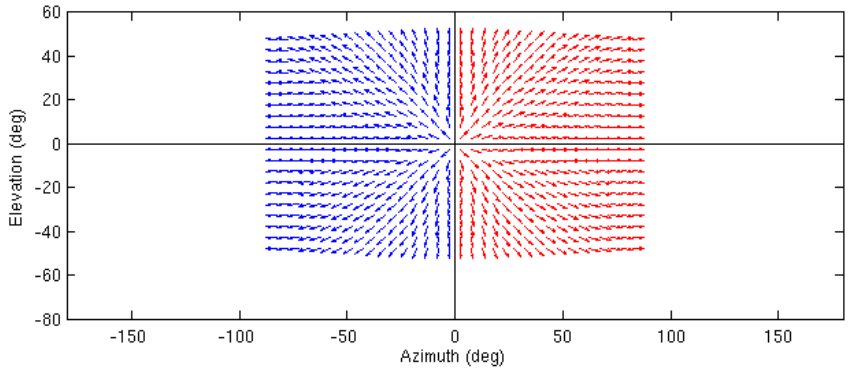


Figure 5.15: An alternative CA filter pair, with a single frontally-centred expansion pattern split down the midline. This would produce saccades in response to simple rotation of the visual field, so is also inappropriate.

Consequently I have chosen filters that represent a compromise between these two extremes (fig 5.16). They have the same spatial extent to either side of the expansion pole, meaning that yaw rotation cancels out. However, they are only offset from the centre by 3°, resulting in a large overlap area. These filters could not be confined to EMDs from a single eye, because each eye can only see up to ~15° into the contralateral visual field (Krapp & Henstenberg, 1996). In my opinion, this does not represent a serious problem for the plausibility of the model, as several binocularly sensitive LPTCs have been identified, albeit in blowflies (Krapp et al, 2001; Farrow et al, 2006; reviewed in Borst & Haag, 2002).

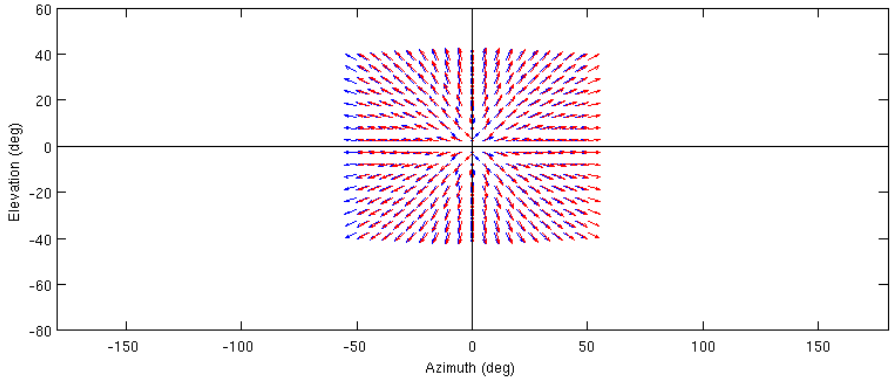


Figure 5.16: The actual CA filters used in the model. Elevations of EMD 'from' channels are at 5° intervals from –37.5° to 37.5°, azimuths are at 5° intervals from -50.5 to 44.5 (blue) or -44.5 to 50.5 (red). EMD orientations are aligned with translational optic flow originating from (-3,0) (blue) or (3,0) (red).

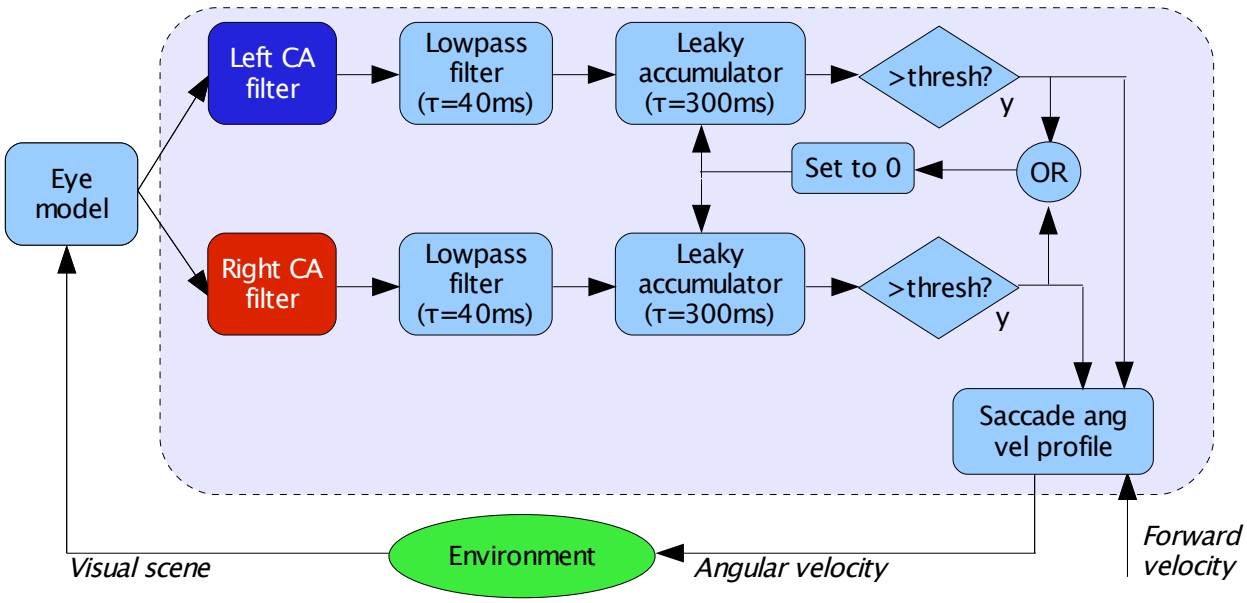


Figure 5.17: Control diagram for collision avoidance. The dark blue and red boxes represent the wide-field filters in fig 5.13. *thresh* = 3.8. Equations 5.4 and 5.5 explain how the saccade angular velocity profile is generated.

The full CA control scheme is shown in fig 5.17. The left and right expansion filters feed into leaky accumulators, and if the signal exceeds a set threshold, a saccade in the opposite direction will be initiated. The model fly then turns according to the predefined angular velocity profile described by equation 5.4:

$$angvel(t) = amplitude \times \left[ 0.7 \exp\left( \frac{-(t-160)^2}{2 \times 28^2} \right) + 0.3 \exp\left( \frac{-(t-160)^2}{2 \times 56^2} \right) \right] \tag{5.4}$$

which is the weighted sum of two Gaussians, where $t$ is in milliseconds from the instant at which the saccade is triggered. Thus the peak angular velocity is reached after 160ms, when the term inside the square brackets is equal to 1. This profile is based upon free-flight data, as shown in fig 5.18.

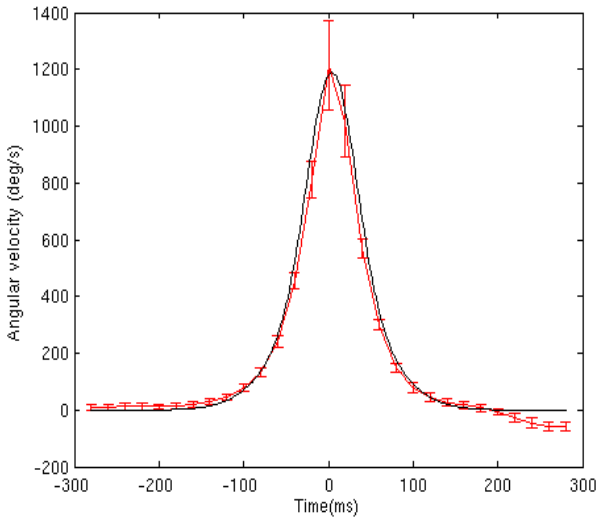


Figure 5.18: The mean angular velocity profile for saccades within 6cm of the centre of the HS arena is shown in red. Due to the lack of vertical contrast and perspective cues, these saccades are minimally affected by visual feedback, and thus provide the best estimate of the 'pure' motor output that occurs in the absence of optomotor compensation. Bars are 1 s.e.m. The sum-of-Gaussians fit is in black, with amplitude = 1180°s$^{-1}$.

The reset of the leaky accumulators upon initiating a saccade (fig 5.17) introduces a kind of relative refractory period, decreasing the probability of triggering a subsequent saccade for several hundred milliseconds. A hard constraint also exists preventing another saccade from being initiated until 200ms after the saccade peak. Thus, the minimum midpoint-to-midpoint interval between saccades is 360ms, corresponding to a distance of ~10cm assuming a typical speed of 0.3ms$^{-1}$ (see equation 5.6). This explains why wall collisions can still occur despite the emergency avoidance mechanism (section 5.2.2).

The amplitude of the saccade angular velocity profile depends on the fly's flightspeed, as I identified a relationship between these variables in the free-flight data (fig 5.19, also see section 4.4.2). Thus amplitude (in °s$^{-1}$) is given by equation 5.5, where *speed* is in ms$^{-1}$ and $N$ denotes a random Gaussian variable. The parameters in this equation are determined by performing a linear regression on the free-flight data. While visual input might also influence saccade amplitude (section 4.5.6), I ignore this possibility a) for the sake of parsimony and b) because I have insufficient behavioural data to implement a mechanism of this kind.

$$amplitude = (1550 - 1106 \times speed) \times N(1, 0.26) \tag{5.5}$$

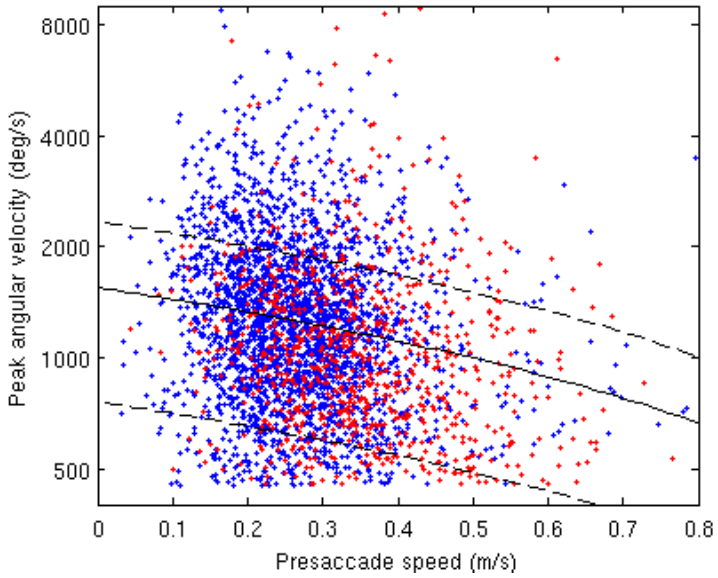


Figure 5.19: Saccade amplitude as a function of presaccadic speed. Blue is CB arena, red is HS. The black line shows the relationship between these variables defined by equation 5.5, with the dashed lines giving the 95% confidence interval of the Gaussian distribution. While the free-flight data is somewhat more variable than the model fit, it should be borne in mind that the more extreme datapoints may represent tracking errors.

During a saccade the fly's forward velocity is reduced according to equation 5.6, which represents the effect of forward thrust being diverted into yaw torque. Again, the scaling parameter is based on free-flight data (fig 5.20).

$$speed(t) = preSaccadeSpeed \times \left(1 - \frac{|angvel(t)|}{4000}\right) \tag{5.6}$$

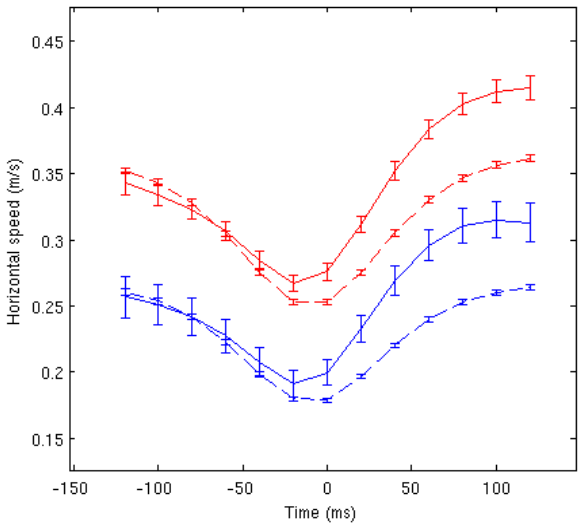


Figure 5.20: Saccade-triggered horizontal speed profiles. Blue is CB arena, red is HS. The solid lines represent free-flight data, the dashed lines are predictions produced by equation 5.6 based on the real fly's angular velocity profile and presaccadic speed. The model is only an approximation of the animal data, failing to capture the asymmetry created by the fly's rapid acceleration out of the saccade. Bars are ±1 s.e.m.

## 5.4: Parameter tuning

In the previous section I described how some modelling parameters could be set based on animal data. Unfortunately, many remain which must be manually tuned to produce behaviour approximating that of flies. Because of the complex ways in which the subsystems interact, it would be impractical (not to mention very tedious) to give a thorough account of the parameter space of the model. Therefore, in this section I simply discuss some relationships between parameter values and model behaviour that I identified during my tuning efforts. First though, it is necessary to describe how closed-loop tests of the full visuomotor model were performed.

### 5.4.1: Methodology

As shown in section 5.1.2.1, it is vital to allow the model to adapt before performing an experiment, because of the many temporal filters used (especially the slow highpass filters ($\tau$=10s) modelling photoreceptor adaptation). In this case it is rather less straightforward to determine how this should be carried out, as a simple constant-velocity visual stimulus no longer exists. The approach I take is to place the model in a different randomly chosen (x,y) position in the arena, with a random yaw orientation, every 125ms for 40 simulated seconds prior to the experiment.

The model is then initialised in a new random position with a velocity of 30cms$^{-1}$. A simulation timestep of 3ms is used. The first five simulated seconds of flight are discarded, as the LPFs and leaky accumulators in the visuomotor systems will take some time to reach normal operating conditions. The trial is only included for analysis if the model continues for a further 30s without colliding with the wall. (Despite the emergency wall avoidance mechanism (section 5.2.2), collisions are still possible, e.g. if the resultant saccade is too small.) Each trial is ended after 40s of recorded flight. Twenty-four trials are recorded for each visual condition, and these are analysed using exactly the same procedures as the free-flight data.

## 5.4.2: Speed tuning

The most important parameter in the SR subsystem is the set-point (fig 5.12), as this defines the desired level of translational optic flow the model attempts to achieve by moving forward. The model's mean intersaccadic speed is rather sensitive to the setting of this parameter, and exhibits an approximately linear relationship with it (fig 5.21a).

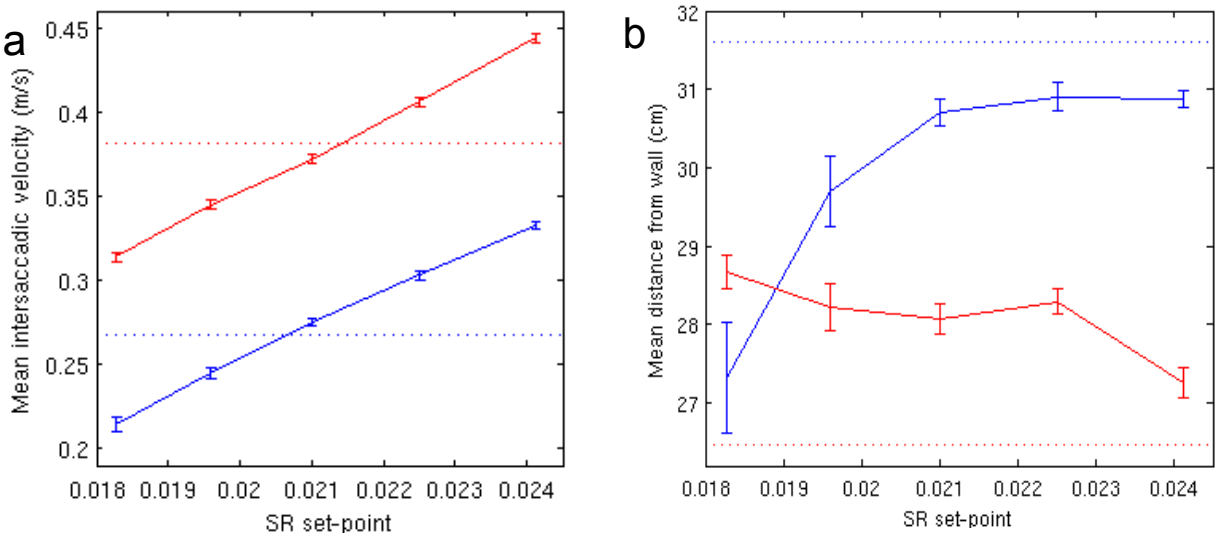


Figure 5.21: SR tuning. Blue lines are CB, red HS. The central datapoint (on the x-axis) is the value used in the final model. Dotted lines show the corresponding statistics from the fly data. Bars are ±1 s.e.m. **a** Intersaccadic speed displays an approximately linear relationship with the SR set-point over this range. **b** The model's mean distance from the wall has a more complex dependency on this parameter. Also, note that while the difference between CB and HS is significant and in the same direction as the fly data over much of the range, the model fails to reproduce the magnitude of the effect seen in real flies.

Fig 5.21b shows that altering the SR set-point not only changes the model's speed, but also its level of wall-aversion. As the model's mean flightspeed drops towards 0.2ms$^{-1}$ in the CB arena, its average

proximity to the arena walls increases sharply. Evidently, the reduction in the expansion signal received by the CA system due to the decreased forward velocity outweighs the shortening of the distance needed by the fly to perceive and turn away from the looming wall. Interestingly, the opposite appears to be true in the HS arena. These observations demonstrate that due to the complex interactions between the model's subsystems, altering any given parameter is likely to have many unpredictable side-effects.

### 5.4.3: Collision avoidance tuning

The key parameter of the CA system is the threshold at which a saccade is initiated to avoid an impending collision (fig 5.17). As one would expect, the higher the threshold, the closer the model approaches the arena walls (fig 5.22a). While this relationship is roughly linear in the HS arena, the same is not true of CB, where wall-aversion drops off quickly as this parameter increases.

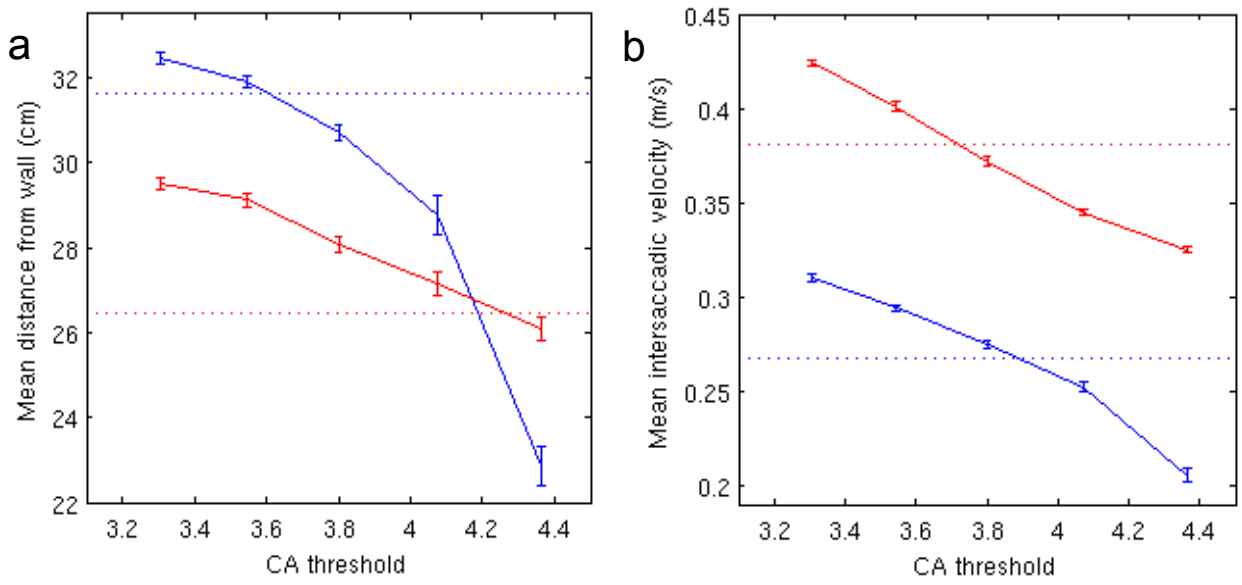


Figure 5.22: CA tuning. Blue is CB, red is HS. As in fig 5.21, the central datapoint (on the x-axis) is the value used in the final model. Dotted lines show the fly data. Bars are ±1 s.e.m. **a** The model's average distance from the arena walls drops as the threshold increases in both visual conditions, but at different rates. **b** Decreasing the sensitivity of the CA system (i.e. raising the threshold) results in slower flight in both environments.

Just as the tuning of the SR system affected wall-aversion (fig 5.21b), the CA threshold has a clear effect on flightspeed (5.22b). This effect is a consequence of the fact the speed of translational optic flow is proportional to the proximity of the visual object. Thus as the model approaches the wall more closely, the SR system causes it to slow down.

Recall that flies are neither attracted to nor repelled by a single vertical stripe in an otherwise horizontally striped arena (the SL arena, see section 4.2). Fig 5.23 shows that the setting for the CA saccade initiation threshold modulates the model's attraction to this vertical landmark. The metric used to quantify this behaviour is the odour localisation index (OLI, section 3.5.1), although of course there is no odour present in the simulation at this stage. Instead, the OLI is used to compare the time spent near the water-filled vial perfectly aligned with the landmark *versus* the other two. A value higher than .333 indicates attraction to the stripe; lower shows repulsion.

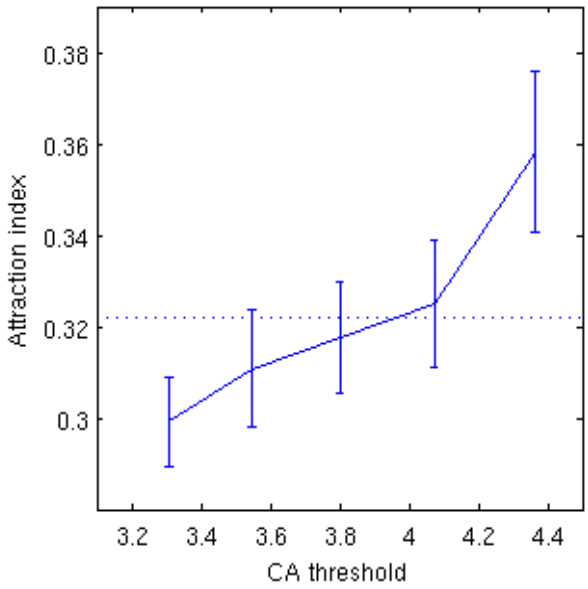


Figure 5.23: Landmark attraction in the SL arena. The statistic used is the OLI (section 3.5.1), calculated as if a vial aligned with the stripe (i.e. positioned midway between the stripe and the arena centre) contained odorant. Increasing the CA threshold promotes attraction to the landmark.

Increasing the CA threshold increases the model's tendency to fly close to the stripe, and vice versa. This finding can be understood in light of fig 5.22a: at high threshold values the model becomes less averse to the the vertical contrasts of the CB arena than the exclusively horizontal contrast of HS, so in the SL arena its flight will become biased towards the vertical stripe and away from the horizontal stripes covering the rest of the wall.

## 5.4.4: Optomotor response tuning

Finally, I turn my attention to the OMR and the gain parameter which determines how strong an effect this has on the model's steering. I shall look in detail at how the model reproduces the optomotor rebound phenomenon (identified in section 4.4.3) in section 5.5.2.2. For now, this effect can be quantified by measuring the average angular velocity 160ms after the saccade peak as a

proportion of the peak angular velocity (fig 5.24).

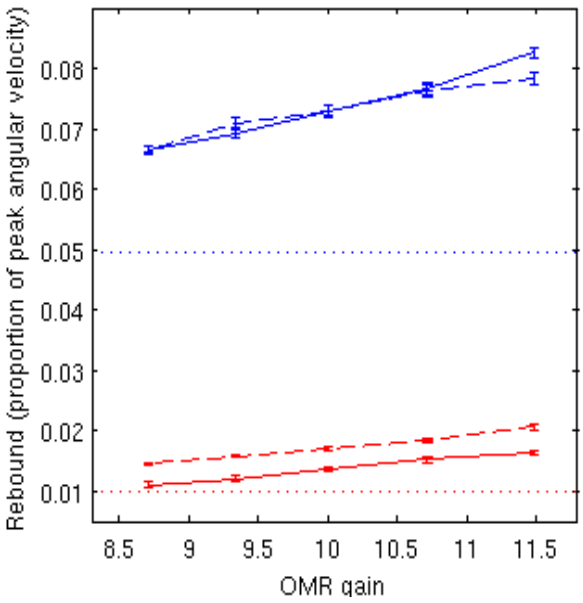


Figure 5.24: Optomotor rebound as a function of OMR gain. Blue is CB, red is HS. The metric used is the mean angular velocity 160ms after the saccade peak divided by the peak angular velocity (which is in the opposite direction). Solid lines are experiments using the frontally concentrated OMR filters (fig ), dashed lines are the uniform filters (fig 5.8). The central datapoint (on the x-axis) is the value used in the final model. Dotted lines show the fly data. Bars are ±1 s.e.m.

Unsurprisingly, the size of the counter-turn following a saccade increases as the OMR gain is raised. Whether the evenly distributed (fig 5.8) or frontally biased (fig ) filters are used makes little difference, especially in the CB arena. This is because the optic flow experienced during a saccade is predominantly rotational, and the retinal velocity of rational flow is independent of object distance, and thus will be equal throughout the image. (More accurately, it is equal for all azimuths of any given elevation, but in fact the distortion created by the Mercator projection means it is equal everywhere.) The difference between the two filter types in the HS arena reflects the fact that the sparse vertical contrast (created by the apparent bulging of the horizontal stripes due to perspective) is not uniformly distributed in the visual field of the model.

Fig 5.25 shows the influence of OMR gain on landmark attraction in the SL arena. Though the data is rather variable, two points are apparent. Firstly, as the gain is increased, the model spends more of its time in the vicinity of the vertical stripe. Second, the frontally-biased OMR filters produce a higher level of landmark attraction than the uniformly distributed ones.

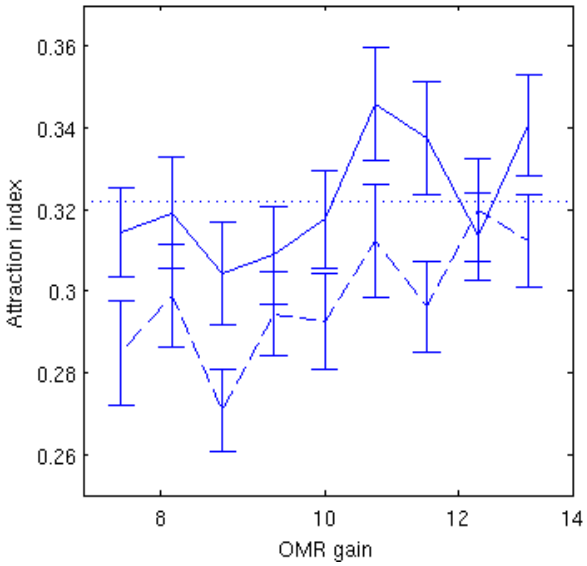


Figure 5.25: Proportion of time spent in a region near the vertical stripe in the SL arena. As in fig fig 5.23, OLI (section 3.5.1) is used to quantify attraction; baseline level is .333. Solid line is using the frontally concentrated OMR filters (fig ), dashed line is the uniform filters (fig 5.8). The central datapoint (on the x-axis) is the value used in the final model. Dotted line shows the fly data. Bars are ±1 s.e.m.

There are many parameters I have not discussed in this section, e.g. the threshold for suppressing the OMR during translational optic flow (fig 5.10), or the gain with which the SR system regulates flightspeed (fig 5.12). Furthermore, the configurations of the wide-field motion filters could be altered in countless ways. However, I have attempted to highlight some of the most important trade-offs involved in tuning the model, and give some impression of the difficulty of 'programming' a non-linear analogue controller of this type.

In the following section I characterise the behaviour of the model implementation that represents the end-result of this tuning process, before discussing in section 5.6 how successfully it reproduces fly behaviour.

## 5.5: Behaviour of the complete visuomotor model

Having implemented local motion detectors, assembled these into wide-field filters forming the input to three closed-loop controllers, built a simulation of the visual environment, and then manually tuned the whole system, I finally present model data similar to that collected from the fly experiments in chapter 4. My methodology is the same as in section 5.4.1; the model is allowed to adapt in random positions in the arena for 40s, then initialised in a random starting position. The first 5s of flight are discarded, then up to 40s of behaviour is recorded to produce one experimental replicate. The

simulation timestep is again 3ms.

### 5.5.1: Spatial distribution

Just as I did in my analysis of the animal data in the previous chapter, I shall begin by discussing the general shape of the model fly's trajectories in each visual environment. Fig 5.26 shows some sample trajectories (c.f. fig 4.2). As in the fly data, flightpaths in the CB arena are slightly concave, while those in HS are convex. Fig 5.27 shows transit probability plots (c.f. fig 4.3). Like its biological counterpart, the model maintains a more centralised position in the CB arena than the HS one.

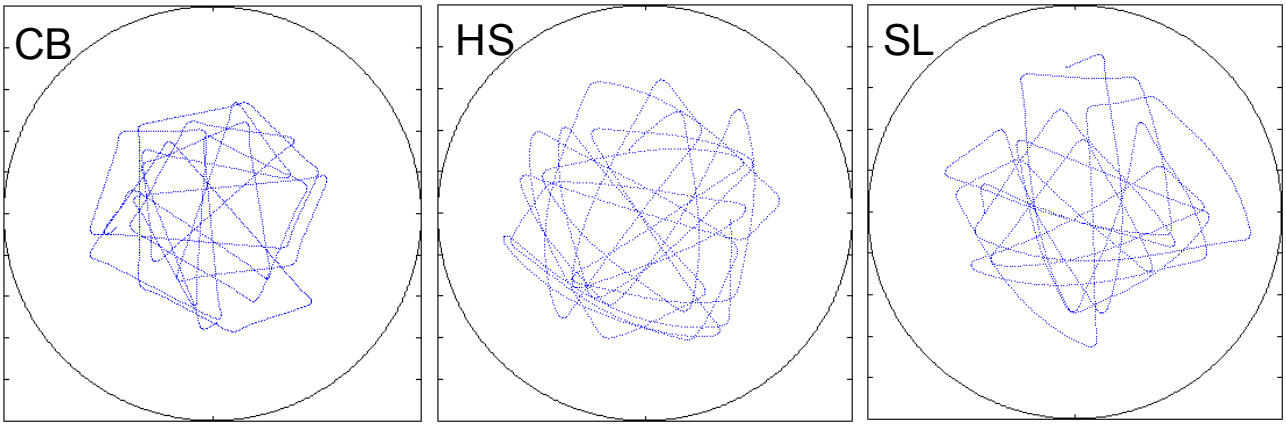


Figure 5.26: Sample trajectories of the model fly. Dots represent its position at 20ms intervals, giving an impression of speed. In the SL arena, the stripe is located at the 12 o'clock position. Fig 4.2 shows analogous data for real flies. 3D data is not presented because the model fly is restricted to a horizontal plane.

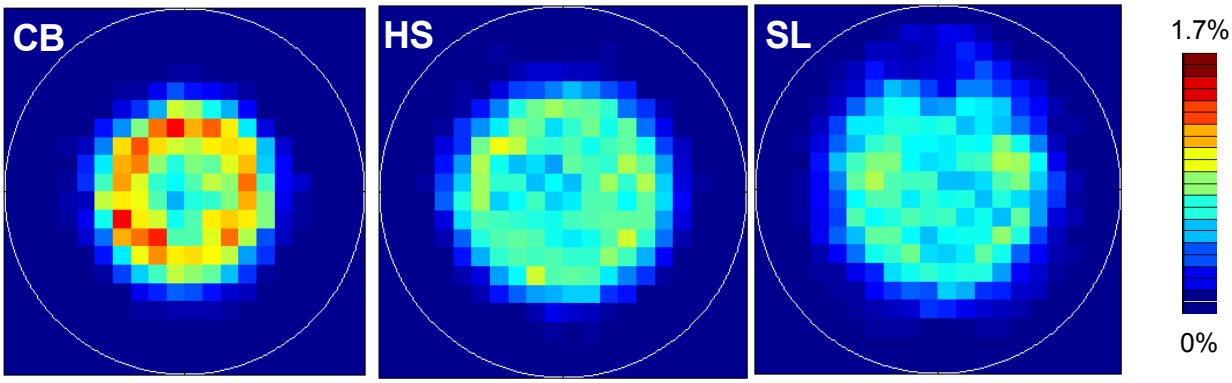


Figure 5.27: Plots of transit probability, i.e. how frequently the fly passes through each grid square (size 5cm). Fig 4.3 shows analogous data from real flies, using the same heat-scale.

### 5.5.2: Homogeneous environments

Fig 5.28 compares a number of flight statistics for the real flies and the model in the two spatially homogeneous environments, CB and HS. Most of these metrics are explained fully in section 3.5. We

have seen that complex relationships exist between many of these statistics, so the following effects should not be considered independent.

Some of the statistics in fig 5.28 were used to tune the model (section 5.4), so it is unsurprisingly that they match closely. One measure of this kind is the model's average distance from the arena wall (fig 5.28a). However, figs 5.28b,c show that the model may be achieving this behaviour in a slightly different way to the fly. These charts show how close to the wall saccades take place on average, in terms of radial distance (fig 5.28b) and distance in the direction of flight prior to the saccade (fig 5.28c). While the model produces the same environment-dependent differences, both measures indicate that the model fly tends to approach the wall more closely before saccading than its biological counterpart.

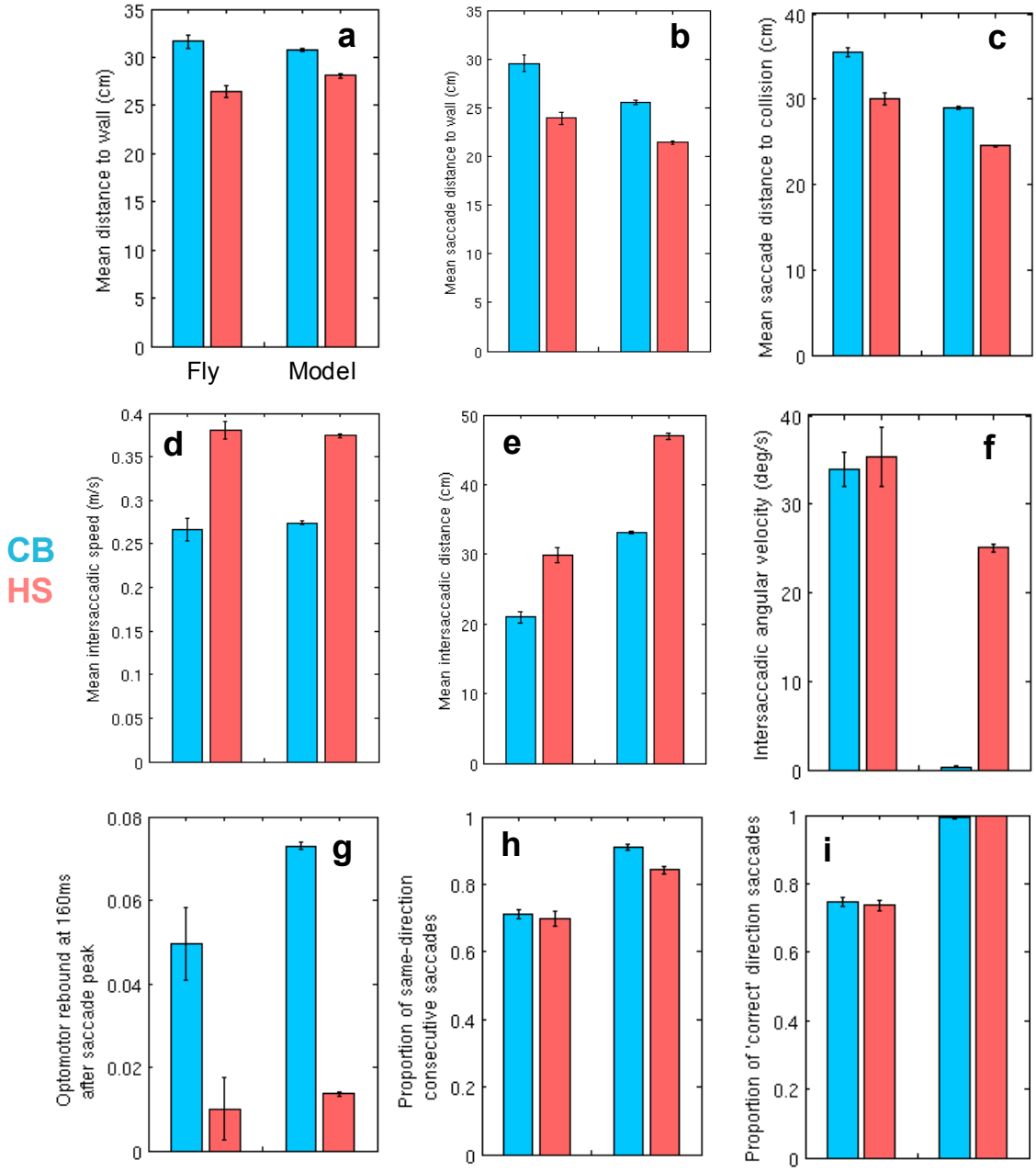


Figure 5.28: Comparison of real (left on each chart) and modelled (right) flight performance in the two homogeneous arenas, CB (blue) and HS (pink). Data is averaged over experimental replicates; n=24 in all four conditions. Bars represent ±1 s.e.m. The standard errors are generally smaller for the model data, reflecting that the behaviour of the model is less variable than that of flies. See section 3.5 for details on how the measures used in **a**-**f** are calculated. **g** Optomotor rebound is the negative angular velocity 160ms after the saccade peak, as a proportion of the peak angular velocity (see fig 5.24). **h** gives the probability that each saccade will be followed by another in the same direction. **i** is the proportion of saccades directed away from the side on which the arena wall is closer, see section 4.4.1 for details.

Another statistic that was explicitly used to tune the model is intersaccadic speed (fig 5.28d), and thus a close match is seen between fly and model. However, the model produces much longer intersaccadic segments than the flies (fig 5.28e), indicating that saccades are less frequent (though

once again the between-arena effects are still reproduced). The model's intersaccadic flight is also straighter (fig 5.28f), especially in the CB arena where almost no intersaccadic turning is seen.

Even though the amplitude of the post-saccade optomotor rebound (fig 5.28g) was used for parameter tuning, the model somewhat exaggerates this effect in the CB arena. However, the gain of the OMR cannot be reduced without making the model averse to the landmark in the SL arena (section 5.4.4).

The final two charts are concerned with the polarity of saccades. The model is more likely than real flies to saccade repeatedly in the same direction, despite having no endogenous bias to do so (fig 5.28h). Furthermore, the model turns in the appropriate direction to avoid the wall more frequently than the flies (fig 5.28i) – in fact, it almost never turns towards the wall. Possible reasons for all of the differences between the flies and model that are mentioned above – and what they allow us to infer about the fly - are discussed in section 5.6.3.

#### 5.5.2.1 Intersaccadic turning

Intersaccadic angular velocity (fig 5.28f) would appear to be the feature of the model's behaviour most at odds with the animal data, so I shall elaborate a little more on this issue. Fig 5.29 shows how the model fly's intersaccadic turning varies as a function of the angle at which it is approaching the wall.

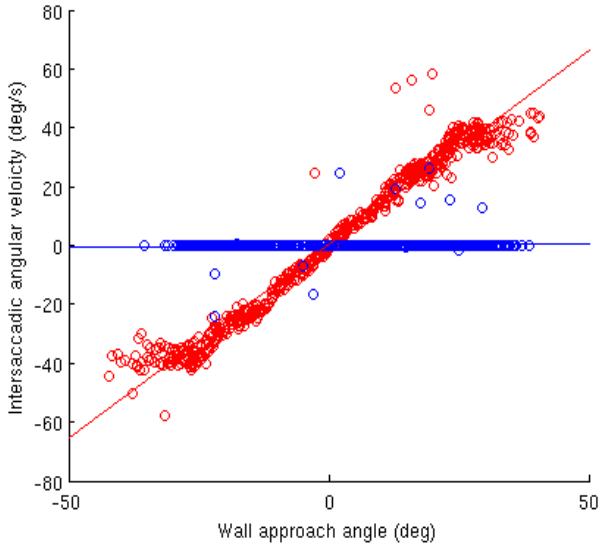


Figure 5.29: Intersaccadic turning and wall approach angle. CB arena is in blue, HS in red. Analogous free-flight data is shown in fig 4.4. If the angular velocity has the same sign as the wall approach angle, the fly is turning away from the wall. Lines are linear regression fits.

This data looks rather different to the animal results (fig 4.4), because it has much less variability. There are of course many potential sources of noise in the fly data which do not apply to the model and could thus account for this discrepancy: e.g. tracking errors, turbulence, spontaneous behaviour (see section 5.6.3.2), uncontrolled visual contrasts in the arena, between-animal differences, and countless other factors. Nevertheless, the same general pattern is seen; the model fly veers away from the wall in the HS arena, but has no clear bias in CB.

This veering is the reason for the convexity of flight trajectories in the HS arena (fig 5.26). In the model, it occurs for the reason hypothesised in 4.5.4, i.e. perspective effects combined with a lack of vertical contrast produce optic flow consistent with yaw rotation although the model is translating. The slight concavity of flight paths in the CB arena is caused by the optomotor rebound following saccades, since there very little turning occurs during the actual intersaccadic segments (which are defined to begin 500ms after the preceding saccade; see section 3.5.3).

### 5.5.2.2 Optomotor rebound

Fig 5.30 presents the saccade-triggered angular velocity profiles showing the optomotor rebound in the model (c.f. fig 4.8). The model data matches that of the insects quite closely, although as mentioned previously, the amplitude of the model's rebound is a little larger.

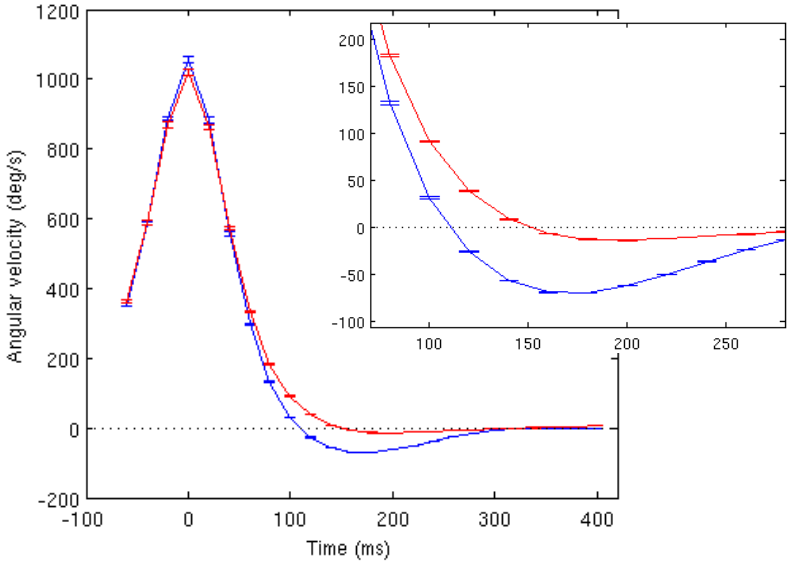


Figure 5.30: Event-triggered angular velocity profile, normalised such the the saccade direction is positive. CB arena is blue, HS is red. Bars are ±1 s.e.m. Inset: Zoomed view of the plots, showing the 'rebound' phase following the saccade. Fig 4.8 shows exactly equivalent data from flies.

When I introduced the optomotor rebound phenomenon in section 4.4.3, I argued that the difference in amplitude seen between CB and HS was directly caused by the differing abundance of visual rotational cues. However, it is difficult to demonstrate that the effect cannot be explained as some indirect consequence of the visual environment. For instance, flies fly considerably faster in the HS arena; could this account for their smaller rebound? The model provides a way to test whether visual environment alone can produce the observed effect, by controlling all other variables.

Fig 5.31 shows the results of 'staging' identical saccades in the CB and HS arenas. To perform these experiments, the SR and CA subsystems are disabled, the model's speed is set to 30cms$^{-1}$, and a saccade is manually triggered 25cm from the wall. Flightspeed is only modulated according to equation 5.6, and the model's angular velocity is determined by the saccade profile (equations 5.4 and 5.5, omitting the Gaussian noise), modulated by the OMR system in a closed-loop manner. Following the standard pre-adaptation procedure (section 5.4.1), the model flies for 500ms before reaching the peak of its saccade. The temporal resolution is increased by reducing the simulation timestep to 1ms. The difference in rebound amplitudes is still clearly exhibited, suggesting that the difference in visual environment alone is sufficient to produce the effect. Of course, the possibility that indirect effects also contribute to the phenomenon in flies cannot be discounted.

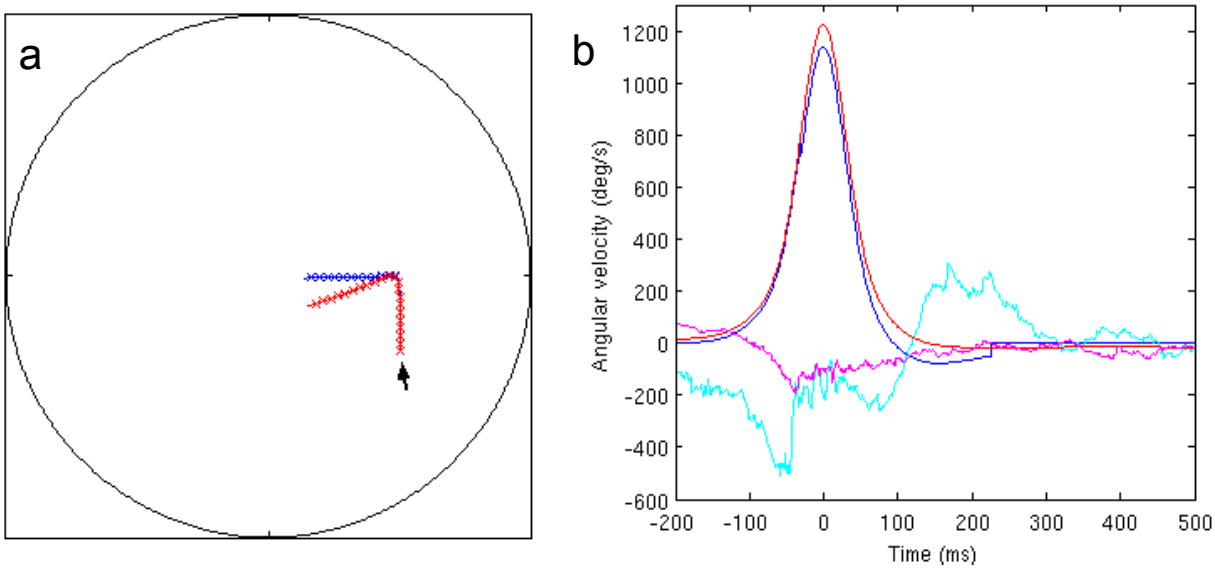


Figure 5.31: 'Staged' optomotor rebounds. **a** The paths taken by the model in the CB (blue) and HS (red) arenas, 'x's mark 50ms intervals. Flight begins at t = -500ms; the arrow marks the start. **b** Blue and red lines show angular velocity during the saccade in CB and HS respectively, as in fig 5.30. The two discontinuities in the CB profile (at t = -35 and 225ms) are caused by OMR suppression due to translational optic flow disengaging and re-engaging. Cyan (CB) and magenta (HS) lines are recordings of OMR filter response (left and right summed), measured immediately downstream of the filters (fig 5.10). Units are arbitrary.

Another benefit of the model is that it allows the internal workings of the system to be investigated. The output of the OMR filters (fig 5.31b) sheds some light on what happens during the optomotor rebound. The filter response is generally much larger in the CB case, because the vertical contrasts offer a far greater rotational cue than the bulging caused by perspective in the HS arena. The CB response is largest at moderate angular velocities, dipping at the peak of the saccade. This is because the wavelength of the pattern is on the order of tens of degrees, and therefore the temporal frequency experienced by the fly exceeds the optimal value of ~7Hz. The HS pattern, effectively having a wavelength of 360°, is not subject to this effect, and thus the signal has a single peak when the angular velocity is maximal. Also, note that the illusory rotational cue experienced before the saccade at t = -200ms generates a response of approximately 40% of the peak seen when the model is actually rotating at over $1000°s^{-1}$.

### 5.5.3: Landmark behaviour

In the previous chapter, I found very little evidence that flies were either attracted to or repelled by a single vertical bar in an otherwise horizontally striped arena. In this section I ask whether the same can be said of the model.

The model spends 31.8% of the time in the zone aligned with landmark (section 3.5.1), which is neither significantly different from the real flies' behaviour (32.3%, U(42,24)=484, p=.79), nor from chance (T(24)=86, p=.067). However, the model does show some tendency to approach the landmark. Fig 5.32 is a plot of the frequency with which the fly and model orient towards different parts of the arena wall. The model displays a preference for 'aiming' at the landmark, which the real flies do not. Comparing the proportion of time spent pointed at the wall within ±15° of the landmark (i.e. a region 26.2cm wide), this difference is significant (model: 11.1% *versus* fly: 7.8%; U(42,24)=756, p=.0008).

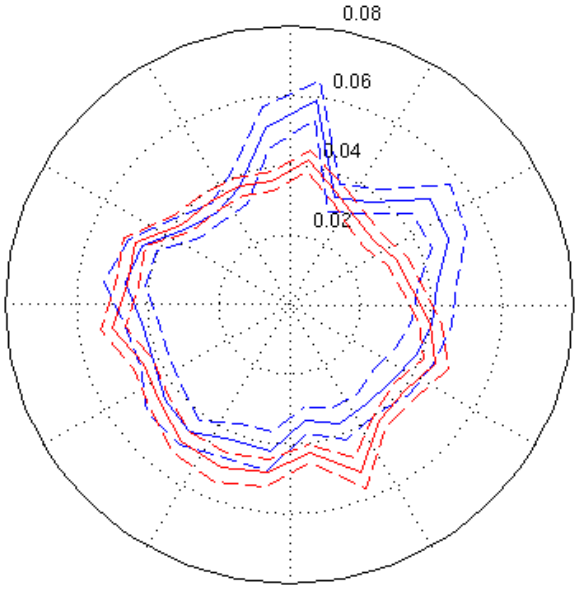


Figure 5.32: Polar plot of the proportion of time spent oriented toward different parts of the SL arena wall (binned in 15° / 13.1cm intervals). Model data in blue, flies in red. The landmark is, as always, at the 12 o'clock position. Dashed lines are ±1s.e.m.

It appears that the cause of this bias is intersaccadic turning. While real flies exhibit no tendency to steer towards the landmark (section 4.3.2), the model turns towards the landmark when it is the frontal visual hemisphere (angle to landmark *versus* intersaccadic angular velocity: $\rho(270)=.790$; $p<.0001$). It should be borne in mind that the model's trajectories are much less noisy than the recorded ones so it is possible that even small-magnitude correlations will have high significance. This being the case, it is noteworthy that the duration of intersaccadic segments is uncorrelated with the absolute angle to the landmark in the model ($\rho(501)=-.032$; $p=.47$, whereas real flies are found to make longer segments towards the vertical stripe than away from it.

# 5.6: Discussion

## 5.6.1: Summary

This chapter has described my efforts to implement and validate a model of visuomotor behaviour in flying *Drosophila*, based upon recordings of flies (chapter 4). Delay-and-correlate elementary motion detectors (EMDs) are used to identify local image motion. To detect wide-field motion, the responses of many EMD 'half-detectors' are pooled before comparing them to their mirror image counterparts (section 5.1.2.1).

These EMD ensembles are used to drive behaviour in three parallel controllers. These are:

- The optomotor response (OMR, section 5.3.2) which detects yaw rotation and causes the fly to turn gradually in the same direction. I found it necessary to suppress this system when the optic flow more closely resembles a translation than rotation pattern.
- Speed regulation (SR, section 5.3.3) using an estimate of forward velocity based on fronto-ventral translational optic flow.
- Collision avoidance (CA, section 5.3.4) which initiates saccades based on expansion detection. Following some experimentation to find suitable optic flow filters, two overlapping but slightly laterally offset translational patterns were adopted.

Due to the difficulties of validating the subsystems individually, the entire visuomotor model had to be carefully tuned to attempt to match the behaviour of the fly. The resulting implementation successfully reproduced the following effects seen in the free-flight experiments (section 4.5.1):

- Walls are approached more closely in the HS arena than the CB one.
- Flight is significantly faster in the HS arena.
- The model fly veers away from the walls in the HS arena but not in CB.
- In terms of spatial distribution of trajectories, the model fly is neither significantly attracted nor repelled by a vertical landmark.
- A larger post-saccade 'optomotor rebound' occurs in the CB arena than the HS one.

In section 5.6.3 I discuss in detail the discrepancies between the behaviour of the model and that of real flies. Before that, it is worthwhile to reflect on the scope of the model by discussing the the sensorimotor mechanisms that are absent from it.

## 5.6.2: Limitations of the model

There are many well-documented aspects of *Drosophila* vision and behaviour which are not included in my model. These are not necessarily weaknesses; as I argued back in section 1.6, a model is only useful inasmuch as it helps people to better understand the nature of the target system. For this reason, a simple model which approximates the target behaviour is likely to be of greater use than a more accurate but very complicated one. Nevertheless, it is important to be explicit about the simplifying assumptions one makes. Towards this end, this section lists phenomena which I have not attempted to model.

### 5.6.2.1 Visual processing

- At the most peripheral level, I have ignored the fact that the ommatidia of the eye must be

arranged in a hexagonal pattern. However, the interommatidial and acceptance angles are realistic (section 5.1.1). Also, the eyes are modelled as cylinders rather than spheres for computational simplicity.

- Perhaps the greatest simplification I have made to the motion detection system is to ignore motion adaptation. The relationship between image temporal frequency and the response of a blowfly LPTC is not constant, but rather the sensitivity of the cell is modulated according to the input such that its dynamic range is fully utilised, maximising information transmission (Brenner et al, 2000).
- Similarly, I have not modelled contrast adaptation. This is a well-established phenomenon; for instance, dronefly LPTCs adapt such that responses to low-contrast motion stimuli are depressed for several hundred milliseconds following prolonged exposure to high-contrast ones (Harris et al, 2000). As my experimental paradigm uses only environments with high contrast throughout their extent, this simplification is unlikely to make much difference to behaviour.
- The model visual system is entirely based on motion. Clearly *Drosophila* can also process and recognise the structure of visual objects, as they can be conditioned to avoid certain stationary shapes (Wolf et al, 1998).

#### 5.6.2.2 Flight behaviour

- The most obvious simplification I have made is to omit altitude regulation by confining the fly to a horizontal plane.
- The model fly's pitch and roll are held constant at all times, because I lacked data on the orientation of flying flies due to the limited resolution of the tracking system (see section 5.2.1).
- Flying flies obviously must land at some point, and indeed they are occasionally observed to do so in my experiments. Tethered *Drosophila* extend their legs and attempt to decelerate when faced with a frontally-positioned expanding pattern (Tammero & Dickinson, 2002b), whereas my model could only attempt to saccade away from the looming obstacle in the same situation.
- Saccades only occur as a response to visual expansion. This is in contrast to real flies, which produce spontaneous saccades (Maye et al, 2007). See section 5.6.3.2 for further discussion of this point.
- No attempt is made to model muscular control of the wings, aerodynamic or inertial forces, or the role of the halteres in regulating flight manoeuvres. These processes are treated as a black box and approximated using empirical data where appropriate, e.g. the relationship between

flightspeed and saccade amplitude (section 5.3.4).

## 5.6.3: Validity of the model

The model does not perfectly reproduce the behaviour of the fly. In this section I identify the most significant discrepancies and discuss what might cause them and what bearing they have on subsequent experiments.

### 5.6.3.1 Optomotor rebound amplitude

I noted that the model produces a rather larger post-saccade counter-turn than the flies, particularly in the CB arena (fig 5.30, c.f. Fig 4.8). There are a number of reasons why this behavioural response may be attenuated in the animal experiments relative to the model:

- Blowflies' heads rotate faster than their bodies during saccades (van Hateren & Schilstra, 1999), which serves to shorten the duration and increase the velocity of visual rotation. Since the motion stimulus is already at a supraoptimal temporal frequency (see fig 5.31), both of these effects will tend to attenuate the LPTC response. This would in turn reduce the size of optomotor rebound.
- It is possible that the amplitude of the optomotor rebound is curtailed by kinematic factors, i.e. *Drosophila* can only turn at a certain rate without initiating a saccade. Of course, there is also no particular reason to assume that the transfer function from LPTC to flight motor is linear.
- The existence of a visual environment-dependent rebound merely indicates that the fly does not entirely suppress optomotor feedback when performing saccades. Some attenuation due to an efference copy (i.e. the fly anticipating the sensory consequences of its action) could still occur. However, in light of the above points and the fact that the model's optomotor rebound amplitude is comparable to that of the flies, I am inclined to support Warzecha & Egelhaaf's (1996) view that the decreasing response of EMDs to supraoptimal temporal frequencies alone is sufficient to prevent instability in the OMR controller.

### 5.6.3.2 Spontaneous saccades

As mentioned previously, the model differs from flies in that it will not saccade without visual stimulation. Postulating that real flies make additional, non-CA-triggered saccades provides a parsimonious explanation for many of the discrepancies that exist between the model and insect data.

Firstly, this suggests a reason why the model tends to saccade closer to the wall (figs 5.28b,c) despite

being tuned to match flies' general level of wall-aversion (fig 5.28a). It could be the case that saccades triggered by the CA system occur at roughly the same distance from the wall in real flies as in the model, but that spontaneous saccades (which are likely to occur in more central positions than CA-triggered ones) pull the average up in the case of the flies. Spontaneous saccades would also break up intersaccadic segments, shortening their mean length. Again, this account is consistent with the data (fig 5.28e).

Fig 5.28i shows that the model saccades away from the wall more frequently than real flies do. In fact, it always turns away in the perfectly regular HS arena, suggesting that its rare failures to do so in the CB arena are due to the random nature of the chequerboard pattern. Clearly, if the model were to make random spontaneous saccades one would expect these figures to agree more closely with the free-flight data.

In the previous chapter's discussion I suggested that these 'wrong direction' turns might not be due to endogenous saccades but rather a tendency for the fly to persistently saccade in one direction (section 4.5.5). Fig 5.28h shows that the model repeatedly saccades in the same direction to a *greater* extent than real flies simply by virtue of avoiding the walls of the circular arena. This result thus provides evidence against the persistent-direction hypothesis, and can be seen as further supporting the notion that the fly generates random saccades. This is because a spontaneous saccade's direction would be truly independent of the fly's previous movements, and would thus pull the statistic towards the chance level of 0.5.

Given the accumulating evidence for the existence of spontaneous saccades, it may seem surprising that I have not included them in my implementation. The main reason for this decision is because it would further complicate the model, and add at least one more free parameter, thereby increasing the risk of overfitting. A further reason is that it is unclear what mechanism should be used to generate these endogenous saccades. A Poisson process is the obvious choice, but Maye et al (2007) argue that the timecourse of these saccades has fractal properties which cannot be captured by so simple an algorithm.

Reynolds & Frye (2007) claim that a negative linear relationship exists between the log length of segments between spontaneous saccades and their log frequency. If interpreted naively, this means that very short segments should be very frequent, resulting in nonsensical trajectories. It seems that some lower bound would have to be put on segment length (if only to capture the fact that a fly presumably cannot initiate a new saccade until it has finished executing the current one), which would

mean introducing yet another free parameter. Worse still, this parameter would likely have a rather profound effect on behaviour.

#### 5.6.3.3 Landmark behaviour

The model features no explicit target fixation mechanism, because I found little or no evidence that flies were attracted to the vertical stripe in the SL arena. However, the optomotor response (OMR) can give rise to landmark orientation behaviour, as evidenced by the model's tendency to steer towards the stripe (section 5.5.3). The reason for this is as follows: because the landmark is the only source of vertical contrast in the arena, if the model is flying with the landmark to its left, it will experience front-to-back motion of the left hand side, but see little movement on its right. This is consistent with rightward yaw rotation, so the OMR system (section 5.3.2) will attempt to compensate by steering left, i.e. towards the landmark. Huber et al (1999) investigate in detail how a single rotational-sensitive visuomotor system can achieve both optomotor stability and target fixation in sparsely textured environments.

As a result of this effect, the model shows a clear bias to orient towards the region of the landmark (figure 5.32). Neither this effect nor the intersaccadic steering towards the stripe are observed in real flies. I am forced to concede that the model does not behave in exactly the same way as a real fly when faced with a single conspicuous landmark in its environment; it fails to reproduce the indifference with which flies appear to regard the landmark. It is possible this discrepancy is due to real flies' behaviour being much more variable than the model's, for the reasons discussed in section 5.5.2.1. This heightened level of noise could mask subtle target fixation effects.

As my eventual aim is to investigate odour localisation, the important point for my purposes is that the model - like the fly - spends no more or less time in the vicinity of the stripe than chance would predict. This is why I have used the OLI to quantify landmark attraction, as this metric shall also be used to measure odour localisation in later chapters.

I explained in section 5.4 that achieving the model's indifference to the landmark was in fact a delicate balancing act, with the sensitivity of both the CA and OMR systems having a clear effect on landmark attraction or repulsion. I shall return to these points in chapter 8 when I come to discuss how olfaction could modulate the functioning of the visuomotor model to achieve odour localisation. First though, I must turn my attention to the olfactory behaviour of real flies in the free-flight arena, which is the subject of the next chapter.

# 6. Odour localisation behaviour

Having observed and modelled the visuomotor behaviour of flying *Drosophila*, this chapter covers the behaviour seen when a new stimulus modality is introduced. First, I describe the methodology of my odour localisation experiments (section 6.1). I then present the results of these experiments, and discuss how the flies' behaviour changes in the presence of food odour (section 6.2). In section 6.3, I investigate what possible mechanisms allow the insects to locate the odour source, and finally discuss the implications of my findings in section 6.4.

## 6.1: Methodology

Once again, the general methodology for these experiments is covered in detail in chapter 3. Details of the visual stimuli can be found in section 4.1.1. This section describes those procedures and analyses specific to experiments featuring odour.

The substance selected for use as an attractive odorant is balsamic vinegar. Though *Drosophila melanogaster* are commonly referred to as fruit flies, some authors (e.g. Zhu et al, 2003) insist that they should be called 'vinegar flies', as they are most strongly attracted to fruit that has rotted and fermented, and the resulting alcohol has oxidised to vinegar. The most effective *Drosophila* attractant found by Zhu et al (2003) is a blend of 22 parts ethanoic acid (i.e. vinegar) to five parts 2-phenylethanol (a compound found in many flowers and fruits, most notably roses) and one part ethanol.

Previous olfactory experiments on flies (Frye et al, 2003; Duistermars & Frye, 2008; Chow & Frye, 2008) have typically employed apple cider vinegar, but preliminary tests (on Canton-S flies, rather than the 'Super Fly' strain used in the eventual experiments; see section 3.2) suggested that balsamic vinegar acted as a stronger attractant.

As described in section 3.1, the floor of the arena features three evenly spaced slots which are occupied by small black vials. For all experiments described in this chapter, one of these vials contained vinegar and the other two water. The vinegar vial was put into its slot ten minutes before the commencement of an experimental trial, in order to allow the odour to diffuse. Once the trial was completed, the vial was removed and the blackout curtain was opened to ventilate the arena. After six

minutes the process was repeated with a fresh vial of vinegar. These timings are based on measurements of the diffusion of ethanol (see section 7.3). The vinegar was handled and disposed of at least 10m away from the arena to prevent contamination. During any single day's 3hr experimental session the odorant would always appear in the same vial, to minimise the effect of residual plumes lingering from previous experiments.

All data for the homogeneous environments (i.e. chequerboard (CB) and horizontal stripes (HS)) consists of equal numbers of trials with the vinegar in each slot, to control for any directional bias that may exist in the arena. Clearly, is is not sensible to do this for the single-landmark (SL) arena, so I define two separate conditions: *SL-near* describes the situation where the odour source is aligned with the vertical stripe, and *SL-far* refers to when it is in one of the two slots offset by 120° from the stripe.

# 6.2: Behavioural results

## 6.2.1: Spatial distribution

Sample trajectories are given in fig 6.1 (c.f. no-odour experiments in fig 4.2). Perhaps the most striking difference between these trajectories and the controls is the decrease in altitude when odour is present. As table 6.1 shows, this difference is significant in all environments. The same effect was observed by Frye et al (2003).

| | No odour | | Odour | | | |
|---|---|---|---|---|---|---|
| Condition | Altitude (cm) | n | Altitude (cm) | n | U | p |
| CB | 46.6 | 24 | 32.5 | 27 | 132 | .0003 |
| HS | 46.9 | 24 | 39.1 | 27 | 194 | .014 |
| SL-near | 51.2 | 42 | 36.2 | 24 | 207 | .0001 |
| SL-far | | | 38.9 | 24 | 203 | .0001 |

Table 6.1: Flies decrease altitude when vinegar is concealed in the arena floor.

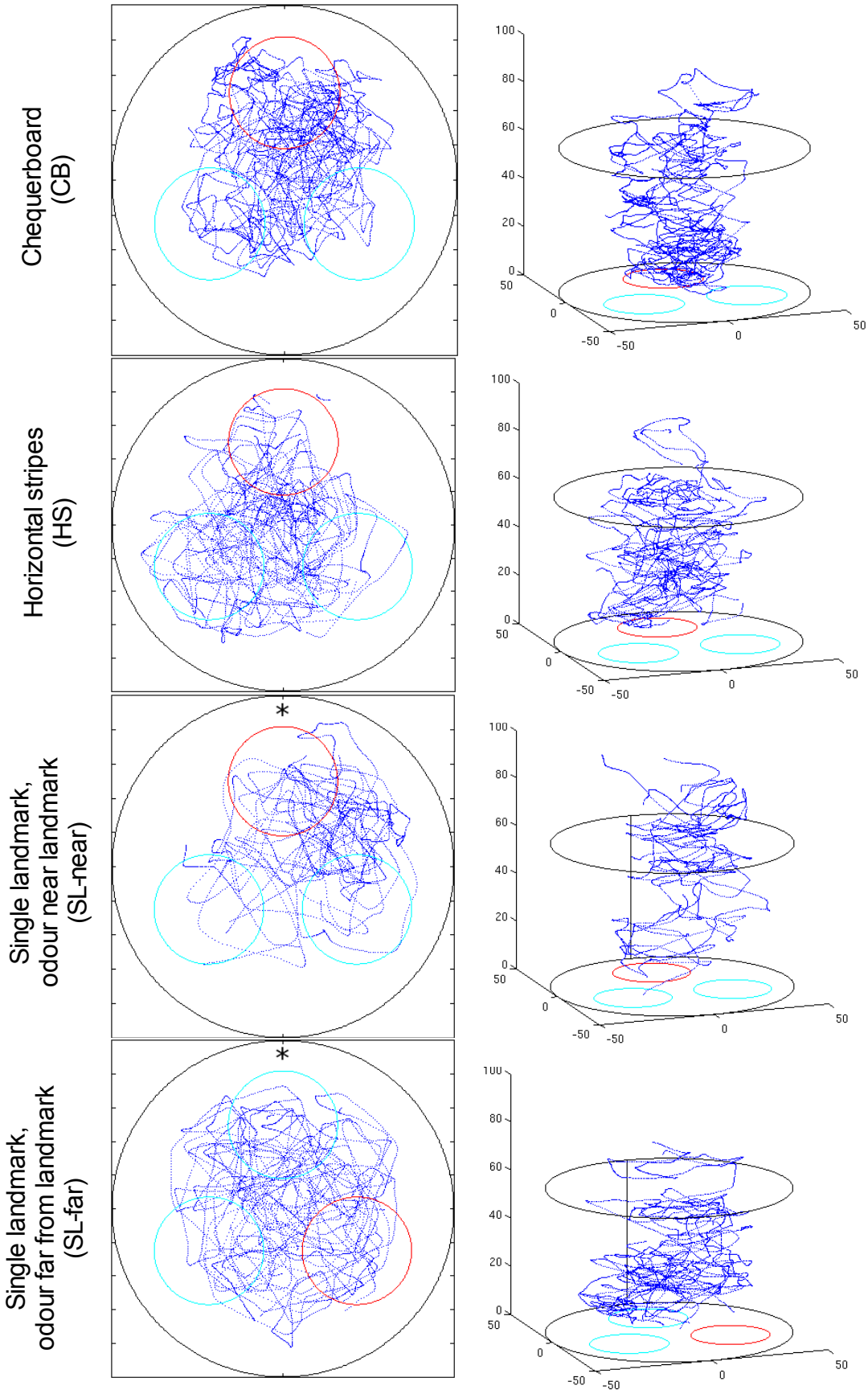


Figure 6.1: Sample trajectories from the four conditions. Dots represent the fly's position at 20ms intervals. The overhead and 3D views show the same trajectories. Small circles show the zones used to compute the OLI (equation 3.9), with the red one denoting the vial containing vinegar. In both *SL-near* and *SL-far*, the stripe is located at the 12 o'clock position on the overhead plot (marked '*'), which is the far side of the 3D plot (marked by the vertical black line). See fig 4.2 for no-odour trajectories.

Fig 6.2 shows plots of transit probability. While the general patterns are rather similar to those seen when no vinegar is present (fig 4.3), the distributions are shifted towards the odour source to varying degrees in the different conditions. OLI calculations (equation 3.9) can be used to rigorously measure this odour localisation (OL) behaviour. This data can be found in fig 6.3.

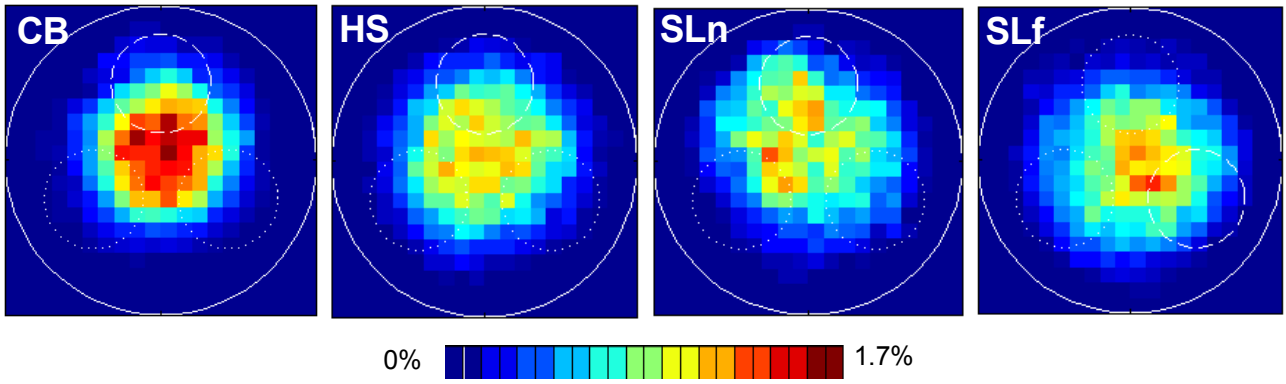


Figure 6.2: Plots of transit probability for the odour experiments. As usual, the landmark in the SL arena is at the 12 o'clock position. SLn is short for SL-near, i.e. the case where the odour source is aligned with the landmark; SLf is SL-far. The small circles show the boundaries of the zones, with a dashed line representing the zone containing vinegar, and the dotted line representing water-filled controls. The trajectories in the CB and HS arenas were rotated in order that the odour source position was constant. See fig 4.3 for no-odour data; note that the same colour scale is used. $n_{CB}$ = 27, $n_{HS}$=27, $n_{SLn}$=24, $n_{SLf}$=24.

Highly significant OL is observed in the CB arena (fig 6.3a, OLI=.467). In disagreement with Frye et al (2003), my experiments reveal OL also taking place in the HS arena (fig 6.3b, OLI=.378). However, the performance is significantly stronger in the CB case (U(27,27)=237, p=.038).

For the single landmark arena, it is important to note that in the absence of odour (fig 6.3c), flies spend no more or less time in the zone next to the landmark than the other two (OLI=.322, T(42)=406, p=.57). When vinegar is put in this zone, significantly more time is spent there (fig 6.3d, OLI=.512). If the odorant is placed in one of the other two slots, however, significant OL does not take place (fig 6.3e, OLI=.398). (Note that the OLI is in fact higher in SL-far than it is in HS, but fails to achieve significance due to its higher variability.) The difference between SL-near and SL-far is significant (U(24,24)=171, p=.016).

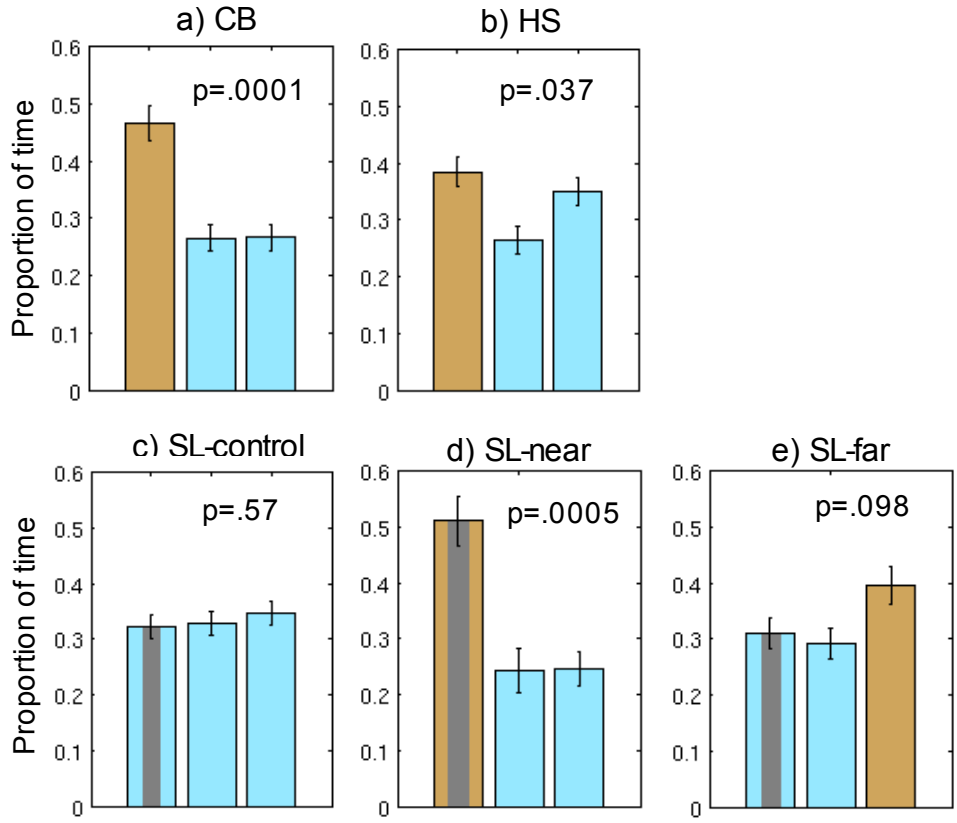


Figure 6.3: Odour localisation performance. Bars show the mean proportion of time spent by flies in each zone, i.e. the OLI. Brown bars denote zones containing odour, cyan bars are water-filled controls. In the SL arena (**c**-**e**), the bar containing a grey stripe represents the zone aligned with the landmark. Significance values are based on Wilcoxon Matched Pairs tests comparing the OLI of the odour zone with the mean of the two control zones. In the SL-control case (**c**), the zone next to the landmark is compared to the mean of the other two. Error bars are ±1s.e.m.

## 6.2.2: Flight statistics

I have demonstrated that flies are able to locate a concealed food odour source significantly better in certain visual conditions than others. The question I seek to address in this section is how the fly's behaviour alters in the presence of odour. I shall repeat many of the analyses performed in previous chapters, but instead of looking for differences between visual environments, or between flies and the model, I am now concerned with differences between odour and control experiments.

Fig 6.4 shows comparisons of various flight statistics for the two homogeneous arenas (CB and HS) with and without food odour present. Recall that significant OL takes place in both visual environments, but to a greater degree in CB. When odour is present, flies in the HS arena become more wall-averse, both in terms of their overall average distance from the wall (fig 6.4a) and the distance at which saccades are initiated (fig 6.4b). No change occurs in the CB arena.

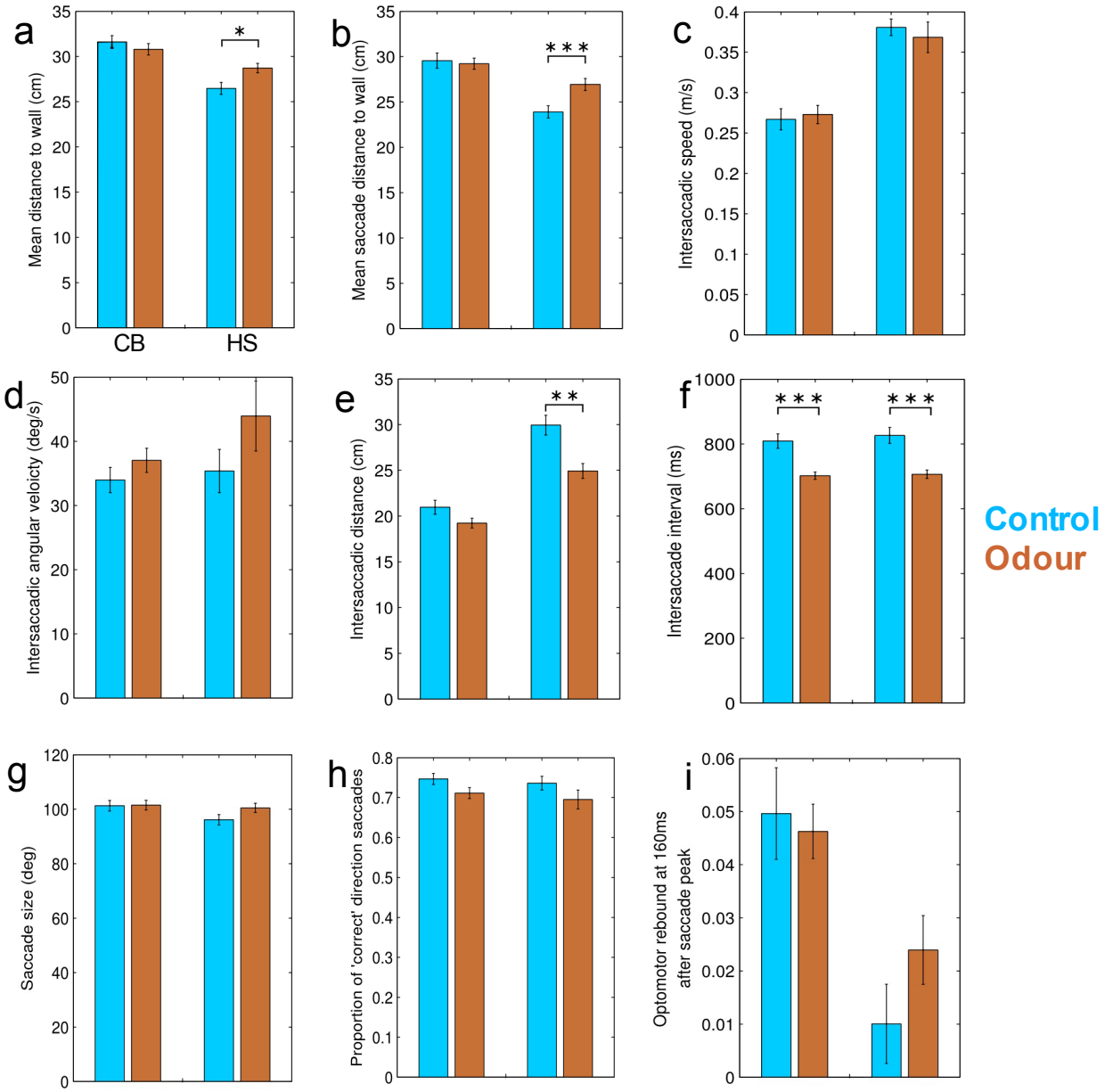


Figure 6.4: Comparison of flight performance of flies in the CB (left on each chart) and HS (right) arenas in the presence (brown) and absence (blue) of food odour. Data is averaged over experimental replicates; n=24 in both control conditions and 27 in both odour conditions. Stars show significance of differences: * p<.05, ** p<.01, *** p<.001. Note that only within-arena comparisons are shown. Bars represent ±1 s.e.m. See fig 5.28 for more detail.

Flightspeed in each environment changes very little when vinegar is introduced (fig 6.4c), and no significant difference is seen in the straightness of intersaccadic segments either (fig 6.4d). Segments do however become shorter in distance in the HS arena (fig 6.4e), and in both environments there is a clear reduction in their duration, i.e. saccades become more frequent (fig 6.4f). The size of saccades is unchanged (fig 6.4g), as is their probability of being in the appropriate direction to avoid a collision with the wall (fig 6.4h). Finally, the amplitude of the optomotor rebound is similar between odour and

control experiments (fig 6.4i).

A couple of general observations can be made about these results. Firstly, rather little appears to change when odour is introduced to the arena, so the behavioural modulation required for odour localisation may be rather subtle. Of course, it must always be borne in mind that failure to find significant differences is not equivalent to demonstrating that no such differences exist. It does however indicate that if they do exist, they must be of relatively small magnitude. Secondly, despite OL being stronger in the CB arena, more odour-dependent effects are found in HS.

It is also instructive to ask whether the correlations identified between certain flight parameters persist when OL is occurring. As before, saccade size is negatively correlated with presaccade velocity in both arenas (CB: $\rho(2931)=-.162$, $p<.0001$; HS: $\rho(1142)=-.063$, $p=.033$). While intersaccadic segments showed neither a bias towards nor away from the wall in an odour-free CB arena, when vinegar is added a significant negative correlation is seen ($\rho(446)=-.148$, $p=.0017$; fig 6.5). This means that flies veer *towards* the wall between saccades.

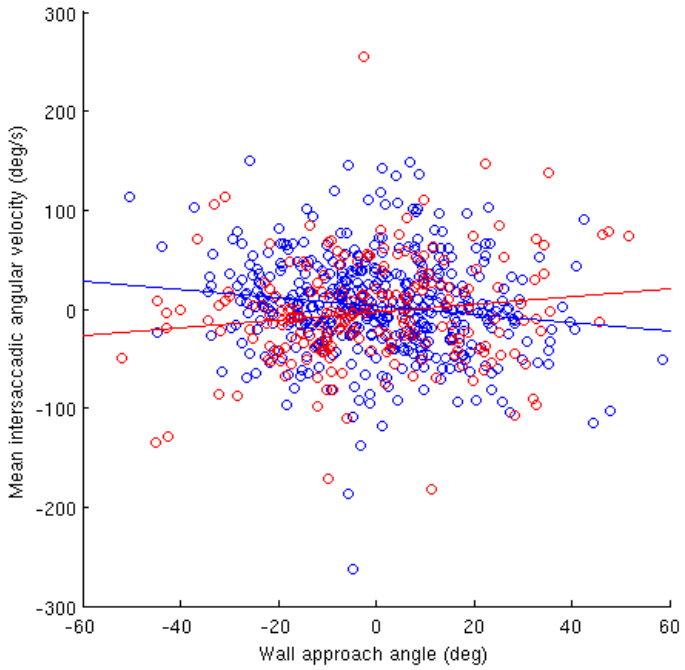


Figure 6.5: Intersaccadic turning as a function of the fly's angle to the wall at the beginning of the segment. Data is from odour experiments, c.f. no-odour control in fig 4.4. Blue is the CB arena, red is HS. Linear regression lines are shown. Flies in the CB arena turn significantly towards the wall. While the HS flies' tendency to steer away from the wall is not longer significant ($\rho(208)=.129$, $p=.063$), the gradient of the regression line is in fact steeper (odour: 0.40 *versus* control: 0.27).

I have not discussed the issue of whether the flies' behaviour towards the landmark in the SL arena changes when odour is present. This is because this analysis becomes rather difficult, since there are now two directional cues in the arena - one visual and one olfactory – and picking their influences apart is quite a delicate process. However, I shall return to this point in section 6.3.5.

## 6.3: Mechanisms of odour localisation

The previous section identified some ways in which *Drosophila*'s flight behaviour changes when food odour is present. In this section I investigate how these and other behavioural modulations could actually cause the fly to approach the odour source. A central difficulty is that the olfactory environment is unknown. Thus while I can approximately reconstruct the visual stimuli experienced by a fly at any given instant, the same is not true of its olfactory input. To overcome this problem, I must use a somewhat complicated analysis technique, which is explained in the following section.

### 6.3.1: Analysis methodology

Although I attempt to characterise the structure of odour plumes in the arena using a chemical sensor (chapter 7), the odorant distribution is highly variable, so it is impossible to reconstruct a fly's olfactory experience from its flight trajectory. A smooth odour gradient is very unlikely to exist, due to the heterogeneous and unpredictable nature of turbulent plumes (see sections 2.5.1, 7.3). However, it is reasonable to assume that *on average* odour intensity will be highest near to the source (see section 7.3). Thus, proximity to the source can be used as a crude proxy for odour intensity, as long as one has enough data to achieve the statistical power needed to overcome the high level of variability introduced by this approximation.

Thus, I make the unrealistic assumption that an appreciable odour gradient exists throughout the arena, and points in the direction of the odour source. When considering saccades, the estimate of the local odour gradient is computed based on the fly's position and orientation prior to the saccade, in a similar manner to the calculation of *distance to collision* (section 3.5.2). For intersaccadic flight, it is based on the beginning of the segment (section 3.5.3). I relax the inclusion criteria for intersaccadic segments a little for this analysis; these are now deemed to begin 320ms after the offset of the previous saccade and end 80ms before the onset of the next. This step was taken to increase the number of observations for the reasons discussed above, but carries the risk of the data being slightly more contaminated by peri-saccade effects (e.g. optomotor rebound).

Under the assumption of a smooth odour distribution, the cosine of the azimuthal angle of the odour source relative to the fly is proportional to the local odour gradient in the direction the fly is moving. To look for chemokinetic effects (i.e. non-directional odour attraction, see section 6.3.2) on flight behaviour, I assess whether this statistic is correlated with features of saccades or intersaccadic segments. (Since I compute correlations using a non-parametric method, the negative absolute value of the angle is equivalent to its cosine.) To investigate whether flies have any chemotactic ability (i.e. directional odour attraction, see sections 6.3.3, 6.3.4), I test whether their turning is correlated with the direction of the hypothetical gradient. Even if the fly exhibited perfect chemokinesis or chemotaxis, it would frequently modulate its behaviour in the 'wrong' direction (e.g. turning away from the source) according to this analysis because of irregularities in the plume. However, on average it would alter its behaviour in the appropriate way to achieve odour localisation, and thus a significant (but possibly weak) correlation would exist.

There are some additional complications to this analysis. Firstly, if the fly is roughly above the odour source then all directions are down-gradient. For this reason, events (i.e. saccades or beginnings of intersaccadic segments) occurring less than 15cm (horizontally) from the odorant vial are ignored. Secondly, a significant correlation in itself is meaningless, as it could be merely a by-product of the arena geometry. Quantifying this baseline correlation is not straightforward, as it depends on the flies' spatial distribution in the arena (fig 6.2), which clearly cannot be assumed to be uniform if successful OL is occurring, by definition.

I adopt a Monte Carlo approach to overcome this problem. For each event, a random source position 25cm from the centre of the arena is generated. The angles to these fictive odour sources are used to compute the baseline correlation. As above, if the segment begins within 15cm of the fictive source, it is discarded. Only if the correlation obtained using the true source position differs significantly from that obtained using the random fictive positions can I conclude that an odour-dependent effect exists. Details of how two correlation coefficients can be compared are given in the Appendix.

## 6.3.2: Chemokinesis

Kinesis, like taxis, is movement of an organism in response to a stimulus. Unlike taxis, the response to the stimulus is non-directional, e.g. the feeding behaviour of *E.coli* (see section 2.5.3). Briefly, this bacterium suppresses random turns when it senses the concentration of nutrients increasing, and promotes them when it is falling, thereby moving on average towards regions high in nutrients. Could it be that *Drosophila* use a similarly simple algorithm to find food? If this were the case, one would expect intersaccadic segments to be longer when moving towards regions of higher odour intensity,

and shorter when moving away.

The methodology explained in section 6.3.1 is used to investigate this hypothesis, by calculating the correlation between absolute angle to the odour source and intersaccadic segment length. Table 6.2 shows the results of the analysis. Highly significant correlations are seen in all conditions even when randomly generated source locations are used, which illustrates the importance of using the Monte Carlo method to establish a baseline. However, in the CB arena a significantly stronger correlation is seen between segment length and angle to the actual odour source, suggesting that chemokinesis is indeed occurring. No such effect is found in the HS arena.

| Condition | Actual | | | Monte Carlo | | | $p_{difference}$ |
|---|---|---|---|---|---|---|---|
| | ρ | n | p | ρ | n | p | |
| CB | -.214 | 1573 | <.0001 | -.136 | 1606 | <.0001 | .024 |
| HS | -.150 | 638 | .0001 | -.139 | 654 | .0004 | .85 |
| SL-near | -.214 | 496 | <.0001 | -.154 | 577 | .0002 | .31 |
| SL-far | -.166 | 710 | <.0001 | -.201 | 746 | <.0001 | .49 |

Table 6.2: Correlations between absolute angle to odour source and (spatial) length of intersaccadic segments. 'Actual' refers to the analysis using the real position of the odour source, 'Monte Carlo' to random fictive source locations (see section 6.3.1 for details). $p_{difference}$ is the significance of the difference between the two correlations (see Appendix for details of statistical method). There are generally fewer observations in the 'actual' case because segments starting near the source are excluded, and trajectories are of course biased towards the real source location.

No significant chemokinesis in seen in the SL arena for either odour location. In the case of SL-near, this may be in part due to a lack of data, as the correlation coefficients are quite similar to those observed in CB. On the other hand, it may be the case that other mechanisms are responsible for the strong OL performance seen in the SL-near case, as I shall investigate in section 6.3.5.

As well as flying further up-gradient than down-gradient, we might also hypothesise that flies will fly faster towards the source than away from it. Table 6.3 shows the results of repeating this analysis for mean segment speed instead of length. There is no clear evidence of an odour-dependent modulation of flight speed, although something curious happens in the SL-near condition. When the data is randomly resampled for the Monte Carlo analysis, there is a significant (p=.013) tendency for segments directed towards fictive source locations to be faster. However, this effect is not seen when the actual position of the odour is used. Given the borderline significance of this difference, I am inclined to dismiss this result as an anomaly.

| Condition | Actual | | Monte Carlo | | $p_{difference}$ |
|---|---|---|---|---|---|
| | ρ | n | ρ | n | |
| CB | -.060 | 1573 | -.075 | 1676 | .67 |
| HS | -.012 | 638 | -.023 | 658 | .84 |
| SL-near | +.021 | 496 | -.103 | 585 | .043 |
| SL-far | -.048 | 710 | -.006 | 734 | .42 |

Table 6.3: Correlations between absolute angle to odour source and intersaccadic speed. See section 6.3.1 for details of analysis.

### 6.3.3: Saccadic chemotaxis

In the previous section I presented evidence that flies use non-directional chemotaxis to localise odour, at least in the CB arena. Do they also have a directional sense of the odour gradient? As discussed in section 2.5.3, it seems unlikely that flies are able to obtain usable gradient information by comparing their antennae due to the very small separation between them. However, gradient information could conceivably be built up by recording odour intensities it experiences as it flies around the arena.

The question addressed in this section is whether saccades are more likely to be directed towards the odour source than chance would predict. Saccades are slightly (though not significantly) less likely to be in the appropriate direction for collision avoidance when odour is present (fig 6.4h), so could the flies be turning towards the odour instead of avoiding the wall?

To assess this question, only those saccades that occur when the odour source (be it real or fictive) is at an azimuth in the range ±(45° ~ 135°) relative to the fly (i.e. to its side) are analysed, since it is difficult to see how a fly could saccade towards a frontally or posteriorly positioned location. Since the side on which the source is positioned and the direction of the saccade are both binary variables, the analysis (section 6.3.1) must be modified slightly; $\chi^2$ rather than a difference-of-correlations is computed, but the principle remains the same. Results are shown in table 6.4.

| Condition | Actual | | Monte Carlo | | $p_{difference}$ |
|---|---|---|---|---|---|
| | freq | n | freq | n | |
| CB | .693 | 1146 | .644 | 1294 | .010 |
| HS | .670 | 442 | .631 | 499 | .22 |
| SL-near | .642 | 369 | .622 | 455 | .55 |
| SL-far | .725 | 523 | .706 | 545 | .43 |

Table 6.4: Proportion of saccades directed towards a laterally positioned odour source, excluding those occurring within 15cm of the source.

It appears that in the CB arena (where OL is successful) flies do saccade in the direction of the odour source more frequently than chance would predict. However, one should be careful not to jump to the conclusion that these flies 'know' which side the source is on. How this result should be interpreted is discussed in section 6.4.3.

### 6.3.4: Intersaccadic chemotaxis

Saccading towards the odour source is just one way that chemotaxis could be manifested. This section asks whether flies steer gradually towards it during intersaccadic flight, by investigating the relationship between angle to the odour and intersaccadic angular velocity. I exclude all segments that begin with the source behind the fly (i.e. at an absolute azimuth >90°). This is because the any chemotactic turning response would presumably be maximal when the odour gradient was perpendicular to the fly's heading, so including cases where the angle to the source is obtuse may weaken the correlation. As table 6.5 shows, no evidence is found to support the hypothesis that flies turn in an up-gradient direction between saccades.

| Condition | Actual | | Monte Carlo | | $p_{difference}$ |
|---|---|---|---|---|---|
| | ρ | n | ρ | n | |
| CB | -.148 | 769 | -.075 | 760 | .15 |
| HS | +.059 | 299 | +.064 | 320 | .95 |
| SL-near | +.028 | 246 | -.122 | 291 | .085 |
| SL-far | +.063 | 388 | +.036 | 390 | .71 |

Table 6.5: Correlations between angle to odour source and intersaccadic angular velocity. Cases where the odour source is behind the fly are excluded.

### 6.3.5: Landmark fixation

In chapter 4 I found little evidence of flies modulating their behaviour to either approach or avoid the vertical stripe in the SL arena. This section addresses the question of whether this situation changes when food odour is introduced to the arena.

First I consider whether flies saccade towards the stripe when odour is introduced. I employ the same analysis as detailed in section 6.3.3, but using the position of the landmark rather than the odour source. For the Monte Carlo analysis, random points on the arena perimeter are generated. As table 6.6 shows, there is no indication that flies saccade towards the stripe whether odour is present or not.

| | Actual | | Monte Carlo | | |
|---|---|---|---|---|---|
| Condition | freq | n | freq | n | $p_{difference}$ |
| SL-near | .545 | 479 | .579 | 515 | .28 |
| SL-far | .550 | 645 | .563 | 606 | .66 |
| SL-control | .536 | 832 | .555 | 879 | .43 |

Table 6.6: Proportion of saccades directed towards the vertical stripe when laterally positioned, excluding those occurring within 15cm of it. See section 6.3.3 for more detail.

Next, I ask whether flies steer towards the stripe between saccades, using the same method as in section 6.3.4 but with the stripe rather than the odour source as a target. Results are given in table 6.7. Flies in the SL-near condition show a highly significant tendency to steer towards the landmark when it is in their frontal visual field. This result is somewhat difficult to interpret, as the visual and olfactory directional cues are aligned in this condition. However, given that the correlation is much stronger when the stripe as opposed to the odour source is used as a target (c.f. table 6.5), together with the fact that we see no evidence for intersaccadic chemotaxis in any other visual condition, I consider the most reasonable interpretation to be that flies are indeed orienting towards the landmark.

| | Actual | | Monte Carlo | | |
|---|---|---|---|---|---|
| Condition | ρ | n | ρ | n | $p_{difference}$ |
| SL-near | +.200 | 321 | -.080 | 345 | .0003 |
| SL-far | -.042 | 397 | +.008 | 406 | .48 |
| SL-control | -.023 | 626 | -.033 | 612 | .86 |

Table 6.7: Correlations between angle to landmark and intersaccadic angular velocity. Cases where the stripe is behind the fly or within 15cm of it at the start of the segment are excluded.

## 6.4: Discussion

### 6.4.1: Summary

Odour localisation behaviour was assessed by concealing one vial of vinegar in the arena floor. Flies spent a disproportionate amount of time in the vicinity of the odorant vial in both the random chequerboard (CB) and horizontally striped (HS) arenas, but odour localisation (OL) performance was significantly stronger in the richly textured CB arena. In the single landmark (SL) arena, significant odour localisation only occurs when the odour is aligned with the landmark. This cannot be trivially explained as a visual effect because no such bias is seen when odour is absent.

When odour is introduced, flies reduce their altitude and saccade more frequently. In the CB arena, flies veer significantly towards the wall between saccades, which they do not in no-odour control experiments. Other than these effects, broad behavioural metrics show remarkably little response to the addition of the olfactory stimulus.

Using proximity to the odour source as a very crude proxy for the odour intensity perceived by the fly, I investigate how behaviour might be modulated by the local odour gradient. I present evidence for non-directional chemokinesis taking place. There is also some suggestion that flies in the CB arena may perform saccadic chemotaxis, i.e. saccading in the direction of the odour gradient. In the SL arena, flies appear to steer towards the visual landmark when the odour source is positioned close to it – a behaviour not exhibited in the absence of odour.

### 6.4.2: Comparison to previous studies

My findings are broadly in line with those of Frye et al (2003). However, they reported that odour localisation did not take place in a horizontally striped arena, leading them to conclude that vertical contrasts were essential for this behaviour. I do find significant OL in the HS arena. I think there are two possible reasons for this discrepancy:

- My arena may be more poorly constructed than theirs, meaning that uncontrolled contrasts exist due to uneven lighting, joins, etc. These residual vertical contrasts facilitate OL in the HS arena.
- With all due respect to their pioneering study, their analysis was rather less rigorous than mine, in that OL performance was assessed by inspection rather then being statistically quantified. Looking at fig 13C of their paper (p851, c.f. fig 6.2b in this thesis) it seems possible that subtle OL could be occurring, which my analysis would be able to detect.

In any case, both Frye et al (2003) and the current study can agree that vertical contrasts improve OL performance. Another phenomenon they identify is the pronounced change in flies' behaviour in the HS arena when odour is introduced:

> "The structure of flight trajectories exhibited by animals flying within [the horizontally striped arena] is qualitatively different to those produced in all other visual conditions . ... Remarkably, when flying in an arena of horizontal stripes in the presence of odor, flies displayed the pattern of straight flight sequences interspersed with saccades that is characteristic of other visual treatments." (p849)

At first glance, it would appear that my results fail to replicate this observation. However, more behavioural changes are seen between odour and control experiments in the HS than in CB (fig 6.4), despite that fact that a higher degree of OL is occurring in CB. In particular, flies in HS become more wall-averse (fig 6.4a,b) in the presence of odour and fly shorter distances between saccades (fig 6.4e), both of which effects are reported by Frye et al (2003). Their observation that intersaccadic flight becomes straighter is not replicated in my data, however (fig 6.4d). The fact that the changes I see are considerably less dramatic than the ones they report is once again consistent with the notion that my HS arena contained more residual vertical contrast than theirs.

While Frye et al (2003) is the only previous study I know of specifically looking at *Drosophila*'s ability to locate odour plumes when flying freely in static air, I shall briefly comment on my findings in light of other related experiments. Duistermars & Frye's (2008) finding that tethered *Drosophila* can successfully track an odour plume given wide-field vertical visual contrast, but not a single vertical stripe offset by 90° from the plume, would appear to match very closely with my results. However, I would caution against trying to draw any strong parallels between these experiments. The tethered fly is in a very unnatural situation where it experiences no translational optic flow and a quasi-binary olfactory signal. These points are not criticisms of the methodology, but merely mean that it is difficult to relate the results to free-flight OL.

Chow & Frye's (2008) tethered flight experiment finds that in the presence of food odour, turning responses to expanding visual stimuli are attenuated, while those to rotating stimuli are enhanced. Interpreting this result somewhat naively, one would have to conclude that these observations are not supported by my results, since neither wall-aversion (presumably mediated by visual expansion detection) nor the optomotor rebound size change significantly in the CB arena when odour is present. However, if one considers these effects to occur when odour intensity is rising, or in some

other sense 'elevated', then they provide plausible mechanisms for visually-mediated chemokinesis (table 6.2) and target attraction (table 6.7), respectively.

Tethered (Frye & Dickinson, 2003) and wind-tunnel (Budick & Dickinson, 2006) experiments on *Drosophila*, (not to mention countless studies on other animals such as moths; see section 2.5.2), suggest that flightspeed is increased when moving up the odour gradient. I fail to find any evidence for this effect, but that is not to say that it does not occur in my paradigm. This point is discussed further in the next section.

### 6.4.3: Mechanisms of odour localisation

As I have stressed in previous chapters, one must expect a high degree of noise in behavioural data from free-flying insects. To investigate the ways olfactory input could affect behaviour, I have made the assumption that odour intensity is proportional to proximity to the source. While this assumption is reasonable on average, this correlation is likely to be rather loose (see section 7.3). For these reasons, the analyses presented in section 6.3 are hampered by a very high degree of variability. Given these conditions, it bears repeating that failure to identify a significant effect is in no way equivalent to demonstrating that such an effect does not exist.

A further problem is that of separating cause and effect in an observational paradigm such as this one. All kinds of correlations exist between flight statistics, many of them due to the confined nature of the experimental space. For instance, we saw that segments directed towards *any* position 25cm from the arena centre are longer than those directed away (table 6.2), simply by virtue of the animals flying inside a cylinder. This issue necessitated the random resampling of data using fictive targets to obtain suitable baseline statistics. Consequently, these analyses become rather difficult to grasp intuitively. Fortunately, it is possible to use the model – a system whose internal workings are known – as a kind of sanity check for these methods (section 8.4.3).

With these warnings in mind, I shall discuss the behavioural effects identified in section 6.3. In the CB arena, intersaccadic segments directed towards the odour source are longer than those directed away from it (table 6.2). This chemokinesis could be achieved by modulating the probability of spontaneous saccades (section 4.5.5), or by adjusting the sensitivity of visual collision avoidance. The latter hypothesis seems more promising, as it is in accord with Chow & Frye's (2008) findings, and could potentially explain why vertical contrast facilitates OL.

I am doubtful that flies have any directional sense of the odour plume. Certainly, they show no strong

tendency to steer into the plume during intersaccadic flight (table 6.5). Intriguingly, flies in CB do saccade towards the source more often than chance would predict (table 6.4). However, this could be linked to their tendency to veer towards the wall in the presence of odour (fig 6.5). If this behaviour was promoted when moving up-gradient, it would tend to make the fly steer away from the source (though non-significant, we do see a trend in this direction in table 6.5). This in turn could bias the subsequent saccade towards the source.

In the SL-near condition, it appears that flies steer towards the landmark rather than the odour source (table 6.7). This could in fact explain why they appear to fly more slowly when moving up-gradient (table 6.3); it is possible that forward thrust is being reduced in order to perform these steering manoeuvres. In any case, this observation suggests that there may be two complimentary mechanisms for OL: visually mediated chemokinesis and odour-dependent landmark attraction.

These tentative hypotheses could of course be tested by more sophisticated behavioural experiments (section 10.2.2.4). However, I take the approach of modelling these putative mechanisms to assess whether they could really account for the observed behaviours. This is the subject of chapter 8. Before I can test a visual-olfactory model though, I must find a way to simulate an odour plume. I address this problem in the next chapter.

# 7. Plume characterisation

Before a visual/olfactory model can be implemented, a method of simulating the olfactory environment must be found. It would be very difficult to model the dynamics of diffusing odorant molecules, because while there is no wind inside the arena the air cannot be assumed to be completely static. Instead, difficult-to-measure processes such as convection currents will determine how the odour diffuses.

For this reason I take the approach of empirically measuring the structure of the odour plume. How the resulting data is used to simulate the flies' olfactory environment is covered in chapter 8, but first this short chapter describes how I went about characterising a typical odour plume in the experimental arena. Section 7.1 is concerned with the details of measuring chemical concentrations in air, while section 7.2 describes the process by which the spatio-temporal structure of the plume was recorded. Finally, section 7.3 presents the results of these experiments and discusses their validity.

## 7.1: Gas sensor

### 7.1.1: Choice of sensor

In order to characterise the structure of an odour plume, I use a chemical sensor to repeatedly record the odorant intensity at various points in space. An alternative approach would have been to use a visible tracer (i.e. smoke) to visualise the plume (e.g. Willis & Cardé, 1990; Geier et al, 1999; Budick & Dickinson, 2006). This method was not adopted for the following reasons:

- It would be difficult to introduce smoke to the arena without creating any unwanted air currents.
- Though by no means impossible, it would be technically challenging to reconstruct a 3D representation of the plume from 2D images.
- I had initially intended to build a robotic implementation of my model, and a point sensor would clearly be more suited to this application.

My requirements for a gas sensor are rather different from those of the industrial applications for which most are designed. As a single odorant is to be used, I am not concerned with the issue of gas identification, so selectivity is unimportant. Furthermore, since I can perform experiments in

controlled conditions, robustness to changes in temperature or humidity is not vital. However, temporal resolution is desirable because I want to record the fine spatio-temporal structure of the plume as experienced by *Drosophila* as accurately as possible. Crude time-averaged recordings will not capture the variability that is likely to exist.

There are two main types of gas sensor suitable for my purposes: photoionisation detectors (PID) and metal oxide semiconductor (MOS) sensors. PIDs use ultraviolet light to ionise organic molecules and measure the resultant electrical current to calculate the gas concentration. They offer very high temporal resolution, with a frequency response in the hundreds of Hz (Justus et al, 2005). They are comparatively expensive though, costing several thousand pounds. MOS sensors offer a much cheaper alternative. These contain a metal oxide film, the electrical resistance of which decreases as organic compounds bond to it. For my purposes, their main weakness is the rather slow response time associated with this bonding process, and the often even slower dissociation process. Typical response time constants are on the order of seconds (i.e. cutoff frequency $\approx$ 0.1Hz).

I searched for the fastest MOS sensor available, and found the MiCS 5521 volatile organic compound (VOC) sensor, manufactured by Microelectronics SA (Corcelles, Switzerland). This device consists of a metal oxide film and a heater element to ensure that bonded molecules rapidly dissociate from the film.

### 7.1.2: Interpreting sensor readings

To take measurements from the VOC sensor, I put the sensor resistor in series with a load resistor of a value similar to that of the sensor in clean air (fig 7.1). While continuously supplying the heater element with the appropriate voltage, the resistance of the sensor relative to the load resistor can be computed by measuring the voltage across it. The measurement was carried out using a Velleman K8055 USB experiment interface board, which acts as an 8-bit analogue-to-digital converter. A custom-written C++ program was used to log readings.

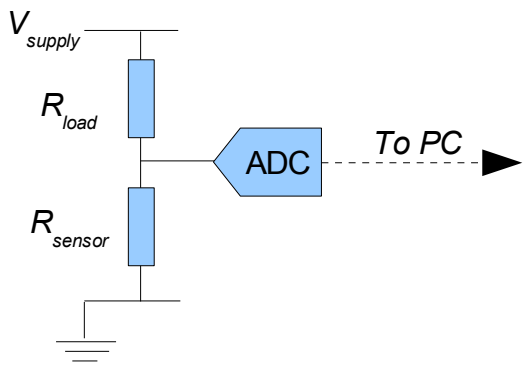


Figure 7.1: VOC sensor circuit diagram. Heating circuit not shown. The analogue-to-digital converter sends an 8-bit reading to a computer via USB. $V_{supply}$=5V.

Because the baseline resistance of the sensor depends on atmospheric conditions (especially humidity), it is necessary to calibrate the circuit while the sensor is in clean air. This is done by adjusting the gain of the ADC so that its output is just below the saturation value of 255. This maximises the dynamic range of the sensor reading, thus improving its accuracy.

It is straightforward to calculate $V_{sensor}$, as the gain of the ADC is known. $R_{sensor}$ can then be obtained using equation 7.1. As $R_{load}$ is a constant, we can ignore it as long as we bear in mind that the resistance measurement is no longer in ohms. To ascertain how the resistance of the sensor relates to odorant concentration, I consulted the sensor datasheet, which gives the response characteristics for carbon monoxide (fig 7.2). I am measuring a different organic compound, but I make the assumption that while the gain may differ, the same log/log relationship will hold. Thus, the concentration in arbitrary units is given by equation 7.2.

$$R_{sensor} = R_{load} \frac{V_{sensor}}{V_{supply} - V_{sensor}} \tag{7.1}$$

$$concentration = \exp(-\ln(R_s / R_0)) \tag{7.2}$$

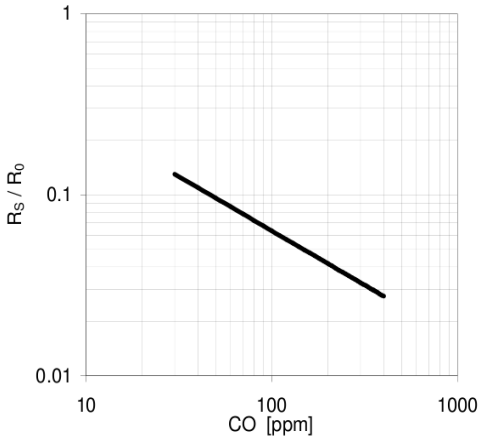


Figure 7.2: VOC sensor response to carbon monoxide. $R_s$ is the sensor resistance, $R_0$ is the resistance in clean air. Data recorded at 25°C and 50% humidity. Taken from the product datasheet, © Microchemical Systems SA.

## 7.1.3: Sensor temporal dynamics

To assess the temporal resolution of the VOC sensor, it was positioned in front of an electric fan and apparatus was constructed allowing an ethanol-soaked swab to be quickly placed upwind of the sensor, and removed equally quickly. The airflow ensures a rapid rise or fall in the odorant concentration in the vicinity of the sensor. Control experiments showed that the effect of air moving over the sensor (which could potentially cool it down, changing its resistance) was negligible. Fig 7.3 shows the readings obtained during a test of this type. Looking at the raw sensor data, the off-response appears much slower than the on-response. However, following the non-linear transformation to an estimate of concentration, the two transitions happen at comparable rates.

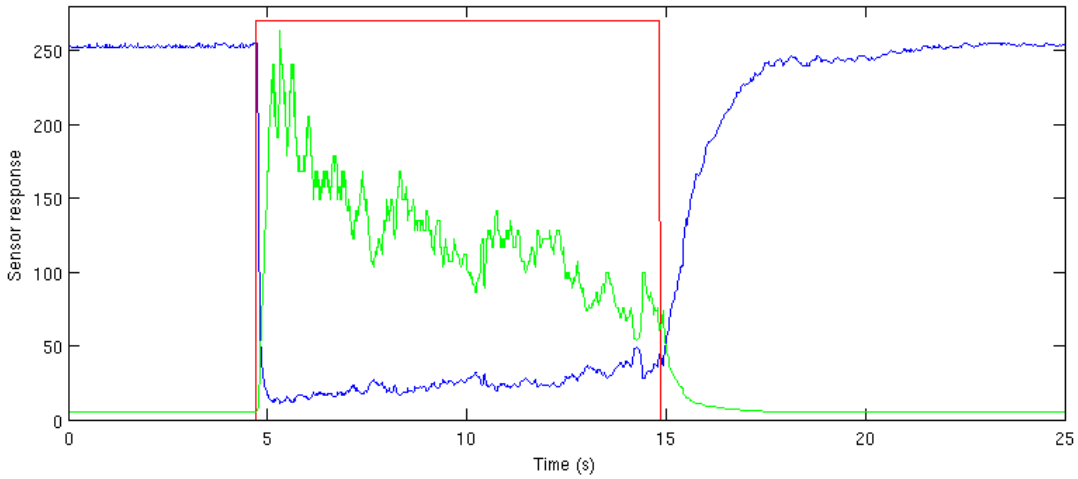


Figure 7.3: VOC sensor dynamics. The red line shows whether the sensor is downwind of an ethanol-soaked cotton wool ball (high) or in clean air (low). The blue line is the raw sensor reading, which has an integer value between 0 and 255. The green line is this signal transformed into a concentration estimate using the procedure explained in section 7.1.2, with an arbitrary scale.

Due to the crude nature of the experimental set-up, there is no stable high value. This is because the air flow is likely turbulent, creating pronounced fluctuations in the concentration of ethanol vapour at the sensor. The concentration decreases over the 10s period, presumably because the ethanol on the cotton wool is depleting due to evaporation.

These difficulties aside, it is still possible to estimate the rise and fall time of the VOC sensor. Repeating the procedure shown in fig 7.3 several times, and fitting exponential curves to the transitions, yields a time constant of approximately 160ms for both rise and fall. Assuming the sensor has first-order low-pass filter characteristics, this corresponds to a cut-off frequency of ~1Hz. This is around one order of magnitude slower than the fly olfactory system (see section 2.6.2), which is not ideal but should at least ensure that the measurements I obtain will feature a reasonable level of temporal variability, rather than representing crude time-averages.

## 7.2: Methodology

To characterise the 3D structure of the plume I sample the odorant concentration at many different points in the arena. It is also desirable to record at different times after the odorant vial is introduced to the arena to investigate the temporal development of the plume. Thus, the task faced is one of sampling a 4D space.

### 7.2.1: Apparatus

To facilitate recording from different spatial locations, the VOC sensor was mounted on a gantry robot which the University of Sussex kindly allowed me to use. It is a three degree-of-freedom robot with sub-millimetre precision over a workspace of 3x2x2m (Smith et al, 2007). It is controlled using a C++ program written by its designer, Lincoln Smith.

The sensor was mounted at the bottom of a 65cm metal pole, which was put tightly inside a carbon fibre tube to increase its rigidity. The other end of the pole was attached to a baseplate which was bolted to the robot (fig 7.4). The purpose of this pole was to minimise the disturbance of the air caused by the movement of the robot.

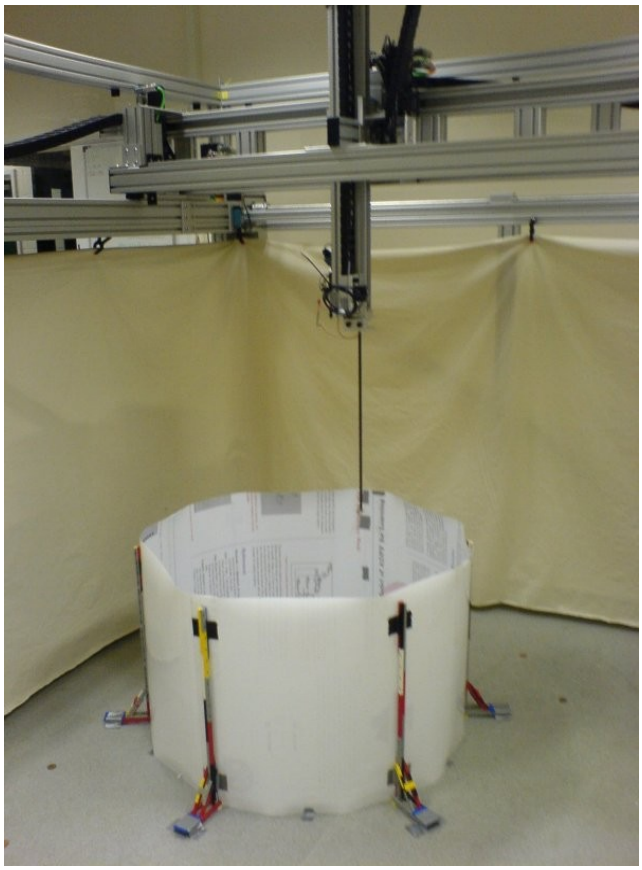

Figure 7.4: The Sussex gantry robot with VOC sensor attached, sampling inside the mock arena.

A mock arena of the same dimensions as the free-flight arena (i.e. 1m diameter, 60cm radius) was constructed from laminated paper with six plastic (Lego) stanchions for support. Note that the curtain extending from the top edge of the arena wall was absent. As it was not possible to make holes in the floor, the odorant was contained in a small (<1cm tall) flat-bottomed vial which was placed on the floor in the appropriate position.

The odorant used was 70% ethanol solution, not vinegar. This step was taken because the sensor was found to have very low sensitivity to balsamic vinegar, possibly because of the different chemical properties of ethanol and ethanoic acid (the primary, but by no meals only, volatile organic compound found in balsamic vinegar), or possibly because the vinegar is simply a much weaker solution, at only 6% ethanoic acid.

It is reasonable to assume that ethanol and ethanoic acid diffuse similarly, as they have comparable molecular masses (46 and 60) and boiling points (74°C and 118°C, respectively). More importantly, molecular diffusion, which depends on the characteristics of the odour molecules, typically only takes place over a scale of a few centimetres. On larger scales turbulent diffusion, i.e. that due to odorant molecules being carried by currents in the air, dominates and "the plume structure becomes practically independent of the properties of the material within it" (Murlis et al, 1992, p509).

### 7.2.2: Procedure

Prior to the introduction of odorant, a baseline reading from the VOC sensor was taken, for reasons explained in section 7.1.2. This was repeated before every experiment to control for drift in ambient atmospheric conditions. Based on preliminary VOC recordings from a handful of points in the free-flight arena, it appeared to take several minutes for odour to diffuse enough to reach appreciable levels throughout the arena volume. Thus I decided to take measurements from five to twenty minutes after the odour vial was introduced. A temporal resolution of one minute is used, by which I mean that for every point in the arena I take 15 measurements, i.e. one from each one-minute interval of the recording period.

I decided upon a spatial resolution of 10cm, which gives 69 positions that fall within the 1m diameter circle of the arena. Fig 7.5 shows a route by which all of these can be visited without travelling further than 14.1cm between any consecutive pair of points. Minimising the amount the robot must move minimises the extent to which it perturbs the air in the arena.

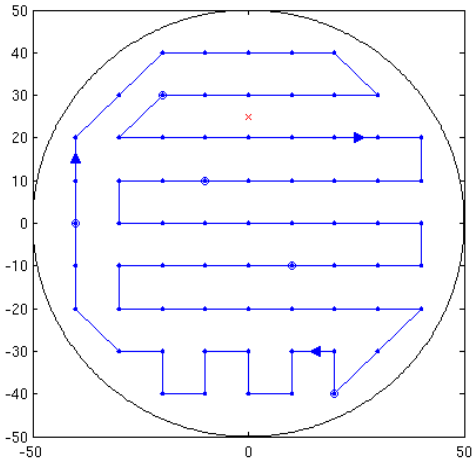


Figure 7.5: The trajectory used to traverse a layer. Small dots show the 69 grid-points at which samples are taken. Circles represent the five offset points, placed approximately 14 points apart. Arrows show the direction of movement, and the red x represents the location of the odour vial.

The time taken for the robot moving at its default speed to traverse this path stopping at all the points is ~62s. Thus a pass of all 69 points in one horizontal plane (which I shall henceforth call a 'layer') can be completed in five minutes if the gantry pauses for 3.4s at each point to take sensor readings. Repeating this process five times but starting at different 'offsets' on the circuit (fig 7.5) means that each point can be sampled once in each one-minute interval.

There are six layers, at heights from 5 to 55cm from the floor. Three layers can be sampled in any 15-minute experiment (i.e. from t=5 to 20min). The robot always moves downwards when changing layers, because the air at lower levels will be less perturbed by the robot's previous movements than that at the same or higher levels. The experimental regime is summarised in fig 7.6. Between trials the ethanol vial is removed, the lab is ventilated, and the arena is fanned to expel lingering vapour.

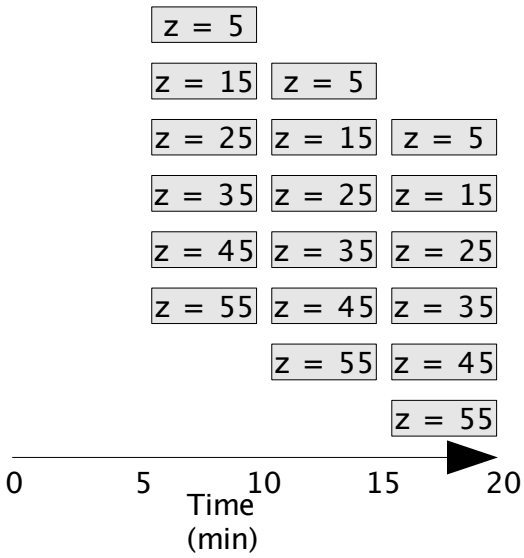


Figure 7.6: Experimental procedure, z is altitude in cm. Rows are separate experimental trials. In each trial, between 1 and 3 layers (fig 7.5) are sampled. If multiple layers are sampled, they are always in descending order of altitude. These eight trails are repeated for each of the five offsets, giving a total of 40.

Data is read from the VOC sensor at 20Hz; there is little point in sampling at any higher frequency due to the sensor's response characteristics (section 7.1.3). Thus recording for 3.4s gives 68 individual readings. Therefore, a total of 68 samples x 69 positions x 6 layers x 15 minutes = 422,280 measurements were taken, not counting the pre-trial baseline recordings.

## 7.3: Results and discussion

Fig 7.7 shows the spatial structure of the odour plume averaged over the interval from 10 to 15 minutes after the odorant vial was introduced, corresponding to roughly the period when I conduct the fly experiments. Note that the heat scale is logarithmic. As one would expect, odorant concentration is highest near to the source.

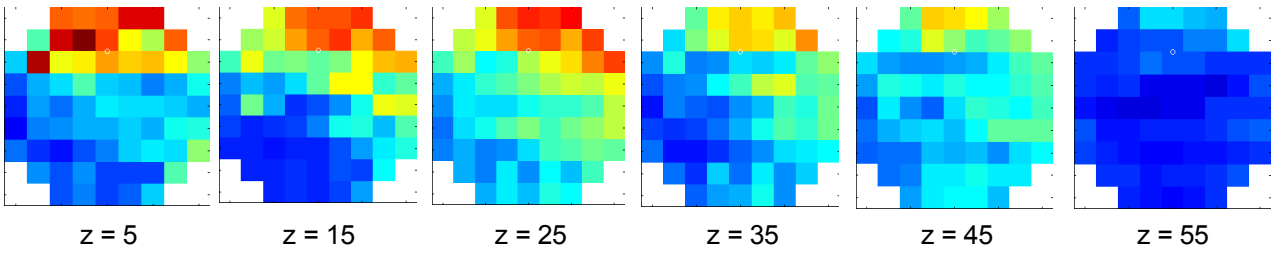


Figure 7.7: Mean odour intensities throughout the arena for the 11th to 15th minutes. Each image is a horizontal slice at the altitude (in cm) shown. The white o shows the position of the vial. Note that the colour scale is logarithmic, units are arbitrary.

There are some less obvious points to note about the spatial characteristics of the plume:

- Odour appears to gather at the walls of the arena, particularly at higher altitudes.
- The plume has a slight 'mushroom cloud' shape, as evidenced by the fact that intensity at the opposite side of the arena to the vial is greater in higher layers than those close to the floor (compare z=5 to z=45), despite these points being further away from the source in 3D space.
- A slight bias towards the right side of the arena is seen. This could be due to the robot's perturbation of the air as it traverses the layer (fig 7.5), or subtle air currents in the laboratory.

Fig 7.8 gives an impression of how the plume develops over time. The z=35cm layer is shown, since this is the one closest to the average altitude at which flies fly in the presence of odour (section 6.2.1), and thus closest to the altitude set for the model (section 5.2.2). As one might expect, odour intensity generally increases over time as the ethanol vapour reaches this height. The distribution also becomes more uniform as time passes (compare the second and fifth intervals of fig 7.8).

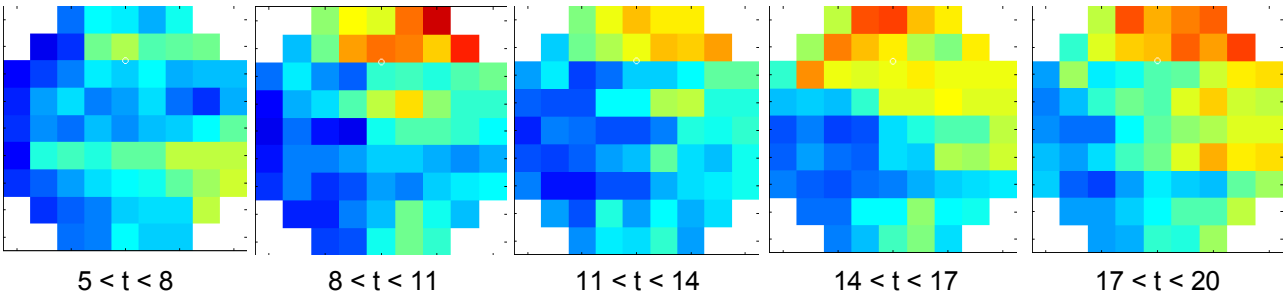


Figure 7.8: Temporal plume structure, time is in minutes after odorant introduction. Mean odour intensities for the z=35cm layer are shown. Heat scale is in arbitrary logarithmic units.

While steps have been taken to minimise the perturbation of the air caused by the robot's movements, there remains the distinct possibility that some disruption of the plume is caused in this way. To assess the magnitude of this effect, I made a series of recordings with the robot stationary for the entire 15 minute experimental period. Fig 7.9 shows these recordings from three different locations, compared to the measurements taken by the moving robot in the same positions.

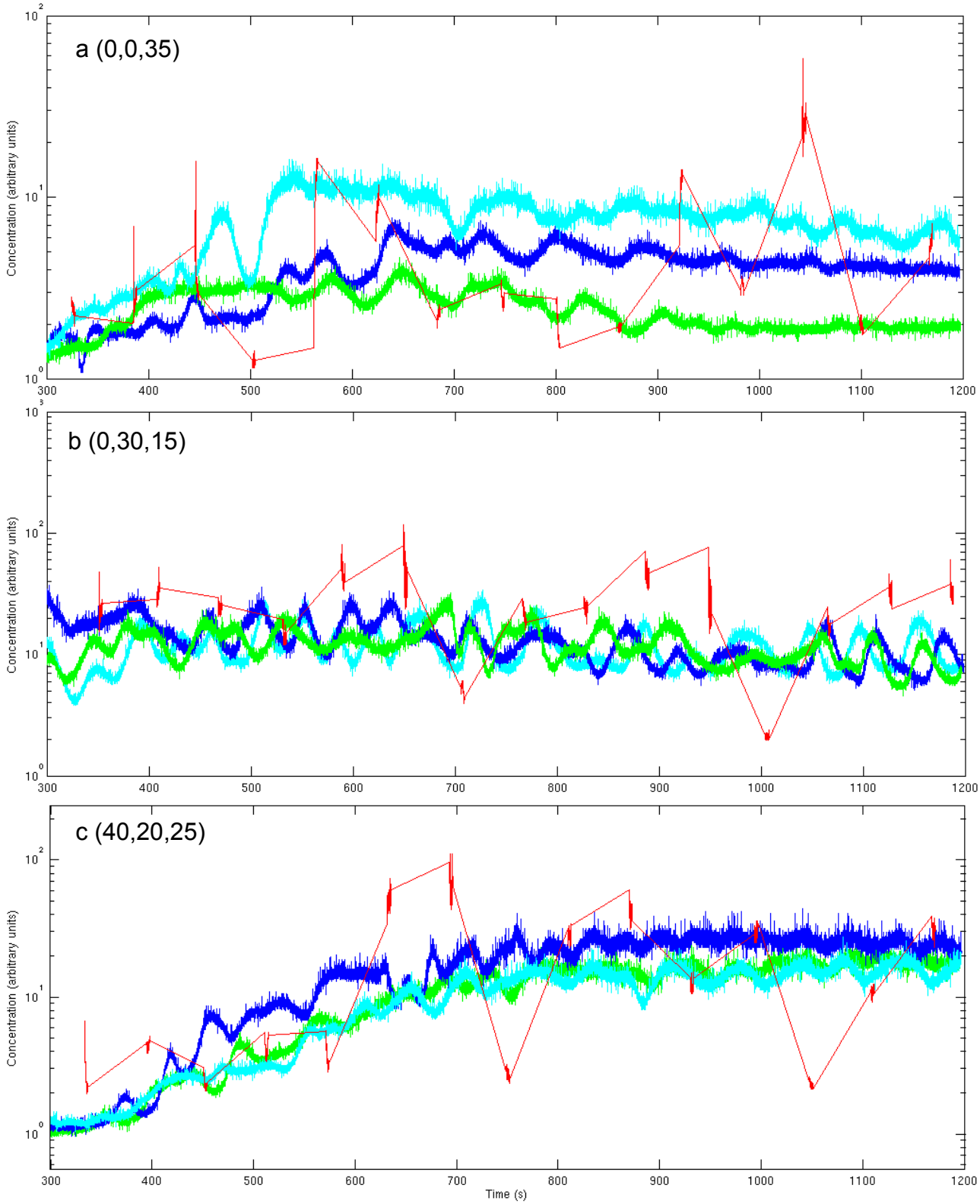


Figure 7.9: Static *versus* moving recordings. These three graphs each show intensity recorded over three 15-minute runs at a single point: **a** near the centre of the arena, **b** close to the vial, and **c** close to the wall. The blue, green and cyan lines are three separate static recordings, while the red shows the measurements taken from the moving gantry experiments corresponding to the same spatial point. Note that the 15 samples come from 15 different experiments.

The static recordings reveal some interesting properties of the odour signal. The trial-to-trial variation is quite large, and appears to vary between positions, being most pronounced at (0,0,35). Another striking feature is the existence of large fluctuations in intensity happening over a timescale of several tens of seconds.

The measurements from the moving robot (fig 7.9, red) often fall outside the range of concentrations seen in the three static recordings, especially in positions b and c. Thus I must conclude that the movement of the gantry affects the odour plume, and therefore the data presented above is not entirely representative of an odorant diffusing without external perturbation. Of course, a somewhat higher degree of variability is to be expected in the moving recordings, as they are composed of data taken from 15 different experiments potentially performed on different days with different ambient conditions.

In any case, the stationary and moving recordings do not differ wildly, so I am of the opinion that the measurements taken by the moving robot represent a useful, if noisy, dataset. As is discussed at greater length in 8.1, it is better for the validity of the model that the simulation over- rather than underestimates the level of noise in the environment.

# 8. Modelling odour localisation

This chapter is concerned with adding an olfactory sense to the existing visuomotor model (chapter 5) to model the odour localisation behaviour of *Drosophila* (chapter 6). I begin by describing how the odour plume is simulated (section 8.1) based upon recordings of real plumes (chapter 7). After describing how the odour signal is preprocessed (section 8.2), I investigate various ways in which this information could modulate the visuomotor model (section 8.3). Having identified the minimally complex crossmodal model able to reproduce the odour localisation behaviour of flies, I characterise its behaviour and compare it to that of the insect (section 8.4). After summarising the main findings, I conclude the chapter with a discussion of the model's validity (section 8.5).

## 8.1: Plume simulation

To test models of odour localisation, the arena simulation must be extended to include the olfactory environment. Chapter 7 described how the odour plume was measured empirically; this section addresses the issue of how to use that data to simulate the olfactory input of the model fly as it moves around the arena.

One approach would be to fit some kind of parametric model to the data, e.g. a 3D mixture of Gaussians. This would be a compact, analytically elegant representation which would allow for very straightforward generation of new data, i.e. producing estimates of the odour intensity at arbitrary points in the arena. The variability could be modelled in a similar way, thereby generating a realistic level of noise.

However, the main problem with this approach is that one risks introducing regularities to the data that do not exist in reality. Fitting $n$ Gaussians to a distribution makes the implicit assumption that it is at most $n$-modal. Similarly, adding Gaussian noise would be inappropriate if the noise distribution was not in fact normal. When modelling, it is imperative to avoid simplifying the environment in any way that makes it possible for algorithms that would fail in the real world to be successful. Only in this way one can avoid the oft-heard criticism that models are 'doomed to succeed'. For this reason, I take a non-parametric approach where the data itself *is* the model. (In the machine learning community, techniques of this kind are called 'lazy learning', because no attempt is made to abstract any structure from the training data.)

As described in section 7.2.2, for every point on a 10cm grid inside the arena, I have 15 measurements of the odorant concentration taken between five and 20 minutes after odorant was added to the arena. Each measurement consists of 68 individual readings from the VOC sensor. Thus there is a pool of 15 x 68 = 1020 samples associated with each grid-point. Since the animal experiments take place between approximately 10 and 14 minutes after odour introduction, it could be argued that I should only use the samples taken between these times. However, I take the position that adding more variability can only make odour localisation more difficult, increasing one's confidence in any model that successfully reproduces the target behaviours (see above).

It is undesirable to include the left/right bias (fig 7.7) in the plume simulation, since this is most probably particular to the measurement paradigm. Therefore, mirror-symmetric positions about the y-axis are treated as equivalent, meaning that all grid-points not on this line actually have 2040 associated samples.

The simulated odour level at any grid point can be generated by simply choosing a random sample from the pool of 2040 (or 1020) for that point, trivially guaranteeing that the simulation distribution will be identical to that recorded (fig 8.1). Note that this method is likely to overestimate the moment-to-moment variability of the plume at a given point, since data is aggregated from many different experimental trials (see fig 7.9).

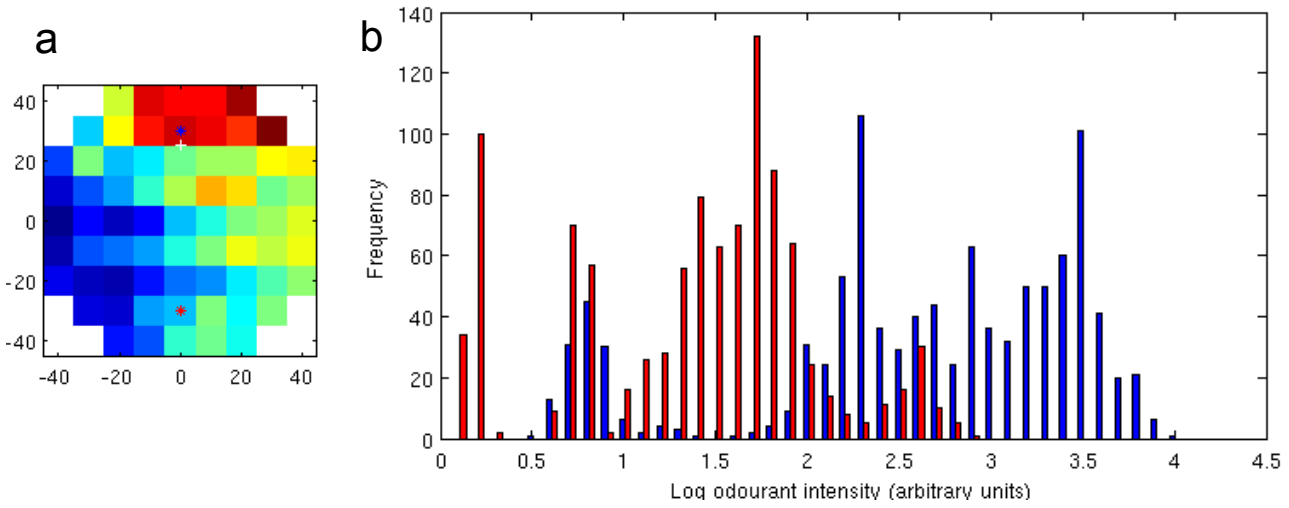


Figure 8.1: Odour plume datasets. **a** Map of mean log odorant intensity for the horizontal slice of altitude 35cm (arbitrary heat scale) over the full 15 minute period. The white '+' indicates the odour source position. **b** Histogram showing the full set of readings for the points marked by the blue and red stars in **a**. Each dataset consists of a total of 1020 readings, in 15 batches of 68 readings. Each batch is taken from a separate experimental trial, accounting for the multimodal nature of the distributions.

The question remains of how to select a grid point to sample from when the model is in some arbitrary location between grid points. Choosing the nearest neighbour is perhaps the most obvious approach, but this could create unrealistic discontinuities. Instead, I select using the probability distribution defined in equation 8.1:

$$p(gridPoint) = \frac{\exp\left(\frac{-distanceTo(gridPoint)^2}{5^2}\right)}{\sum_{g \in gridPoints} \exp\left(\frac{-distanceTo(g)^2}{5^2}\right)} \quad (8.1)$$

i.e. a 3D Gaussian of s.d. = 5cm centred on the model's current position. Note that as the s.d. approaches 0, this mechanism becomes nearest-neighbour.

## 8.2: Olfactory pre-processing

I ignore the issue of odour identification altogether, since the chemical composition of the attractant is constant. Thus the model's olfactory input signal can be taken as a scalar value. Olfactory receptor neurons are known to have lowpass (Justus et al, 2004; Schuckel et al, 2008) as well as highpass (i.e. adaptation) characteristics (Störtkuhl et al, 1999; see section 2.6.2). Adaptation is also found at the first synapse of the olfactory system in the antennal lobe (Kazama & Wilson, 2008), and *Drosophila* larvae exhibit marked behavioural adaptation to the prolonged presentation of odour (Cobb & Domain, 2000). Indeed, it seems clear that the temporal derivative of odour intensity is more useful than the absolute value to an animal attempting to locate an odour source, given that baseline conditions may be highly variable.

To obtain a suitable olfactory signal I feed the raw odour level to two parallel first-order low-pass filters with different time constants. Subtracting the output of the slower filter from that of the faster filter gives an approximation of the temporal derivative, which I call *OD'* (fig 8.2). I then employ an adaptive gain mechanism to keep the range of this signal constant despite changes in the overall amplitude of the odour signal. This is achieved by keeping an incremental estimate of the variance of the signal, with a time constant of 4s. This is compared to a desired value (specifically, 1.0) for the variance, and the difference causes a compensatory change in the gain by means of a simple proportional controller. The output of the system, *OD**, is given by OD' multiplied by the adaptive gain parameter. This process is summarised in fig 8.2, and the behaviour of the system is illustrated in fig 8.3.

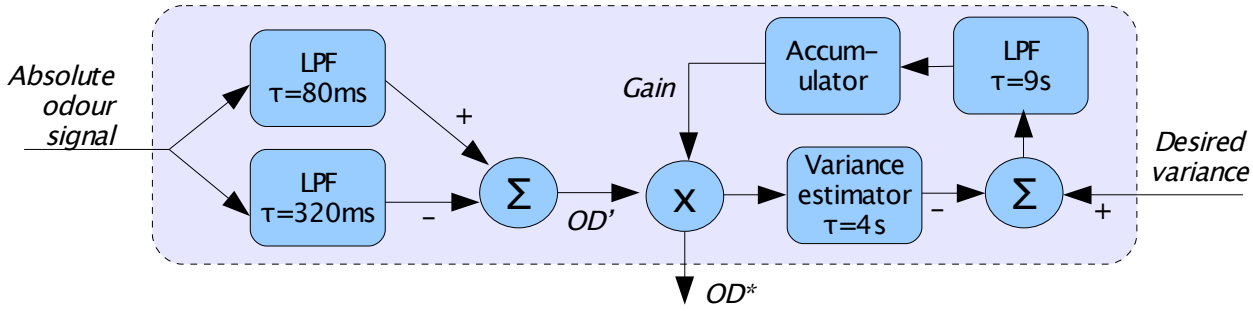


Figure 8.2: Overview of olfactory pre-processing. An estimate of the temporal derivative of the odour signal (*OD'*) is obtained by comparing two first order low-pass filters (LPFs) with different time constants. The gain of this signal is then adjusted by a slow feedback system which attempts to keep the variance equal to 1. This gives *OD**, which is used to modulate visuomotor behaviours (section 8.3).

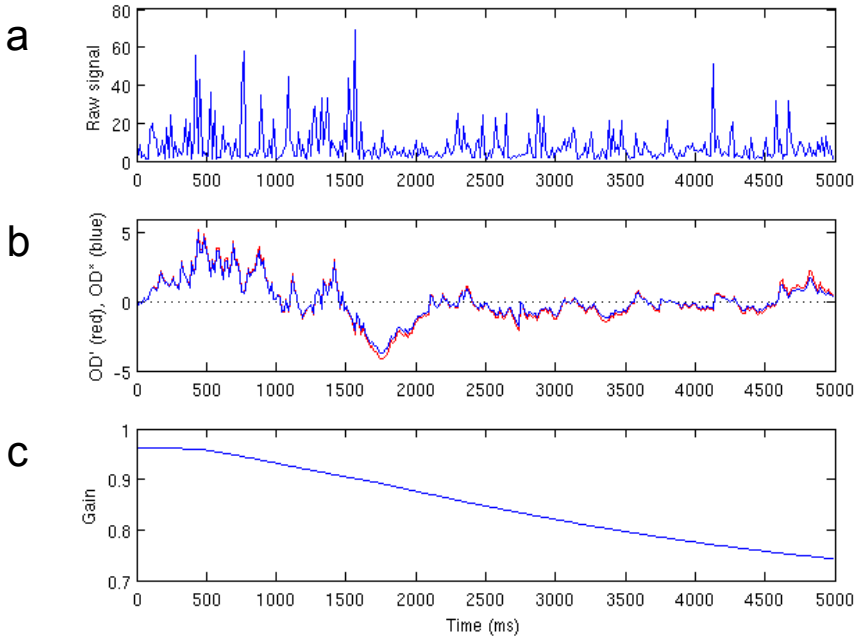


Figure 8.3: Behaviour of the olfactory pre-processing system (fig 8.2). **a** Sample olfactory input during five seconds of simulated flight in the arena. Units are arbitrary, scale is linear. **b** The estimate of the temporal derivative of the odour signal, both before being subjected to adaptive gain (OD', red) and after (OD*, blue). The values are similar because the gain is close to 1. Note the slight lag due to the use of LPFs: there is a sharp drop in the raw signal at t≈1600, but the minimal level of OD* is not reached until >100ms later. **c** The adaptive gain. This changes slowly and with a considerable lag; as a result of the high variance of the OD* signal during the first 2s, the gain continues to decrease for the following 3s.

Fig 8.4 shows the distribution of OD* values experienced by the model flying in the CB arena. Note that at this stage the odour signal does not modulate any aspect of behaviour. Also shown in fig 8.4 is the Gaussian distribution that the adaptive gain mechanism attempts to maintain. While it is a

reasonable match, it is instructive to reflect on the differences. There is some positive skewness (i.e. the mode is less than the mean), indicating that due to the arena geometry and the plume structure, moves up the odour gradient tend to be steeper than those going down. The distribution is also slightly more heavy-tailed than a Gaussian, so extreme values are seen relatively often.

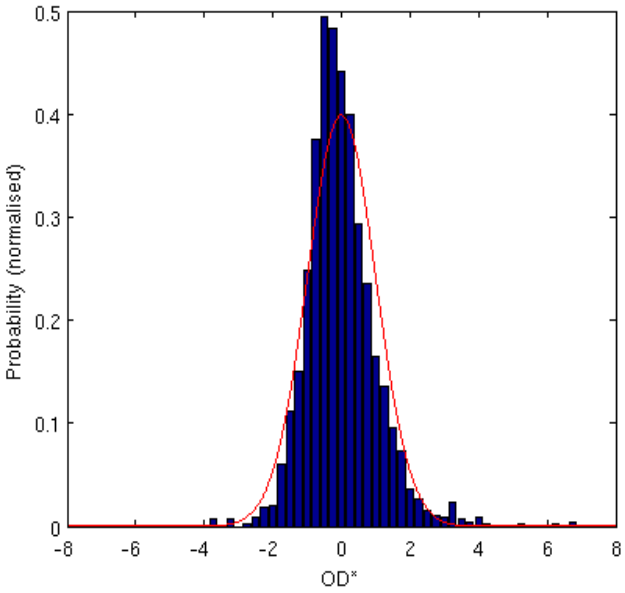


Figure 8.4: Distribution of OD* values experienced by the model in the CB arena. Here, the olfactory signal does not influence the model's behaviour in any way. Probability is normalised such that the total area of the histogram is 1, to facilitate comparison with the Gaussian distribution (mean=0, s.d.=1) plotted in red.

## 8.3: Models of visual-olfactory interaction

Now that a plume simulation has been implemented and a suitable olfactory signal devised, I address the question of how this signal can modulate the existing visuomotor model (chapter 5) to reproduce the odour localisation behaviour seen in flies (chapter 6). Clearly, there are almost limitless ways in which olfaction could modulate flight control. I therefore employ the principle of Occam's razor, starting with the very simplest ways in which olfactory information could shape flight behaviour and only attempting more complex schemes if simple ones can be shown to be insufficient to reproduce the experimental results. The OL performance of all of the following models, compared to the insect data, is summarised at the end of this section in fig 8.10.

### 8.3.1: Model 0: Non-visual chemokinesis

Perhaps the simplest known algorithm that could produce odour localisation behaviour is undirected

kinesis, a mechanism used, for instance, by *E. coli* to find food (Berg & Brown, 1972; see section 2.5.3). This refers to a process whereby the animal will continue to move forward while odour intensity is rising, and turn randomly when it falls. The model is numbered 0 because it does not in fact involve any modulation of the visuomotor system by olfaction, but rather has the two systems operating entirely in parallel. Whenever OD* falls below a certain negative threshold value, a saccade is initiated with a 50/50 probability regarding the direction. Each odour-triggered saccade will inhibit visually triggered (CA) ones in just the same way as shown in fig 5.17.

This mechanism introduces a free parameter: what threshold value of OD* should trigger a saccade? Fig 8.5 shows the results of systematically varying this parameter. At low values clear OL is observed, with higher OLIs than those seen in flies. At high values no significant OL takes place, as olfaction-triggered saccades becoming increasingly infrequent. The key point is that at no point in this range is there a significant difference in OL performance between the CB and HS arenas, so this model is unable to reproduce the pattern seen in the biological data.

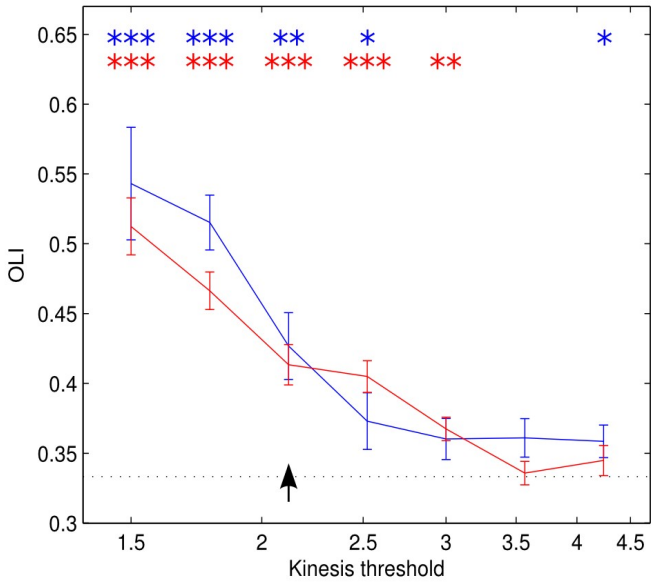


Figure 8.5: OLI in the CB (blue) and HS (red) arenas for a range of settings of the threshold for olfactory saccade initiation, n=24 for each observation. The dotted black line is the chance baseline level. Asterisks denote significance of OL performance: *** p<.001, ** p<.01, * p<.05. In none of the cases is the difference between CB and HS significant. The black arrow shows the setting used to produce the data in Fig. 8.10. As the threshold increases, chemokinetic saccades become less frequent, and behaviour tends towards that seen in the absence of odour. Bars represent ±1s.e.m.

Fig 8.10 illustrates the OL behaviour of this model (with a mid-range parameter setting, fig 8.5) in all four experimental conditions. It achieves significant OL in both SL-near and SL-far, but once again

there is no significant difference between the two results.

Model 0's ability to locate the odour in all arenas demonstrates that the simulated plume (section 8.1), despite all its noise and variability, contains sufficient structure to allow its source to be found. It seems remarkable that a control scheme as simple as kinesis can outperform flies in terms of OL, and indeed prompts the question of why flies do not make use of it. The reason for this may be that the algorithm implicitly assumes that the air is static. An animal in the wild cannot generally assume that it is moving forward just because it is making the appropriate wing movements, and must therefore make use of visual input to obtain information about its movement relative to the world (Srinivasan et al, 1997).

### 8.3.2: Model 1: Collision avoidance (CA) modulation

Clearly, olfaction must interact with the visual system to produce the environment-dependent odour localisation that we see in flies. As discussed in section 6.4.3, an obvious way to produce kinesis-like behaviour *via* the visuomotor controller is to have the olfactory signal modulate the threshold for initiating CA saccades, such that saccades are inhibited by a rising odour intensity (positive OD*), and promoted by a falling one. Model 1 does just that, using OD* to continually modulate the threshold parameter in the CA system as described in equation 8.2 (*CAthresh* = 3.8, see fig 5.17).

$$CAthresh_{Model1} = CAthresh + OD^{*} \times modulationGain \tag{8.2}$$

Once again, this mechanism introduces a free parameter: how much should the odour signal alter the sensitivity of the CA system? Fig 8.6 shows the results of varying this parameter in the SL-near and SL-far conditions. For all values tested, a higher degree of OL is seen in the SL-far case, which is the opposite of the effect seen in flies. However, as fig 8.10 shows, this model is able to produce the desired difference in behaviour between the CB and HS arenas.

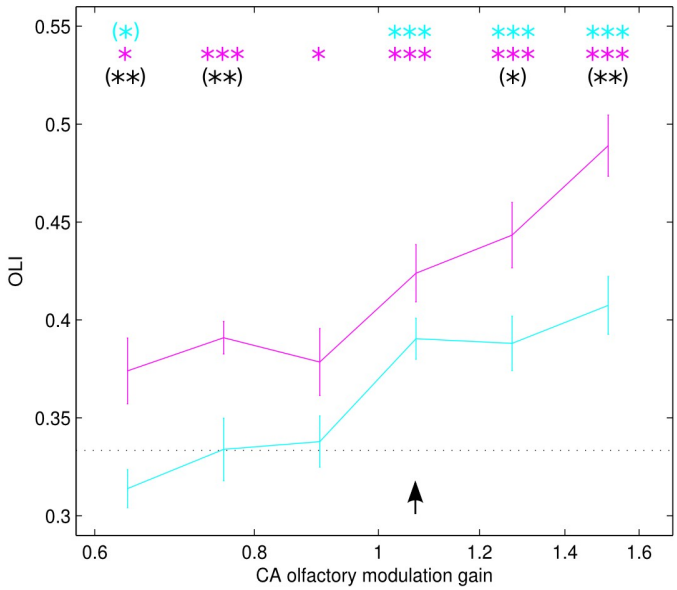


Figure 8.6: Model 1 (CA modulation) parameter sweep. OLI in the SL-near (cyan) and SL-far (magenta) arenas for a range of settings of the threshold for olfactory saccade initiation. The dotted black line is the chance baseline level. Asterisks denote significance of OL performance: *** p<.001, ** p<.01, * p<.05. Black symbols refer to the significance of the difference between the conditions. Brackets denote significant effects in the opposite direction to that seen in the fly data. The black arrow shows the setting used to produce the data in fig 8.10. Bars represent ±1s.e.m.

In section 6.4.3 I speculated that the fly may possess at least two distinct mechanisms for OL: a visually-mediated chemokinesis behaviour that is seen in textured but homogeneous environments, and an odour-dependent landmark attraction behaviour. Consistent with this account, it seems that Model 1 achieves the former competence but not the latter.

### 8.3.3: Model 2: CA modulation + optomotor response (OMR) boost

Tethered flies increase the amplitude of responses to visual rotation in the presence of food odour, as well as decreasing their response to expansion stimuli (Chow & Frye, 2008). I found evidence that flies steer towards the landmark when localising odour in the SL arena (section 6.3.5), and I demonstrated that increasing the gain of the OMR system results in landmark attraction (section 5.4.4). In light of these points, Model 2 introduces an odour-dependent strengthening of the OMR system. Note that unlike the continuous modulation of the CA threshold based on OD*, this takes the form of a step change in OMR gain which occurs according to the presence or absence of food odour and persists for the entire experimental trial. This is shown in equation 8.3, where *OMRgain* = 10.0 (fig 5.10):

$$OMRgain_{Model2} = \begin{cases} OMRgain \times (1 + OMRboost) & if\ odourPresent \\ OMRgain & otherwise \end{cases} \quad (8.3)$$

The size of this boost is a free parameter, and I cannot assume the relationship between CA modulation gain and OL behaviour identified for Model 1 will persist for this model, so both parameters must be investigated. Since the parameters may well exhibit a non-linear interaction, a systematic search of the 2D parameter space is called for. This was carried out, but since the results of such an analysis are rather difficult to present on paper, fig 8.7 merely illustrates two 1D slices through this space. As summarised in fig 8.10, this model successfully reproduces the findings that OL is stronger in CB than HS (OLI = .437 *versus* .361, U(24,24)=110, p=.0002), and in SL-near than SL-far (OLI = .436 *versus* .332, U(24,24)=41, p<.0001).

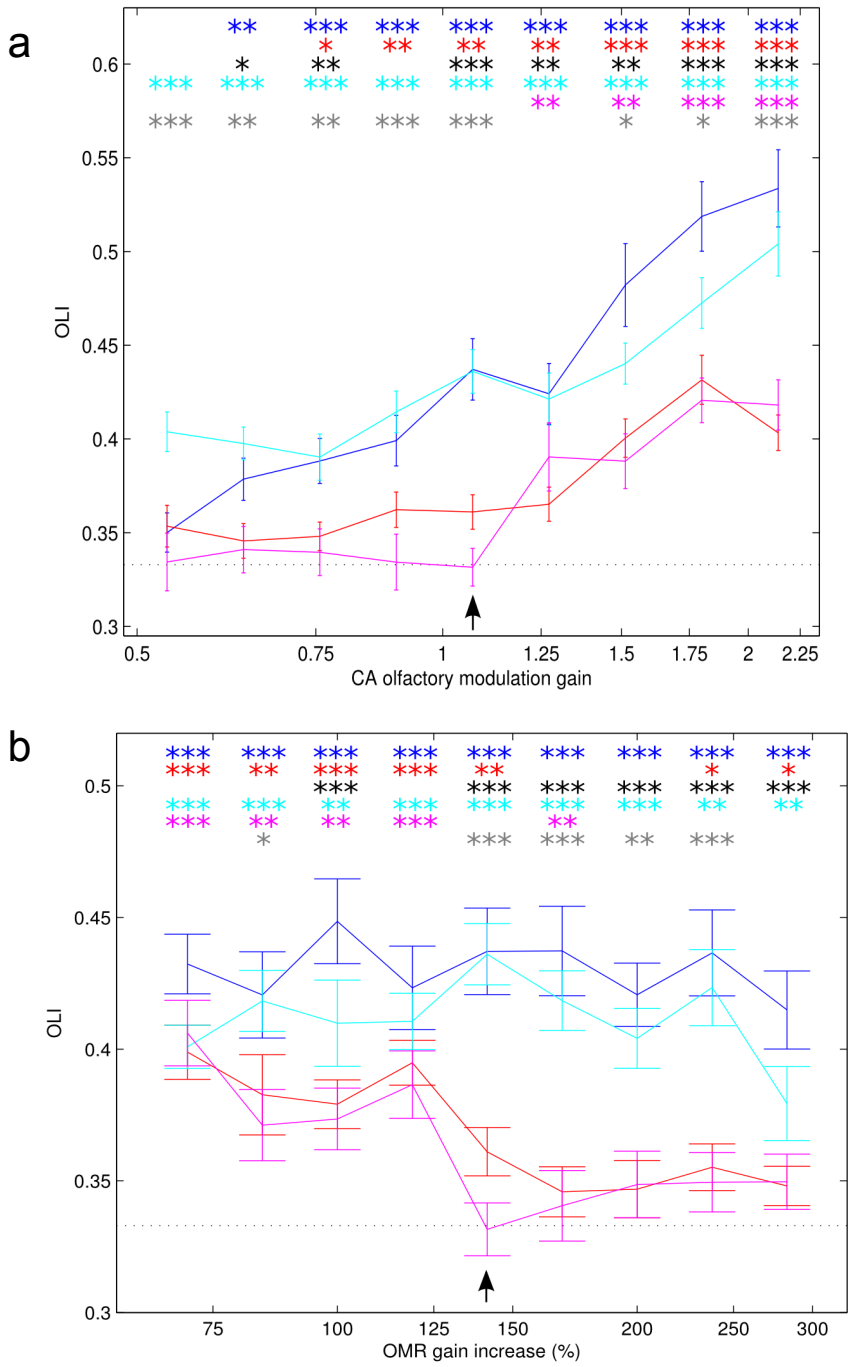


Figure 8.7: Model 2 (CA modulation + OMR boost) parameter sweep. OLI in the CB (blue), HS (red), SL-near (cyan) and SL-far (magenta) arenas. In **a** the OMR boost is held constant while the CA modulation gain is varied, and vice versa in **b**. The dotted black line is the chance baseline level. Asterisks denote significance of OL performance: *** p<.001, ** p<.01, * p<.05. Black symbols refer to the significance of the CB/HS difference, grey ones to SL-near/far. The black arrow shows the setting used to produce the data in Fig. 8.10., which is also the setting employed whilst sweeping the other parameter.

## 8.3.4: Model 3: CA modulation + OMR modulation

It could be argued that it would be more parsimonious to have OD* continually modulate the OMR

gain as it does for the CA threshold, rather than introducing the binary distinction between the presence and absence of odour seen in the previous model. Furthermore, the fact that flies veer towards the landmark in SL-near but not SL-far (table 6.7) could suggest that the OMR is only strengthened when the odour intensity is increasing. Model 3 explores this possibility by having OD* influence the OMR gain as shown in equation 8.4:

$$OMRgain_{Model3} = OMRgain \times 2^{OD^* \times modulationGain} \tag{8.4}$$

I chose an exponential rather than linear relationship, as it seems more appropriate that the gain approaches zero for a sharply falling odour signal (i.e. large negative OD*), rather than reversing polarity. Sample results from Model 3 are shown in fig 8.10. Like Model 1, it reproduces the CB/HS difference seen in flies, but fails to exhibit the SL-near/far effect.

The settings of both gain parameters must be investigated before this model may be rejected. Fig 8.8 shows two illustrative slices through this 2D parameter space. As in Model 1, by altering the CA modulation gain one can achieve very strong OL in both SL-near and SL-far, or no OL in neither, but significantly stronger OL in SL-near than SL-far is never observed (fig 8.8a). Very weak OMR modulation renders this model equivalent to Model 1, and the same reverse effect (i.e. better OL in SL-far than SL-near) is seen (c.f. fig 8.6). While this gap closes when OMR modulation gain is increased, the desired difference is still not found. It should be noted that the rightmost datapoint on fig 8.8b very probably represents an unrealistically high gain. Since OD* values of 4 and above are not unheard of (fig 8.4), these instances would result in a 48-fold increase in OMR gain (equation 8.4; $2^{4 \times 1.396} = 48.0$). With gains this high, 'pseudo-saccades' produced by the OMR system rather than the CA system are observed (fig 8.9).

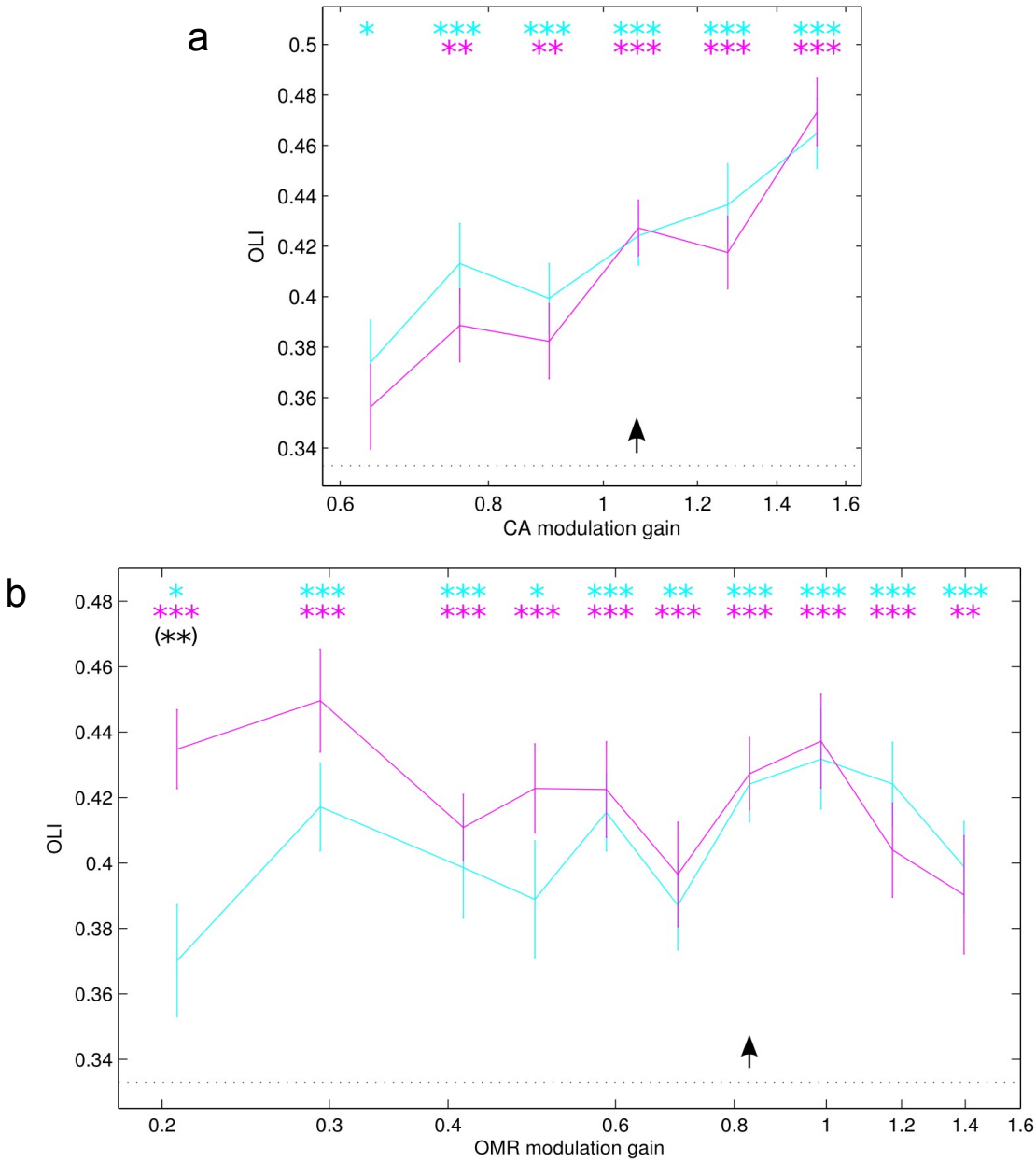


Figure 8.8: Model 3 (CA modulation + OMR modulation) parameter sweep. OLI in the SL-near (cyan) and SL-far (magenta) arenas. In **a** the OMR modulation is held constant while the CA modulation gain is varied, and vice versa in **b**. The dotted black line is the chance baseline level. Asterisks denote significance of OL performance: *** p<.001, ** p<.01, * p<.05. Black symbols refer to the significance of the difference between arenas, brackets denote an effect in the opposite direction to that seen in flies. The black arrow shows the setting used to produce the data in Fig. 8.10., which is also the setting employed whilst sweeping the other parameter.

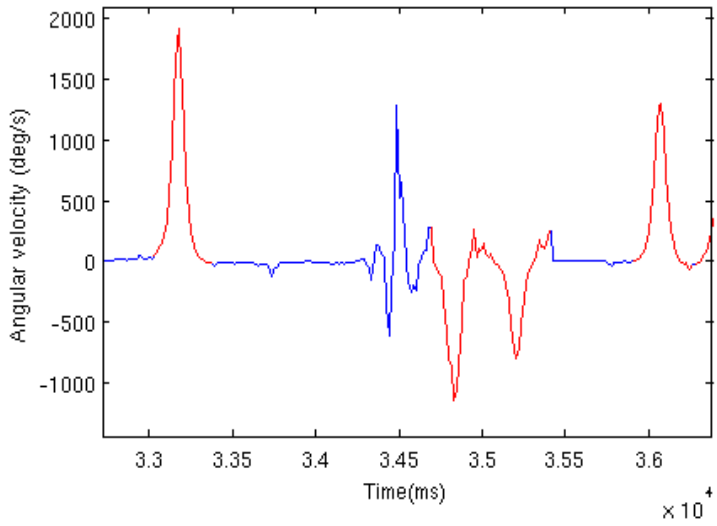


Figure 8.9: A 'pseudo-saccade' in the SL-near arena. This example is taken from the rightmost datapoint of fig 8.8b, i.e. Model 3 with $modulationGain_{OMR}$ = 1.39, $modulationGain_{CA}$ = 1.07. Red denotes times when the CA system was producing a saccade following the predefined angular velocity profile (section 5.3.4). At t = 34.5s an unrealistic rapid turning manoeuvre is produced by the over-amplified OMR system.

### 8.3.5: Model 4: OMR boost

Having shown that increasing the OMR gain in the presence of odour is necessary to reproduce fly behaviour (Model 2), I must now show that it is not sufficient, i.e. that CA gain modulation is also required. The final model therefore features only the odour-dependent alteration to the OMR system described by equation 8.3. Note that since this is a step-change, no use is made of the actual odour signal intensity.

No significant OL is seen in either the CB or the HS arenas (fig. 8.10). This is to be expected, since these patterns are homogeneous and therefore provide no directional cues. If the model is unable to make use of the structure of the odour plume, then clearly it has no way of locating the odour source. However, a weak but significant effect still exists between SL-near and SL-far, as the model can locate the odour by simply increasing its tendency to approach the landmark.

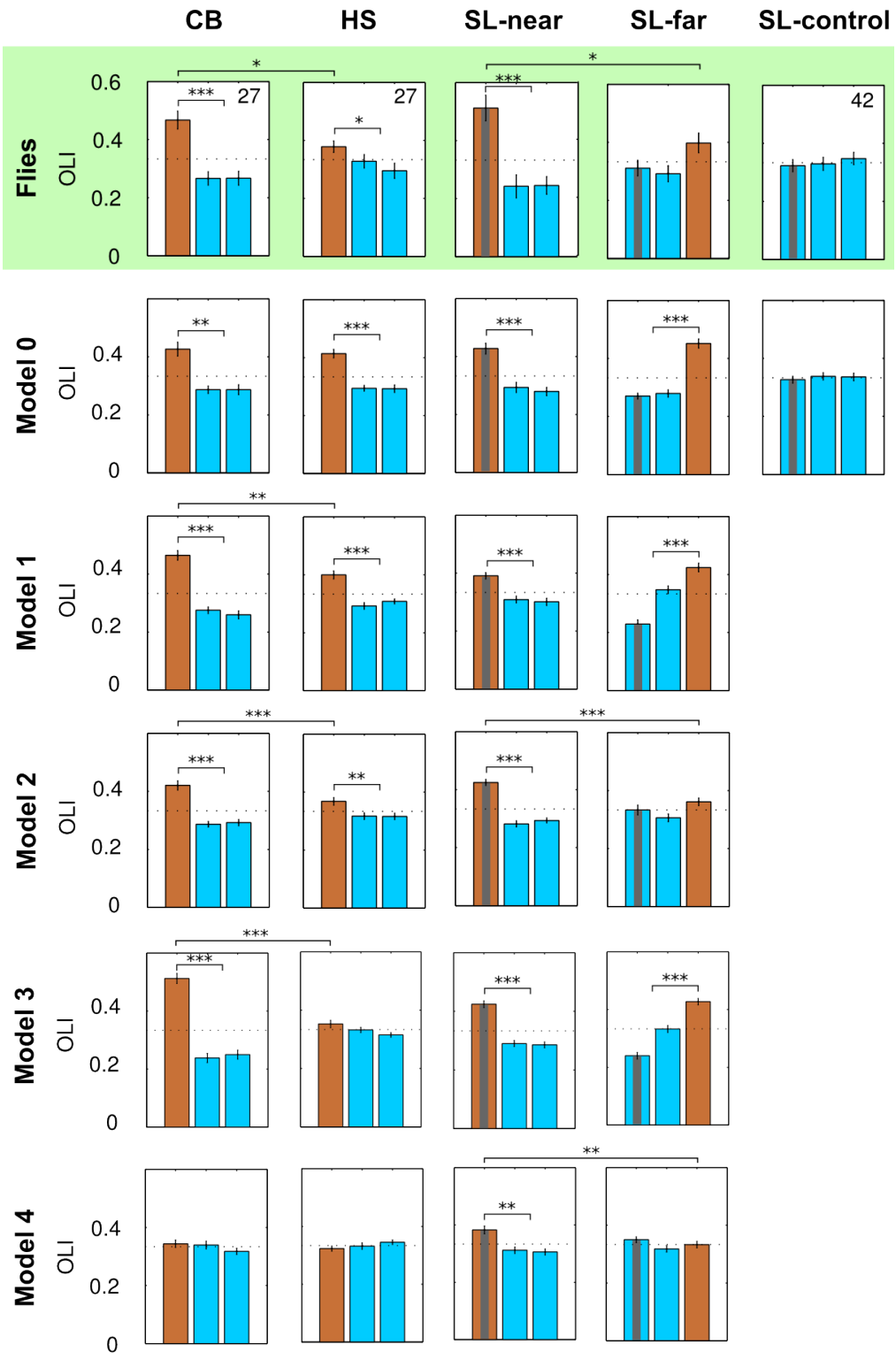


Figure 8.10: Odour localisation performance of real and modelled flies**.** Animal data is highlighted in green. Bars show the OLI for each vial, error bars represent ±1s.e.m. Brown bars are for vials containing vinegar, blue for ones containing water. In the SL arena, the striped bar represents the vial aligned with the landmark. In the absence of odour all models are equivalent, so the SL no-odour control data is only shown once. In the case of the models, the parameter settings that result in behaviour most closely matching that of the fly are chosen. Stars inside graphs refer to the significance of OL within that condition (i.e. odour vial *versus* mean of control vials), while those between graphs show differences in OLI between conditions. Only Model 2 reproduces all of the effects seen in the animal data, i.e. significant OL in CB and SL-near, and significantly stronger OL performance in CB than HS, and in SL-near than SL-far. Unless otherwise specified, n=24 experimental replicates. *** means p<.001, ** p<.01, * p<.05.

## 8.4: Behaviour of the visual-olfactory model

In the previous section I demonstrated that Model 2 (which modulates CA sensitivity according to the odour signal and increases OMR gain whenever odour is present) was the minimally complex model capable of reproducing the OL behaviour of flies. I shall now perform many of the analyses used in previous chapters on the trajectories produced by this model in order to characterise its behaviour and assess its similarity to that of the insects.

As the desired OL effects were observed for a range of parameter values (fig 8.7) the actual settings for $modulationGain_{CA}$ and *OMRboost* were set somewhat arbitrarily at 1.07 and 1.41 respectively – the values used the generate the OL data in fig 8.10. It should be noted that this choice was further constrained by results from the tripartite arena, which is introduced in the next chapter.

### 8.4.1: Spatial distribution

Fig 8.11 shows sample trajectories of the model from the four experimental conditions. Perhaps the most striking difference between these trajectories and the corresponding no-odour experiments is the more pronounced intersaccadic veering in the environments lacking widespread vertical contrast (i.e. all but CB), as a result of the odour-dependent amplification of the OMR. Also, due to the high level of attraction to the stripe in the SL arena, the emergency wall avoidance mechanism (section 5.2.2) must quite often be employed to prevent collisions with it, especially in SL-near. Transit probability plots are given in fig 8.12.

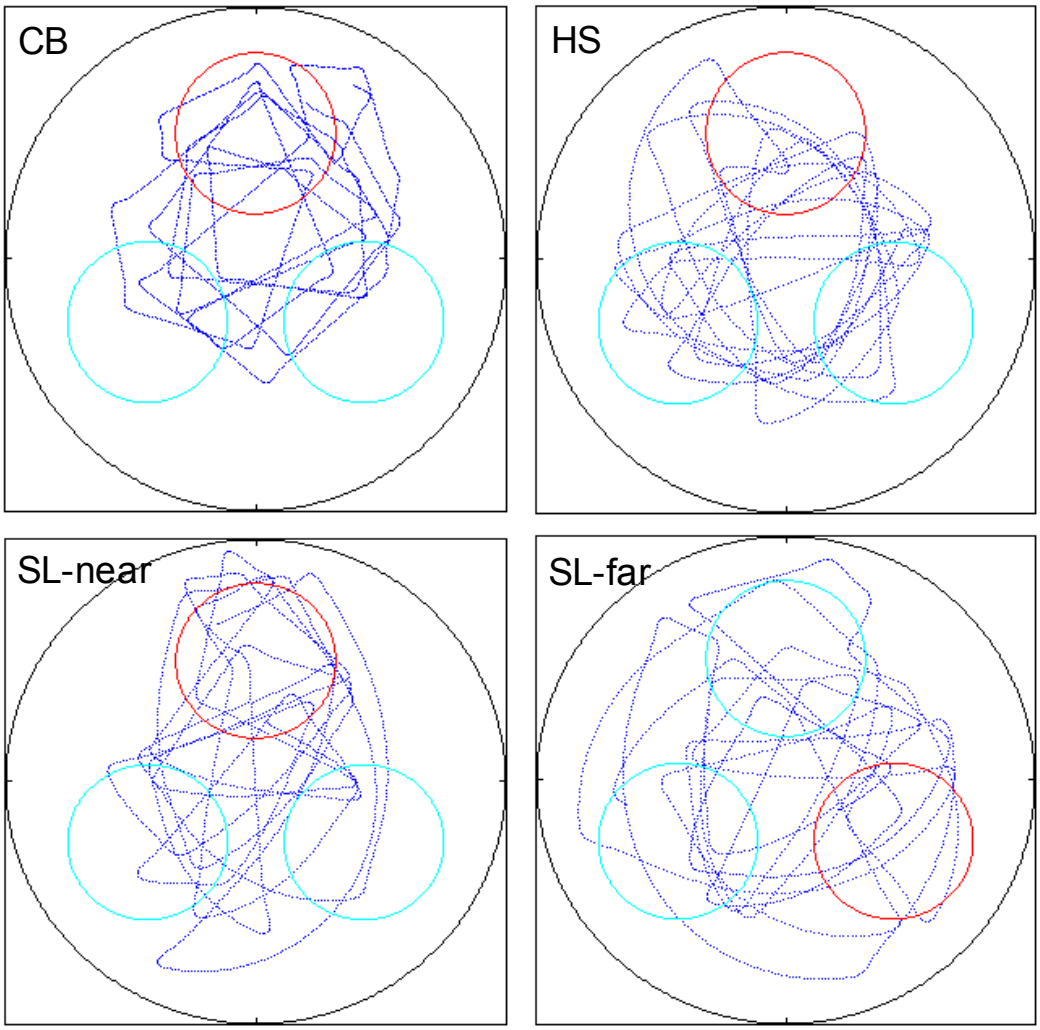


Figure 8.11: Sample trajectories of the model fly. Dots represent its position at 20ms intervals, giving an impression of speed. Small circles show the zones used to compute the OLI (equation 3.9), with the red one denoting the vial containing vinegar. In the SL arena, the stripe is located at the 12 o'clock position. Fig 6.1 shows analogous animal data, while fig 5.26 shows the model's behaviour in these arenas without odour present.

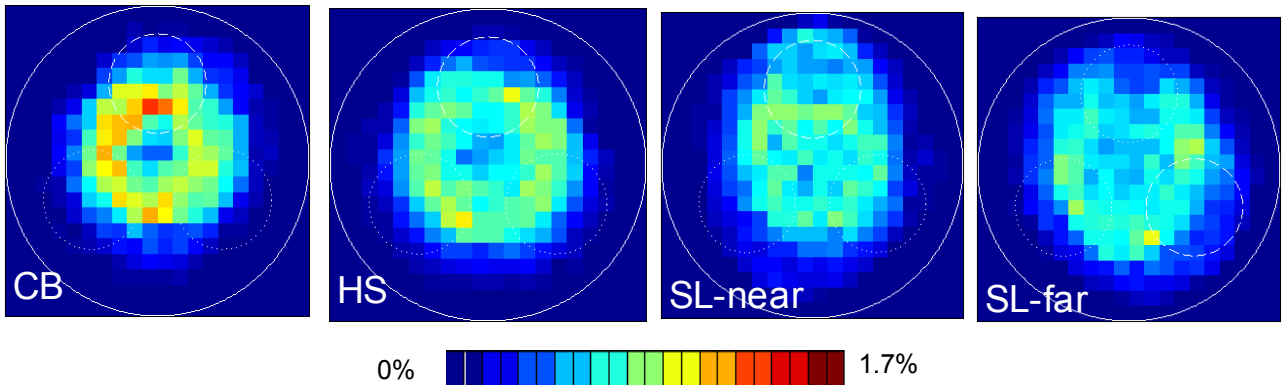


Figure 8.12: Plots of the model's transit probability for the odour experiments (n=24 in each case). As usual, the landmark in the SL arena is at the 12 o'clock position. The small circles show the boundaries of the zones, with a dashed line representing the zone containing vinegar, and the dotted line representing water-filled controls. Fig 6.2 shows analogous animal data, while fig 5.27 shows the model's behaviour without food odour present. The same heat-scale is used in all of these figures.

## 8.4.2: Flight statistics

Fig 8.13 presents charts comparing various flight statistics of the model in the two homogeneous arenas. Analogous data for real flies is given in fig 6.4. Comparing the real and modelled data, a number of differences are apparent. I shall list these and comment briefly on them here, but detailed discussion of their causes will be left for section 8.5.2.

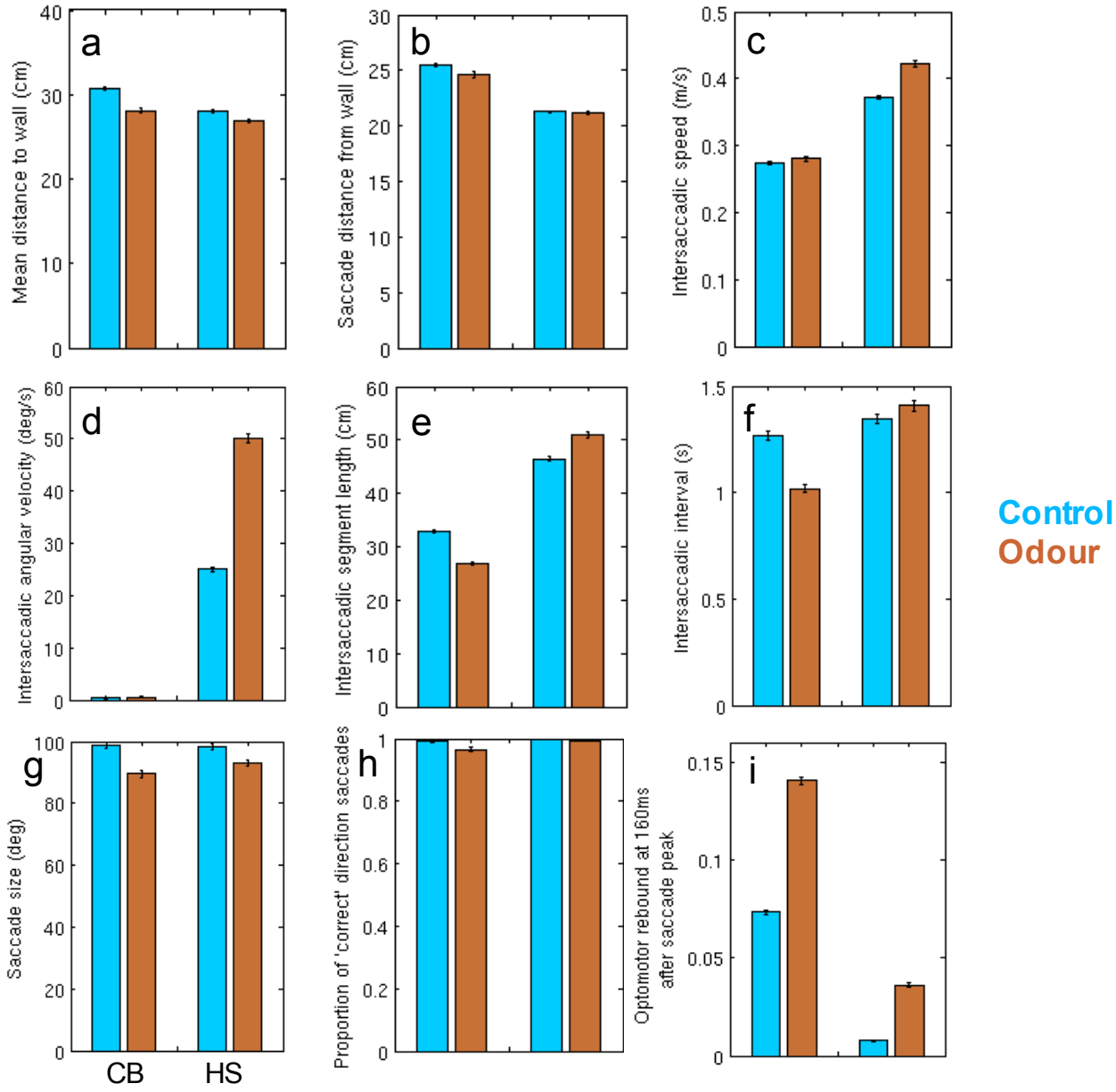


Figure 8.13: Comparison of flight performance of the model in the CB (left on each chart) and HS (right) arenas in the presence (brown) and absence (blue) of food odour. See fig 6.4 for identical analysis of animal data; also see fig 5.28 for direct comparison of fly and model data in no-odour controls. Bars are ±1 s.e.m. Due to the low level of variability in the model data, virtually all differences are significant, so significance is not shown.

Little difference in overall wall-aversion is seen (fig 8.13a,b), whereas the real flies became slightly more wall-averse in HS when odour was introduced. Unlike real flies, the model moves considerably faster in the presence of odour in HS (fig 8.13c), despite the fact that olfaction does not influence the speed regulation system.

While flies may participate in slightly more intersaccadic turning in the presence of odour (fig 6.4d),

the model's mean intersaccadic angular velocity approximately doubles for odour experiments in the HS arena (fig 8.13d). This is a direct consequence of the increased OMR gain, and may in fact be the cause of many of the other effects seen here, as discussed in 8.5.2. The reason why almost no intersaccadic turning is observed in the CB arena is discussed in section 5.5.2.1.

In the CB arena, the model reproduces the flies' pattern of shortening intersaccadic segments (both in distance and duration) when odour is added. However, the opposite is seen in the HS arena (fig 8.13e,f). Saccades are slightly smaller in amplitude in both arenas when odour is present (fig 8.13g), which is not the case for the flies. The model still almost never saccades towards the arena wall, though the occasional 'wrong' direction saccade is observed in the CB-odour case (fig 8.13h). Lastly, in stark contrast to the fly data, the optomotor rebound approximately doubles in amplitude when odour is introduced to the CB arena (fig 8.13i). Again, this can be directly attributed to the increased OMR gain.

Fig 8.14 shows the relationship between wall approach angle and intersaccadic turning. As before (fig 5.29), the model veers away from the wall in the HS arena, but the steepness of the correlation is considerably greater because of the OMR boost. No correlation is found for the CB arena ($\rho(492)=.028$, $p=.54$), whereas the flies displayed a significant tendency to steer towards the wall in this condition (fig 6.5). This effect can in fact be reproduced (whilst preserving the OL effects) by disabling the suppression of the OMR for translational optic flow (fig 5.10) when odour is present (data not shown). However, it is my opinion that this marginal improvement in the model's accuracy does not justify the corresponding reduction of its parsimony, so this mechanism is not adopted.

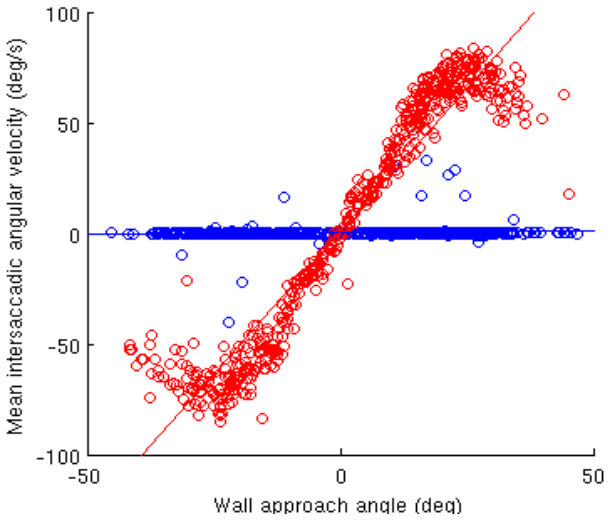


Figure 8.14: Intersaccadic turning as a function of the model's angle to the wall at the beginning of the segment. Blue is the CB arena, red is HS. Linear regression lines are shown. See fig 6.5 for analogous fly data, and fig 5.29 for the model in the absence of odour.

## 8.4.3: Mechanisms of odour localisation

In section 6.3 I attempted to uncover clues in the fly data as to what behavioural modifications occur to facilitate OL. In the case of the model, obviously I, as the designer, know exactly how olfaction alters flight control. However, it is not straightforward to predict the behavioural consequences of algorithmic changes, so it is worthwhile to perform a similar analysis on the model data. As mentioned in section 6.4.3, one can also validate the analyses used by applying them to a system whose mechanisms are known. It should be borne in mind that because the model's behaviour is much less variable than that of the flies, very small effects can potentially achieve high significance.

I have assumed that olfactory modulation of CA results in visually-mediated chemokinesis, i.e. longer intersaccadic segments are produced when the model is moving up-gradient than down-gradient. This hypothesis can be assessed directly using the analysis explained in section 6.3.1. Briefly, I make the rather unrealistic assumption that a smooth circular odour gradient exists around the source (c.f. plume recordings, section 7.3). I then compute the correlation between segment length and the angular position of the source with the respect to the model's orientation. This correlation is then compared to a Monte Carlo baseline computed using random fictive source positions to control for effects of the arena geometry. Results are in table 8.1.

| Condition | Actual | | Monte Carlo | | $p_{difference}$ |
|---|---|---|---|---|---|
| | ρ | n | ρ | n | |
| CB | -.548 | 679 | -.353 | 721 | <.0001 |
| HS | -.276 | 489 | -.195 | 493 | .18 |
| SL-near | -.225 | 445 | -.210 | 506 | .81 |
| SL-far | -.490 | 516 | -.248 | 495 | <.0001 |

Table 8.1: Correlations between absolute angle to odour source and (spatial) length of intersaccadic segments. 'Actual' refers to the analysis using the true position of the simulated odour source, 'Monte Carlo' to random fictive source locations (see section 6.3.1 for details). $p_{difference}$ is the significance of the difference between the two correlations (see Appendix for details of statistical method). Table 6.2 shows the same data for real flies.

In the richly textured CB arena, there is clear evidence that the model does indeed perform chemokinesis, as does its biological counterpart (table 6.2). Also in agreement with the fly data, significant chemokinesis is not seen in HS, where OL is significantly weaker. A more unexpected result is the observation that chemokinesis occurs in SL-far, even though significant OL does not occur. This is probably because the vertical stripe in the SL arena provides a strong translational cue, and is more likely to be in the receptive field of the CA system (fig 5.16) when the fly is moving away from the source than towards it. The converse could explain why chemokinesis does not take place in SL-near.

| Condition | Actual | | Monte Carlo | | $p_{difference}$ |
|---|---|---|---|---|---|
| | ρ | n | ρ | n | |
| CB | +.078 | 679 | +.066 | 721 | .84 |
| HS | -.025 | 489 | -.036 | 493 | .86 |
| SL-near | -.074 | 445 | -.086 | 506 | .85 |
| SL-far | +.036 | 516 | -.079 | 495 | .068 |

Table 8.2: Correlations between absolute angle to odour source and the intersaccadic speed, c.f. fly data in 6.3.

Table 8.2 shows a similar analysis for intersaccadic speed as opposed to segment length. No significant effects are found, which is as one would expect since speed regulation is not affected by olfaction in the model. Thus, the difference in flightspeed seen in the HS arena (fig 8.13c) is a generalised effect and not linked to the model's position within the plume. There is however an almost significant bias in SL-far. This too can be explained by the point made in the previous paragraph, since the SR receptive field (fig 5.11) is also restricted to the frontal portion of visual space.

| Condition | Actual | | Monte Carlo | | $p_{difference}$ |
|---|---|---|---|---|---|
| | freq | n | freq | n | |
| CB | .916 | 370 | .912 | 397 | .96 |
| HS | .949 | 257 | .924 | 276 | .23 |
| SL-near | .949 | 253 | .866 | 291 | .0011 |
| SL-far | .852 | 305 | .832 | 274 | .65 |

Table 8.3: Proportion of saccades directed towards a laterally positioned odour source. $p_{difference}$ is the significance of the difference between the actual and Monte Carlo result, calculated using $\chi^2$ tests. See table 6.4 for fly data.

Table 8.3 is concerned with whether saccades are directed towards the odour source more often than chance would predict. Note that even when fictive source positions are used, over 80% of saccades are in the 'correct' direction, demonstrating the influence that the arena geometry has and underlining the need for the Monte Carlo baseline. Interestingly, in SL-near the model saccades toward the real odour source significantly more frequently than fictive ones, despite having no explicit memory or representation regarding the plume structure. The bias must therefore be caused by the asymmetry of the visual environment and/or of the model's spatial distribution.

In light of this observation, one might suspect that the positive result observed for real flies in the CB arena (section 6.3.3) is similarly artefactual. However, it is curious that the model does not display the same behaviour. I suggested that this effect may be linked to flies' tendency to veer towards the walls of the CB arena when odour is present. The negative result here is consistent with this account, since this veering phenomenon is not reproduced by the model (fig 8.14).

| Condition | Actual | | Monte Carlo | | $p_{difference}$ |
|---|---|---|---|---|---|
| | ρ | n | ρ | n | |
| CB | +.696 | 376 | +.570 | 412 | .0031 |
| HS | +.622 | 307 | +.621 | 321 | 1.0 |
| SL-near | +.902 | 255 | +.540 | 315 | <.0001 |
| SL-far | +.458 | 315 | +.550 | 306 | .13 |

Table 8.4: Correlations between angle to odour source and intersaccadic angular velocity. See table 6.5 for fly data.

Table 8.4 addresses the question of whether the model steers towards the odour source during intersaccadic flight, despite having no explicit chemotactic mechanism of this kind. A significant

tendency to do so is observed in the CB arena. However, very little intersaccadic turning actually occurs in the CB arena (fig 8.14). I therefore consider this effect to be artefact caused by catching the tail-end of optomotor rebounds at the beginning of segments. (As with the fly data, the inclusion criteria for intersaccadic segments are relaxed for this analysis (section 6.3.1).) The tendency in the SL-near case, on the other hand, is clearly due to the model steering towards the stripe, rather than the odour source. It seems probable that the same is true of the flies (section 6.3.4).

| Condition | Actual | | Monte Carlo | | $p_{difference}$ |
|---|---|---|---|---|---|
| | ρ | n | ρ | n | |
| SL-near | +.661 | 253 | +.151 | 313 | <.0001 |
| SL-far | +.643 | 304 | +.169 | 309 | <.0001 |
| SL-control | +.750 | 295 | +.098 | 308 | <.0001 |

Table 8.5: Correlations between angle to landmark and intersaccadic angular velocity. See table 6.7 for fly data.

Lastly, table 8.5 shows the model's tendency to steer towards the vertical stripe in different olfactory situations. This data is rather different to that observed in flies (section 6.3.5), making comparisons difficult. The main problem is that the model, unlike flies, has a highly significant tendency to turn towards the landmark in the control condition, as I discussed in section 5.6.3.3. In any case, the similarity between SL-near and SL-far reflects the fact that the OMR boost size is invariant with regard to position in the plume. This is at odds with the fly data, where significant target attraction behaviour is only seen in SL-near.

# 8.5: Discussion

## 8.5.1: Summary

I have added a simulation of a food odour plume to my visual simulator, based upon my VOC sensor recordings described in the previous chapter. The simulation makes minimal assumptions about the distribution of odorant, in that it randomly resamples from the sensor readings rather than fitting any generative model of the data (section 8.1). I have erred on the side of making the simulation more noisy than a real plume, to ensure that no spurious structure exists for my visual-olfactory model to exploit. The model's olfactory input is preprocessed by passing it through two parallel low-pass filters of different speeds and comparing their outputs to estimate the temporal derivative (section 8.2). An adaptive gain control mechanism attempts to keep the variance of this signal constant in order to achieve behavioural invariance to the overall intensity of the odour plume.

With these elements in place, I investigate models of how olfaction could modulate the existing visuomotor controller (section 8.3). In accordance with the principle of Occam's razor, I attempt to identify the minimally complex model that reproduces fly OL behaviour. The results are as follows:

- Non-visual chemokinesis (i.e. saccading whenever the odour intensity is falling sharply, Model 0), is a viable mechanism for OL. I shall return to this point in section 10.2.4. However, it is unable to reproduce the difference in OL performance exhibited by flies between the CB and HS arenas.
- Modulating the collision avoidance (CA) threshold based on the odour signal, such that a rising intensity inhibits saccades and a falling one promotes them (Model 1), reproduces the CA/HS difference seen in flies. However, it fails to reproduce the OL effects seen in the SL arena.
- Increasing the gain of the optomotor response (OMR) whenever odour is present in the arena (Model 4) produces some limited attraction to the stripe in the SL arena, but is clearly unable to produce OL behaviour in a visually homogeneous environment like the CB arena.
- Combining CA modulation with an increase in OMR gain (Model 2) reproduces the fly data, i.e. OL is stronger in CB than HS, and in SL-near than SL-far.
- The arguably simpler and/or more plausible approach of modulating OMR gain (rather than increasing it in a stepwise manner) whilst also modulating CA sensitivity (Model 3) fails to reproduce the OL effects in the SL arena.

Having found a model of crossmodal interaction that reproduces the desired effects, I looked in detail at its behaviour to assess whether it localises the odour in the same manner that flies do (section 8.4). I found evidence for both chemokinesis and intersaccadic steering towards the visual landmark, broadly in line with what I observed in flies (section 8.4.3). However, there are some serious discrepancies between the model and animal data in terms of flight statistics (section 8.4.2) and landmark attraction, which I discuss in the following section.

### 8.5.2: Validity of the visual-olfactory model

In section 8.4.2, I identified a number of ways in which the flight behaviour of the model differs from that of flies in olfactory experiments, particularly those in the HS arena. In some sense this is to be expected. The visuomotor model was carefully tuned to match the fly data in as many respects as possible (section 5.4), whereas the visual-olfactory model represents the simplest possible algorithm that satisfies a different set of requirements, namely the OL competencies of flies.

It is my opinion that the various discrepancies in fig 8.13 can be attributed to a single cause: because of the odour-dependent OMR boost, the OMR gain is too high. This affects behaviour in the following ways:

- An increased OMR gain directly generates an increased optomotor rebound (fig 8.13i) as the compensatory post-saccade turn becomes larger (fig 5.24).
- Boosting the OMR increases the curvature of intersaccadic segments in the HS arena (fig 8.13d) due to the illusion described in fig 4.10. No difference is seen in the CB arena because the OMR is suppressed.
- Because the model makes tighter intersaccadic turns in the HS arena, it experiences less visual expansion and thus the SR system accelerates to compensate (fig 8.13c). To understand why this is the case, imagine the model flying in a circle maintaining a constant distance from the wall of the HS arena. It would experience no visual motion whatsoever. (Of course, if it were experiencing no visual motion, it would stop steering away from the wall. It would then experience the illusory rotational cue once again and veer away. With the OMR gain high enough, this oscillatory process could continue indefinitely.)
- This decrease in visual expansion caused by increased intersaccadic veering will make the model less wall-averse in the HS arena (fig 8.13a,b), because the CA system is also based on expansion detection.
- Saccade amplitude decreases for different reasons in the CB and HS arenas (fig 8.13g). In the former, the increased post-saccade rebound reduces the total angular size of the manoeuvre. In the latter, the reduction is a direct consequence of the increased flightspeed (equation 5.5).

Of course, the reason the OMR gain is so high is because this was found to be necessary to produce stronger OL in SL-near than SL-far (fig 8.7b). That is to say, the OMR was boosted in order to increase the model's tendency to approach the landmark. While I have presented strong evidence that flies do become more attracted to a vertical stripe when odour is present, in light of the above points I am forced to conclude that they do so by some means other than simply amplifying the optomotor response.

One alternative approach I considered in Model 3 was to amplify the OMR only when odour intensity was rising, and attenuate it when falling. Since the average effect would be zero (depending on how one computes averages), this would avoid all the problems listed above. Furthermore, it would very likely mean that a stronger tendency to steer towards the landmark would be seen in SL-near than SL-far, as is the case for flies (table 6.7) but not my model (table 8.5).

Unfortunately, Model 3 did not produce the appropriate OL behaviour. However, some combination of Models 2 and 3, i.e. a modulation of the OMR with an average gain greater than one (but less than the current boost size), may fare better. This would correspond to a phasic-tonic response as found in a wide variety of biological systems (e.g. Barth, 1964; Grace, 2000), including *Drosophila* visuomotor behaviour (Tammero et al, 2004). One reason I have not pursued this approach is that it would mean reducing the model's parsimony and adding at least one more free parameter, for what might be a rather marginal increase in accuracy, since there is little indication that real flies increase their OMR gain in the presence of odour at all (fig 6.4). More importantly though, data presented in the next chapter indicates that such an approach would fail when applied to other visual conditions.

Another alternative would be to introduce a new visuomotor subsystem specifically responsible for tracking small-field targets, which would be activated in the presence of odour. Although such models exist (see section 2.4.2), this approach would be problematic for two (related) reasons. First, having demonstrated that there is virtually no evidence for landmark attraction in control experiments (chapter 4), to introduce a whole new mechanism for target tracking in odour experiments seems like an exercise in overfitting, rather like postulating epicycles on epicycles to explain planetary orbits. Indeed, a similar criticism could be made of the way I increase the OMR gain whenever odour is present, as it does in some sense mean that two different models are being used to explain behaviour in the presence and absence of odour. In my defence, I would argue that changing a single parameter in this way is far more valid than introducing a new control loop, especially since experimental evidence of such an increase exists (Chow & Frye, 2008).

A second problem is that it is unclear what form such a mechanism would take, because the only examples I have of target attraction behaviour to analyse are from the SL arena. Should the model only be attracted to long vertical stripes? What about a combination of horizontal and vertical contrasts, as one would obtain by inverting a vertical band of the HS area? It is not even necessarily the case that such a mechanism should be based on motion detection. While attempts have made to characterise how target attraction/repulsion depends on visual parameters (Maimon et al, 2008; see also section 2.2.5), it would be very difficult to extrapolate a predictive model from this limited data.

In section 5.6.2 I argued that a parsimonious but inaccurate model could be of greater interest than an accurate but complex one. For this reason I shall persist with the visual-olfactory model I have described in this chapter in spite of its shortcomings. Besides being more understandable, another benefit of a simpler model is that it is more likely to generalisable to novel circumstances. This is the

subject of the next chapter.

# 9. Validation of the model

Based upon recordings of free-flying *Drosophila* (chapters 4, 6) I have implemented a model that approximates their odour localisation behaviour in a variety of experimental conditions (chapters 5, 8). While I have attempted to avoid overfitting by favouring parsimony throughout the modelling process, the possibility remains that the model is only relevant to the specific experimental conditions I have considered during its development. For this reason, it is essential to assess its predictive validity by testing it in novel environments.

My intention was to finalise the model before performing the experiments described in this chapter, but unfortunately errors in the model implementation came to light after they were performed. Thus I revised and retuned the model in the knowledge of the results presented in section 9.2. I feel it is important to make this point explicit in the interests of transparency. However, the processes of parameter tuning (section 5.4) and model selection (section 8.3) were performed as described, using only the data from the CB, HS and SL arenas. The only influence the results of this chapter had was to act as a 'tie-breaker' by further constraining the choice of parameter values for crossmodal Model 2 (section 9.3.2; see also section 8.3.3).

Section 9.1 describes the new visual environment I introduce, and explains the reasoning behind its selection. The results of fly experiments are presented in 9.2, and these are compared to the behaviour of the model in section 9.3. I discuss the successes and failures of the model in this new condition in section 9.4.

## 9.1: A novel environment

In devising a new experimental condition to assess the predictive validity of the model, I must ensure that it is sufficiently different from the existing conditions to represent a genuine test of its generality. For instance, a regular as opposed to random chequerboard pattern, or a CB arena with squares subtending 10° instead of 5° (section 4.1.1) would most likely fail in this regard, as they would probably not elicit behaviour significantly different to that seen in the existing CB arena.

On the other hand, practical limitations constrain the types of environments I can investigate. Interesting as it would be to record behaviour in a 5x5x2m room (not to mention easy to simulate),

my tracking rig is limited to ~1m diameter arenas. Similarly, while other experimenters have used moving visual stimuli to great effect (Srinivasan et al, 1991; Mronz & Lehmann, 2008; Fry et al, 2009), my tracking system would be unable to operate in such conditions because it assumes a static background (section 3.3.2).

The scope of the model imposes even more fundamental constraints. To make my visuomotor model tractable I had to make a number of simplifying assumptions, which are listed in section 5.6.2. For instance, because contrast adaptation is not modelled, any new visual condition must contain strong contrasts throughout its extent, just as CB, HS and SL do. This constraint is rather limiting; since blank spaces are not permitted I can only really vary the relative levels of horizontal and vertical contrast in different parts of the arena.

The compromise I have struck between the conflicting requirements of novelty and applicability is a stimulus consisting of familiar visual elements combined into a single arena in a novel way. The tripartite arena (henceforth abbreviated TP) consists of three sectors each covering 120° of azimuth (fig 9.1). These contain a random chequerboard pattern, horizontal stripes, and vertical stripes (identical to the horizontal ones but rotated 90°). A water/odorant slot is aligned with the centre of each sector.

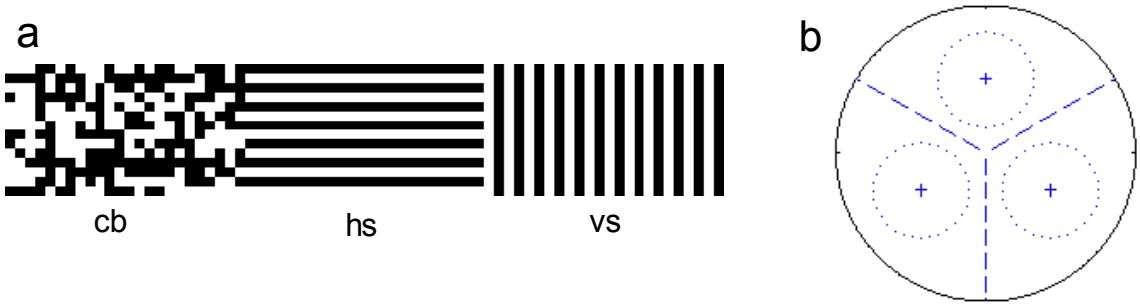


Figure 9.1: The tripartite (TP) arena. **a** The wallpaper design used. **b** Plan view showing the arrangement of the three sectors and the circular zones used for computing OLI.

## 9.2: Fly results

Experiments were carried out in the TP arena using an identical methodology to the previous OL trials. It should however be noted that it is inappropriate to make direct comparisons between this and the previous batch of experiments, since they were performed roughly a year apart and in different buildings, with the animals reared in different labs. Vinegar either appears in one of the vials, with

water in the other two (a condition referred to as TP-cb, TP-hs, or TP-vs, depending on the odorant sector), or water would be put in all three (TP-control).

### 9.2.1: No-odour experiments

Fig 9.2 shows the results of the no-odour control. Behaviour in this composite environment matches fairly well with what one might expect based upon data from the homogeneous CB and HS conditions. The wall is approached most closely in the *hs* sector and least closely in *cb*. An intermediate level of wall aversion is exhibited in the *vs* sector. This is consistent with the notion that vertical contrasts offer greater expansion cues than horizontal ones for an animal translating in a roughly horizontal direction, but that both vertical and horizontal texture provides the strongest collision avoidance cue. I cannot rule out the possibility that some attraction to the vertical stripes exists, but this seems improbable given the lack of such a phenomenon in the SL-control condition. Computing OLIs for the three sectors (fig 9.4) indicates that significantly more time is spent in the vicinity of the *hs* vial than the *vs* one ($T(36)=89$, $p=.0001$), and in the *vs* zone than the *cb* one ($T(37)=66$, $p<.0001$).

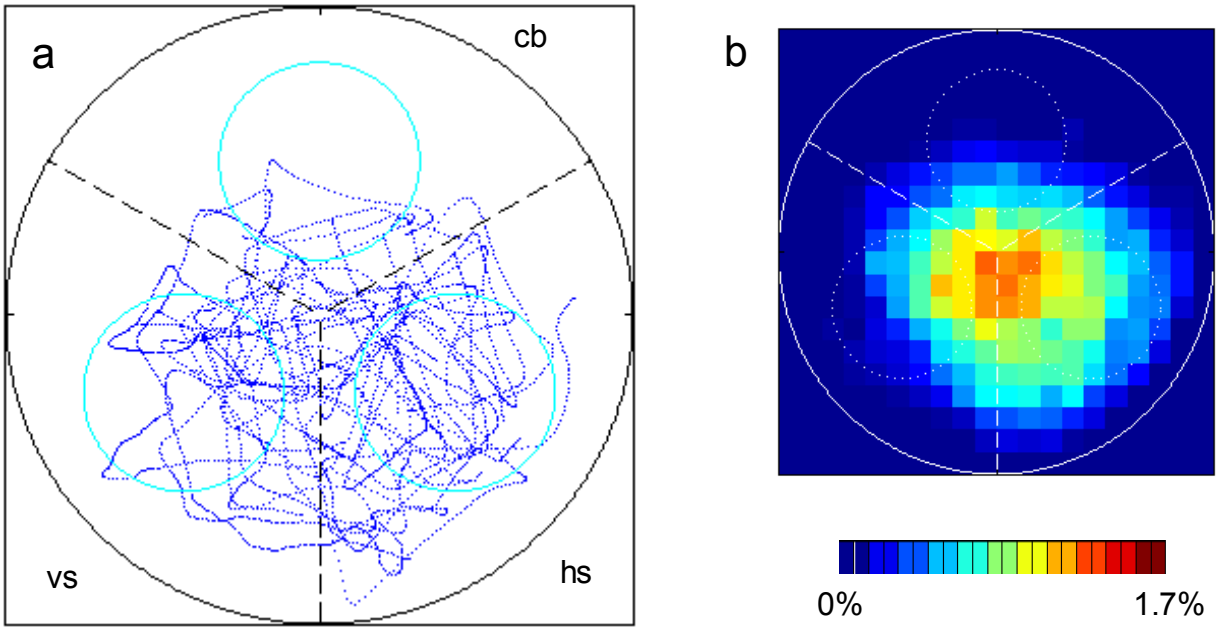


Figure 9.2: Spatial distribution of flies in the TP-control arena. See fig 9.1 for details of arena layout. **a** Sample trajectory. Dots represent the fly's position at 20ms intervals. **b** Transit probability plot. The same heat-scale is used as in all previous plots of this kind. n=37 flies.

### 9.2.2: Odour localisation experiments

Fig 9.3 shows spatial distribution data for odour experiments in the TP arena, and fig 9.4 summarises

the OL results. To determine whether OL is occurring, I compare the OLI for each experimental condition with the proportion of time spent in the corresponding zone in the control experiment. By this definition, significant OL is exhibited when the vinegar is in either the *cb* sector ($U(37,22)=690$, $p=<.0001$) or the *vs* one ($U(37,23)=571$, $p=.027$).

Something remarkable happens when the odorant is put in the *hs* sector: for the first time, significant odour *repulsion* is seen ($U(37,21)=88$, $p=<.0001$), with flies instead spending a significantly greater proportion of time in the *vs* sector than they do in control experiments ($U(37,21)=642$, $p<.0001$). In fact, they spend a comparable amount of time in the *vs* sector as they do when the vinegar is located there ($U(23,21)=308$, $p=.12$). The implications of this unexpected result will be discussed in section 9.4.2. First though, I turn my attention to how the model behaves in this environment.

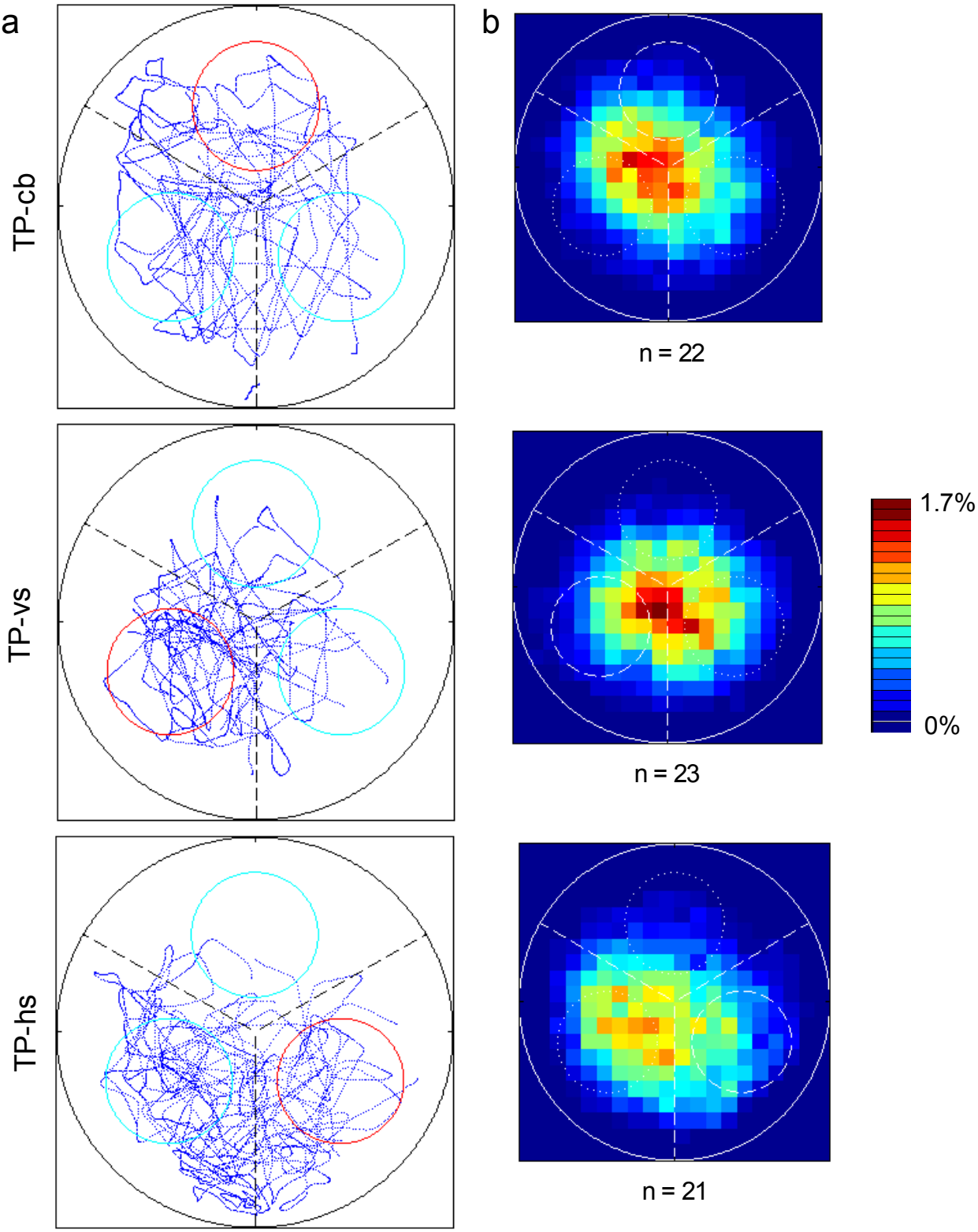


Figure 9.3: Spatial distribution in odour experiments in the TP arena. See fig 9.1 for details of arena layout; see fig 9.2 for controls. **a** Sample trajectories. Dots represent the fly's position at 20ms intervals, the red circles denote the zones containing the vinegar vial. **b** Transit probability plot. The dashed circles represent the odorant zones. The same heat-scale is used as in all previous plots of this kind.

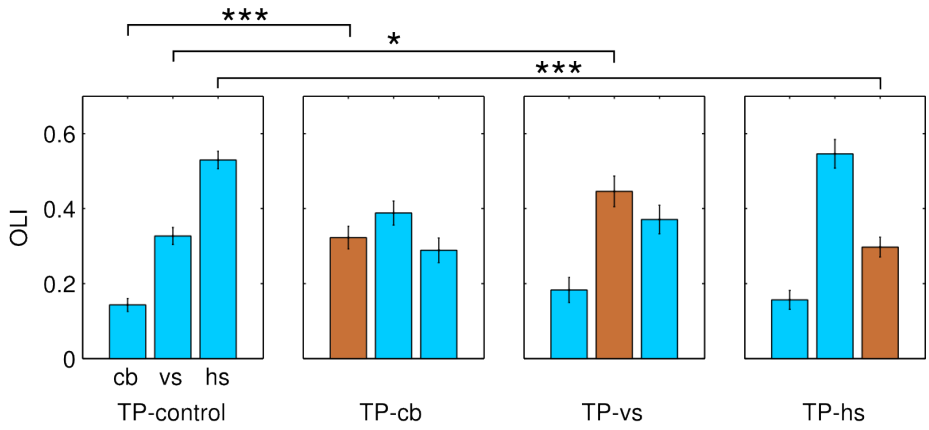


Figure 9.4: Odour localisation performance of flies in the TP arena. Bars show the OLI for each vial, error bars represent ±1s.e.m. Brown bars are for vials containing vinegar, blue for ones containing water. *** means p<.001, ** p<.01, * p<.05.

# 9.3: Model results

## 9.3.1: No-odour experiments

I shall present the results of running the model in a simulation of the TP arena in exactly the same way as I did the fly data, to facilitate straightforward comparisons. Fig 9.5 shows the model's behaviour in the TP arena in the absence of odour, while OLI statistics are presented in fig 9.7. Qualitatively, the model's behaviour matches that of the flies: more time is spent in the *hs* sector than *vs* (T(24)=44, p=.0025), and in *vs* than *cb* (T(24)=p=.040). The difference between *vs* and *cb* is rather less pronounced than it is for the flies, however. This could be because real flies, unlike the model, have a vertical component to their flight, for which the horizontal contrasts of the *cb* sector would provide additional translation cues.

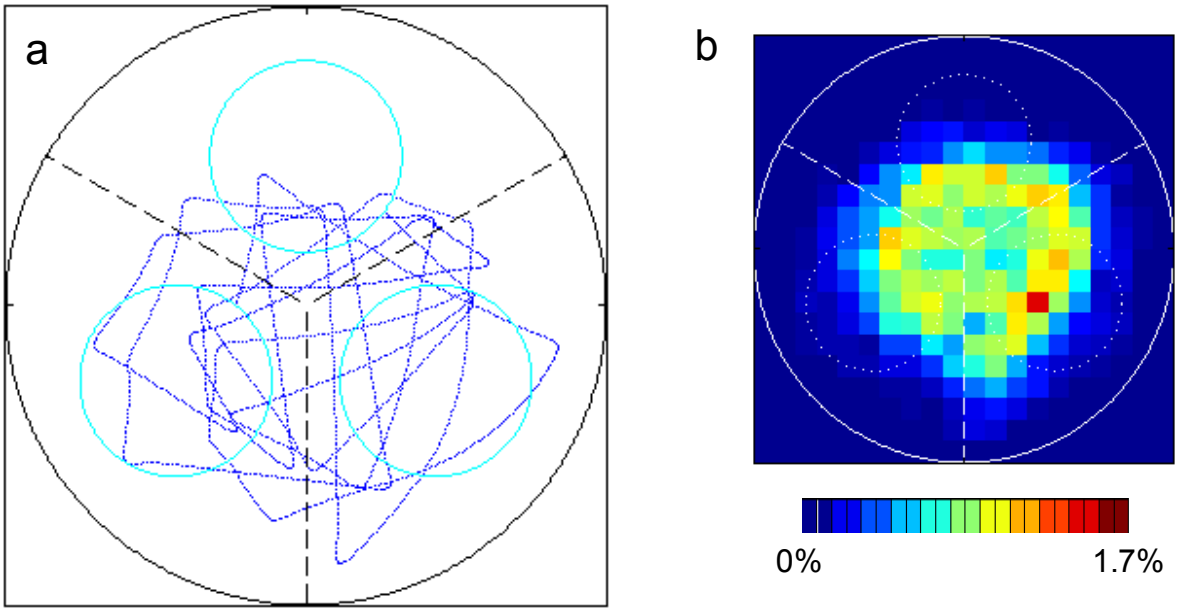


Figure 9.5: Spatial distribution of the model in the TP-control arena, c.f. fly data in fig 9.2. **a** Sample trajectory. Dots represent the model's position at 15ms intervals. **b** Transit probability plot. The same heat-scale is used as in all previous plots of this kind. n=24 experimental replicates.

## 9.3.2: Odour localisation experiments

Fig 9.6 shows the model's behaviour when a simulated odour source (section 8.1) is added to each of the three sectors, and the OLI statistics are presented in fig 9.7. As in the fly data, a significant shift towards the vinegar is observed when it is put in either the *cb* ($U(24,24)=473$, $p=.0001$) or the *vs* sector ($U(24,24)=484$, $p=.0001$). However, the repulsion from the odorant in the *hs* sector is not reproduced. Out of the cluster of parameter settings for the CA modulation gain and the OMR boost that produce the desired effects in the CB, HS and SL arenas (section 8.3.3), the closest that the model can achieve is for there to be no significant OL effect in this condition ($U(24,24)=345$, $p=.24$). Substantially strengthening the CA modulation and/or weakening the OMR boost results in significant OL in all three sectors.

While two out of three of the qualitative OL effects of flies are reproduced, quantitatively the data looks rather different. The large shift out of the *hs* sector and into the *vs* one that flies make across all odour conditions (fig 9.4) is not really evident in the model's behaviour (fig 9.7). What this means for the model is discussed in the next section.

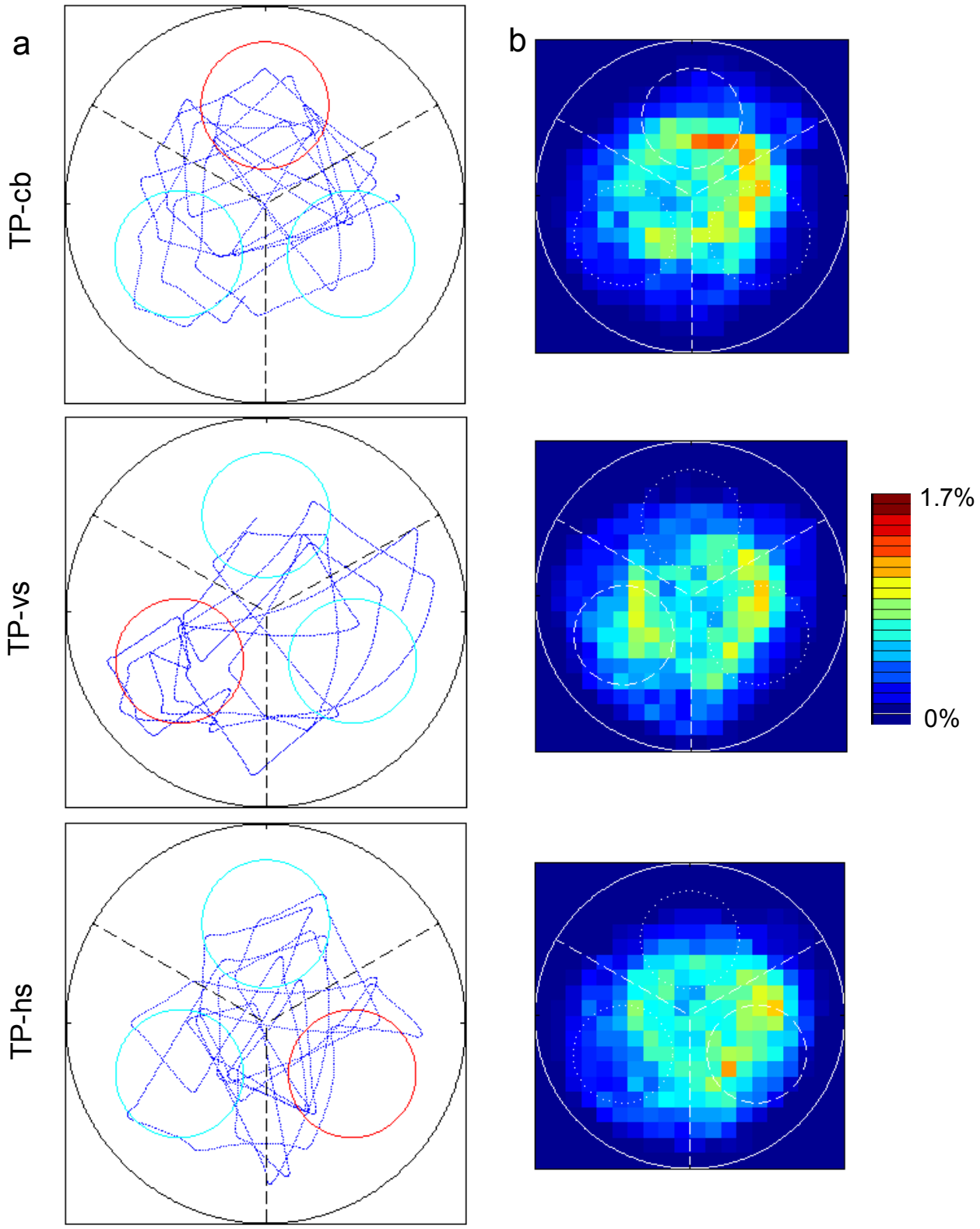


Figure 9.6: Spatial distribution of the model in odour experiments in the TP arena, c.f. fly data in fig 9.3. **a** Sample trajectories. Dots represent the model's position at 20ms intervals, the red circles denote the zones containing the vinegar vial. **b** Transit probability plot. The dashed circles represent the odorant zones. Once again, the same heat-scale is used.

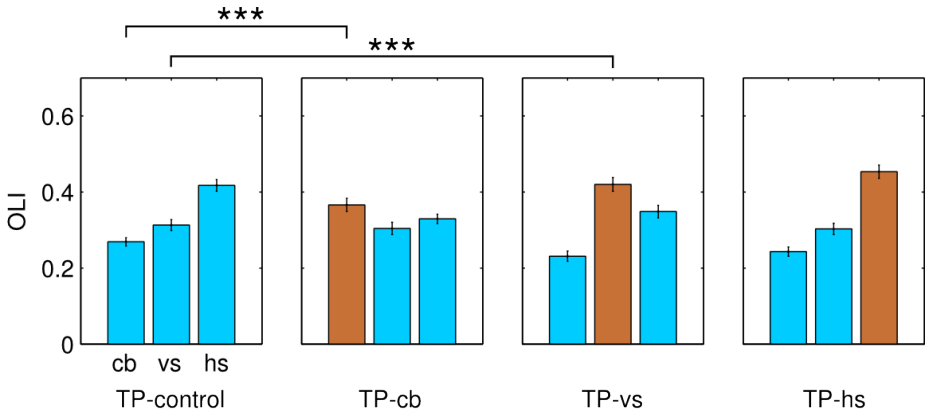


Figure 9.7: Odour localisation performance of the model in the TP arena, c.f. fly data in fig 9.4**.** Bars show the OLI for each vial, error bars represent ±1s.e.m. Brown bars are for vials containing vinegar, blue for ones containing water. *** means p<.001, ** p<.01, * p<.05.

# 9.4: Discussion

## 9.4.1: Summary

To investigate the predictive validity of the visual-olfactory model, I devised a new visual environment: the tripartite (TP) arena. This consists of three 120° sectors containing a random chequerboard pattern (*cb*), regular vertical stripes (*vs*) and regular horizontal stripes (*hs*). In the absence of food odour, the flies' flight is distributed highly unevenly across the three sectors, such that *hs* > *vs* > *cb*. This pattern is replicated by the model, albeit not quite as strongly.

Compared to the no-odour control, flies spend significantly more time in the vicinity of an odorant vial in both the *cb* and *vs* sectors. However, when vinegar is put in the *hs* sector they spend *less* time there than they do in controls, moving instead into the *vs* sector. While the model reproduces the OL seen in *cb* and *vs*, it fails to replicate this odour repulsion effect in the *hs* sector – at best it merely displays no significant tendency to locate the odour source in this condition.

## 9.4.2: Validity of the model

Although the match between fly and model data is not perfect in the control case, it is my opinion that the fact that the same general pattern is seen represents a significant vindication of my visuomotor model. As discussed in section 9.1, the TP arena may not be an especially exacting test of the model's generality, as it does contain many visual elements that have been used previously. However, combining areas of differing textural properties in one arena is in itself a novel and thus non-trivial

step.

In particular, one would imagine that the receptive fields of the visuomotor subsystems (section 5.3) could have a pronounced effect on behaviour in such an environment, as these define the areas in the arena where the visual input will be dominated by a certain type of texture. Given that these had to be implemented more through engineering intuition than by constraints from biological or behaviour data, it is encouraging that the control results match as well as they do. Having said this, one might speculate that the more uneven distribution of the flies between sectors (fig 9.4 *versus* fig 9.7) suggests that the CA receptive field is narrower in the fly than the model (fig 5.16), i.e. the model is more wall-averse than the fly in the *hs* sector because its CA subsystem can more often see vertical contrasts from the neighbouring regions.

The olfactory component of the model is validated rather less well by these experiments. In section 8.5.2 I identified that my crossmodal model was an oversimplification: while it is clear that flies perform some kind of odour-dependent target attraction behaviour, this is most probably not achieved by simply increasing the gain of the OMR system. Unfortunately, there was insufficient data to determine the nature of this hypothetical mechanism. The behavioural data yielded by the tripartite arena of experiments provides a few tantalising clues about its properties.

It would appear that there is something special about vertical stripes. When flies are 'repelled' from the vinegar in the *hs* sector, they are displaced to the *vs* sector, spending no more or less time in the *cb* sector than in control experiments ($U(37,21)=422.5$, $p=.58$). The *cb* sector contains abundant vertical contrasts, so it must be either the long, unbroken nature of the visual edges and/or the lack of accompanying horizontal contrast that makes the *vs* sector so attractive.

Of course, there is nothing new about the notion that flies are attracted to vertical stripes. As I discussed in section 4.5.2, this is a well-established behaviour, and it is remarkable that I do not see evidence for it in my experiments until odour is introduced. What is perhaps more surprising is that a series of 24 alternating black and white vertical stripes covering a third of the experimental arena (fig 9.1) would appear to be more attractive than a single vertical landmark – no odour 'repulsion' is observed in the SL-far condition (section 6.2.1). However, I must reiterate that caution should be exercised when drawing comparisons between the first and second batch of experiments.

The reason I say this is surprising is that studies of target fixation have typically focussed on small-field stimuli (see sections 2.2.5, 2.3.3.1). Flight responses to small-field stimuli in *Drosophila* have a

different frequency tuning to wide-field ones, suggesting that a separate sensory pathway is devoted to tracking small targets (Duistermars et al, 2007). It is difficult to see how the *vs* sector, taking up as much visual space as it does, could elicit a greater response than the SL arena's single stripe from a system of this kind. Perhaps then, odour-dependent attraction to vertical objects is mediated by neither the optomotor response nor the small-field tracking system. Potential experiments to investigate this possibility, as well as the implications it has for modelling odour localisation, will be discussed in the next (and final) chapter.

# 10. Conclusions

In this the last chapter, I first reiterate what I consider to be the main contributions of this study (section 10.1). I then discuss possible directions for future research (section 10.2) before offering my final conclusions (section 10.3).

## 10.1: Summary

The objective of this study was to derive an algorithmic account of why the ability of flying *Drosophila* to locate a hidden odour source depends on features of the visual environment, as reported by Frye et al (2003). I feel I have successfully achieved this goal. In more detail, the contributions of this study are as follows:

- Having implemented a free-flight tracking system, I extend the experiments of Frye et al (2003) (also, Tammero & Dickinson (2002a); Frye & Dickinson (2007)) and, broadly speaking, replicate the previous findings. I go beyond the previous work by investigating a new visual condition containing a single landmark in an otherwise homogeneous arena, and by performing more rigorous and detailed statistical analyses of the recorded flight trajectories. For instance, I quantify odour localisation numerically, allowing me to compare its strength in different experimental conditions. I present evidence for both chemokinesis and odour-dependent target attraction contributing to odour localisation behaviour.
- I identify a distinctive 'rebound' turning response immediately following saccades, and present evidence that it is visually mediated. To my knowledge, this behaviour has not been previously described in *Drosophila.*
- I implement a systems-level visuomotor model consisting of three parallel mechanisms: the optomotor response, speed regulation, and expansion-based collision avoidance, and demonstrate that this model can in simulation provide a reasonable approximation of the free-flight behaviour observed in flies. While more sophisticated models of the neural computation involved in visual motion processing exist (Lindemann et al, 2008; Hennig et al, 2008), I believe that my work represents the most detailed behavioural model of *Drosophila* visual flight control proposed to date. Unlike previous studies, it is able to account for the specific differences in behaviour caused by changes in the visual setting. Additionally, it reproduces and thus provides a plausible explanation for the rebound phenomenon mentioned above.
- Based on measurements from a real odour plume, I simulate the fly's olfactory environment.

By extending the visuomotor model to include odour sensing, I demonstrate the minimal interaction between visual and olfactory modalities required to qualitatively reproduce the odour localisation behaviour of flies. Specifically, the odour signal modulates the sensitivity of the CA system, resulting in visually-mediated chemokinesis, while the gain of the OMR is increased whenever odour is present, producing odour-gated target attraction.

- Lastly, I validate my crossmodal model using a novel heterogeneous environment. The model accurately predicts the spatial distribution of flies in this arena in the absence of odour. It correctly predicts some of the observed effects when odour is introduced, but fails to account for the pronounced attraction exhibited by flies towards vertical stripes.

## 10.2: Future work

In answering the question of why flies' ability to locate odour sources depends on their visual environment, I have uncovered many more questions that still lack answers. Furthermore, the model is not perfect (see sections 8.5.2 and 9.4.2), so there is ample opportunity for extending and refining it. In this section I give my thoughts on avenues for further research, beginning with relatively straightforward questions and moving on to more far-reaching ideas.

### 10.2.1: Extensions to the free-flight paradigm

There are countless ways in which the experimental arena could be altered or elaborated: one could use natural scenes for wallpaper, add coloured stimuli, change the shape of the arena, etc. However, experiments should be based on well-formed hypotheses rather than the whim of the researcher. Accordingly, one straightforward extension I recommend pursuing would be to add a textured pole to the arena, taking a leaf from the book of Maimon et al (2008). This would mean that the fly would experience parallax cues, i.e. discontinuities in the optic flow field, which could elicit the target fixation behaviour that proved so elusive in the SL-control experiments. Might this small-field motion cue enhance OL in the HS arena? Would OL performance depend on the position of the pole relative to the odour, as it did for the landmark in the SL arena? Answers to these questions would contribute considerably to our understanding of odour-dependent target fixation (sections 6.3.5, 9.4.2). Furthermore, one could investigate whether olfaction affects the fly's tendency to behave differently towards long and short objects (Maimon et al, 2008).

Given the time and budget, I would very much like to improve the tracking system itself. While it has proved sufficient for my needs, the intermittency of the recorded trajectories it produces is a

drawback, as not having complete trajectories constrains one's options for analysis, and possible artefacts due to non-uniform sampling (i.e. the fly being more likely to tracked in certain regions of the arena) are a perennial concern. The tracker's inability to measure the fly's orientation is another serious limitation, as it necessitates the assumption that the fly is always aligned with its direction of movement. I would say that this is the single biggest weakness of my study, particularly in light of recent publications demonstrating the impressive aerobatic agility of *Drosophila* (Ristroph et al, 2009; Sugiura & Dickinson, 2009). It may be feasible to estimate yaw orientation using higher-resolution cameras (perhaps utilising pan-tilt equipment for active tracking (Fry et al, 2000)), which would represent a significant improvement. However, estimating parameters such as roll orientation and the position of the head relative to the body is still likely to prove challenging with currently available hardware. To date, it has only been possible to record this kind of data from a volume of space much smaller than my free-flight arena (e.g. Fry et al, 2003; Ristroph et al, 2009).

It would also be desirable to project, rather than glue, shapes onto the walls. Moving wallpaper patterns could be used to perform some interesting experiments; for instance, could a fly overcome the repulsive effect of an expansion pole if the odour source was positioned close to it? One could even follow Fry et al's (2008) lead, and change the patterns on the walls dependent on the fly's position in real time. This would open up all kinds of experimental possibilities. For instance, could a fly still use a landmark to locate an odour source if the landmark vanished whenever the fly approached it (c.f. walking flies in Strauss & Pichler (1998))?

## 10.2.2: Tethered flight experiments

My experiments are observational in nature. While I can alter certain stimulus parameters, the flies have considerable freedom to determine their own visual input *via* their behaviour. While this ensures that they have a naturalistic visuomotor experience, it can be a little frustrating as cause and effect are so difficult to distinguish. I have had to employ very careful statistical analysis to avoid drawing spurious conclusions.

By contrast, a tethered flight paradigm sacrifices realism to some extent in order to offer manipulative control of the animal's sensory input. I lack the facility to perform tethered experiments, but given the opportunity there are a number of questions that I would like to settle using this method.

### 10.2.2.1 Optomotor rebound

I have described a post-saccade turning behaviour that I term the optomotor rebound, and presented

evidence from both real (section 4.4.3) and modelled flies (section 5.5.2.2) that it can be best understood as compensation for the visual feedback a fly receives as a result of its own saccade. However, it is difficult to conclusively demonstrate this without performing a direct experiment. A magnetic tether would be appropriate for this purpose, as it allows flies to produce relatively unimpeded saccades. Assuming a sufficiently low-latency closed-loop flight simulator system could be implemented, one could induce a saccade (or wait until the fly performed one spontaneously), and then manipulate the visual panorama such that the fly would appear to be rotating at a different speed than it actually was. Any differences in post-saccade behaviour could then be unequivocally attributed to visual feedback during the saccade. However, it should be borne in mind that tethered saccades are significantly smaller and slower than the real thing (Bender & Dickinson, 2006).

#### 10.2.2.2 Spontaneous saccades

I have hypothesised that flies perform (at least) two distinct types of saccades in my experiments: those triggered by visual input, and those initiated endogenously (sections 4.5.5, 5.6.3.2). Furthermore, I have suggested that these manoeuvres may differ kinematically, such that the latter category of saccades have a larger average amplitude. These hypotheses must be considered tentative; due to the limitations of my experimental paradigm I cannot say with any certainty which category any given saccade belongs to. Maye et al (2007) perform a detailed analysis of the temporal structure of spontaneous saccades in tethered flies, and Reynolds & Frye (2007) investigate how they could give rise to optimal foraging behaviour. However, I am not aware of any studies directly comparing the properties of spontaneous *versus* visually-evoked saccades. A magnetic tether would again be the most appropriate paradigm for such an investigation.

#### 10.2.2.3 Receptive fields

The receptive fields for the three subsystems of my visuomotor model (section 5.3) were based more on guesswork, trial and error, and engineering insight than hard biological data. Furthermore, simplifying assumptions had to be made, such as that of uniform weighting for all EMDs in a filter. While the receptive fields of some LPTCs have been characterised in detail, it is unclear how this relates to behaviour. The tethered flight paradigm would allow one to map local motion sensitivity fields like those of e.g. Krapp & Hengstenberg (1996), but for behavioural rather than electrophysiological responses. Huston & Krapp (2008) perform an analysis of this kind for motoneurons in the necks of blowflies, so my proposed approach could be viewed as simply moving rather further downstream in the control loop. These experiments would be in a similar vein to those of Tammero et al (2004), but more spatially detailed. Of course, care would have to be taken with this analysis as one would expect spatial integration of motion signals to be highly non-linear.

#### 10.2.2.4 Olfactory temporal dynamics

A vexatious issue that I have repeatedly encountered during this study is whether behavioural responses to odour should be considered predominantly phasic or tonic. Chow & Frye (2008) compare visuomotor responses when odour is either present or absent in a binary fashion, but behavioural responses to odorants can be attenuated by prolonged pre-exposure in both larval (Cobb & Domain, 2000) and adult *Drosophila* (Störtkuhl, 1999). Indeed, I make use of both a steady-state (tonic) and a high-pass (phasic) mechanism for different parts my crossmodal model. This could be viewed as a prediction, namely that target fixation will be strengthened throughout an extended presentation of odour, but that collision avoidance will exhibit only transient odour-dependent effects. This hypothesis would be straightforward to test by using an approach very similar to Chow & Frye's (2008), but focussing on changes in the amplitude or coherence of visuomotor behaviours as a function of the time elapsed since the on- or offset of odour presentation.

#### 10.2.2.5 Target fixation

I find evidence for target attraction behaviour in the SL arena when odour is present, but not when it is absent. This would seem to be at odds with Chow & Frye's (2008) observation that the presence of odour does not affect tethered flies' tracking of a small-field target. Further tethered experiments could help to clarify the picture. One possible reason for the discrepancy is that my free-flight environment featured horizontal stripes but their visual stimulus did not, so the disruptive effects of background horizontal edges of varying spatial extents and contrasts could be explored.

In section 9.2.2, I observed a remarkably strong odour-dependent attraction towards a wide region of homogeneous, exclusively vertical contrast. This could not be considered a small-field target in any conventional sense. Assuming that this finding can be replicated, tethered studies would allow this behaviour to be investigated in detail. Does the attraction depend on a total absence of horizontal contrast? This could be explored by arithmetically adding horizontal contrasts of various waveforms, amplitudes and spatial frequencies to a vertical stripe pattern. Does the response scale sub- or supralinearaly with the size of the vertical pattern? How does the response attenuate as the stripes are rotated from vertical? Is the behaviour better understood as a repulsion from regions lacking in vertical contrast? Answers to these questions would make it possible to begin modelling this behaviour, which at present is impossible as too little is known about it.

#### 10.2.2.6 A more realistic closed loop

Comparisons between free- and tethered-flight studies are complicated by the fact that even a closed-

loop tethered paradigm offers a rather unrealistic coupling of perception and action from the fly's perspective. For instance, a tethered fly may steer until a vertical stripe is frontally positioned and then hold it there indefinitely, producing very clear fixation behaviour. In free-flight, a fly may orient towards a landmark but then be repelled by expansion cues shortly afterwards (see Maimon et al, 2008), making the behaviour more difficult to detect.

This could be resolved to some extent by programming the closed loop system to simulate flying in an arena, rather than simply controlling the yaw orientation of a visual scene. Essentially, this would mean using my simulation but with a real tethered fly in the place of the model. While realistic optic flow patterns have been presented to tethered flies for electrophysiological experiments (e.g. van Hateren et al, 2005), I am not aware of any studies that close the loop in this way. I find this a little surprising, as it seems like an obvious logical step.

Of course, there would be some considerable difficulties associated with mapping, say, torques generated at the simulator to the manoeuvres that would result in an unrestrained animal. Furthermore, the simulation would still be a pale imitation of real flight, since mechanosensory cues from the halteres and antennae would be lacking. Nevertheless, I think this approach could represent a valuable step towards reconciling data from tethered and free-flight experiments.

#### 10.2.2.7 Genetic dissection of flight behaviour

As discussed in section 1.4, the chief advantage of using *Drosophila* as an experimental animal is the wealth of genetic techniques available. Genetic dissection could be used to investigate which areas of the central brain are involved in odour localisation behaviour – a question I have remained deliberately agnostic about throughout this thesis. While mutant flies could of course be used in the free-flight paradigm, the finer control offered by tethered experiments may be more appropriate to investigate this issue, as it would allow for a more direct causal linkage to be established between neural causes and sensorimotor effects. As a starting point, I would suggest investigating the behaviour of central complex (CX) mutants. This brain region appears to be involved in the high-level co-ordination of walking behaviour, and target orientation in particular (reviewed in Strauss, 2002). Tethered flight experiments reveal some intriguing effects on visuomotor control caused by defects in the ellipsoid body of the CX in *Drosophila* (Ilius et al, 1994). It would be interesting to assess the extent to which the olfactory modulation of flight behaviour (see section 10.2.2.4) is affected in these animals.

### 10.2.3: Biorobotic model

An original aim of this study was to implement the crossmodal model on a gantry robot. Robotic implementations of behavioural models can often offer a more convincing demonstration of their validity than simulated ones, as they show that the model can handle all the noise and unpredictability of the real world (Webb & Consi, 2001; Webb, 2002). Since the physical world no longer needs to be simulated, the bioroboticist sidesteps the kinds of concerns I had about using an unrealistically benign model of the environment (section 8.1). However, because we generally lack the technology to manufacture robots on the scale of insects with insect-like sensorimotor capabilities, compromises must always be made.

In my opinion, there is not a great deal to be gained by using cameras instead of a simulation to generate visual input in this case. If the paradigm involved natural three-dimensional scenes with movement and complex lighting (e.g. a breezy woodland setting), then real video would be highly preferable to the simple simulation I employ. However, since the visual environment in my paradigm has been specifically engineered to be as controlled and artificial as possible, it lends itself to simulation. While it is true that robot-mounted video cameras would introduce noise, both in terms of pixel noise and variability in motion cues resulting from positional uncertainty, it is not clear that this noise would be in any way similar to that experienced by a fly. I would argue that it is preferable to have a perfect simulation which can be corrupted by artificial noise in a controlled, quantifiable manner as the experimenter requires.

The real strength of a biorobotic model would be in the olfactory domain. As I have discussed at length, simulating an odour plume is a very difficult problem. Because I was so keen to avoid oversimplifying the task of odour localisation in my simulation, I may have underestimated the richness of the plume structure. Specifically, my random resampling of recorded VOC sensor data destroys any frequency information that may exist. Static recordings (fig 7.9) clearly reveal slow oscillations over the course of tens of seconds. It may be that higher frequency components also exist, which could conceivably confer valuable information to the fly. Using a real plume would allow these features to be preserved, assuming the sensor had sufficient temporal resolution to detect them. However, any robot is likely to be considerably larger than a fly, and thus its movements will perturb the plume structure to a greater degree. Any biorobotic modeller tackling this problem would do well to take great efforts to minimise this influence, perhaps by using smoke plumes for visualisation of the robot's wake.

### 10.2.4: Extending the model to non-static air

As I detailed in section 5.6.2, there are many features of *Drosophila* physiology and behaviour that are absent from my model. Thus there are countless ways in which the model could be elaborated to make it more realistic. However, as with devising new experiments (section 10.2.1), this should be done in a principled way. Parsimony is crucial to a model's success, so complication for complication's sake must be avoided.

With this in mind, I think the most useful way the model could be extended would be to take wind into account. While the still-air paradigm is good for characterising behaviour in a simple, controlled setting, it must be recognised that it represents a special case which does not generally apply to a fly in the wild. Indeed, I show that simple non-visual chemotaxis of the type performed by *E. coli* is sufficient for odour localisation in still air (section 8.3.1), but hypothesise that it would fail in windy conditions, and that this is the reason why the fly employs the more complex algorithm represented by my model.

Wind perturbs a flying insect's position and orientation, necessitating compensatory mechanisms to maintain a straight course. While I imagine that my current model's optomotor response system would be able to correct for yaw disturbances, I would predict that additional expansion-detection mechanisms would be required to deal with translational drift due to wind. In my simulation, the model only experiences expansion patterns with roughly frontally-positioned poles, but a fly in windy conditions could be blown in any direction, and thus would require expansion detectors with many different alignments to avoid collisions. Indeed, this could be the purpose of the Hx cell shown in fig 2.7. Tethered flight experiments like those of Bender & Dickinson (2006) would help to establish how turning responses vary as a function of the orientation of the expansion pole – information that would be essential for implementing the extended model.

There is evidence that anemotaxis in *Drosophila* is achieved not only using vision, but also mechanosensory information, most likely from the antennae. The presence of such cues can alter visuomotor behaviours; for instance, flies that feel as if they are moving upwind display less aversion to expansion patterns (Budick et al, 2006). Thus, a third modality would need to be added to the crossmodal model, complete with its interactions with the existing visuomotor controller. Furthermore, even dead flies display some anemotactic ability due to passive aerodynamic effects (Budick et al, 2006), rather like a dart or shuttlecock maintains its orientation in flight. This observation illustrates that some simulation of the physics of *Drosophila* flight may be required. Fortunately, this is a very active area of research (e.g. Ramamurti & Sandberg, 2007; Hesselberg &

Lehmann, 2007; Sugiura & Dickinson, 2009).

Of course, in order to inform and validate the model, one must be able to perform analogous experiments on the fly. This could be achieved by adapting the free-flight paradigm to take place inside a wind tunnel. This would naturally impose some constraints on the type of environment that could be used; the circular geometry of my arena, for instance, would probably not be suitable. However, fine mesh screens could perhaps be used to present visual stimuli (which could potentially be dynamic, see section 10.2.1) whilst allowing air currents to pass through them. The presence of wind may in fact simplify the problem of olfactory simulation by imposing more structure on the odour plume.

A trimodal model of this kind would be a significant step towards a 'general theory' of odour localisation. One could investigate how well it generalised to other animals such as moths, and the different spatial scales over which their odour localisation behaviours take place. This would offer insights into the extent to which the algorithms identified were constrained by universal features of turbulent plumes, *versus* those aspects which were specific to the particular evolutionary niche of *Drosophila.*

## 10.3: Closing remarks

What is the moral of this story? While vision and olfaction cannot be considered independent, reasonably simple interactions between the two modalities can account for the puzzling (to me at least) observations of Frye et al (2003). When I began this study, I hypothesised that *Drosophila* relied on visual odometry to construct some spatial representation of the odour plume, and that horizontal stripes offered insufficient odometric feedback for this map-making exercise. While I would by no means rule out the existence of such a mechanism – there is evidence for at least rudimentary spatial memory in *Drosophila* (Putz & Heisenberg, 2002) – this study demonstrates that it is not necessary to explain the observations in question.

I am reminded of one of my undergraduate robotics lectures. The lecturer, Chris Malcolm, put a wheeled vehicle on the table and set it moving. When it encountered an obstacle, it would bump into it and then change direction, moving in a fluid, loopy manner. Dr Malcolm asked us to guess how many sensors and motors the robot possessed. At least two motors, we reasoned, since it could steer; and at least one contact sensor, possibly more. He then removed the casing to reveal one motor and no sensors, at least in the conventional sense. The drive wheels were powered via a differential gear such that the vehicle would move forward as long as it was unimpeded, but as soon as the wheels

experienced resistance, the torque was diverted into rotating their axis, causing the robot to turn away from whatever had obstructed its progress. My fellow students and I had not properly used Occam's razor.

My point is not that *Drosophila* are simple automatons; they are most certainly not. It is simply that it is all too easy to ascribe excessive complexity to a system that one does not properly understand. Taking a synthetic approach (i.e. model building) as opposed to an analytic one can be a very enlightening exercise (Braitenberg, 1984), as it encourages one to consider the simplest possible mechanisms that could account for the behaviour of the target system. However, as argued by Webb (2009), it is vital to perform analytic experiments on real animals to ensure that one has a well-defined target system against which to assess one's model. Tempting though it may be to escape the messiness of the natural world by implementing abstract agents in idealised environments, it is my opinion that models must ultimately be grounded in reality if they are to be useful. To achieve this goal, experimentalists and modellers should co-operate very closely, as each group has much to offer the other (section 1.7). Better still, the same researchers can practise both of these modes of investigation, as I have done in this study.

# Appendix: Comparing correlation coefficients

Spearman's $\rho$, the correlational statistic used throughout this study, is the non-parametric version of Pearson's $r$, and is calculated by simply computing $r$ on the ranks of the data rather than the data itself. Thus, for a suitably large $n$, the distribution of $\rho$ approximates that of $r$.

It is possible to calculate the significance of the differences between two $r$s. Because this is not a standard statistical technique, the method is given here. The general formula, yielding a z-score, is given by equation A1.

$$z = \frac{z'_1 - z'_2}{\sigma_{z'_1 - z'_2}} \tag{A1}$$

$z'$ is computed from $r$ as shown in equation A2.

$$z' = \frac{\log(1+r) - \log(1-r)}{2} \tag{A2}$$

The denominator of A1 is the standard error of the difference between $z$'s, and is given by equation A3, where $n_1$ and $n_2$ are the sample sizes of the correlations.

$$\sigma_{z'_1 - z'_2} = \sqrt{\frac{1}{n_1 - 3} + \frac{1}{n_2 - 3}} \tag{A3}$$

# References


**MD Adams, SE Celniker, RA Holt, CA Evans, JD Gocayne, PG Amanatides, SE Scherer, PW Li, RA Hoskins, RF Galle *et al*** (2000) The genome sequence of *Drosophila melanogaster*. *Science*, **24**, 2185-95.

**H Autrum** (1958) Electrophysiological analysis of the visual systems in insects. *Expl Cell Res*, **Suppl. 5**, 426-39.

**T Balch, Z Khan & M Veloso** (2001) Automatically tracking and analyzing the behaviour of live insect colonies. *Proc Intl Conf Auton Agents 2001*, 521-8.

**FG Barth** (1964) A phasic-tonic proprioceptor in the telson of the crayfish *Procambarus clarki* (Girard). *J Comp Physiol A*, **48**, 181-9.

**J Bau, KA Justus & RT Cardé** (2002) Antennal resolution of pulsed pheromone plumes in three moth species. *J Ins Physiol*, **48**, 433-42.

**JH Belanger & EA Arbas** (1998) Behavioral strategies underlying pheromone-modulated flight in moths: lessons from simulation studies. *J Comp Physiol A*, **183**, 345-60.

**JA Bender & MH Dickinson** (2006) Visual stimulation of saccades in magnetically tethered *Drosophila*. *J Exp Biol,* **209**, 3170-82.

**HC Berg & DA Brown** (1972) Chemotaxis in *Escherichia coli* analysed by three-dimensional tracking. *Nature*, **239**, 500-4.

**M Blanchard, FC Rind & PFMJ Verschure** (2000) Collision avoidance using a model of the locust LGMD neuron. *Robotics and Autonomous Systems,* **30**, 17-38.

**N Boeddeker & M Egelhaaf** (2003) Steering a virtual blowfly: simulation of visual pursuit. *Proc R Soc Lond B*, **270**, 1971-8.

**N Boeddeker, R Kern & M Egelhaaf** (2003) Chasing a dummy target: smooth pursuit and velocity control in male blowflies. *P R Soc B*, **270**, 393-99.

**N Boeddeker, JP Lindemann, M Egelhaaf & J Zeil** (2005) Responses of blowfly motion-sensitive neurons to reconstructed optic flow along outdoor flight paths. *J Comp Physiol A*, **191**, 1143-55.

**A Borst** (2009) *Drosophila*'s view on insect vision. *Curr Biol*, **19**, 36-47.

**A Borst & S Bahde** (1988) Spatio-temporal integration of motion: A simple strategy for safe landing in flies. *Naturwissenschaften*, **75**, 265-7.

**A Borst, M Egelhaaf & J Haag** (1995) Mechanisms of dendritic integration underlying gain control in fly motion-sensitive interneurons. *J Comp Neurosci*, **2**, 5-18.

**A Borst, VL Flanagin & H Sompolinsky** (2005) Adaptation without parameter change: Dynamic gain control in motion detection. *PNAS*, **102**, 6172-6.

**A Borst & J Haag** (2002) Neural networks in the cockpit of the fly. *J Comp Physiol A*, **188**, 419-37.

**A Borst & M Heisenberg** (1982) Osmotropotaxis in *Drosophila melanogaster*. *J Comp Physiol A*, **147**, 479-84.

**V Braitenberg** (1984) *Vehicles: Experiments in synthetic psychology*. Cambridge, MA: MIT Press.

**N Brenner, W Bialek & R de Ruyier van Steveninck** (2000) Adaptive rescaling maximizes information transmission, *Neuron*, **26**, 695-702.

**SA Budick, & MH Dickinson** (2006) Free-flight responses of *Drosophila melanogaster* to attractive odors. *J Exp Biol,* **209**, 3001-17.

**SA Budick, MB Reiser & MH Dickinson** (2007) The role of visual and mechanosensory cues in structuring forward flight in *Drosophila melanogaster. J Exp Biol*, **210**, 4092-103.

**JR Carlson** (1996) Olfaction in *Drosophila*: from odor to behavior. *Trends Genet*, **12**, 175-80.

**JS Chahl, MV Srinivasan & SW Zhang** (2004) Landing strategies in honeybees and applications to uninhabited airborne vehicles. *Int J Robot Res*, **23**, 101-10.

**WP Chan, R Prete & MH Dickinson** (1998) Visual input to the efferent control system of a fly's "gyroscope". *Science*, **280**, 289-92.

**DC Chang** (2006) Neural circuits underlying circadian behaviour in Drosophila melanogaster. *Behav Process*, **71**, 211-25.

**DM Chow & MA Frye** (2008) Context-dependent olfactory enhancement of optomotor flight control in *Drosophila*. *J Exp Biol,* **211**, 2478-2485.

**M Cobb & I Domain** (2000) Olfactory coding in a simple system: adaptation in *Drosophila* larvae. *Proc R Soc Lond B,* **267**, 2119-25.
**D Coombs & K Roberts** (1992) Bee-bot: Using peripheral optic flow to avoid obstacles. *Proc SPIE (Boston)*, **1825**, 714-21.
**A Couto, M Alenius & BJ Dickson** (2005) Molecular, anatomical, and functional organization of the *Drosophila* olfactory system. *Curr Biol*, **15**, 1535-47.
**H Cuntz, J Haag, F Forstner, I Segev & A Borst** (2007) Robust coding of flow-field parameters by axo-axonal gap junctions between fly visual interneurons. *PNAS*, **104**, 10229-33.
**CT David** (1982) Compensation for height in the control of groundspeed by *Drosophila* in a new, 'barber's pole' wind tunnel. *J Comp Physiol A*, **147**, 485-93.
**J-M Devaud** (2003) Experimental studies of adult *Drosophila* chemosensory behaviour. *Behav Proc*, **64**, 177-96.
**AA Dobritsa, W van der Goes van Naters, CG Warr, RA Steinbrecht & JR Carlson** (2003) Integrating the molecular and cellular basis of odour coding in the Drosophila antenna. *Neuron,* **37**, 827-41.
**JK Douglass & NJ Strausfeld** (1995) Visual motion-detection circuits in flies: Peripheral motion computation by identified small-field retinotopic neurons. *J Neurosci*, **15**, 5596-611.
**JK Douglass & NJ Strausfeld** (1996) Visual motion-detection circuits in flies: Parallel direction- and non-direction-sensitive pathways between the medulla and lobula plate. *J Neurosci*, **16**, 4551-62.
**BJ Duistermars, DM Chow, M Condro & MA Frye** (2007) The spatial, temporal and contrast properties of expansion and rotation flight optomotor responses in *Drosophila. J Exp Biol*, **210**, 3218-27.
**BJ Duistermars & MA Frye** (2008) Crossmodal visual input for odor tracking during fly flight. *Curr Biol,* **18**, 270-275.
**S Edwards, AJ Rutkowski, RD Quinn & MA Willis** (2005) Moth-inspired plume tracking strategies in three-dimensions. *Proc IEEE Intl Conf Rob & Autom 2005*, **5**, 1669-74.
**M Egelhaaf** (1987) Dynamic properties of two control systems underlying visually guided turning in house-flies. *J Comp Physiol A*, **161**, 777-83.
**M Egelhaaf, A Borst & W Reichardt** (1989) Computational structure of a biological motion-detection system as revealed by local detector analysis in the fly's nervous system. *J Opt Soc Am A*, **6**, 1070-87.
**HY Fadamiro, TD Wyatt & MC Birch** (1998) Flying beetles respond as moths predict: optomotor anemotaxis to pheromone plumes at different heights, *J Ins Behav*, **11**, 549-57.
**K Farrow, J Haag & A Borst** (2003) Input organization of multifunctional motion-sensitive neurons in the blowfly. *J Neurosci*, **23**, 9805-11.
**K Farrow, J Haag & A Borst** (2006) Nonlinear, binocular interactions underlying flow field selectivity of a motion-sensitive neuron. *Nat Neurosci,* **9**, 1312-20.
**TC Ferrée & SR Lockery** (1999) Computational rules for chemotaxis in the nematode *C. elegans*. *J Comp Neurosci*, **6**, 263-77.
**N Franceschini, C Blanes & L Oufar** (1986) Passive, non-contact optical velocity sensor (in French). *Dossier technique ANVAR/DVAR No. 51 549*, Paris.
**N Franceschini, JM Pichon & C Blanes** (1992) From insect vision to robot vision. *Phil Trans R Soc Lond B*, **337**, 283-94.
**N Franceschini, F Ruffier & J Serres** (2007) A bio-inspired flying robot sheds light on insect piloting abilities. *Curr Biol*, **17**, 329-35.
**MO Franz & HG Krapp** (2000) Wide-field, motion-sensitive neurons and matched filters for optic flow fields. *Biol Cybern*, **83**, 185-94.
**MO Franz, TR Neumann, M Plagge, HA Mallot & A Zeil** (1999) Can fly tangential neurons be used to estimate self motion? *Proc. Artificial Neural Networks*, 994-9.
**SN Fry, M Bichsel, P Müller & D Robert** (2000) Tracking of flying insects using pan-tilt cameras. *J Neurosci Meth*, **101**, 59-67.
**SN Fry, N Rohrseitz, AD Straw & MH Dickinson** (2008) TrackFly: Virtual reality for a behavioral system analysis in free-flying fruit flies. *J Neurosci Meth*, **171**, 110-7.
**SN Fry, N Rohrseitz, AD Straw & MH Dickinson** (2009) Visual control of flight speed in

*Drosophila melanogaster. J Exp Biol*, **212**, 1120-30.
**SN Fry, R Sayaman & MH Dickinson** (2003) The aerodynamics of free-flight maneuvres in *Drosophila*. *Science*, **300**, 495-8.
**MA Frye & MH Dickinson** (2004) Motor output reflects the linear superposition of visual and olfactory inputs in *Drosophila*. *J Exp Biol*, **207**, 123-31.
**MA Frye & MH Dickinson** (2007) Visual edge orientation shapes free-flight behavior in *Drosophila. Fly* **1**, 153-4.
**MA Frye, M Tarsitano & MH Dickinson** (2003) Odor localization requires visual feedback during free flight in *Drosophila melanogaster*. *J Exp Biol*, **206**, 843-55.
**V Gauck & A Borst** (1999) Spatial response properties of contralateral inhibited lobula plate tangential cells in the fly visual system. *J Comp Neurol*, **406**, 51-71.
**M Geier, OJ Bosch & J Boeckh** (1999) Influence of odour plume structure on upwind flight of mosquitoes towards hosts. *J Exp Biol*, **202**, 1639-48.
**JJ Gibson** (1950) *The perception of the visual world*. Boston: Houghton Mifflin.
**JJ Gibson** (1979) *The ecological approach to perception*. Boston: Haughton Mifflin.
**C Gilbert, W Gronenberg & NJ Strausfeld** (1995) Oculomotor control in calliphorid flies: head movements during activation and inhibition of neck motor neurons corroborate neuroanatomical predictions. *J Comp Neurol,* **361**, 285-97.
**M Giurfa & R Menzel** (1997) Insect visual perception: complex abilities of simple nervous systems. *Curr Opin Neurobiol*, **7**, 505-13.
**KG Götz** (1964) Optomotorische Untersuchung des visuellen Systems einiger Augenmutanten der Fruchtfliege *Drosophila*. *Kybernetik*, **2**, 77-92.
**KG Götz** (1968) Flight control in *Drosophila* by visual perception of motion. *Biol Cybern*, **4**, 199-208.
**J Goyret, PM Markwell & RA Raguso** (2007) The effect of decoupling olfactory and visual stimuli on the foraging behavior of *Manduca sexta. J Exp Biol*, **210**, 1368-405.
**AA Grace** (2000) The tonic/phasic model of dopamine system regulation and its implications for understanding alcohol and psychostimulant craving. *Addiction*, **95**, 119-28.
**FW Grasso & J Atema** (2002) Integration of flow and chemical sensing for guidance of autonomous marine robots in turbulent flows. *Environmental Fluid Mechanics*, **2**, 95-114.
**RJ Greenspan** (2004) *Fly pushing: The theory and practice of* Drosophila *genetics, 2nd ed*. Cold Spring Harbor Laboratory Press.
**RJ Greenspan & B van Swinderen** (2004) Cognitive consonance: complex brain functions in the fruit fly and its relatives. *Trends Neurosci*, **27**, 707-11.
**J Guo & A Guo** (2005) Crossmodal interactions between olfactory and visual learning in *Drosophila*. *Science*, **309**, 307-10.
**J Haag & A Borst** (2002) Dendro-dendritic interactions between motion-sensitive large-field neurons in the fly. *J Neurosci*, **22**, 3227-33.
**J Haag, W Denk & A Borst** (2004) Fly motion vision is based on Reichardt detectors regardless of the signal-to-noise ratio. *PNAS*, **101**, 16333-8.
**J Haag, A Vermeulen & A Borst** (1999) The intrinsic electrophysiological characteristics of fly lobula plate tangential cells: III. Visual response properties. *J Comput Neurosci*, **7**, 213-34.
**RA Harris, DC O'Carroll & SB Laughlin** (2000) Contrast gain reduction in fly motion adaptation. *Neuron*, **28**, 595-606.
**RR Harrison & C Koch** (1999) A robust analog VLSI motion sensor based on the visual system of the fly, *Auton Robot*, **7**, 211-24.
**B Hassenstein & W Reichardt** (1956) Systemtheoretische Analyse der Zeit-, Reihenfolgen- und Vorzeichenauswertung bei der Bewegungsperzeption des Rüsselkäfers Chlorophanus. *Z Naturforsch*, **9**, 513-24.
**AT Hayes, A Martinoli & RM Goodman** (2002) Distributed odor source localization. *IEEE Sens J*, **2,** 260-71.
**M Heisenberg & R Wolf** (1984) *Vision in* Drosophila. Springer.
**P Hennig, R Möller & M Egelhaaf** (2008) Distributed dendritic processing facilitates object detection: A computational analysis on the visual system of the fly. *PloS ONE*, **3**, e3092.
**R Hengstenberg** (1993) Multisensory control in insect oculomotor systems. *Rev Oculomot Res*, **5**, 285-98.
**T Hesselberg & FO Lehmann** (2007) Turning behaviour depends on frictional damping in the

fruit fly *Drosophila*. *J Exp Biol,* **210**, 4319-34.
**CM Higgins, JK Douglass & NJ Strausfeld** (2004) The computational basis of an identified neuronal circuit for elementary motion detection in dipterous insects. *Vis Neurosci*, **21**, 567-86.
**CM Higgins & V Pant** (2004) An elaborated model of fly small-target tracking. *Biol Cybern*, **91**, 417-28.
**ES Hodgson & RF Mathewson** (1971). Chemosensory orientation in sharks. *Ann NY Acad Sci,* **188**, 174–82.
**MH Holmqvist & MV Srinivasan** (1991). A visually evoked escape response of the housefly. *J Comp Physiol A,* **169**, 451-9.
**E Horn & R Wehner** (1975) The mechanism of visual pattern fixation in the walking fly, *Drosophila melanogaster*. *J Comp Physiol*, **101**, 39-56.
**G Hoyle** (1984) The scope of neuroethology. *Behav Brain Sci*, **7**, 367-412.
**KG Hu, H Reichert & WS Stark** (1978) Electrophysiological characterization of the *Drosophila* ocelli. *J Comp Physiol A*, **126**, 15-24.
**SA Huber, MO Franz & HH Bülthoff** (1999) On robots and flies: Modeling the visual orientation behavior of flies. *Rob & Auton Sys*, **29**, 227-42.
**SJ Huston & HG Krapp** (2008) Visuomotor transformation in the fly gaze stabilization system. *PloS Biol*, **6**, e173.
**M Ilius, R Wolf & M Heisenberg** (1994) The central complex of *Drosophila melanogaster* is involved in flight control: studies on mutants and mosaics of the gene *ellipsoid body open*. *J Neurogenet*, **9**, 189-206.
**M Joesch, J Plett, A Borst, & DF Reiff** (2008) Response properties of motion-sensitive visual interneurons in the lobula plate of *Drosophila melanogaster. Curr Biol,* **18**, 368-74.
**KA Justus, RT Cardé & AS French** (2005) Dynamic properties of antennal responses to pheromone in two moth species. *J Neurophysiol*, **93**, 2233-9.
**K Karmeier, HG Krapp & M Egelhaaf** (2003) Robustness of the tuning of the fly visual interneurons to rotatory optic flow. *J Neurophysiol*, **90**, 1626-34.
**K Karmeier, HG Krapp & M Egelhaaf** (2005) Population coding of self-motion: Applying Bayesian analysis to a population of visual interneurons in the fly. *J Neurophysiol*, **94**, 2182-94.
**H Kazama, & RI Wilson** (2008) Homeostatic matching and nonlinear amplification at identified central synapses. *Neuron,* **58**, 401-13.
**JS Kennedy** (1940) The visual response of flying mosquitoes. *Proc Zool Soc Lond A*, **109**, 221-42.
**R Kern, JH van Hateren, C Michaelis, JP Lindemann & M Egelhaaf** (2005) Function of a fly motion-sensitive neuron matches eye movements during free flight. *PLoS Biol*, **3**, e171.
**T Komiyama & L Luo** (2006) Development of wiring specificity in the olfactory system. *Curr Opin Neurobiol*, **16**, 67-73.
**KP Körding & DM Wolpert** (2004) Bayesian integration in sensorimotor learning. *Nature*, **427**, 244-7.
**HG Krapp, B Hengstenberg & R Hengstenberg** (1998) Dendritic structure and receptive-field organization of optic flow processing interneurons in the fly. *J Neurophysiol*, **79**, 1902-17.
**HG Krapp & R Hengstenberg** (1996) Estimation of self-motion by optic flow processing in single visual interneurons. *Nature*, **384**, 463-6.
**HG Krapp, R Hengstenberg & M Egelhaaf** (2001) Binocular contributions to optic flow processing in the fly visual system. *J Neurophysiol*, **85**, 724-34.
**SA Kreher, D Mathew, J Kim & JR Carlson** (2008) Translation of a sensory input into behavioural output via an olfactory system. *Neuron,* **59**, 110-24.
**LPS Kuenen & TC Baker** (1982) Optomotor regulation of ground velocity in moths during flight to sex pheromone at different heights. *Physiol Entomol*, **7**, 193-202.
**Y Kuwana, S Nagasawa, I Shimoyama & R Kanzaki** (1999) Synthesis of the pheromone-oriented behaviour of silkworm moths by a mobile robot with moth antennae as pheromone sensors. *Biosens & Bioelec*, **14**, 195-202.
**DN Lee** (1976) A theory of visual control of braking based on information about time-to-collision. *Perception*, 5, 437-59 .
**DN Lee & DE Reddish** (1981). Plummeting gannets: A paradigm of ecological optics. *Nature,*

**293**, 293-4.
**FO Lehmann & MH Dickinson** (2001) The production of elevated flight force compromises manoeuvrability in the fruit fly *Drosophila melanogaster*. *J Exp Biol* **204**, 627-35.
**A Lilienthal & T Duckett** (2003) Gas source localisation by constructing concentration gridmaps with a mobile robot. *Proc Euro Conf Mob Rob 2003*.
**A Lilienthal, A Zell, M Wandel & U Weimar** (2001) Sensing odour sources in indoor environments without a constant airflow by a mobile robot. *Proc IEEE Intl Conf Rob & Autom 2001*, 4005-10.
**JP Lindemann, R Kern, JH van Hateren, H Ritter, & M Egelhaaf** (2005) On the computations analyzing natural optic flow: Quantitative model analysis of the blowfly motion vision pathway. *J Neurosci* **25**, 6435-48.
**JP Lindemann, H Weiss, R Möller & M Egelhaaf** (2008) Saccadic flight strategy facilitates collision avoidance: closed-loop performance of a cyberfly. *Biol Cybern,* **98**, 213-27.
**S-C Liu & A Usseglio-Viretta** (2001) Fly-like visuomotor responses of a robot using aVLSI motion-sensitive chips. *Biol Cybern*, **85**, 449-57.
**M Louis, T Huber, R Benton, TP Sakmar & LB Vosshall** (2004) Bilateral olfactory sensory input enhances chemotaxis behavior. *Nat Neurosci*, **11**, 187-99.
**G Maimon, AD Straw & MH Dickinson** (2008) A simple vision-based algorithm for decision making in flying *Drosophila*. *Curr Biol,* **18**, 464-70.
**A Maye, CH Hsieh, G Sugihara & B Brembs** (2007) Order in spontaneous behaviour. *PloS ONE,* **2**, e443.
**DK Modrak** (1987) *Aristotle: The Power of Perception*. Chicago: Univ. of Chicago Press.
**M Mronz & FO Lehmann** (2008). The free-flight response of *Drosophila* to motion of the visual environment. *J Exp Biol,* **211**, 2026-2045.
**J Murlis, JS Elkinton & RT Cardé** (1992) Odor plumes and how insects use them. *Annu Rev Entomol*, **37**, 505-32.
**RR Murphy** (1996) Biological and cognitive foundations of intelligent sensor fusion. *IEEE Trans Sys Man Cybern A*, **26**, 42-51.
**G Nalbach** (1994) Extremely non-orthogonal axes in a sense organ for rotation: Behavioural analysis of the dipteran haltere system. *Neuroscience*, **61**, 149-163.
**LA Necker** (1832) Observations on some remarkable optical phaenomena seen in Switzerland; and on an optical phaenomenon which occurs on viewing a figure of a crystal or geometrical solid. *London Edinburgh Philosoph Mag J Sci*, **1**, 329–37.
**TR Neumann** (2002) Modeling insect compound eyes: Space-variant spherical vision. Proc *Biologically Motivated Computer Vision 2002*, 360-7.
**TR Neumann & HH Bülthoff** (2002) Behavior-oriented vision for biomimetic flight control. *Proc. EPSRC/BBSRC Intl. Workshop on Biologically Inspired Robotics 2002*, 196-203.
**G Nevitt** (1999) Foraging by seabirds on an olfactory landscape. *Am Sci*, **87**, 46-53.
**RM Olberg & MA Willis** (1990) Pheromone-modulated optomotor response in male gypsy moths, *Lymantria dispar* L.: Directionally selective visual interneurons in the ventral nerve cord. *J Comp Physiol A*, **167**, 707-14.
**SR Olsen, & RI Wilson** (2008) Lateral presynaptic inhibition mediates gain control in an olfactory circuit. *Nature* **452**, 956-60.
**MM Parsons, HG Krapp & SB Laughlin** (2006) A motion-sensitive neurone responds to signals from the two visual systems of the blowfly, the compound eyes and ocelli. *J Exp Biol*, **209**, 4464-74.
**R Petrowitz, H Dahmen, M Egelhaaf & HG Krapp** (2000) Arrangement of optical axes and spatial resolution in the compound eye of the female blowfly *Calliphora*. *J Comp Physiol A*, **186**, 737-46.
**T Poggio & W Reichardt** (1973) A theory of the pattern induced flight orientation of the fly *Musca domestica*. *Kybernetik*, **12**, 185-203.
**G Putz & M Heisenberg** (2002) Memories in *Drosophila* heat-box learning. *Learn Mem*, **9**, 349-59.
**P Pyk, SB i Badia, U Bernardet, P Knüsel, M Carlsson, J Gu, E Chanie, BS Hansson, TC Pearce & PFMJ Verschure** (2006) An artificial moth: Chemical source localization using a robot based neuronal model of moth optomotor anemotactic search. *Auton Robots,* **20**, 197-213.
**R Ramamurti & WC Sandberg** (2007) A computational investigation of the three-dimensional

unsteady aerodynamics of Drosophila hovering and maneuvering. *J Exp Biol*, **210**, 881-96.
**W Reichardt** (1969) Movement perception in insects. In: W Reichardt (ed) *Processing of optical data by organisms and machines*. Academic Press, London New York, 465–93.
**W Reichardt, T Poggio & K Hausen** (1983) Figure-ground discrimination by relative movement in the visual system of the fly. *Biol Cybern*, **46(Suppl.)**, 1-30.
**C Reisenman, J Haag & A Borst** (2003) Adaptation of response transients in fly motion vision. I: Experiments. *Vision Res*, **43**, 1293-309.
**MB Reiser & MH Dickinson** (2003) A test bed for insect-inspired robotic control. *Phil Trans R Soc Lond A*, **361**, 2267-85.
**AM Reynolds & MA Frye** (2007) Free-flight odor tracking in *Drosophila* is consistent with an optimal intermittent scale-free search. *PloS ONE,* **2**, e354.
**A Riehle & N Franceschini** (1984) Motion detection in flies: Parametric control over ON-OFF pathways. *Exp Brain Res*, **54**, 390-4.
**FC Rind & DI Bramwell** (1996) Neural network based on the input organization of an identified neuron signalling impending collision. *J Neurophysiol*, **75**, 967-85.
**L Ristroph, GJ Berman, AJ Bergou, ZJ Wang & I Cohen.** (2009) Automated hull reconstruction motion tracking (HRMT) applied to sideways maneuvers of free-flying insects. *J Exp Biol,* **212**, 1324-35.
**D Robert & MC Göpfert** (2002) Acoustic sensitivity of fly antennae. *J Insect Physiol,* **48**, 189-96.
**A Rosenblueth & N Wiener** (1945) The role of models in science. *Philos Sci*, **4**, 316-21.
**RA Russell** (2001) Survey of robotic applications for odor-sensing technology. *Int J Robot Res*, **20**, 144-62.
**AJ Rutkowski, S Edwards, MA Willis, RD Quinn & GC Causey** (2004) A robotic platform for testing moth-inspired plume tracking strategies. *Proc IEEE Intl Conf Rob & Autom 2004*, **4**, 3319-24.
**MN Safran, VL Flanagin, A Borst & H Sompolinsky** (2007) Adaptation and information transmission in fly motion detection. *J Neurophysiol*, **98**, 3309-20.
**L Sarov-Blat, WV So, L Liu & M Rosbash** (2000) The *Drosophila takeout* gene is a novel molecular link between circadian rhythms and feeding behaviour. *Cell*, **101**, 647-56.
**J Schuckel, S Meisner, PH Torkkeli & AS French** (2008) Dynamic properties of *Drosophila* olfactory electroantennograms. *J Comp Physiol A*, **194**, 483-9.
**FH Schuling, HAK Masterbroek, R Bult & BPM Lenting** (1989) Properties of elementary movement detectors in the fly *Calliphora erythrocephala. J Comp Physiol A*, **165**, 179–92 .
**H Schuppe & R Hengstenberg** (1993) Optical properties of the ocelli of *Calliphora erythrocephala* and their role in the dorsal light response. *J Comp Physiol A*, **173**, 143-9.
**S Schuster, R Strauss & KG Götz** (2002) Virtual-reality techniques resolve the visual cues used by fruit flies to evaluate object distances. *Curr Biol*, **12**, 1591-4.
**J Serres, F Ruffier, S Viollet, & N Franceschini** (2006) Toward optic flow regulation for wall-following and centring behaviours. *Int J Adv Robotic Syst,* **3**, 147-54.
**PA Shoemaker, DC O'Carroll & AD Straw** (2005) Velocity constancy and models for wide-field visual motion detection in insects. *Biol Cybern*, **93**, 275-87.
**A Si, MV Srinivasan & S Zhang** (2003) Honeybee navigation: properties of the visually driven 'odometer'. *J Exp Biol*, **206**, 1265-73.
**H Simon** (1982) *The Sciences of the Artificial, 2nd ed.* Cambridge, Mass.: MIT Press.
**S Single & A Borst** (1998) Dendritic integration and its role in computing image velocity. *Science*, **281**, 1848-50.
**S Single, J Haag & A Borst** (1997) Dendritic computation of direction selectivity and gain control in visual interneurons. *J Neurosci*, **17**, 6023-30.
**KK Siwicki & L Ladewski** (2003) Associative learning and memory in *Drosophila*: beyond olfactory conditioning. *Behav Process*, **64**, 225-38.
**L Smith, A Philippides, P Graham & P Husbands** (2007) Linked local navigation for visual route guidance. *Adapt Behav*, **15**, 257-71.
**HP Snippe & JJ Koenderink** (1994) Extraction of optical velocity by use of multi-input Reichardt detectors. *J Opt Soc Am A*, **11**, 1222-36.
**MV Srinivasan** (1994) An image-interpolation technique for the computation of optic flow and egomotion. *Biol Cybern*, **71**, 401-16.
**MV Srinivasan, M Lehrer, WH Kirchner & SW Zhang** (1991) Range perception through

apparent image speed in freely flying honeybees. *Vis Neurosci*, **6**, 519-35.
**MV Srinivasan, JS Chahl, K Weber, S Venkatesh, MG Nagle & SW Zhang** (1999a) Robot navigation inspired by principles of insect vision. *Robot Auton Syst*, **26**, 203-16.
**MV Srinivasan, M Poteser & K Kral** (1999b) Motion detection in insect orientation and navigation. *Vision Research*, **39**, 2749-66.
**MV Srinivasan, SW Zhang & NJ Bidwell** (1997) Visually mediated odometry in honeybees. *J Exp Biol*, **200**, 2513-22.
**DG Stavenga** (2003) Angular and spectral sensitivity of fly photoreceptors. II. Dependence on facet lens F-number and rhabdomere type in *Drosophila*. *J Comp Physiol A*, **189**, 189-202.
**M Stopfer, V Jayaraman & G Laurent** (2003) Intensity versus identity coding in an olfactory system. *Neuron*, **39**, 991-1004.
**KF Störtkuhl, BT Hovemann, & JR Carlson** (1999) Olfactory adaptation depends on the Trp $Ca^{2+}$ channel in *Drosophila*. *J Neurosci,* **19**, 4839-46.
**R Strauss** (2002) The central complex and the genetic dissection of locomotor behaviour. *Curr Opin Neurobiol*, **12**, 633-8.
**R Strauss & J Pichler** (1998) Persistence of orientation toward a temporarily invisible landmark in *Drosophila melanogaster. J Comp Physiol A*, **182**, 411-23.
**AD Straw, T Rainsford & DC O'Carroll** (2008) Contrast sensitivity of insect motion detectors to natural images. *J Vision*, **8**, 1-9.
**AH Sturtevant** (1913) The linear arrangement of six sex-linked factors in Drosophila, as shown by their mode of association. *J Exp Zool*, **14**, 43-59.
**H Sugiura & MH Dickinson** (2009) The generation of forces and moments during visual-evoked steering maneuvers in flying *Drosophila. PloS ONE*, **4**, e4883.
**LF Tammero & MH Dickinson** (2002a) The influence of visual landscape on the free flight behavior of the fruit fly *Drosophila melanogaster*. *J Exp Biol*, **205**, 327-43.
**LF Tammero & MH Dickinson** (2002b) Collision-avoidance and landing responses are mediated by separate pathways in the fruit fly, *Drosophila melanogaster*. *J Exp Biol*, **205**, 2785-98.
**LF Tammero, MA Frye & MH Dickinson** (2004) Spatial organization of visuomotor reflexes in *Drosophila. J Exp Biol*, **207**, 113-22.
**NK Tanaka, T Awasaki, T Shimada & K Ito** (2004) Integration of chemosensory pathways in the *Drosophila* second-order olfactory centers. *Curr Biol*, **14**, 449-57.
**JR Tresilian** (1999) Visually timed action: time-out for 'tau'? *Trends Cogn Sci*, **3**, 301-10.
**JH van Hateren, R Kern, G Schwerdtfeger & M Egelhaaf** (2005) Function and coding in the blowfly H1 neuron during naturalistic optic flow. *J Neurosci*, **25**, 4343-52.
**JH van Hateren & C Schilstra** (1999) Blowfly flight and optic flow: II. Head movements during flight. *J Exp Biol,* **202**, 1491-1500.
**B van Swinderen & RJ Greenspan** (2003) Salience modulates 20-30 Hz brain activity in *Drosophila*. *Nat Neurosci*, **6**, 579-86.
**NJ Vickers** (2000) Mechanisms of animal navigation in odor plumes. *Biol Bull*, **198**, 203-12.
**NJ Vickers & TC Baker** (1994) Reiterative responses to single strands of odor promote sustained upwind flight and odor source location by moths. *Proc Natl Acad Sci*, **91**, 5756-60.
**NJ Vickers, TA Christensen, TC Baker & JG Hildebrand** (2001) Odour-plume dymanics influence the brain's olfactory code. *Nature*, **410**, 466-70.
**K von Frisch** (1967) *The dance language and orientation of bees*. Harvard University Press.
**H Wagner** (1982) Flow-field variables trigger landing in flies. *Nature*, **297**, 147-8.
**D Walther, DR Edgington & C Koch** (2004) Detection and tracking of objects in underwater video. *Proc Computer Vision & Pattern Recognition 2004*, 544-9.
**Y Wang, A-S Chiang, S Xia, T Kitamoto, T Tully & Y Zhong** (2003) Blockade of neurotransmission in *Drosophila* mushroom bodies impairs odor attraction, but not repulsion. *Curr Biol*, **13**, 1900-4.
**Y Wang, H-F Guo, TA Pologruto, F Hannan, I Hakker, K Svoboda & Y Zhong** (2004) Stereotyped odor-evoked activity in the mushroom body of *Drosophila* revealed by green fluorescent protein-based $Ca^{2+}$ imaging. *J Neurosci*, **24**, 6507-14.
**L Wang, VE Walker, H Sardi, C Fraser & TJC Jacob** (2002) The correlation between physiological and psychological responses to odour stimulation in human subjects. *Clin Neurophys*, **113**, 542-51.

**JP Wann** (1996) Anticipating arrival: Is the tau margin a specious theory? *J Exp Psychol*, **22**, 1031-48.
**A-K Warzecha & M Egelhaaf** (1996) Intrinsic properties of biological motion detectors prevent the optomotor control system from getting unstable. *Phil Trans R Soc Lond B*, **351**, 1579-91.
**A-K Warzecha, M Egelhaaf & A Borst** (1993) Neural circuit tuning fly visual interneurons to motion of small objects. I. Dissection of the circuit by pharmacological and photoinactivation techniques. *J Neurophysiol*, **69**, 329-39.
**B Webb** (2001) Can robots make good models of biological behaviour? *Behav Brain Sci*, **24**, 1033-50.
**B Webb** (2002) Robots in invertebrate neuroscience. *Nature*, **417**, 359-63.
**B Webb** (2004) Neural mechanisms for prediction: do insects have forward models? *Trends Neurosci*, **27**, 278-82.
**B Webb** (2006) Validating biorobotic models. *J Neural Eng*, **3**, R25-35.
**B Webb** (2009) Animals versus animats: Or why not model the real iguana? *Adapt Behav*, in press.
**B Webb & TR Consi** (2001) *Biorobotics: Methods and applications*. MIT Press.
**R Wehner** (2003) Desert ant navigation: how miniature brains solve complex tasks. *J Comp Physiol A*, **189**, 579-88.
**MA Willis & TC Baker** (1984) Effects of intermittent and continuous pheromone stimulation on the flight behavior of the oriental fruit moth, *Grapholita molesta*, *Physiol Entomol*, **9**, 341-58.
**MA Willis, MA Butler & LP Tolbert** (1995) Normal glomerular organization of the antennal lobes is not necessary for odor-modulated flight in female moths. *J Comp Physiol A*, **176**, 205-16.
**MA Willis & RT Cardé** (1990) Pheromone-modulated optomotor response in male gypsy moths, *Lymantria dispar* L.: Upwind flight in a pheromone plume in different wind velocities. *J Comp Physiol A*, **167**, 699-706.
**R Wolf & M Heisenberg** (1991) Basic organization of operant behaviour as revealed in *Drosophila* flight orientation. *J Comp Physiol A*, **169**, 699-705.
**R Wolf, T Wittig, L Liu, G Wustmann, D Eyding & M Heisenberg** (1998) *Drosophila* mushroom bodies are dispensable for visual, tactile and motor learning. *Learn Mem*, **5**, 166-78.
**AM Wong, JW Wang & R Axel** (2002) Spatial representation of the glomerular map in the *Drosphila* protocerebrum. *Cell*, **109**, 229-41.
**L Xue & M Noll** (2000) *Drosophila* female sexual behavior induced by sterile males showing copulation complementation. *PNAS*, **97**, 3272-5.
**CA Yao, R Ignell & JR Carlson** (2005) Chemosensory coding by neurons in the coeloconic sensilla of the *Drosophila* antenna. *J Neurosci*, **25**, 8359-67.
**S Yue & FC Rind** (2005) A collision detection system for a mobile robot inspired by the locust visual system. Proc 2005 Intl Conf on Robotic and Automation, 3832-7.
**JM Zanker, MV Srinivasan & M Egelhaaf** (1999) Speed tuning in elementary motion detectors of the correlation type. *Biol Cybern*, **80**, 109-116.
**J Zhu, K-C Park & TC Baker** (2003) Identification of odors from overripe mango that attract vinegar flies, *Drosophila melanogaster*, *J Chem Ecol*, **29**, 899-909.
**J-C Zufferey & D Floreano** (2006) Fly-inspired visual steering of an ultralight indoor aircraft. *IEEE T Robot*, **22**, 137-46.
**J-C Zufferey, A Klaptocz, A Beyeler, J-D Nicoud & D Floreano** (2007) A 10-gram vision-based flying robot. *Adv Robotics*, **21**, 1671-84.